

STATUS OF THESIS

Title of thesis

INVESTIGATION OF THE EFFECT OF ASPHALTENE
DEPOSITION ON RELATIVE PERMEABILITY
CHARACTERISTICS DURING WAG PROCESS

I AHMAD KHANIFAR

hereby allow my thesis to be placed at the Information Resource Center (IRC) of
Universiti Teknologi PETRONAS (UTP) with the following conditions:

1. The thesis becomes the property of UTP
2. The IRC of UTP may make copies of the thesis for academic purposes only.
3. This thesis is classified as

☐

Confidential

☒

Non-confidential

If this thesis is confidential, please state the reason:

The contents of the thesis will remain confidential for _____ years.

Remarks on disclosure:



Signature of Author

Endorsed by



Signature of Supervisor

Permanent address: No.16,
Amozegar Street, Shohada Square,
Shoosh Danial, Khozestan, Iran,
Post Code, 64719-48461

Date: 21-02-2013

Name of Supervisor
Prof. Dr. Mustafa Onur

Date: 21-02-2013

UNIVERSITI TEKNOLOGI PETRONAS

INVESTIGATION OF THE EFFECT OF ASPHALTENE DEPOSITION ON
RELATIVE PERMEABILITY CHARACTERISTICS DURING WAG PROCESS

by

AHMAD KHANIFAR

The undersigned certify that they have read, and recommend to the Postgraduate Studies Programme for acceptance this thesis for the fulfillment of the requirements for the degree stated.

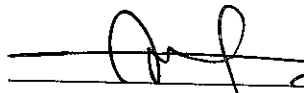
Signature:



Main Supervisor:

Prof. Dr. Mustafa Onur

Signature:

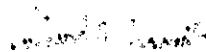
 Assoc Prof Dr Ismail M Saaid
Head, Petroleum Engineering Department
Universiti Teknologi PETRONAS

Head of Department:

Assoc. Prof. Dr. Ismail Bin Mohd Saaid

Date:

21-02-2013



INVESTIGATION OF THE EFFECT OF ASPHALTENE DEPOSITION ON
RELATIVE PERMEABILITY CHARACTERISTICS DURING WAG PROCESS

by

AHMAD KHANIFAR

A Thesis

Submitted to the Postgraduate Studies Programme

as a Requirement for the Degree of

DOCTOR OF PHILOSOPHY

PETROLEUM DEPARTMENT

UNIVERSITI TEKNOLOGI PETRONAS

BANDAR SERI ISKANDAR,

PERAK

FEBRUARY 2013

DECLARATION OF THESIS

Title of thesis

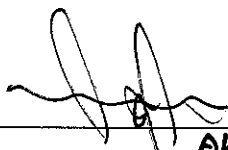
INVESTIGATION OF THE EFFECT OF ASPHALTENE
DEPOSITION ON RELATIVE PERMEABILITY
CHARACTERISTICS DURING WAG PROCESS

I AHMAD KHANIFAR

hereby declare that the thesis is based on my original work except for quotations and citations which have been duly acknowledged. I also declare that it has not been previously or concurrently submitted for any other degree at UTP or other institutions.

Witnessed by

Signature of Author


Ahmad Khanifar

Signature of Supervisor



Permanent address: No.16,

Amozegar Street, Shohada Square,

Shoosh Danial, Khozestan, Iran,

Post Code, 64719-48461

Name of Supervisor

Prof. Dr. Mustafa Onur

Date: 21-02-2013

Date: 21-02-2013

DEDICATION

This thesis is dedicated to:

First to my lovely and patient wife that she helps me a lot during residence time in UTP and second to my cute daughter which born and grew up during my PhD time and now she is almost three years old.

ACKNOWLEDGEMENTS

I would like to express my deepest gratitude and respect to my supervisor, Professor Dr. Mustafa Onur for his support, constructive ideas, valuable and precise advices, and extensive discussions and knowledge. Also I would like to take this opportunity to thank my previous supervisor, Professor Dr. Birol Demiral, and my field supervisor Dr. Nasir Darman for their guidance, encouragement, support, and advice. I also would like to thank Petroleum Engineering Department and Center of Excellence in EOR in Universiti Teknologi PETRONAS for awarding me with a financing support to pursue my PhD study.

I greatly acknowledge the technicians of the EOR laboratory in UTP, Mrs. Riduan, Shahrul, Saiful, and Aliman for their efforts and supports during implementation of my experiments.

Enormous thanks to my patient wife and my family who prayed for me and took care of my daughter and provided all kinds of support to me. I am especially grateful to my wife, Maryam Jam and my kid Einas Khanifar which without them, I would not have achieved to this milestone.

Finally much gratitude is extended to all my colleagues and the people that I cannot mention their names individually, who helped to eliminate facing any difficulty during my living and study in UTP and also this thesis to be completed and delivered accordantly in a timely manner.

ABSTRACT

Pressure depletion, temperature changes, and injection of CO₂ or solvents into reservoirs can induce asphaltene precipitation and deposition in porous media. The dynamic displacement efficiency of a water alternating gas (WAG) process is controlled by relative permeability. Asphaltene deposition may alter the original characteristics of the relative permeability curves. To the best of the author's knowledge, the effects of asphaltene deposition on three-phase relative permeability data have not been investigated in detail in the literature. In this study the effects of asphaltene deposition on the three-phase relative permeability using dynamic displacement experiments are investigated. A synthetic experimental approach is used to simulate the effect of in-situ asphaltene deposition on three-phase relative permeability for a water-wet system. This approach uses a chemical solvent as the precipitating agent to create in-situ asphaltene deposition. Independent coreflooding experiments are conducted on the different core-plug samples which have almost similar rock properties under reservoir conditions for both water-oil and gas-liquid systems. One dimensional two-phase black oil model is used for analyses of the experimental data. The two-phase relative permeability data are estimated using the history matching process in both water-oil and gas-oil systems. The three-phase relative permeability data for an oil-gas-water system are computed based on the Stone II model. Modeling and simulation of asphaltene phenomena during WAG process in conventional compositional simulators are also investigated. Parameters which can control the asphaltene simulation process are adjusted by matching process of the experimental absolute permeability reduction data. The weight factors of relative permeability alteration as function of asphaltene deposition are also obtained using coreflooding experimental results and non-linear multi-regression analysis. The experimental results show that as the asphaltene deposition increases the relative permeability curves are changed from water-wet to mixed-wet. The oil relative

permeability in three-phase system show different trajectories for oil iso-perm with different levels of asphaltene deposition until a certain gas saturation is achieved. For gas saturations above, all oil iso-perm trajectories merge together indicating no significant effect of asphaltene deposition. The effect of asphaltene deposition on relative permeability data is experimentally identified and investigated in this study.

ABSTRAK

Susutan tekanan, perubahan suhu, dan suntikan CO₂ atau pelarut ke dalam reserbor boleh menyebabkan pemendapan asphaltene dan pemendapan dalam media berliang. Kecekapan anjakan dinamik gas seli air (WAG) proses dikawal oleh kebolehtelapan relatif. Pemendapan Asphaltene boleh mengubah ciri-ciri asal lengkung kebolehtelapan relatif. Berdasarkan pengetahuan pengarang, kesan pemendapan asphaltene terhadap data kebolehtelapan relatif pada tiga fasa belum lagi dikaji secara terperinci dalam kesusasteraan. Dalam kajian ini, kesan pemendapan asphaltene pada kebolehtelapan relatif tiga fasa menggunakan eksperimen anjakan dinamik telah dikaji. Satu pendekatan eksperimen sintetik telah digunakan untuk menyelakui kesan pemendapan asphaltene in-situ pada tiga fasa kebolehtelapan relatif bagi sistem basah air. Kajian ini menggunakan bahan kimia pelarut sebagai ejen pemendapan untuk mewujudkan pemendapan asphaltene in-situ. Eksperimen teras membanjir (coreflooding) dijalankan ke atas sampel teras palam yang mempunyai ciri-ciri batu yang hampir sama dengan keadaan reserbor bagi kedua-dua sistem air-minyak dan gas-cecair. Satu dimensi dua fasa model minyak hitam telah digunakan untuk analisa data eksperimen. Dua-fasa data kebolehtelapan relatif telah dianggarkan menggunakan proses sejarah yang sepadan dalam kedua-dua air minyak dan sistem gas-minyak. Data kebolehtelapan relatif tiga fasa bagi sistem minyak-gas-air telah dikira berdasarkan model Stone II. Pemodelan dan penyelakui bagi fenomena asphaltene semasa proses WAG dalam penyelaku konvensional kerencaman juga dikaji. Parameter yang boleh mengawal proses penyelakui asphaltene diselaraskan dengan pemadanan proses data eksperimen pengurangan kebolehtelapan mutlak. Faktor-faktor pengubahan kebolehtelapan relatif dari segi fungsi pemendapan asphaltene juga diperolehi dengan menggunakan keputusan eksperimen teras membanjir dan analisa regresi bukan linear. Keputusan eksperimen menunjukkan bahawa pemendapan asphaltene dapat meningkatkan lengkung kebolehtelapan relatif

berubah dari basah air kepada basah bercampur. Kebolehtelapan relatif minyak dalam sistem tiga fasa menunjukkan trajektori yang berbeza untuk minyak seketelapon (iso-perm) dengan tahap pemendapan asphaltene yang berbeza sehingga ketepuan gas tertentu tercapai. Untuk ketepuan gas tersebut, semua minyak trajektori seketelapon yang bergabung menunjukkan tiada kesan pemendapan asphaltene yang ketara. Kesan pemendapan asphaltene kepada data kebolehtelapan relatif eksperimen dikenalpasti dan dikaji dalam kajian ini.

In compliance with the terms of the Copyright Act 1987 and the IP Policy of the university, the copyright of this thesis has been reassigned by the author to the legal entity of the university,

Institute of Technology PETRONAS Sdn Bhd.

Due acknowledgement shall always be made of the use of any material contained in, or derived from, this thesis.

© Ahmad Khanifar, 2012

Institute of Technology PETRONAS Sdn Bhd

All rights reserved.

TABLE OF CONTENTS

ABSTRACT.....	vii
ABSTRAK.....	ix
LIST OF FIGURES	xvii
LIST OF TABLES.....	xxv
LIST OF ABBREVIATIONS.....	xxvi
NOMENCLATURE	xxvii
CHAPTER 1 INTRODUCTION	1
1.1 Background.....	1
1.2 Problem Statement.....	3
1.3 Research Objectives.....	4
1.4 Brief Description of Chapters.....	4
1.5 Summary.....	6
CHAPTER 2 LITURATURE REVIEW.....	7
2.1 Overview.....	7
2.2 General Description of Asphaltene.....	7
2.2.1 Asphaltene Introduction	7
2.2.2 Definition of Asphaltene	8
2.2.3 Characteristics of Asphaltene.....	9
2.2.4 Resin and Asphaltene	11
2.2.5 Wax and Asphaltene.....	11
2.2.6 SARA Analysis	12
2.2.7 State of Asphaltene in Petroleum	13
2.2.8 Precipitation and Onset of Asphaltene Instability.....	15
2.2.9 Asphaltene Stability Evaluation	17
2.2.10 Flocculation and Deposition.....	18
2.2.11 Reversibility of Asphaltene Precipitation and Deposition	20
2.2.12 Formation Damage due to Asphaltene Deposition.....	20
2.3 General Description of WAG Injection.....	22
2.3.1 WAG Introduction.....	22

2.3.2 Classification of WAG Process	23
2.3.3 WAG Efficiency	24
2.3.4 Three-Phase Flow Region during WAG Process	25
2.3.5 Asphaltene Deposition during WAG Process	27
2.4 General Description of Relative Permeability	27
2.4.1 Introduction to Relative Permeability	27
2.4.2 Effect of Wettability on Relative Permeability	28
2.4.3 Experimental Measurement of Relative Permeability	32
2.4.3.1 Two-Phase Flow	32
2.4.3.2 Three-Phase Flow	35
2.4.4 Experimental Computation of Relative Permeability Values	36
2.4.4.1 Two-Phase Relative Permeability	36
2.4.4.2 Three-Phase Relative Permeability	41
2.4.5 Factors Affecting Relative Permeability	41
2.4.6 Relative Permeability Correlations	42
2.4.6.1 Two-Phase Relative Permeability Correlations	43
2.4.6.2 Three-Phase Relative Permeability Correlations	44
2.4.6.3 Stone's I Model	45
2.4.6.4 Stone's II Model	48
2.5 Summary	48
CHAPTER 3 RESEARCH METHODOLOGY	49
3.1 Overview	49
3.2 Experimental Materials and Apparatus	49
3.2.1 Core Samples Specification	49
3.2.2 Fluid Samples Specification	50
3.2.3 Experimental Apparatuses	51
3.3 Basic Experiments and Measurements	51
3.3.1 Core Samples Preparation	52
3.3.2 Gas Porosity and Absolute Permeability Measurements	52
3.3.3 Core Saturation and Liquid Porosity Measurement	54
3.3.4 Viscosity Measurement	56
3.3.5 Density Measurement	57

3.3.6 Asphaltene Content Measurement	57
3.3.7 Cores Cleaning and Drying	59
3.4 General Flowchart of Dynamic Experiments	60
3.5 Dynamic Experimental Approach	61
3.6 Dynamic Experimental Set-Up and Materials	63
3.7 Coreflooding Procedure in Water-Oil System.....	66
3.8 Coreflooding Procedure in Gas-Oil System	69
3.9 Core Flow Simulator	70
3.10 Relative Permeability Correlations.....	73
3.11 Summary.....	74
CHAPTER 4 ANALYSIS OF DATA AND DISCUSSION OF RESULTS.....	75
4.1 Overview.....	75
4.2 Experimental Results.....	76
4.2.1 Fluid Properties Measurements	76
4.2.2 Core Properties Measurements.....	78
4.2.3 Asphaltene Weight Percent	82
4.2.4 Brine Permeability and Fluid Saturation	83
4.2.4.1 Water-Oil System.....	89
4.2.4.2 Gas-Oil System	90
4.2.5 End-Point of Relative Permeability Curves	93
4.2.5.1 Water-Oil System.....	93
4.2.5.2 Gas-Oil System	96
4.2.6 Reduction in Effective Oil Permeability at Irreducible Water Saturation.....	99
4.2.7 Oil Recovery and Sweep Efficiency Performance	100
4.2.7.1 Water-Oil System.....	101
4.2.7.2 Gas-Oil System	104
4.3 Estimation of Relative Permeability Curves.....	106
4.3.1 Oil-Water Relative Permeability	106
4.3.2 Gas-Oil Relative Permeability.....	109
4.4 Three-Phase Relative Permeability.....	111
4.5 Water-Oil Relative Permeability Correlations.....	117

4.6 Summary	124
CHAPTER 5 ASPHALTENE MODELING AND SIMULATION.....	125
5.1 Overview.....	125
5.2 Asphaltene Modeling and Simulation	125
5.3 Fluid Modeling	127
5.4 Asphaltene Simulation and Control Parameters	128
5.4.1 Asphaltene Precipitation	128
5.4.2 Asphaltene Flocculation-Dissociation.....	128
5.4.3 Asphaltene Deposition	129
5.4.4 Porosity and Absolute Permeability Reduction	130
5.4.5 Viscosity Changes	131
5.4.6 Relative Permeability Alteration	132
5.5 Workflow for Asphaltene Modeling and Simulation	133
5.5.1 Synthetic Model	133
5.5.2 Fluid Modeling.....	135
5.5.3 Asphaltene Control Parameters	142
5.5.4 Relative Permeability Alteration.....	144
5.5.5 Simulation Results.....	147
5.6 Summary.....	152
CHAPTER 6 CONCLUSIONS AND RECOMENDATIONS.....	153
6.1 Overview.....	153
6.2 Conclusions	153
6.3 Recommendations for Future Work	155
6.4 Summary.....	156
REFERENCES	157
APPENDIX A EXPERIMENTS AND SIMULATION RESULTS	169
APPENDIX B PVT CELL SYSTEM AND ASPHALTNE MEASUREMENTS	202
B.1 Introduction.....	203
B.2 Sample Restoration	205
B.2.1 Restoration Methods.....	205
B.2.2 Recombination During This Study	208
B.2.3 Basic Live Crude Oil Sample Measurements.....	209

B.3 Quality Control	211
B.4 SDS System	213
B.4.1 How SDS System Work	213
B.4.2 SDS Procedure during This Study	216
B.5 HPM System	217
B.6 SOF System	221
APPENDIX C ASPHALTENE SIMULATION INPUT FILE DATA FOR ECLIPSE 300	224
APPENDIX D PAPER PUBLICATION.....	239

LIST OF FIGURES

Figure 2.1: Effect of paraffin carbon number on asphaltenes.....	10
Figure 2.2: Schematic illustration of SARA analysis	13
Figure 2.3: Simplified view of asphaltene in crude oil solution	14
Figure 2.4: Precipitation, flocculation, and deposition processes.....	19
Figure 2.5: Ideal vertical cross section of WAG process.....	26
Figure 2.6: Wettability effect, pore scale (a) water-wet, (b) oil wet.....	30
Figure 2.7: Intermediate wet systems	31
Figure 2.8: Steady-state procedure to measure relative permeability data in a water-oil system	32
Figure 2.9: Unsteady-state procedure to measure relative permeability data in a water-oil system	34
Figure 2.10: Average water saturation as function of pore volume injection.....	38
Figure 2.11: Relative pressure drop as a function of pore volume injection	39
Figure 2.12: Relative injectivity as a function of pore volume injection.....	39
Figure 3.1: Core cutter machine.....	52
Figure 3.2: Poroperm apparatus	53
Figure 3.3: Manual saturator instrument.....	55
Figure 3.4: Electromagnetic viscometer instrument	56
Figure 3.5: Digital densitometer instrument	57
Figure 3.6: Rotary evaporator instrument.....	58
Figure 3.7: Soxhlet distillation extraction instrument.....	59
Figure 3.8: General flowchart of core flooding experiments, water-oil system	62
Figure 3.9: General flowchart of core flooding experiments, gas-oil system.....	63
Figure 3.10: Schematic of experimental set-up used for displacement experiments...	64
Figure 3.11: Schematic of three-phase separator in coreflooding system	66
Figure 3.12: Main functionalities of main window of Sendra at start up	71
Figure 3.13: Plot window with several plots after matching process	72
Figure 4.1: Calculated brine viscosity versus different temperatures.....	76
Figure 4.2: Crude oil viscosity versus different temperature.....	77

Figure 4.3: Nitrogen viscosity vs. pressure at different temperatures	78
Figure 4.4: Amount of asphaltene deposition at various ratios of n-heptane crude oil injections.....	83
Figure 4.5: Oil injection pressure during simultaneously n-heptane and oil injection (50%, water-oil system)	86
Figure 4.6: Pressure drop during gas injection (50%, gas-oil system)	91
Figure 4.7: Irreducible water and initial oil saturation at various ratios of n-heptane–crude oil injections (water-oil system).....	94
Figure 4.8: Residual oil and final water saturation at various ratios of n-heptane–crude oil injections (water-oil system).....	95
Figure 4.9: Effective water and oil permeability at various ratios of n-heptane–crude oil injections (water-oil system).....	95
Figure 4.10: Irreducible water and initial oil saturation at various ratios of n-heptane–crude oil injections (gas-oil system)	96
Figure 4.11: Residual liquid and final gas saturation at various ratios of n-heptane–crude oil injections (gas-oil system)	97
Figure 4.12: Effective gas and oil permeability at various ratios of n-heptane–crude oil injections (gas-oil system)	97
Figure 4.13: Ratio of effective oil permeability at irreducible water saturation at various ratios of n-heptane–crude oil injections (water-oil system).....	99
Figure 4.14: Ratio of effective oil permeability at irreducible water saturation at various ratios of n-heptane–crude oil injections (gas-oil system)	100
Figure 4.15: Cumulative oil production versus cumulative water injection at various ratios of n-heptane–crude oil injections (water-oil system).....	103
Figure 4.16: Oil recovery factor for first pore volume injection at various n-heptane–crude oil ratios injections (water-oil system).....	103
Figure 4.17: Ultimate oil recovery factor at various n-heptane–crude oil ratios injections (water-oil system).....	104
Figure 4.18: Cumulative oil production versus cumulative gas injection at various ratios of n-heptane–crude oil injections (gas-oil system)	105
Figure 4.19: Ultimate oil recovery factor at various n-heptane–crude oil ratios injections (gas-oil system)	105

Figure 4.20: Pressure drop history match of 20% case, Corey (water-oil system)....	107
Figure 4.21: Oil production history match of 20% case, Corey (water-oil system) ..	108
Figure 4.22: Water production history match of 20% case, Corey (water-oil).....	108
Figure 4.23: Effect of asphaltene on relative permeability at various n-heptane–crude oil ratios injections, Corey correlation (water-oil system).....	109
Figure 4.24: Oil production history match of 20% case, Corey (gas-oil system).....	110
Figure 4.25: Effect of asphaltene on relative permeability at various n-heptane–crude oil ratios injections, Corey (gas-oil system)	111
Figure 4.26: Oil relative permeability at zero % ratio of n-heptane–crude oil injection	113
Figure 4.27: Oil relative permeability at 20 % ratio of n-heptane–crude oil injection	113
Figure 4.28: Oil relative permeability at 50 % ratio of n-heptane–crude oil injection	114
Figure 4.29: Oil relative permeability at 80 % ratio of n-heptane–crude oil injection	114
Figure 4.30: Comparison of oil relative permeability 0.1 for all cases.....	115
Figure 4.31: Comparison of oil relative permeability 0.2 for all cases.....	115
Figure 4.32: Comparison of oil relative permeability 0.3 for all cases.....	116
Figure 4.33: Comparison of fluid saturation distribution for oil relative permeability equal to zero for all cases.....	116
Figure 4.34: Behavior of oil relative permeability, Corey-parameter	118
Figure 4.35: Behavior of oil relative permeability, LET correlation.....	119
Figure 4.36: Oil-water relative permeability matching between Corey Correlation and this study correlation (zero % ratio of n-heptane–crude oil injection)	122
Figure 4.37: Oil-water relative permeability matching between Corey Correlation and this study correlation (20 % ratio of n-heptane–crude oil injection)	123
Figure 4.38: Oil-water relative permeability matching between Corey Correlation and this study correlation (50 % ratio of n-heptane–crude oil injection)	123
Figure 4.39: Oil-water relative permeability matching between Corey Correlation and this study correlation (80 % ratio of n-heptane–crude oil injection)	124
Figure 5.1: Asphaltene modeling and simulation processes.....	126

Figure 5.2: Synthetic model.....	134
Figure 5.3: Initial asphaltene precipitation curve	139
Figure 5.4: Asphaltene precipitation curve after adjusting related parameters	141
Figure 5.5: Asphaltene precipitation curve for saturation pressure 2500 psi	142
Figure 5.6: Asphaltene precipitation curve for saturation pressure 2050 psi	142
Figure 5.7: Absolute permeability reduction matching between experiments and simulation.....	143
Figure 5.8: Injection pattern during this study simulation.....	147
Figure 5.9: Field oil efficiency factors, asphaltene and without asphaltene cases	148
Figure 5.10: Field average pressure, asphaltene and without asphaltene cases.....	149
Figure 5.11: Field oil production rate, asphaltene and without asphaltene cases	150
Figure 5.12: Well gas oil ratio (GOR) for production well	150
Figure 5.13: Well bottomhole pressure for water injection well	151
Figure 5.14: Well bottomhole pressure for gas injection well.....	152
Figure A.1: Pressure drop across core sample during water injection (zero % ratio of n-heptane–crude oil injection, water-oil system).....	170
Figure A.2: Pressure drop across core sample during water injection (20 % ratio of n- heptane–crude oil injection, water-oil system)	171
Figure A.3: Pressure drop across core sample during water injection (50 % ratio of n- heptane–crude oil injection, water-oil system)	171
Figure A.4: Pressure drop across core sample during water injection (80 % ratio of n- heptane–crude oil injection, water-oil system)	172
Figure A.5: Water production from core sample during water injection (zero % ratio of n-heptane–crude oil injection, water-oil system)	172
Figure A.6: Water production from core sample during water injection (20 % ratio of n-heptane–crude oil injection, water-oil system).....	173
Figure A.7: Water production from core sample during water injection (50 % ratio of n-heptane–crude oil injection, water-oil system).....	173
Figure A.8: Water production from core sample during water injection (80 % ratio of n-heptane–crude oil injection, water-oil system).....	174
Figure A.9: Oil production from core sample during water injection (zero % ratio of n-heptane–crude oil injection, water-oil system).....	174

Figure A.10: Oil production from core sample during water injection (20 % ratio of n-heptane–crude oil injection, water-oil system)	175
Figure A.11: Oil production from core sample during water injection (50 % ratio of n-heptane–crude oil injection, water-oil system)	175
Figure A.12: Oil production from core sample during water injection (80 % ratio of n-heptane–crude oil injection, water-oil system)	176
Figure A.13: Pressure drop history matching for zero % ratio of n-heptane–crude oil injection (Corey correlation, water-oil system)	176
Figure A.14: Pressure drop history matching for 20 % ratio of n-heptane–crude oil injection (Corey correlation, water-oil system)	177
Figure A.15: Pressure drop history matching for 50 % ratio of n-heptane–crude oil injection (Corey correlation, water-oil system)	177
Figure A.16: Pressure drop history matching for 80 % ratio of n-heptane–crude oil injection (Corey correlation, water-oil system)	178
Figure A.17: Water production history matching for zero % ratio of n-heptane–crude oil injection (Corey correlation, water-oil system)	178
Figure A.18: Water production history matching for 20 % ratio of n-heptane–crude oil injection (Corey correlation, water-oil system)	179
Figure A.19: Water production history matching for 50 % ratio of n-heptane–crude oil injection (Corey correlation, water-oil system)	179
Figure A.20: Water production history matching for 80 % ratio of n-heptane–crude oil injection (Corey correlation, water-oil system)	180
Figure A.21: Oil production history matching for zero % ratio of n-heptane–crude oil injection (Corey correlation, water-oil system)	180
Figure A.22: Oil production history matching for 20 % ratio of n-heptane–crude oil injection (Corey correlation, water-oil system)	181
Figure A.23: Oil production history matching for 50 % ratio of n-heptane–crude oil injection (Corey correlation, water-oil system)	181
Figure A.24: Oil production history matching for 80 % ratio of n-heptane–crude oil injection (Corey correlation, water-oil system)	182
Figure A.25: Oil-water relative permeability for zero % ratio of n-heptane–crude oil injection, (Corey correlation, water-oil system)	182

Figure A.26: Oil-water relative permeability for 20 % ratio of n-heptane–crude oil injection, (Corey correlation, water-oil system)	183
Figure A.27: Oil-water relative permeability for 50 % ratio of n-heptane–crude oil injection, (Corey correlation, water-oil system)	183
Figure A.28: Oil-water relative permeability for 80 % ratio of n-heptane–crude oil injection, (Corey correlation, water-oil system)	184
Figure A.29: Pressure drop history matching for zero % ratio of n-heptane–crude oil injection (LET correlation, water-oil system).....	184
Figure A.30: Pressure drop history matching for 20 % ratio of n-heptane–crude oil injection (LET correlation, water-oil system).....	185
Figure A.31: Pressure drop history matching for 50 % ratio of n-heptane–crude oil injection (LET correlation, water-oil system).....	185
Figure A.32: Pressure drop history matching for 80 % ratio of n-heptane–crude oil injection (LET correlation, water-oil system).....	186
Figure A.33: Water production history matching for zero % ratio of n-heptane–crude oil injection (LET correlation, water-oil system)	186
Figure A.34: Water production history matching for 20 % ratio of n-heptane–crude oil injection (LET correlation, water-oil system).....	187
Figure A.35: Water production history matching for 50 % ratio of n-heptane–crude oil injection (LET correlation, water-oil system).....	187
Figure A.36: Water production history matching for 80 % ratio of n-heptane–crude oil injection (LET correlation, water-oil system).....	188
Figure A.37: Oil production history matching for zero % ratio of n-heptane–crude oil injection (LET correlation, water-oil system).....	188
Figure A.38: Oil production history matching for 20 % ratio of n-heptane–crude oil injection (LET correlation, water-oil system).....	189
Figure A.39: Oil production history matching for 50 % ratio of n-heptane–crude oil injection (LET correlation, water-oil system).....	189
Figure A.40: Oil production history matching for 80 % ratio of n-heptane–crude oil injection (LET correlation, water-oil system).....	190
Figure A.41: Oil-water relative permeability for zero % ratio of n-heptane–crude oil injection, (LET correlation, water-oil system).....	190

Figure A.42: Oil-water relative permeability for 20 % ratio of n-heptane–crude oil injection, (LET correlation, water-oil system).....	191
Figure A.43: Oil-water relative permeability for 50 % ratio of n-heptane–crude oil injection, (LET correlation, water-oil system).....	191
Figure A.44: Oil-water relative permeability for 80 % ratio of n-heptane–crude oil injection, (LET correlation, water-oil system).....	192
Figure A.45: Effect of asphaltene on relative permeability at various n-heptane–crude oil ratios injections, (LET correlation, water-oil system).....	192
Figure A.46: Pressure drop across core sample during gas injection (zero % ratio of n-heptane–crude oil injection, gas-oil system).....	193
Figure A.47: Pressure drop across core sample during water injection (20 % ratio of n-heptane–crude oil injection, gas-oil system)	193
Figure A.48: Pressure drop across core sample during water injection (50 % ratio of n-heptane–crude oil injection, gas-oil system)	194
Figure A.49: Oil production from core sample during gas injection (zero % ratio of n-heptane–crude oil injection, gas-oil system).....	194
Figure A.50: Oil production from core sample during gas injection (20 % ratio of n-heptane–crude oil injection, gas-oil system).....	195
Figure A.51: Oil production from core sample during gas injection (50 % ratio of n-heptane–crude oil injection, gas-oil system).....	195
Figure A.52: Oil production history matching for zero % ratio of n-heptane–crude oil injection (Corey correlation, gas-oil system).....	196
Figure A.53: Oil production history matching for 20 % ratio of n-heptane–crude oil injection (Corey correlation, gas-oil system).....	196
Figure A.54: Oil production history matching for 50 % ratio of n-heptane–crude oil injection (Corey correlation, gas-oil system).....	197
Figure A.55: Comparison of oil relative permeability equal to 0.4 for all cases.....	197
Figure A.56: Comparison of oil relative permeability equal to 0.5 for all cases.....	198
Figure A.57: Comparison of oil relative permeability equal to 0.6 for all cases.....	198
Figure A.58: Comparison of oil relative permeability equal to 0.7 for all cases.....	199
Figure A.59: Comparison of oil relative permeability equal to 0.8 for all cases.....	199

Figure A.60: Fluid saturation distribution for oil relative permeability for zero % ratio of n-heptane–crude oil injection	200
Figure A.61: Fluid saturation distribution for oil relative permeability for 20 % ratio of n-heptane–crude oil injection	200
Figure A.62: Fluid saturation distribution for oil relative permeability for 50 % ratio of n-heptane–crude oil injection	201
Figure A.63: Fluid saturation distribution for oil relative permeability for 80 % ratio of n-heptane–crude oil injection	201
Figure B.1: Fluid evaluation system or PVT cell system	203
Figure B.2: Restoration processes of separator and bottom-hole samples	206
Figure B.3: RCA 1000 instrument, recombination cell	207
Figure B.4: Schematic of recombination instruments.....	207
Figure B.5: Schematic of transferring separator samples into PVT cell.....	208
Figure B.6: Schematic of transferring bottom-hole samples into PVT cell.....	208
Figure B.7: Main window during CME experiment in PVT system	210
Figure B.8: Total PVT Cell volume versus pressure	211
Figure B.9: Pre-filtration flow diagram before loading	212
Figure B.10: Pre-filtration flow diagram after loading	212
Figure B.11: Solid detection system (SDS)	213
Figure B.12: Principle of light scattering technique	213
Figure B.13: Density and light transmittance versus pressure without asphaltene....	215
Figure B.14: Density and light transmittance versus pressure with asphaltene.....	215
Figure B.15: Transmitted power as function of pressure.....	216
Figure B.16: Schematic of the HPM system.....	218
Figure B.17: Main window of the particle size analysis.....	219
Figure B.18: Example of main output graphs from HPM system	220
Figure B.19: Effect of inhibitor on asphaltene precipitation	221
Figure B.20: Schematic of SOF system inside the PVT cell system	223
Figure B.21: Asphaltene phase behavior envelope.....	223

LIST OF TABLES

Table 3.1: Properties of crude oil sample	50
Table 4.1: General properties of crude oil sample	77
Table 4.2: Basic core properties from Poroperm instrument	81
Table 4.3: Basic core properties from saturation method	81
Table 4.4: Equivalent values of asphaltene deposition inside core samples	82
Table 4.5: Brine absolute permeability of core samples (water-oil system)	85
Table 4.6: Brine absolute permeability of core samples (gas-oil system)	85
Table 4.7: Effective and relative oil permeability (water-oil system)	87
Table 4.8: Effective and relative oil permeability (gas-oil system)	87
Table 4.9: Initial oil saturation and irreducible water saturation (water-oil system) ...	88
Table 4.10: Initial oil saturation and irreducible water saturation (gas-oil system)	88
Table 4.11: Effective and relative water permeability (water-oil system)	89
Table 4.12: Residual oil saturation and final water saturation (water-oil system)	90
Table 4.13: Effective and relative gas permeability (gas-oil system)	91
Table 4.14: Residual liquid saturation and final gas saturation (gas-oil system)	92
Table 4.15: Effective and relative gas permeability, Standing (gas-oil system)	98
Table 4.16: Average amount of asphaltene deposition during coreflooding experiment	120
Table 5.1: Experimental fluid properties	134
Table 5.2: Experimental asphaltene precipitation at 212 °F	135
Table 5.3: Splitting heaviest component to obtain asphaltene mole percent	137
Table 5.4: Adjusted asphaltene control parameters	144
Table 5.5: Weight factor as function of asphaltene deposition	146
Table B.1: General description of PVT cell system	204
Table B.2: Crude oil composition (dead and live oils)	209
Table B.3: Description of HPM system	217
Table B.4: Description of SOF system	222

LIST OF ABBREVIATIONS

AOP	Asphaltene precipitation onset pressure
API	American petroleum institute
BHP	Bottomhole pressure
BV	Bulk volume
CII	Colloidal instability index
CME	Constant mass expansion experiment
CMG	Computer modeling group
DV	Differential vaporization
EOR	Enhanced oil recovery
EOS	Equation of state
GOR	Gas-oil ratio
GV	Grain volume
HPM	High pressure microscope
JBN	Johnson, Bossler, and Naumann
LET	Lomeland, Ebeltoft, and Thomas
MSCF	Thousand standard cubic feet per day
NIR	Near infrared
OAD	Asphaltene deposition onset pressure
PSA	Particle size analysis
PV	Pore volume
PVT	Pressure, volume, and temperature
RCA	Recombination apparatus
RTD	Resistance temperature detector
SARA	Saturated aromatic resin asphaltene
SCCM	Standard cubic centimeter
SDS	Solid detection system
SOF	Solid organic filter
STB	Stock tank barrel
WAG	Water alternating gas

NOMENCLATURE

Symbol	Description, Unit, (Equation No.)
a	Constant, dimensionless, (5.6)
A	Area of the core sample, cm^2 , (4.5)
A	Constant, dimensionless, (2.10)
A_1, A_2, A_3	Constants, dimensionless, (4.19)
B	Constant, dimensionless, (2.11)
B_1, B_2, B_3	Constants, dimensionless, (4.20)
BV	Bulk volume of the core plug sample, cc
C_a	Volumetric concentration of fines in oil phase, (5.1)
C_i	Volumetric concentration of flocs in oil phase, (5.1)
C_p	Volume concentration of precipitate, (5.7)
C_{p0}	Volumetric concentration for maximum packing, (5.7)
C_1, C_2, C_3, C_4	Constants, dimensionless, (4.21)
d	Dimension, dimensionless, (5.2)
D	Core plug diameter, cm
D_1, D_2, D_3, D_4	Constants, (4.22)
E_o	Constant exponents-LET, (4.18)
E_w	Constant exponents-LET, (4.17)
F	Weight factor, dimensionless
F_{oi}	Oil Darcy flux, $\text{cc}/\text{min} \cdot \text{cm}^2$, (5.2)
f_s	Solid fugacity, (5.14)
f_s^*	Reference (asphaltene) fugacity, (5.14)
f_{o2}	Fraction of oil in the outlet stream, dimensionless
f_{w2}	Fraction of water in the outlet stream, dimensionless
GV	Grain volume, cc
I_R	Relative injectivity, 1/pore volume, (2.7)
k	Liquid permeability, md, (4.5)

$k_{eo}(S_{wi})$	Effective oil permeability at irreducible water saturation, %
$k_{ew}(S_{or})$	Effective brine permeability at residual oil saturation, md
$k_{eg}(S_{lr})$	Effective gas permeability at residual liquid saturation, md
k_{e-nwt}	Effective non-wetting phase permeability, md, (4.12)
k_o	Initial permeability, md, (5.5)
k_{ro}	Oil relative permeability, %
k_{rg}	Gas relative permeability, %
k_{rw}	Water relative permeability, %
k_{row}	Oil Relative permeability in water-oil system, %
k_{rog}	Oil Relative permeability in gas-oil system, %
$(k_{ro})_{S_{wc}}$	Oil relative permeability at connate water saturation, %
k_{rwo}	Water relative permeability in oil-wet system, fraction, (5.10)
k_{rwa}	Water relative permeability affected by asphaltene deposition
k_{rwo}	Water relative permeability in oil-wet system, fraction, (5.10)
k_{roa}	Oil relative permeability affected by asphaltene deposition
k_{roo}	Oil relative permeability in oil wet-system, fraction, (5.11)
k_{rww}	Water relative permeability in water-wet system, fraction, (5.10)
k_{row}	Oil relative permeability in water-wet system, fraction, (5.11)
$k_{ro}(S_{wi})$	Relative oil permeability at irreducible water saturation, %
$k_{ro}(S_w^*)$	Relative oil permeability at normalize water saturation, %
$k_{rw}(S_{or})$	Relative brine permeability at residual oil saturation, md
$k_{rw}(S_w^*)$	Relative brine permeability at normalize water saturation, md
$k_{rg}(S_{lr})$	Relative gas permeability at residual liquid saturation, md
k_{rw}^0	Effective water permeability at S_{or} , md, (4.15)
k_{ro}^0	Effective oil permeability at S_{wi} , md, (4.16)
L	Length of the core sample, cm

L_o	Constant exponents-LET, (4.18)
L_w	Constant exponents-LET, (4.17)
m	Constant, dimensionless, (2.11)
$MW_{Asphaltene}$	Molecular weight of asphaltene, kg/kmol (5.12)
MW_i	Molecular weight of oil components, kg/kmol (5.13)
\overline{MW}_{Oil}	Average molecular weight of oil, kg/kmol (5.12)
n	Constant, dimensionless, (2.10, 2.27)
N_o	Exponent on oil relative permeability-Corey, (4.16)
N_P	Cumulative oil production, cc
N_w	Exponent on water relative permeability-Corey, (4.15)
P	Pressure, psi, (5.14)
P_0	Reference conditions for pressure, psi, (5.14)
P_{sat}	Saturation pressure, psi
PV	Pore volume, cc
q_o	Oil flow rate, cc/sec
q_w	Water flow rate, cc/sec
Q	Liquid (brine) flow rate, cc/sec, (4.5)
Q_i	Cumulative water injected, pore volumes
R	Gas constant, $\text{ft}^3 \text{ psi R}^{-1} \text{ lb-mol}^{-1}$, (5.14)
R_a	Aggregations rate of fines, (5.1)
r_{ai}	Dissociation rate coefficient of flocs, day^{-1} , (5.1)
r_{ia}	Flocculation rate coefficient of fines, day^{-1} , (5.1)
S_g	Gas saturation, %
S_{gc}	Critical gas saturation, %
S_{gf}	Final gas saturation, fraction
S_{lr}	Residual liquid saturation, fraction
S_{nw}	Non-wetting phase saturation, %
S_o	Oil saturation, %
S_{oi}	Initial oil saturation, fraction

S_{om}	Minimum oil saturation, fraction
S_{ora}	Residual oil saturation affected by asphaltene deposition
S_{org}	Residual oil saturation in gas-oil, fraction
S_{oro}	Residual oil saturation in oil-wet system, fraction, (5.8)
S_{orw}	Residual oil saturation in water-wet system, fraction, (5.8)
S_{orw}	Residual oil saturation in water-oil system, fraction
S_{or}	Residual oil saturation, fraction
S_w	Water saturation, %
$S_{w,av}$	Average water saturation, %
S_{wc}	Critical wetting saturation, fraction
S_{wf}	Final brine saturation, fraction
S_{wi}	Irreducible water saturation, fraction
S_{wia}	Irreducible water saturation affected by asphaltene deposition
S_{wio}	Irreducible water saturation in oil-wet system, fraction, (5.9)
S_{wiw}	Irreducible water saturation in water-wet, fraction, (5.9)
S_{w2}	Water saturation in the outlet stream, fraction
S_g^*	Effective gas saturation, fraction
S_o^*	Effective oil saturation, fraction
S_w^*	Effective wetting saturation, fraction
S_{wtr}	Residual wetting phase saturation, fraction, (5.12)
t	Time, day
T_0	Reference conditions for temperature, °R, (5.14)
T_0	Reference conditions for temperature, °R, (5.14)
T_o	Constant exponents-LET, (4.18)
T_w	Constant exponents-LET, (4.17)
U_{cr}	User input critical velocity, ft/day, (5.2)
U_{oi}	Oil phase velocity ($F_{oi} / A\phi$), ft/day, (5.2)

v_s	Molar volume of the solid, L/mol, (5.14)
V_{oil-g}	Recovered oil during gas injection, cc
V_{oil-w}	Recovered oil during waterflooding, cc
V_p	Core pore volume, cc
V_{water}	Recovered water during oil flooding, cc
$w_{Asphaltene}$	Weight percent of asphaltene in oil, wt%, (5.12)
W_{Dry}	Weight of dry core, g
W_{Sat}	Weight of wet or saturated core, g
$x_{Asphaltene}$	Mole fraction of asphaltene, fraction, (5.12)
x_i	Mole fraction of oil components, fraction, (5.13)
Greek	
α	Mass of asphaltene deposition to pore volume, g/cc
α	Adsorption or static deposition coefficient, day ⁻¹ , (5.2)
α	Weight parameter, dimensionless, (2.25)
α^*	Volume of asphaltene deposition to bulk volume, vol/vol
β	Entrainment coefficient, m ⁻¹ , (5.2)
β	Weight parameter, dimensionless, (2.28)
β_g	Weight parameter, dimensionless, (2.21)
β_w	Weight parameter, dimensionless, (2.21)
γ	Plugging coefficient, m ⁻¹ , (5.2)
δ	User constant parameter, dimensionless, (5.5)
ΔP	Differential pressure across the core sample, psi, (4.5)
ΔP_i	Initial differential pressure, psi, (2.7)
ΔP_p	Current differential pressure, psi, (2.7)
ε	Cumulative volume of asphaltene deposition, cc, (5.3)
ε_i	Volume of deposition in i direction of flow, fraction, (5.2)
η	Intrinsic viscosity, dimensionless, (5.7)

μ	Viscosity of the flowing liquid (brine), cp, (4.5)
μ_o	Oil viscosity, cp
μ_o	Initial viscosity of oil, cp, (5.6)
μ_w	Water viscosity, cp
ρ_{Brine}	Brine density at room temperature, g/cc
ϕ	Porosity, fraction
ϕ_0	Initial porosity, fraction, (5.4)

CHAPTER 1

INTRODUCTION

1.1 Background

Asphaltene precipitation and deposition are the severe problems which some oil reservoirs may face during their production life. Asphaltene precipitation and deposition may occur during natural depletion, displacement of reservoir oil by CO₂ or hydrocarbon gas or during WAG application. There are a number of studies in the literature that have addressed asphaltene problems during primary recovery or CO₂ injection as a secondary recovery stage (Kokal and Sayegh, 1995; Nghiem and Coombe, 1997; Kabir and Jamaluddin, 1999; Srivastava *et al.*, 1999; Negahban *et al.*, 2003; Takahashi *et al.*, 2003; Jamshidnezhad, 2005; Wang and Civan, 2005; Oskui *et al.*, 2009; Yi *et al.*, 2009). Despite all researches and studies conducted in the past the definition of asphaltene itself is yet not very well understood and it has been defined based on its solution properties. Asphaltene is arbitrarily defined as a soluble class of petroleum that is insoluble in light alkanes such as n-heptane or n-pentane but soluble in toluene or dichloromethane (Mullins *et al.*, 2007).

Evaluation of the asphaltene stability is the first step toward predicting and avoiding any of asphaltene issues at reservoir conditions. The asphaltene equilibrium conditions can be disrupted due to pressure depletion, change in temperature, change in crude oil composition, addition of miscible gases and liquids to the oil as applied in various EOR techniques (Jamaluddin *et al.*, 2002). The effect of composition and pressure change on asphaltene precipitation is generally believed to be higher than the temperature (Mullins *et al.*, 2007). The onset point of asphaltene is the point at which asphaltene loses its stability from thermodynamic equilibrium in solution and forms a separate and visible phase that it starts the point of precipitation step (Khanifar *et al.*,

2011). During this step, asphaltenes that have tendency to aggregate by their nature may reach to the flocculation and then, deposition steps. Indeed, after asphaltene precipitates from the oil, they may flocculate to form much larger size molecules however, they are still suspended in the solution. The flocculated asphaltenes which can be suspended with oil flow may be deposited on the rock surface because they become so large in size and cannot be carried by the liquid (Sanchez, 2007). Therefore, asphaltene deposition means the settling of the asphaltenes flocculated particles onto the rock surfaces. The flocculated asphaltenes can be adsorbed onto the rock surface by adsorption or may be trapped within the porous media because of their size, thereby blocking the pore throats of the formation by plugging. Moreover, the deposited flocculated asphaltenes can be flushed away by oil due to shearing effect if the local oil velocity is high by entrainment (Yi *et al.*, 2009).

Enhanced oil recovery (EOR) processes can modify flow and phase behavior of reservoir fluids and rock properties. These modifications could lead to asphaltene precipitation and deposition and causing formation damage problems (Minssieux, 1997; Kalantari *et al.*, 2008). Asphaltene deposited particles by impairing the permeability by plugging the pore throat and altering wettability by adsorbing on the rock surface may lead to formation damage (Kokal and Sayegh, 1995). Deposition of solid asphaltenes causes porosity and absolute permeability reduction. This can also result in alteration of rock wettability from water-wet to mixed or oil-wet and plugging of the wellbore and piping in production facilities (Kalantari *et al.*, 2008; Alizadeh *et al.*, 2009). Asphaltene deposition may induce significant changes in relative permeability, end-point saturations and hence, it can affect the displacement efficiency (Al-Maamari and Buckley, 2000). The main mechanisms behind this alteration are still a research topic. However, it has been reported that some of its effects can be captured by wettability change and relative permeability shift from a water-wet to a mixed or oil-wet system.

1.2 Problem Statement

A screening study on Malaysian oil fields has been conducted in 2001 and it has been identified that more oil can be produced through some EOR technologies (Kechut, 2001). The main processes studied in this screening project were chemical, gas flooding and microbial enhanced oil recovery processes that were considered having the most practical aspects in Malaysian oil fields. Thermal was excluded in the study as it was concluded to be impractical in the offshore environment. The hydrocarbon and CO₂ gas flooding in miscible or immiscible modes were found to be the most favorable processes although the applications for miscible processes are limited due to depleted reservoir pressures.

Furthermore, based on some further studies for the way forward, most of the proposed gas flooding should be implemented together with water injection in water alternating gas (WAG) scheme to get higher sweep efficiency, mobility control and optimizing operating cost (Nadeson *et al.*, 2001; Zain *et al.*, 2001; Nadeson *et al.*, 2004; Hamdan *et al.*, 2005; Samsudin *et al.*, 2005; Friedel *et al.*, 2006).

Consequently, the WAG method has been recommended for EOR implementation in Malaysian oil fields. One aspect that should be considered during any WAG process is the asphaltene precipitation and deposition and its effect on recovery performance (Negahban *et al.*, 2003). The dynamic displacement efficiency of WAG process is controlled by three-phase relative permeability data and therefore, asphaltene deposition may alter the original characteristics of the relative permeability curves. Therefore, the effect of asphaltene deposition on three-phase relative permeability data need to be investigated.

In addition, correlations that can be used to compute the relative permeability alteration and end-point saturations as function of asphaltene deposition are not available. Moreover, mechanism of asphaltene modeling and simulation using conventional simulators remain dubious. Therefore, in this study the effect of asphaltene deposition on two-phase and three-phase relative permeability data are investigated using experiments approach. Some correlations to compute the relative permeability alteration as function of asphaltene deposition are proposed. In addition,

a workflow which determines the mechanism of incorporating the coreflooding experimental results into asphaltene modeling and simulation is also presented.

1.3 Research Objectives

This study has three main objectives as follows:

- To investigate the effects of asphaltene deposition on relative permeability during water alternating gas (WAG) process using an experimental approach.
- To develop correlations that can predict relative permeability alteration in the presence of asphaltene deposition for two- and three-phase flow.
- To accomplish a workflow for asphaltene modeling and simulation which determines the mechanism of incorporating the coreflooding experimental results and the asphaltene deposition effects on relative permeability data during WAG process into a conventional compositional simulator.

1.4 Brief Description of Chapters

The thesis contains six chapters as follows:

Chapter 1 is an introduction to the entire research and consists of a brief explanation of the research background, the problem statement, the research objectives, and a brief description of the chapters.

Chapter 2 reviews the literature of topics relevant to this study. This review covers the literature related to description of WAG application, explanation of relative permeability, and description of asphaltene and related issues.

Chapter 3 presents the theory and methodologies which have been adopted in this work toward achieving the aim of this research. This chapter covers detailed description for the experimental methodology, the setup, the material and apparatus, the coreflooding experiments, and the special core analysis method.

Chapter 4 presents the experimental data which have been obtained during the basic core and fluid analysis and coreflooding experiments in both water-oil and gas-oil systems. Then, the detailed analysis and discussions for experimental observation data are provided. Two-phase relative permeability in water-oil system and gas-oil system are estimated based on history matching of experimental data (pressure drop and fluids production data) by using a one dimensional two-phase black oil model. Furthermore, three-phase relative permeability data are computed based on the Stone's II model. The effects of asphaltene deposition on two-phase and three-phase relative permeability are investigated. In addition, this chapter presents the some developed correlations which are obtained from experimental results. These correlations can compute the relative permeability alteration and end-point saturations as function of asphaltene deposition.

Chapter 5 presents a detailed workflow to model and simulate the asphaltene precipitation and deposition by a conventional compositional simulator. A synthetic model in compositional format is built and a fluid model based on live oil fluid properties and asphaltene experimental data is provided. The asphaltene control parameters are adjusted based on the experimental coreflooding data. The required weight factors for relative permeability alteration as function of asphaltene deposition are also obtained based on dynamic displacement experiments results and non-linear multi-regression analysis. The simulation results for this model for two different cases, with asphaltene and without asphaltene options, and during WAG process are presented.

Chapter 6 summarizes the conclusions of the research along with recommendations for future work directions.

Four appendices (A, B, C, and D) are attached at the end of this report. In Appendix A, the observation experimental results are presented. The pressure drop, the oil production, and the water production for all core flooding experiments in water-oil and gas-oil systems are given. Also history-matching of these experimental data with simulation results and predicted relative permeability curves for these experiments are presented. The oil relative permeability data in three-phase system and comparison of different oil iso-perm due to asphaltene deposition are given. Appendix B focuses on

PVT cell system and asphaltene measurements facilities. In this appendix crude oil sample restoration methods, recombination cell method, and PVT system including asphaltene facilities are explained. The efforts to prepare the recombine oil sample and asphaltene onset point measurement are also reported. Appendix C presents a simulation input file data for asphaltene modeling in Eclipse 300 format. In appendix D list of the publications resulted from this study are given.

1.5 Summary

This chapter is an introduction to the entire research. At the beginning, a brief explanation of the research background is given. The motivation to conduct this research problem has been described in the problem statement. The research objectives and brief description of chapters and appendices are outlined at the end of the chapter.

CHAPTER 2

LITURATURE REVIEW

2.1 Overview

This chapter is in compliance with the research topic of this study to review the literatures of three related topics to this research study; asphaltene precipitation and deposition, water alternating gas (WAG) process, and relative permeability.

2.2 General Description of Asphaltene

In this section, a general description of asphaltene is given. The definition, characteristics and state of asphaltene in petroleum followed by precipitation, flocculation, deposition, and onset of asphaltene are all described. Moreover, reversibility and formation damage due to asphaltene are also explained.

2.2.1 Asphaltene Introduction

Heavy organic components such as asphaltenes, resins, and waxes exist in crude oils in various quantities and forms (Ma, 2006; Chen, 2007; Mansoori, 2010). Such compounds could separate out of the crude oil solution due to various mechanisms and deposit (Mansoori, 2010). The reasons for the asphaltenes deposition can be many factors including variations of temperature, pressure, pH, composition, flow regime, wall effect and electro kinetic phenomena (Kamath *et al.*, 1993; Mansoori, 2010). There are many papers that have addressed asphaltene problems during primary recovery or CO₂ injection as secondary recovery stage (Hirschberg *et al.*, 1984; Leontaritis, 1989; Burke *et al.*, 1990; Kokal and Sayegh, 1995; Nghiem and Coombe,

1997; Kabir and Jamaluddin, 1999; Srivastava *et al.*, 1999; Akervoll *et al.*, 2000; Negahban *et al.*, 2003; Takahashi *et al.*, 2003; Jamshidnezhad, 2005; Wang and Civan, 2005; Oskui *et al.*, 2009; Yi *et al.*, 2009).

Formation damage due to asphaltene deposition in the oil industry is an issue for many fields that causes reduction in production and shutting of some of the wells and a severe detrimental effect on the economics of oil recovery (Cenegy, 2001; Sanada and Miyagawa, 2006; Misra *et al.*, 2011; Abdallah, 2012). Once the asphaltene deposition occurs, it may cause severe permeability and porosity reduction and wettability alteration, changing relative permeability in the reservoir and, in the severe cases plugging the wellbore and surface facilities (Kamath *et al.*, 1993; Minssieux, 1997; Al-Maamari and Buckley, 2000; Shedid, 2001; Wang and Civan, 2001; Kocabas, 2003; Nabzar *et al.*, 2005; Okwen, 2006; Kalantari *et al.*, 2008; Alizadeh *et al.*, 2009; Zarrin Nasri 2009; Rezaian *et al.*, 2010). It is clear that the approach taken by most operators is a remedial solution rather than preventive. The remedial measures such as chemical treatment and workover operations are disruptive and expensive (Kokal and Sayegh, 1995). Thus, the probability asphaltene precipitation and deposition occurring during any EOR techniques, its effects on reservoir performance, and preventive measures should be anticipated at earliest stages of each project. This anticipation can be reached through better understanding of the mechanisms up front that initiate such problems (Oskui *et al.*, 2009).

2.2.2 Definition of Asphaltene

The nature and behavior of asphaltenes in crude oils are known complicated (Nghiem *et al.*, 1993). Hence, asphaltene has been defined based on its solution properties (Kokal and Sayegh, 1995). Asphaltenes are arbitrarily defined as a solubility class of petroleum that is insoluble in light alkanes such as n-heptane or n-pentane but soluble in toluene or dichloromethane (Shedid and Abbas, 2005; Mullins *et al.*, 2007). Strictly speaking, asphaltenes are the crude oil components that meet some procedural definition. A common definition is that asphaltenes are the material that is insoluble in n-pentane or n-heptane at a dilution ratio of 40 parts alkane to 1 part crude oil and re-

dissolves in toluene (ASTM D2007-93, IP 143). There are several standard procedures that prove this definition; nevertheless, in reality every laboratory uses its own customized procedure (D2007-93, 1993; IP-143, 2001; Shedid, 2001).

2.2.3 Characteristics of Asphaltene

There have been intensive investigations regarding the chemical structure and molecular weight of asphaltenes. Due to complex nature of asphaltene, the exact chemical structure of asphaltenes is not known (Kokal and Sayegh, 1995; Mullins, 2008). Due to the natural tendency of asphaltene molecules to aggregate, the true molecular weight determination is very difficult and takes too much effort. It is commonly known that applied method for measuring the asphaltene molecular weight has an important effect on the value of the molecular weight. The average molecular weight of asphaltenes present in petroleum crudes is generally very high. Published data record the molecular weight of asphaltene in the range of 500 to 500000 (Jamshidnezhad, 2005; Mullins, 2008).

So far, it is known that asphaltenes are not pure, not crystallized, not identical molecule and cannot be separated into individual components, what's more asphaltenes are polar, polyaromatic and contain in high molecular weight hydrocarbon fraction of crude oil (Srivastava *et al.*, 1999; Oskui *et al.*, 2009). On heating, they are not melted but decompose, forming carbon and volatile products above 300 to 400 °C (Hirschberg *et al.*, 1984; Kawanaka *et al.*, 1991; Jamshidnezhad, 2005). It can be said that asphaltenes are the heaviest components in crude oil (Kawanaka *et al.*, 1991). The carbon number an asphaltene molecule would be around 40 to 80. Asphaltene fraction contains the largest percentage of heteroatom (N, S, O) and organ metallic compounds (Ni, V, Fe) in crude oil (Mullins *et al.*, 2007).

The amount of asphaltenes in petroleum varies with source, depth of burial, and API gravity of the crude oil. Also, the quantity and type of solvent added to the crude oil may be crucial to the amount and characteristics of the asphaltenes precipitated. The various solvents precipitate different amounts of asphaltenes and as the precipitating n-alkane molecule gets smaller, the amount precipitated increases

sharply as shown in Figure 2.1. As can be seen in this figure the precipitated asphaltenes obtained are different both qualitatively and quantitatively. As illustrated in Figure 2.1 n-alkanes induced total asphaltenes precipitated from the same dead oil decrease with increasing titrant carbon number. Moreover, visual inspection reveals variation in textures and characters of the corresponding precipitates. The short n-alkanes yield tacky and sticky asphaltene while, the longer n-paraffins produce powdery and dry asphaltenes (Mullins *et al.*, 2007).

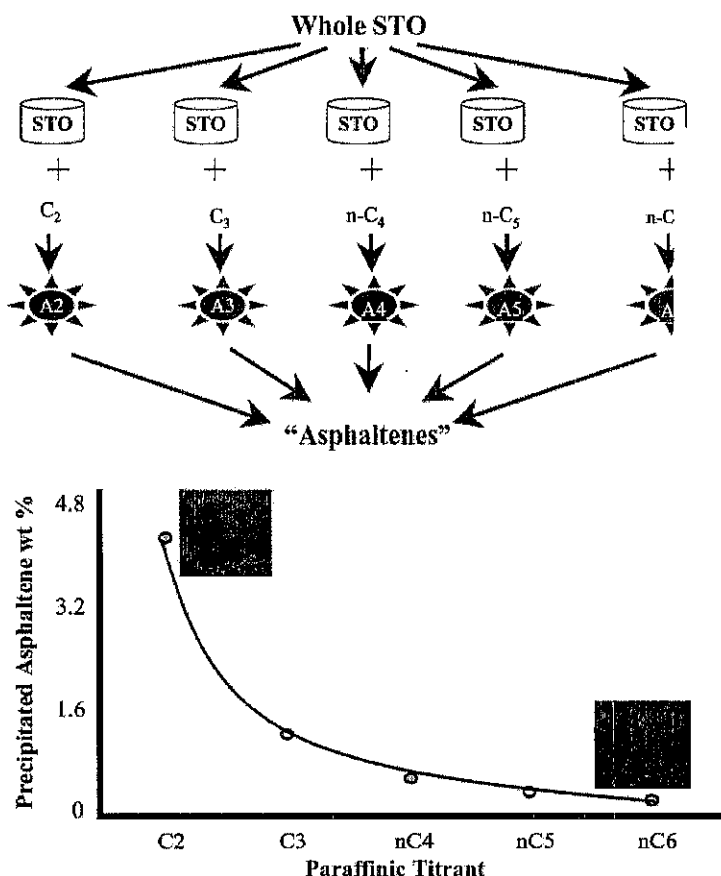


Figure 2.1: Effect of paraffin carbon number on asphaltenes (Mullins *et al.*, 2007)

The amounts of asphaltene precipitated with n-heptane and heavier n-alkanes show very little difference, indicating that the most insoluble materials are precipitated by n-heptane and heavier solvents. This is the primary reason for selecting n-heptane as the most logical solvent for obtaining the asphaltene. Some would argue that the n-C₇ asphaltene is the real asphaltene, whereas the n-C₅ material is a mixture of asphaltene and resin (Long, 1981; Sirota, 2005).

2.2.4 Resin and Asphaltene

Although asphaltenes and resins have similar molecular structure but, resins are less polar, less aromatic and have lower molar mass than asphaltene. Resins are not known to deposit on their own, but they deposit together with asphaltene. Just as the asphaltene has only a procedural definition, resins also are procedurally defined. There are at least two approaches to defining resins (Long, 1981; Sirota, 2005). In one approach the material that precipitates with addition of propane, but not with n-heptane, is considered to constitute the resins. There is no universal agreement about the propane/n-heptane pair, but the general idea is that resins are soluble in higher molecular weight normal alkanes, but are insoluble in lower molecular weight alkanes (Long, 1981; Sirota, 2005). Resin can be converted to asphaltene by oxidation. Unlike asphaltenes, resins are assumed to be soluble in the petroleum fluid. Pure resins are heavy liquids or sticky (amorphous) solids and are as volatile as the hydrocarbons of the same size (Mullins *et al.*, 2007). A SARA analysis is standard method to quantify resins by a completely different approach.

2.2.5 Wax and Asphaltene

Wax and asphaltene co-exist in many reservoirs and there are main differences between wax and asphaltene. Wax is soluble in common precipitant of asphaltene such as n-heptane, also wax has a defined melting point while asphaltene known to have no defined melting point (Mullins *et al.*, 2007). Although both components have differences molecules but their deposition may happen simultaneously. Wax molecules compare with asphaltene and resin; include normal alkane (paraffin) with 15-80 carbon atoms and very few branch chains or even no branch chain. Wax can be separated from the crude oil to form a solid state like a crystal shape due, mostly, to lowering of temperature (Dong *et al.*, 2001).

Just like asphaltenes which start to flocculate before deposition, wax goes through crystallization process which is mainly due to temperature drop. Temperature and composition are two major parameters which influence the solubility of wax in oil, while pressure has a minor effect, unlike in the case of asphaltene where pressure

plays a very important role in the stability of asphaltene. Due to a noticeable temperature drop which happens during oil flow through surface facilities, most of wax depositions occur in these facilities. If the temperature increases the wax will resolve again in crude oil and the process is mostly thermodynamic reversible.

The process of wax deposition like asphaltene includes three stages which are: wax separation, growing up of wax crystals and deposition of wax (Dong *et al.*, 2001). The wax crystals change the flow behavior of crude oil from Newtonian to non-Newtonian which leads to an increase of fluid viscosity; therefore, it requires more pumping energy as pump capacity is decreased with wax deposition. The other wax deposition effect is to reduce the effective cross sectional area of the pipe. Since wax deposition also increases the pipeline roughness, the pressure difference along the pipeline would be higher. Wax deposition in well tubing and process equipment may lead to more frequent shutdowns and operational problems. Also, wax deposition can result in formation damage. If the temperature of the fluid in the formation falls below the cloud point, wax precipitates and may deposit in the formation pores, partially blocking or plugging the fluid flow channels and thus restricting the flow.

In terms of formation damage, it is believed that the damage due to wax deposition is not as much severe as the asphaltene deposition (Venkatesan and Creek, 2007). Wax deposition is due to heat loss which normally is limited to wellbore area unlike asphaltene deposition which can take place a few feet away from wellbore (Venkatesan and Creek, 2007).

2.2.6 SARA Analysis

One simple and useful analysis scheme for characterization of crude oil is fractionation of oil into smaller quantities by a standard method which is documented in Fan *et al.* (2002). This method for characterization of heavy oils based on fractionation, whereby a heavy oil sample is separated into smaller quantities or fractions, with each fraction having a different composition as shown in Figure 2.2. Fractionation is based on the solubility of hydrocarbon components in various solvents used in this test. Each fraction consists of a solubility class containing a

range of different molecular-weight species. In this method, the crude oil is fractionated to four solubility classes, referred to collectively as SARA: saturates, aromatics, resins, and asphaltenes.

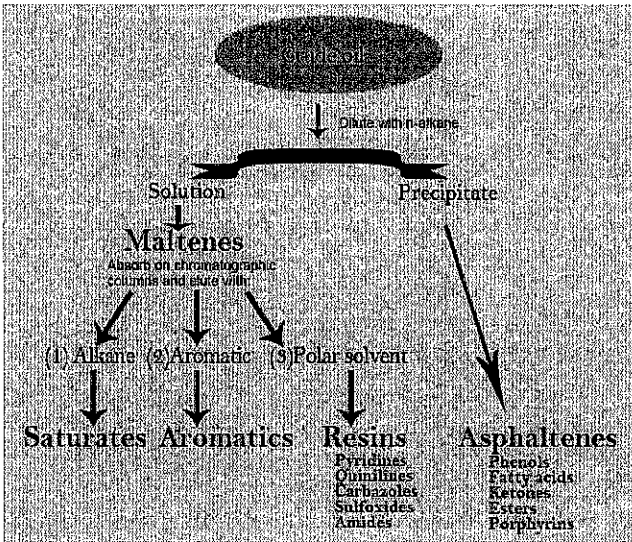


Figure 2.2: Schematic illustration of SARA analysis (Fan *et al.*, 2002)

Each component would be defined based on its solubility in various solvents which later would be used in this test. The saturate fraction consists of nonpolar material including linear, branched, and cyclic saturated hydrocarbons. Aromatics, which contain one or more aromatic rings, are more polarizable (Mullins *et al.*, 2007). The remaining two fractions are resins and asphaltenes which have polar substituents. Typically, this classification is useful because, it identifies the fractions of the oil that pertain to asphaltene stability and thus should be useful in identifying oils with the potential for asphaltene problems. The SARA analysis began with the work of Jewell (1972).

2.2.7 State of Asphaltene in Petroleum

The real solution and colloidal solution approaches are essentially the only two physical models available for description of asphaltene in crude oil (Nghiem *et al.*, 1993; Nghiem and Coombe, 1997; Kabir and Jamaluddin, 1999; Wang and Civan, 2001; Nabzar *et al.*, 2005). The first approach is solubility or real model which considers the asphaltenes to be dissolved in a true liquid state. This model assumes

that asphaltenes dissolve in crude oil completely and form a uniform solution. In other words, asphaltene dissolve in crude oil like other smaller hydrocarbons. The models of this type can be grouped into two subgroups as the regular solution model and the polymer solution model. The regular solution model assumes that asphaltene dissolves in crude oil similar to the small hydrocarbon molecules. The polymer solution model assumes that asphaltene dissolves in crude oil as large molecules, similar to polymer molecules dissolved in water (Burke *et al.*, 1990).

The second approach is the colloidal model that asphaltenes are considered to be solid particles which are suspended colloidal in the crude oil and are stabilized by large resin molecules (Wang and Civan, 2005; Oskui *et al.*, 2009). A simplistic schematic of colloidal model that represent the crude oils in terms of SARA fractions is shown in Figure 2.3. The resins are typically composed of a highly polar end group which often contains heteroatoms such as oxygen, sulfur, and nitrogen, as well as long, nonpolar paraffinic groups. The resins are attracted to the asphaltene micelles through their end group. This attraction is a result of both hydrogen bonding through the heteroatoms and dipole–dipole interactions arising from the high polarities of the resin and asphaltene. The paraffinic component of the resin molecule acts as a tail making the transition to the relatively non-polar bulk of the oil where individual molecules also exist in true solution. The aromatics (such as toluene) are relatively good solvents for both wax and asphaltenes. Petroleum fluids with high-resin content are relatively stable (Mullins *et al.*, 2007).

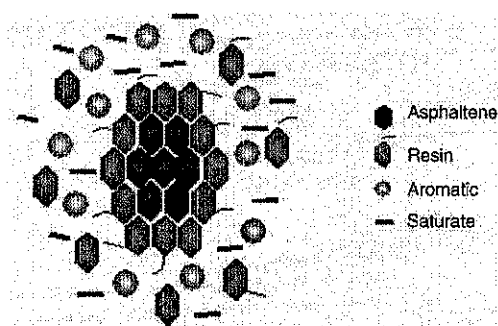


Figure 2.3: Simplified view of asphaltene in crude oil solution (Mullins *et al.*, 2007)

One thing which appears to have universal acceptance is that resins in the crude act as the peptizing agents of the asphaltene particles. According to the solubility

model, asphaltene precipitation is a relatively well-understood reversible thermodynamic process, while in the colloidal model, precipitation of asphaltenes is considered to be a more complex irreversible mechanism. Anderson (1992) and Clarke and Pruden (1996) indicated that the process of asphaltene flocculation and/or precipitation is not completely reversible. Based on this conclusion and wide range of molecular weight and size distribution for asphaltene, the best explanation for asphaltene state in petroleum is to assume that some asphaltenes are dispersed in colloidal suspension form by resins while the rest are dissolved completely (Kocabas, 2003; Negahban *et al.*, 2005).

2.2.8 Precipitation and Onset of Asphaltene Instability

The evaluation of asphaltene stability is the first step toward predicting and avoiding any of asphaltene issues at reservoirs. It is well known that asphaltenes remain in thermodynamic equilibrium into solution by colloidal or solution state under reservoir conditions (Oskui *et al.*, 2009). The asphaltene equilibrium can be disrupted due to pressure reductions, change in temperature, change in crude oil chemical composition, and addition of miscible gases and liquids to the oil as applied in various EOR techniques (Jamaluddin *et al.*, 2002; Oskui *et al.*, 2009). The effect of composition and pressure change on asphaltene precipitation is generally believed to be higher than the effect of temperature. Asphaltenes can form a separate, visible phase if the equilibrium or solubility conditions in the oil falls below the level required maintaining a stable dispersion (Wang and Buckley, 2003). Generally, this level of conditions is named as an onset of asphaltene. In fact, the asphaltene onset point (AOP) is the point that asphaltene loses its stability in terms of pressure, temperature, and composition. So precipitation means the formation of a separate and visible phase from thermodynamic equilibrium in solution (Ju *et al.*, 2001).

In field situations, when the pressure in the reservoir is reduced or when light hydrocarbon or other gaseous are injected, the colloidal suspension may destabilize, resulting in asphaltene and resin molecules precipitating out of the oil, thus, forming a separate and visible phase of asphaltenes. Precipitation occurs above the saturation or

bubble-point pressure, reaches a maximum value around the saturation pressure, and decreases as pressure drops further (Burke *et al.*, 1990; Nghiem and Coombe, 1997; Jamaluddin *et al.*, 2002; Wang and Civan, 2005; Mullins *et al.*, 2007). In other words, further decrease in pressure from the bubble-point pressure gives rise to a decrease in the amount of precipitate (Burke *et al.*, 1990).

Above the saturation pressure, the precipitation is solely due to pressure, while below the bubble-point pressure both pressure and composition affect the precipitation behavior. As the light components come out of the solution, the solubility of asphaltene in the liquid phase increases. Similarly, adding a low molar mass hydrocarbon (precipitant) to a crude oil causes asphaltenes deprecipitation (Wang and Civan, 2005; Mullins *et al.*, 2007). The highest pressure at which asphaltene first precipitates out of solution is known to be upper onset and therefore, the lowest pressure at which asphaltene still precipitate is lower onset pressure. Hence, the asphaltene is stable when pressure is smaller than the lower pressure onset or higher than the upper pressure onset, and only within these two points precipitation is possible to happen (Jamaluddin *et al.*, 2002).

There are different available laboratory techniques which can be used to define the onset of the asphaltene precipitation envelope. These methods are gravimetric, acoustic resonance technique, light scattering, and filtration (Jamaluddin *et al.*, 2002; Negahban *et al.*, 2003). Nowadays, the onset point of asphaltene precipitation is usually measured by using solid detection system (SDS) (Oskui *et al.*, 2009). The window of the visual PVT cell is equipped with fibre-optic light-transmittance probes to measure the onset of asphaltene precipitation. The principle behind the measurement is based on the transmittance of an optimized laser light in the near-infrared (NIR) wavelength through the test fluid undergoing temperature, pressure or fluid composition changes. Some more explanation regarding PVT cell system and asphaltene experiments are given in Appendix B.

2.2.9 Asphaltene Stability Evaluation

Based on available literatures it can be concluded that, whether or not asphaltenes cause problems is unrelated to the amount of asphaltene present in the oil. Asphaltene precipitation is more likely to happen in the light crude oils since the heavier crude with high asphaltene content can dissolve more asphaltene. It has been found difficult to correlate asphaltenes related problems with asphaltene content in the crude oil. The factor that is seen important is the stability of these asphaltenes and stability depends not only on the properties of the asphaltene fraction, but also on how good a solvent the rest of the oil is for its asphaltenes.

As recognized by Boer *et al.* (1995), the light oils with small amounts of asphaltenes are more likely to cause problems during production than the heavy oil with larger amounts of material in the asphaltene fraction. For instance, the Venezuelan Boscan crude with 17.2 wt% asphaltene was produced with nearly no troubles whereas the Hassi-Messaoud in Algeria has numerous production problems with only 0.15 wt% (Shedid, 2001; Takahashi *et al.*, 2003).

The heavier oil also contains plenty of intermediate components that are good asphaltene solvents whereas the light oil may consist largely of paraffinic materials in which, by definition, asphaltenes have very limited solubility. Due to this reason, oils with significant amounts of asphaltenes often can be produced without any asphaltene related problems, whereas severe asphaltene problems have been reported for some oils with amounts of asphaltenes that are barely measurable (Shedid, 2001; Takahashi *et al.*, 2003). Asphaltenes in heavier oils can also cause problems if they are destabilized by mixing with other fluid during transportation or by other steps in oil processing or gas injection processes.

Field experience and experimental observations indicate that asphaltene stability is dependent on various factors including (but not limited to) composition, pressure, and temperature of the oil (Oskui *et al.*, 2006). The general consensus is that effect of composition and, in turn, pressure on asphaltene precipitation is stronger than the effect of temperature (Oskui *et al.*, 2006). However, this fact is seen still grey as few

conflicting arguments is made present in literature specifically regarding the effect of temperature on asphaltene precipitation (Fazelipour, 2007).

Nowadays, SARA test analysis is usually used as a technique to identify the asphaltene stability. The proportions of each of SARA fractions in a crude oil is related to the stability of asphaltenes in that oil (Fan *et al.*, 2002). Some researchers have stated that the high asphaltene content of the reservoir fluids are not cause of asphaltene problems, but the high saturate fractions may lead to asphaltene instability (Leontaritis and Mansoori, 1987; Kamath *et al.*, 1993). Also it has been reported that resins are responsible for asphaltene stability, when resin to asphaltene ratio is high, no problems are anticipated (Shedid and Abbas, 2005; Mullins *et al.*, 2007). But as soon as the ratio decreases asphaltenes become instable and tend to aggregate.

Asphaltene to resin ratio and colloidal instability index (CII) parameters can be calculated and be useful to identify stability or instability of asphaltenes molecules (Shedid and Abbas, 2005; Mullins *et al.*, 2007). The CII is ratio of sum of saturates and asphaltene fractions to sum of the aromatic and resin fractions. As with asphaltene to resin ratio, this index certainly should show some correlation with asphaltene stability, but no critical or definitive cut-off value can be expected. A low ratio of asphaltene to resin ratio implies good colloidal stabilization (Shedid and Abbas, 2005; Mullins *et al.*, 2007). High amounts of resins and aromatics help the asphaltene in this crude to stay in the solution and/or suspended without deposition.

The rule of thumb for the CII values are used to identify if the oil samples would be stable or unstable, i.e. $CII < 0.7$ oils are stable, $0.7 < CII < 0.9$ oils are moderately stable and $CII > 0.9$ oils are very unstable (Mullins *et al.*, 2007; Oskui *et al.*, 2009).

2.2.10 Flocculation and Deposition

Asphaltenes have tendency to aggregate by their nature and this aggregation consists of few stages, asphaltene precipitation, flocculation, and deposition processes that are shown in Figure 2.4. The flocculation of asphaltenes is the process that will happen after precipitation, indeed, after asphaltene precipitates from the oil, it may flocculate

to form much larger size molecules but they are still suspended into solution (Nghiem *et al.*, 1993). The flocculated asphaltenes can be suspended with oil flow or the particles are so large that they cannot be carried by liquid and therefore, settle out on rock surface and cause formation damage (Sanchez, 2007). On the other hand, deposition means settling of asphaltenes flocculated particles onto the rock surfaces (Ju *et al.*, 2001). Precipitation is a necessary, but not sufficient condition for deposition. Unfortunately, precipitation is sometimes incorrectly referred to as deposition (Yi *et al.*, 2009).

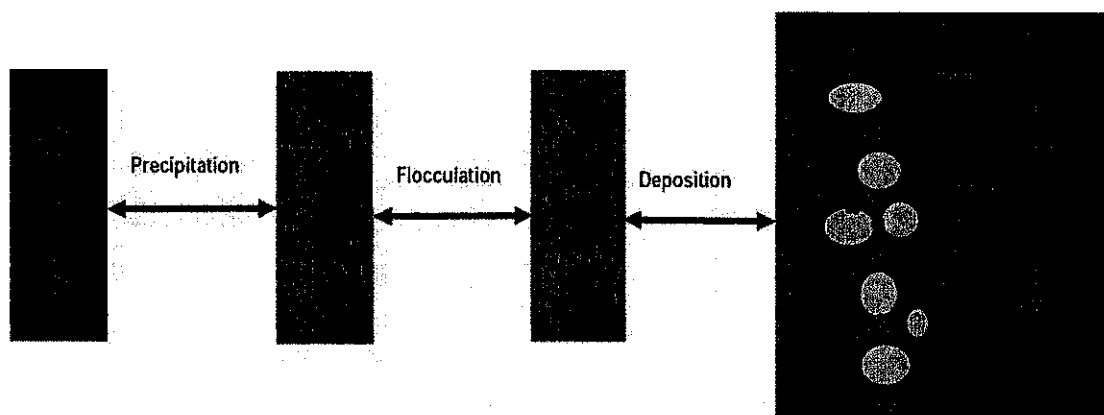


Figure 2.4: Precipitation, flocculation, and deposition processes (Yi *et al.*, 2009)

It must be noted that deposition during production operations is a more complex phenomenon than precipitation. Figure 2.4 shows that asphaltene deposition could be explained in terms of adsorption, plugging, and entrainment. The flocculated asphaltenes can be adsorbed onto rock surface by adsorption or they may be trapped within porous media because of their size, blocking the pore throats of the formation by plugging or the deposited flocculated asphaltenes can be flushed away by oil due to shearing effect if local oil velocity is high by entrainment (Yi *et al.*, 2009). Deposition begins with adsorption of flocculated asphaltene particles on rock surface. Adsorption can be explained in terms of irreversible thermodynamics. Factors which influence asphaltene deposition and adsorption can be summarized due to the presence, thickness, and stability of water film on rock surfaces; brine pH and composition; chemical and structural nature of rock minerals; asphaltenes and resin contents of the crude oil; size distribution of precipitated asphaltenes particles in relation to pore and channel size distribution of rock; and pressure and temperature.

2.2.11 Reversibility of Asphaltene Precipitation and Deposition

Reversibility of asphaltene precipitates is often an issue. Some researchers believe that is not totally reversible and others show that it is largely reversible (Fazelipour, 2007). Fazelipour (2007) has shown that precipitation process, whether it is due to pressure depletion or gas injection, is largely reversible. But other researchers (Mullins *et al.*, 2007) believe that asphaltene precipitation is not reversible mainly due to experimental observation of colloidal behavior of asphaltene suspensions.

Hirschberg *et al.* (1984) have assumed that asphaltene precipitation is reversible but is likely very slow. However, there are possibilities for significant hysteresis in the dissolution process, that is, the time required for asphaltenes to go back into solution may be considerably longer than the time required for the original precipitate to form (Oskui *et al.*, 2009). Pressure reversibility at high temperatures has been addressed by Hirschberg *et al.* (1984) and Oskui *et al.* (2009) and seems to be accepted by others (Fazelipour, 2007; Oskui *et al.*, 2009). Reversibility with respect to composition at low temperatures is still unresolved.

Ramssamdana *et al.* (1996) performed experiments at room temperature to study the reversibility of asphaltene precipitation with respect to composition. The study showed that part of the precipitated asphaltene redissolved into solution, and it was concluded that the asphaltene precipitation process is partially reversible. The dissolution of the precipitated asphaltenes is kinetically a slow process and therefore, the reversibility may require a relatively long time (Fazelipour, 2007; Oskui *et al.*, 2009). One may conclude that the reversibility of asphaltene precipitation process is largely reversible but is still not clear and is an area of specialty that needs more studies and experiments under reservoir conditions and with utilization of live oil samples.

2.2.12 Formation Damage due to Asphaltene Deposition

Civan (2007) has shown that formation damage prevention, assessment, control, and removal are among the important issues dealing with the oil and gas production from

petroleum reservoirs. Any enhanced oil recovery process can modify flow and phase behavior of the reservoir fluid, and rock properties and these modifications could lead to asphaltene precipitation and deposition and causing formation damage problems (Minssieux, 1997; Kalantari *et al.*, 2008; Oskui *et al.*, 2009). In cases of deposition, damage area is normally restricted to the wellbore zone, but in the case of precipitation damage extends over large distances from the wellbore (Oskui *et al.*, 2009).

Asphaltene precipitated particles by impairing the permeability through plugging pore throat and altering wettability through adsorbing on negatively charged mineral sites may lead to formation damage (Kamath *et al.*, 1993; Kokal and Sayegh, 1995). Deposition of solid asphaltenes causes a reduction of the pore space available for fluids i.e. porosity reduction, absolute permeability reduction, alteration of rock wettability from water-wet to mixed wet (or oil-wet) and plugging of the wellbore and piping in production facilities (Ju *et al.*, 2001; Kalantari *et al.*, 2008; Alizadeh *et al.*, 2009; Rezaian *et al.*, 2010). The deposition may induce significant changes in relative permeability, end-point saturations and effects on the displacement efficiency (Al-Maamari and Buckley, 2000).

For instant, wettability controls the flow and distribution of immiscible fluids in an oil reservoir, which plays a key role in any oil recovery process. One way that oil components are thought to alter wettability is by coating pore surfaces with precipitated asphaltenes. The deposited asphaltene may cause alteration of rock wettability from water-wet to oil-wet. Wettability has been shown to affect relative permeability, irreducible water saturation, residual oil saturation, capillary pressures, dispersion and electrical properties. The alteration of relative permeability and end-point saturations has the strongest influence on displacement processes.

It should be emphasized that alteration of wettability from water-wet to oil-wet is not necessary to cause formation damage for all reservoirs. This wettability change may improve displacement performance and efficiency and may be favorable for oil recovery depending on nature of wettability (Ju *et al.*, 2001; Agbalaka *et al.*, 2008). Some researchers have been shown that it is possible for waterflooding to achieve very high displacement efficiencies due to wettability alteration of a system (Morrow,

1990; Kamath *et al.*, 1993; Maeda and Okatsu, 2008; Abeysinghe *et al.*, 2012). In fact, the relation between recovery and wettability is very complex and it is still a controversial subject. Kamath *et al.* (1993) studied the effect of asphaltene deposition on permeability, pressure drop, and displacement performance of oil by water using one core of consolidated Berea sandstone and two unconsolidated sand packs. The results showed that asphaltene deposition caused permeability reduction but improvement of oil displacement by water due to improvement in oil relative permeability.

2.3 General Description of WAG Injection

In this section, a general description of water alternating gas (WAG) process is given. The classifications of WAG process followed by WAG efficiency and three-phase regions during a WAG process are all described.

2.3.1 WAG Introduction

The water alternating gas (abbreviated simply as WAG) process has been proposed as an enhanced oil recovery (EOR) technique to improve sweep efficiency compared to only gas or water injection. In this technique gas and water slugs are alternatively injected into reservoir and therefore, it mainly combines effects from waterflooding and gas injection processes. As reported by Christensen *et al.* (2001) the microscopic displacement of the oil by gas during gas injection is usually better than that of oil by water during waterflooding. In contrast the macroscopic sweep efficiency of water during waterflooding is normally better than that of gas during gas injection. Indeed water helps to control the mobility of the displacing fluid and to stabilize the front.

Therefore, WAG is proposed as a technique that can combine the improved microscopic displacement efficiency of the gas injection with improved macroscopic sweep efficiency of waterflooding. Generally, the WAG injection is expected to result in an improved oil recovery compared to only waterflooding or only gas injection (Surguchev *et al.*, 1992; Christensen *et al.*, 2001). As a brief and general statement,

during a WAG process, a three-phase zone is obtained, which leads to a lower remaining oil saturation than that of gas injection or waterflooding alone. Hence, in reservoirs that have undergone waterflooding, it is still possible to recover a significant quantity of the remaining oil by injecting gas alternately with water. Gas can occupy parts of the pore space that otherwise would be occupied by oil, thereby mobilizing the remaining oil. Water injected subsequently will displace some of the remaining oil and gas, further reducing the residual oil saturation. Repetition of the WAG process can further improve the recovery of oil.

2.3.2 Classification of WAG Process

WAG process can be classified as miscible and immiscible process. Generally the main difference between miscible and immiscible methods is related to the gas injection pressure and the minimum miscibility pressure of the injected gas and reservoir oil.

In a miscible process, the gas is injected at a pressure higher than the minimum miscibility pressure to achieve miscibility between gas and oil either in multi-contact or first-contact miscibility processes. But in an immiscible process, the gas injection pressure should be less than the minimum miscibility pressure between gas and oil. Most of the miscible processes are conducted to increase the reservoir pressure to or above the minimum miscibility pressure of the fluids. Mostly miscible projects are found onshore, and use expensive solvents like propane, which seems to be a less economically favorable process (Christensen *et al.*, 2001).

In many real field projects the multi-contact miscibility may have been obtained during implementing miscible processes. Usually the miscibility condition has been loosed because of inability to maintain adequate pressure. This may cause oscillations between the miscible and immiscible conditions for gas injected during the recovery process. So it can be difficult to distinguish between miscible and immiscible WAG processes. Also there is still much uncertainty about the actual displacement process (Christensen *et al.*, 2001). The immiscible WAG process is usually applied to improve the stability of gas front after gas injection or the oil sweeping of unsweep

zones during waterflooding. Sometimes the gas which is injected during gas slug can be dissolved into oil in some portion. It causes a favorable change in the fluid viscosity and density relations at the displacement front. In this case the displacement can be considered as near miscibility condition (Christensen *et al.*, 2001).

In the literature, it may be found different types of WAG applications. In some reported projects after injection a large slug of gas, a number of small slugs of water and gas were injected. This process is named as hybrid WAG injection (Prieditis *et al.*, 1991; Roper *et al.*, 1992). Also sometimes a WAG process in a few reservoirs was implemented where water and gas were injected simultaneously. This is referred as simultaneous WAG process (Ma *et al.*, 1995; Robie *et al.*, 1995).

Nowadays, there are new techniques that using some chemical additive for water or gas slug to improve more the WAG sweep efficiency (Majidaie *et al.*, 2012). Typically, for this type of cyclic injection, it can be used some alkaline, surfactant, polymer or blending of them as additive for water slug in WAG process. These types of injection are called as chemical WAG Application (Majidaie *et al.*, 2012). In addition, there is a cyclic injection in the literature which use steam instead of water slug in WAG process and it is named as water alternating steam process (Christensen *et al.*, 2001).

2.3.3 WAG Efficiency

The overall efficiency of oil recovery from a WAG process can be related to three efficiencies; vertical sweep efficiency, horizontal sweep efficiency, and microscopic displacement efficiency (Stalkup, 1980; Watts *et al.*, 1982; Moffitt and Zornes, 1992; Christensen *et al.*, 2001; Rao *et al.*, 2004; Majidaie *et al.*, 2012). Consequently, oil recovery from a WAG process can be optimized by maximizing any or all of these three efficiencies. The product of vertical and horizontal sweep efficiencies is named as the macroscopic displacement efficiency. The gas injection normally sweeps oil better than the waterflooding in pore scale. This means that the residual oil saturation after gas injection is lower than that after waterflooding. Hence, the gas injection has better microscopic displacement efficiency than the waterflooding (Christensen *et al.*,

2001). However, the waterflooding can sweep oil from vertical and horizontal areas of the whole reservoir better than the gas injection. This means that waterflooding has a better mobility control compared to the gas injection. As a result, the waterflooding has better macroscopic displacement efficiency than the gas injection. It can be concluded that the WAG process may improve the oil recovery because that the microscopic displacement efficiency from gas slug and the macroscopic displacement efficiency from water slug simultaneously can help.

Righi *et al.* (2004) reported that the oil recovery of WAG process could be higher than the waterflooding because of one or more of the following mechanisms: The free gas presence in the porous medium causes water relative permeability in three-phase zones to be lower than that in the pores occupied by only water and oil, which favors water diversion to previously un-swept areas. This mechanism can improve the volumetric sweep efficiency. The gas dissolution can reduce the oil viscosity in turn which makes the mobility ratio of water-oil displacement more favorable in the case of under-saturated oil. Also dissolved gas can cause oil swelling which causes residual oil to contain less stock-tank oil and thus increases recovery even in the absence of any additional residual oil saturation reduction mechanism. Because the interfacial tension between gas and oil is usually lower than between water and oil, in principle, it allows gas to displace oil through small pore throats not accessible by water alone under the prevailing pressure gradient. The three-phase zone formation and hysteresis effects during WAG application will normally reduce the residual oil saturation more.

2.3.4 Three-Phase Flow Region during WAG Process

Figure 2.5 shows an idealized, homogeneous vertical cross section between an injection and production well during a WAG process, where carbon dioxide gas is injected as alternating scheme with water injection. Presence of gas, water, and oil in the process leads to formation of three-phase flow region as shown in Figure 2.5. The saturation of each phase in this region should be more than each phase's critical saturation so that the three-phase flow occurs. Figure 2.5 schematically shows a WAG

process after waterflooding history of reservoir. Injection of the first gas slug can mobilize some residual oil near the injection well and also can displace water.

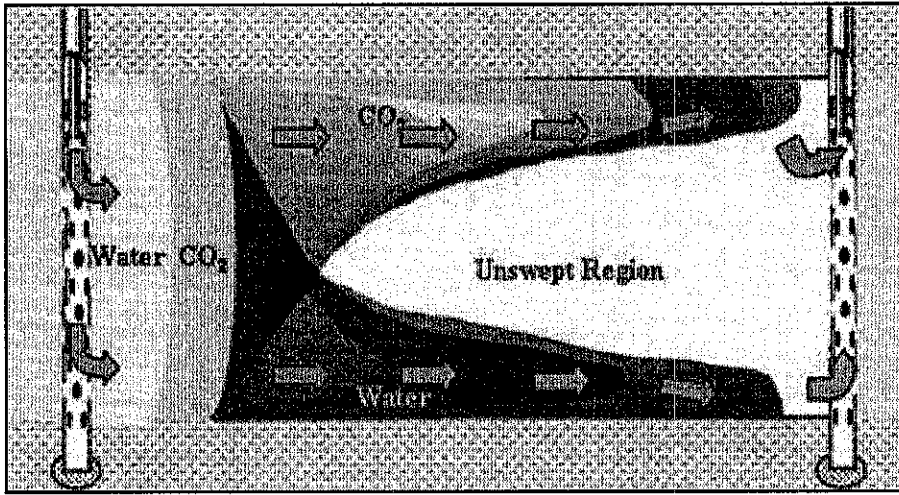


Figure 2.5: Ideal vertical cross section of WAG process (Rao *et al.*, 2004)

In this situation three-phase flow region can be formed. This three-phase flow region is expected to occur initially at near the injection well and towards the top of the reservoir because of gravity segregation, where gas is present. Once the first water slug is injected, again the injected water can mobilize some residual oil and also can displace gas. Once again in this situation the three-phase flow region can be formed. However, this new three-phase flow region is initially located near the injection well too, but towards the bottom of the reservoir where water is present because of gravity segregation.

As injection continues, oil saturation near the injection well reaches to its residual values and the three-phase flow region is moved away from the injection well and separated into two parts; one towards the top the reservoir and second towards the bottom the reservoir, due to gravity segregation. Moreover, once the oil in the top of the reservoir has been swept by gas, the three-phase flow region moves towards the center of the reservoir. Therefore, little gas flows at the bottom of the reservoir and there is no three-phase flow region in these locations. In addition, once the oil in the bottom of the reservoir has been swept by water, the three-phase flow region moves towards the center of the reservoir. Hence, little water flows at the top of the reservoir and there is no three-phase flow region in these locations. The size of the three-phase flow region decreases as oil saturation reaches minimum oil saturation. At the end of

the process may be the three-phase flow region is limited to regions near the production well and to central only.

2.3.5 Asphaltene Deposition during WAG Process

Water-alternating-gas (WAG) injection is the mobility enhancement method of CO₂ injection and it is believed that the presence of water could reduce the asphaltene precipitation. Wolcott et al. (1989); Srivastava et al. (1999); Sarma (2003); Okwen (2006) are researchers who reported that the presence of water could minimize the asphaltene precipitation. In the Hun (2012) work, dynamic core flooding experiments were conducted to study the effect of CO₂ injection and WAG injection on the amount of asphaltene precipitated. The laboratory data based on this study had justified that WAG injection gives less asphaltene precipitation compared to CO₂ injection.

2.4 General Description of Relative Permeability

In this section, a general description of relative permeability is given. Wettability which is important topic in reservoir performance and relative permeability is explained. The experimental measurements and computations of relative permeability followed by some reviews regarding the correlations and factors affecting of relative permeability are all described.

2.4.1 Introduction to Relative Permeability

The permeability of a porous medium is defined as capacity of that porous medium to transmit fluid. When the rock is completely saturated with a single-phase fluid the permeability is properly named as the absolute permeability. On the other hand, when the rock contains more than one fluid being mobile, the effective permeability and relative permeability terms appear. The relative permeability of each phase is defined as the ratio of the effective permeability of that phase to a base permeability that there are alternate definition for this base permeability currently in use. (Honarpour *et al.*,

1988; Tarek, 2001). This base permeability can be considered as the air absolute permeability, the water absolute permeability, or the effective oil permeability at irreducible water saturation but conversion from one base to another is a matter of simple arithmetic. However, experimentally, the base permeability is usually chosen as that measured at the beginning of an experiment. To measure the oil-water relative permeability, the experiment may initially start by measuring the permeability to oil in the presence of irreducible water saturation in the core and then, water is injected into the core to replace oil within the core. The base permeability can be chosen here, the initial oil permeability at irreducible water saturation (Paul, 2000).

In the past, using of three-phase relative permeability data has seldom been necessary, but nowadays, because of using some special EOR methods, an increasing interest in three-phase flow phenomena is anticipated. Practically, a two-phase system of oil and gas may be regarded as a three-phase system in which the water phase is immobile. Moreover, there are some ways which relative permeability data can be obtained. They can be estimated directly from experiments or computed indirectly from other engineering methods (Honarpour *et al.*, 1988).

2.4.2 Effect of Wettability on Relative Permeability

The term of wettability refers to wetting preference of a solid surface in presence of different immiscible fluids. The rock wettability can affect capillary pressure, relative permeability, waterflooding behavior, and electrical properties (Anderson, 1987). It is an important rock property that affects the location, flow, and distribution of fluids in a porous medium. Hence, most measured petrophysical properties must be affected by wettability (Watt, 2008).

Mostly, the assumption is made that the system under consideration is water-wet. Indeed, historically all reservoirs are believed to be strongly water-wet and almost all clean sedimentary rocks are in a water-wet condition. An additional argument for validity of the water-wet assumption was following: the majority of reservoirs were deposited in an aqueous environment, with oil only migrating at a later time. The rock surfaces were consequently in constant contact with water and no wettability

alterations were possible as connate water would prevent oil contacting the rock surfaces. However, Nutting (1934) has expressed that some reservoirs which most of them carbonate reservoirs were, in fact, oil-wet that the rock surface was preferentially wetted by oil in the presence of water.

When a porous medium contains two immiscible fluids, normally, the fluid with more tendency to spread over the surface of a solid consider as wetting phase and the other that has lower tendency consider as non-wetting phase. As well for a porous medium contains three fluids, the fluid with the highest tendency to spread over the surface of a solid consider as wetting phase, the fluid with the lowest lower tendency consider as non-wetting phase, and finally, the third fluid which has intermediate tendency consider as intermediate wetting phase. In most of the times gas is considered as a non-wetting phase but water and oil can be either wetting or intermediate phases that dependent on the rock wettability properties. For water wet rock usually, water is considered as wetting phase, gas as non-wetting phase and oil as intermediate wetting phase. In contrast, for oil-wet rock oil is considered as wetting phase, gas as non-wetting phase and water as intermediate wetting phase (Anderson, 1987; Kantas *et al.*, 1995; Paul, 2000; Watt, 2008).

There are number of different factors that affecting reservoir wettability, including surface-active compounds in crude oil, brine chemistry, brine salinity, brine pH, presence of multivalent metal cations (Ca^{2+} , Mg^{2+} , Cu^{2+} , Ni^{2+} , Fe^{3+}), pressure, temperature, and mineralogy (including clays). For example in some crude oils polar compounds that normally have polar head and hydrocarbon tail, mostly prevalent in the heavier crude fractions resins and asphaltenes that form an organic film or adsorb onto pore walls. This situation can alter the rock wettability from water-wet to oil-wet and thus, it can affect relative permeability of that system (Watt, 2008).

The effects of wettability at pore-scale during waterflooding in water-wet and oil-wet systems are shown in Figure 2.6. In a water-wet system, there is a tendency for water to reside in the tighter pores and to form a film over the grain surfaces whereas oil which is non-wetting phase resides in the larger pores. However in an oil-wet system, situation is exactly reversed, oil now forms a thin film over grain surfaces and water fills larger pores (Watt, 2008).

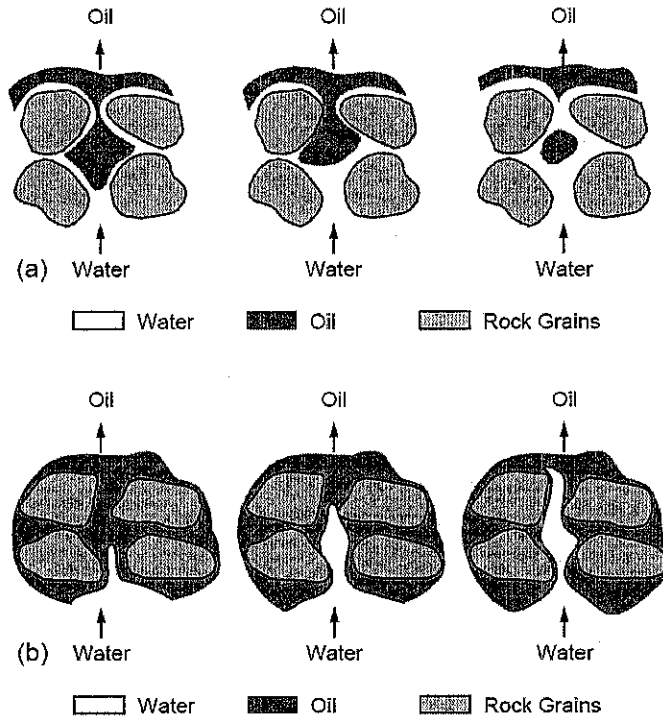


Figure 2.6: Wettability effect, pore scale (a) water-wet, (b) oil wet (Watt, 2008)

Fluid displacement process can be affected by rock wettability, particularly the form of relative permeability and capillary pressure functions (Chen, 2007). As previously explained, wettability can be classified as water-wet, oil-wet, and intermediate-wet systems. The water-wet system is where water is preferred wetting phase. Water occupies smaller pores and forms a film over the entire rock surface, even in the pores containing oil. The waterflooding process in such system will be an imbibition process; water spontaneously imbibes into a core containing mobile oil at the residual oil saturation, thus displacing the oil (Chen, 2007), whereas oil is preferred wetting phase in oil-wet system. In the same basic principle as above, oil occupies smaller pores and forms a film over the entire rock surface, even in pores containing water. Once more, the waterflooding in such system will be a drainage process; oil spontaneously imbibes into a core containing mobile water at the residual water saturation, thus displacing the water (Chen, 2007). An intermediate-wet system is where some degree of both water and oil wetness is displayed by the same rock.

Moreover, two subdivision types of intermediately wet systems can be introduced mixed-wet and fractionally-wet. In the mixed-wet system the wettability preference is depended on size of pores. The pores with large size are oil-wet and the pores have

small sizes are water-wet. However in fractionally-wet system the wettability is no size preference. In this type of rock wettability, some portion of each pore can be water-wet either oil-wet (Chen, 2007; Watt, 2008).

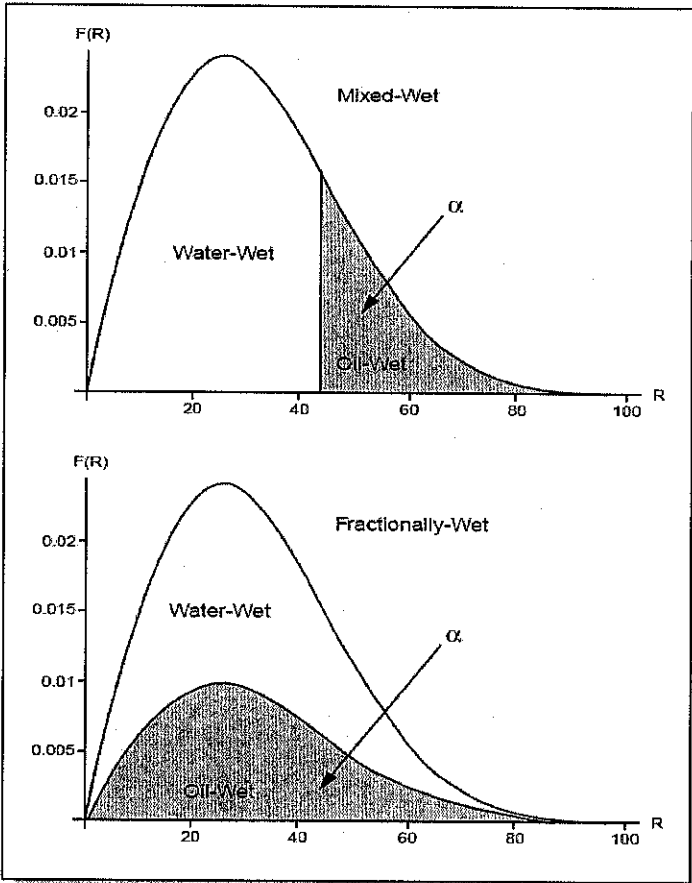


Figure 2.7: Intermediate wet systems (Watt, 2008)

Figure 2.7 shows the mixed-wet and fractionally-wet systems in term of the pore size distribution curves which are the distribution of pore volume with respect to pore size as noted by R in this figure; alternatively, it may be defined by the related distribution of pore area with respect to pore size. In addition, the rock wettability can be grouped as uniform or non-uniform. In uniform rock wettability, the entire pore-space wettability is identical (100% water-wet, 100% oil-wet, or 100% intermediate-wet), and the contact angle is essentially the same in every pore. But in non-uniform wettability, the pore-space wettability exhibits heterogeneous wettability, with variations in wetting from pore to pore, say 70% water-wet pores and 30% oil-wet pores (Watt, 2008).

2.4.3 Experimental Measurement of Relative Permeability

In this section, experimental procedures to measure the relative permeability data are given. The steady-state and unsteady-state methods for estimating the two-phase relative permeability curve are described.

2.4.3.1 Two-Phase Flow

The experimental measurements of two-phase relative permeability mostly include the simultaneous flow of two fluids which is named steady-state method and displacement of one phase with another phase which is referred to as the unsteady-state method.

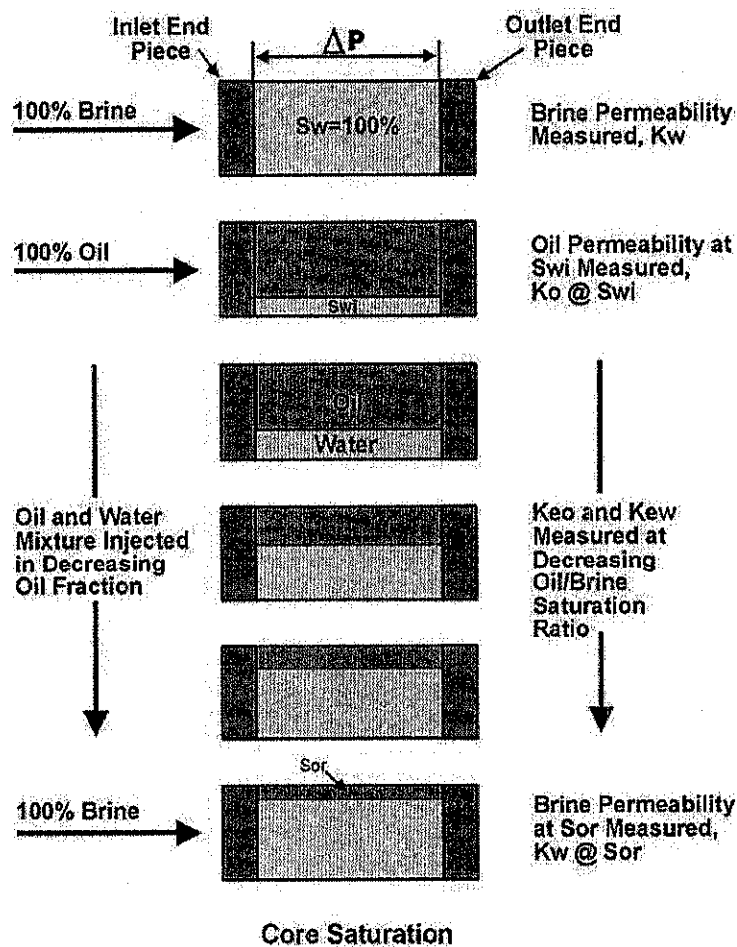


Figure 2.8: Steady-state procedure to measure relative permeability data in a water-oil system (Paul, 2000)

Figure 2.8 describes the steady-state procedure for a water-oil system, but this procedure in principle is the same for gas-oil or water-gas systems (Paul, 2000). In steady-state method, the experimental procedure is begun by saturating the sample with one fluid phase (such as water) and adjusting the flow rate of this phase through the core sample until a predetermined pressure gradient is obtained. Then, injection of a second phase (such as oil) is begun at a low rate and flow of the first phase is reduced slightly so that the pressure differential across the system remains constant. The two fluids are simultaneously injected at a fixed rate ratio until the produced fluids ratio should be equal to the injected fluids ratio. After an equilibrium condition is reached, the two flow rates and pressure drop are recorded and the percentage saturation of each phase within the core sample should be determined. In the next step, the ratio of the injected fluids is changed and again the required parameters are recorded. This procedure is repeated until all saturation ranges are covered. All these steps are illustrated in Figure 2.8. The serious experimental problem with steady-state method is that the in-situ saturations in the core have to be measured or computed. Usually, this saturation measurement after an equilibrium condition can be done by removing the core sample from the core holder and weighting it. However, this procedure introduces a possible source of experimental error. Other methods which have been used for in-situ determination of fluid saturation in core sample include measurement of X-ray absorption, gamma ray absorption, volumetric balance, and microwave technologies (Honarpour *et al.*, 1988).

Another issue in this method is the capillary pressure end effects in the core sample. It may be overcome by using high rate of flow and high pressure differential, or each end of the sample is suitably prepared with porous disks and core sections to minimize end effects. Advantage of this method is that it is conceptually straightforward and gives relative permeability data for the whole saturation range (Honarpour *et al.*, 1988; Tarek, 2001). The steady-state method to assess the effects of asphaltene deposition on the characteristics of relative permeability has not been conducted in this study.

The procedure for performing an unsteady-state experiment is relatively simple and fast and is shown in Figure 2.9 (Paul, 2000). In this figure a water-oil system is

described, but once more procedure in principle is the same for gas-oil or water-gas systems as well. In the beginning, the core is saturated with 100% water and then, the sample is de-saturated by injecting oil until no more production of water is obtained.

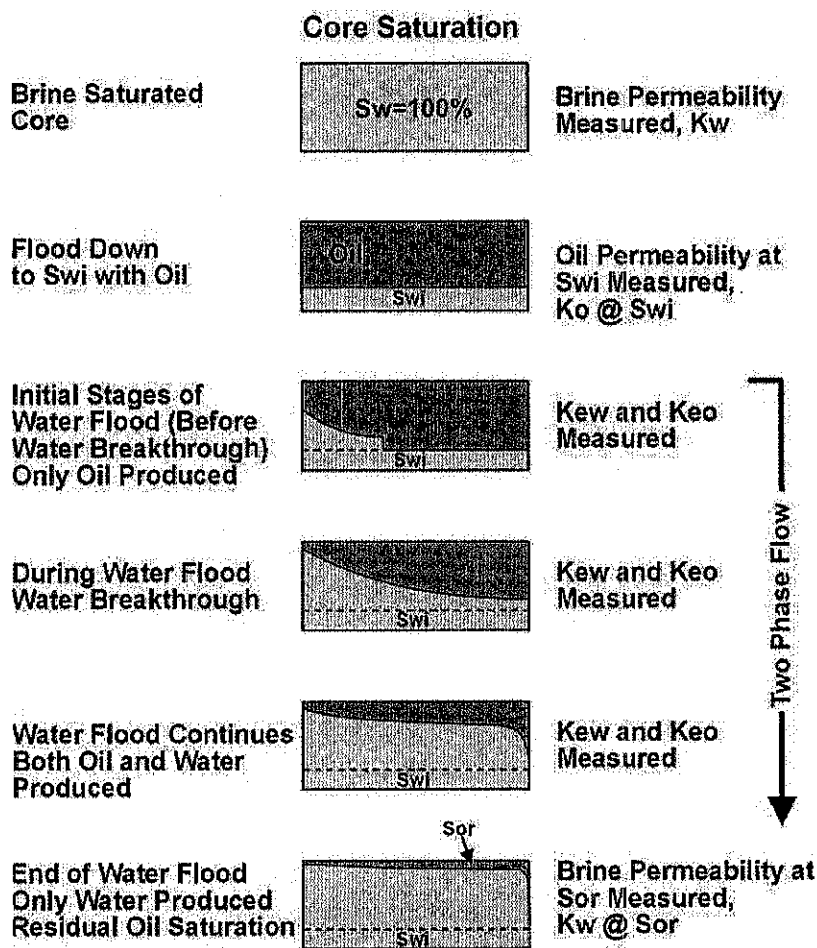


Figure 2.9: Unsteady-state procedure to measure relative permeability data in a water-oil system (Paul, 2000)

The water production in this step is recorded and irreducible water saturation is computed. As result, the effective oil permeability can be then computed at the irreducible water saturation. Then, water is injected at a constant rate to displace the oil inside the core. During this step the pressure drop across the core and fluid production versus time of injection need to be recorded. At end of this step where there is no more oil production, the residual oil saturation can be obtained and the effective water permeability at this saturation point can be computed. With recording of cumulative water injection, pressure drop, and produced oil volume, it is possible to estimate the water and oil relative permeability curves from mathematical

developed model such as extension Welge model (Welge, 1952). Like the steady-state method, pressure across the core must be large enough to make capillary end effects and gravity effects negligible. The unsteady-state method is substantially quicker, simpler experimentally, smaller amounts of fluids required and better adaptable to reservoir condition applications than the steady-state method (Paul, 2000).

2.4.3.2 Three-Phase Flow

The three-phase relative permeability data can be measured similarly as explained above by fluid displacement process under either steady-state or unsteady-state conditions. The unsteady-state method is most frequently applied in reservoir analysis of strong wetting preference, and with homogeneous samples. Oil and water may be displaced by gas to duplicate gas drive processes used in enhanced recovery methods.

However, the estimation of relative permeability values from laboratory data requires analytical solutions of the partial differential equations describing the three-phase fluid flow. Some early studies have made erroneous simplifying assumptions in describing the dynamic condition of the unsteady-state process. Reliable values of relative permeability as a function of saturations may be obtained by mathematical simulation of laboratory data using finite difference calculations. Capillary pressure data should be obtained for gas-oil, water-oil, and water-gas systems to provide basic data necessary for three-phase relative permeability calculations.

These experiments are extremely complex, time consuming, and expensive especially if live fluids need to be used. The average saturation can be measured by gravimetric method that is sufficiently accurate and relatively inexpensive. However, there are various methods of monitoring the saturation of the various fluids inside the core during the experiments that are unnecessarily expensive and elaborate. (Honarpour *et al.*, 1988).

Therefore, in this study two-phase relative permeability in water-oil system and gas-oil system are estimated experimentally based on coreflooding data and unsteady-

state method. However, the three-phase relative permeability data are computed based on Stone's II model and using these two-phase relative permeability data.

2.4.4 Experimental Computation of Relative Permeability Values

In this section, method of computation of relative permeability data from experimental work is given. The procedure for calculating water-oil relative permeability from experimental data and the Welge's extension of the Buckley-Leverett concept based on unsteady-state method are described.

2.4.4.1 Two-Phase Relative Permeability

As previously explained the two-phase relative permeability data can be directly computed from steady-state experiments data and simply using Darcy's Law. In steady-state method the fluid saturations need to be determined in each step and it is more time consuming than the unsteady-state method. It usually takes at least 24 hours for each flow ratio to equilibrate, but this can extend to 72 hours for low permeability samples or samples made from several core plugs abutted to each other to form a long test sample (Paul, 2000). In contrast, the determination of the fluid saturations is not required during an unsteady-state experiment and typically, mathematical relationships are required to compute the fluid saturations and relative permeability values from the unsteady-state experimental data.

Buckley and Leverett (1942) have presented basic equations for describing immiscible displacement in one dimension. The mathematical equations are derived by applying Darcy's law to the flowing phases, and by material balance considerations. Then, Welge (1952) reported a useful analytical method base on extension of Buckley and Leverett theory for computing the average saturation, and hence the oil recovery. The weak point of theory of Buckley and Leverett as extended by Welge is calculating the ratio of relative permeability rather than individual relative permeability. In 1959, a method (abbreviated as JBN) introduced by Johnson *et al.* (1959) further extended the Buckley and Leverett theory and the Welge method.

Based on the JBN method, individual relative permeability can be computed. Some of the relations presented by Welge are needed for the calculation of individual relative permeability in the JBN method.

The procedure for computing water-oil relative permeability from experimental data and the JBN method are given here. The same procedure can be used for calculating the gas-oil relative permeability curves. The experimental data typically recorded during an unsteady-state experiment by waterflooding process include quantity of displacing phase injected, pressure differential across the core, and volumes of oil and water produced. During waterflooding a saturated core with oil, the Welge's extension of the Buckley-Leverett concept states that;

$$S_{w,av} - S_{w2} = (1 - f_{w2}) Q_i \quad (2.1)$$

$$S_{w,av} = \frac{N_p}{V_p} \quad (2.2)$$

where subscript 2 denotes outlet end of the core;

$S_{w,av}$ = average water saturation in the core, fraction

Q_i = cumulative pore volume water injected, fraction

f_{w2} = fraction of water in the outlet stream, fraction

S_{w2} = water saturation in the outlet stream, fraction

N_p = cumulative oil production, cc

V_p = core pore volume, cc

Since the cumulative oil production and core pore volume can be measured experimentally therefore, in the first step Q_i and $S_{w,av}$ can be computed. However, $1 - f_{w2}$ can be determined from Q_i plot as a function of $S_{w,av}$ by using (2.3) and as shown in Figure 2.10;

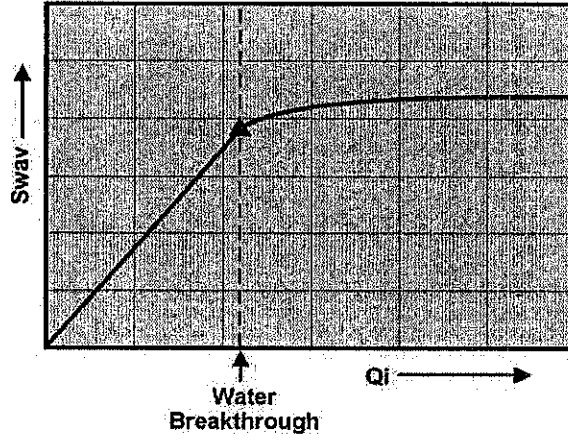


Figure 2.10: Average water saturation as function of pore volume injection (Paul, 2000)

$$1 - f_{w2} = \frac{dS_{w,av}}{dQ_i} \quad (2.3)$$

The water saturation at the outlet face S_{w2} can be computed using (2.1). By definition f_{w2} and f_{o2} may be expressed as;

$$f_{w2} = \frac{q_w}{q_w + q_o} \quad (2.4)$$

$$f_{o2} = 1 - f_{w2} \quad (2.5)$$

where f_{o2} is fraction of oil in the outlet stream, q_w and q_o are instantaneous water and oil flow rates, respectively. By combining (2.4) with Darcy's law (ignoring capillary and gravity effects), it can be shown that;

$$f_{w2} = \frac{1}{1 + \frac{k_{ro}}{k_{rw}} \frac{\mu_w}{\mu_o}} \quad (2.6)$$

Since water and oil viscosities are known, the relative permeability ratio can be determined from (2.6). The JBN method is proposed calculating the individual relative permeability based on definition of relative injectivity parameter. The symbol I_R , designated as the relative injectivity, is a dimensionless function of cumulative injection, describing the manner in which the intake capacity varies with cumulative

injection. From a physical viewpoint, the relative injectivity may be defined as the ratio of the intake capacity at any given flood stage to the intake capacity of the system at the very initiation of the flood (at which moment practically only oil is flowing through the system). This latter definition permits determination of the relative injectivity function for a given type of reservoir rock from measurements of flow rate and pressure drop taken at successive stages of waterflooding susceptibility experiment. Therefore, the relative injectivity is expressed as following;

$$I_R = \frac{\Delta p_i}{\Delta p_p} \frac{1}{Q_i} \tag{2.7}$$

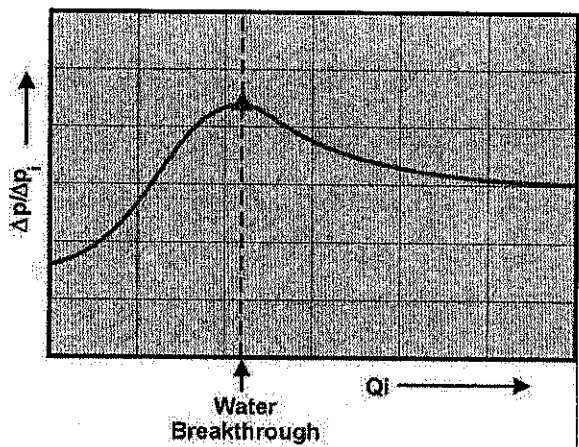


Figure 2.11: Relative pressure drop as a function of pore volume injection (Paul, 2000)

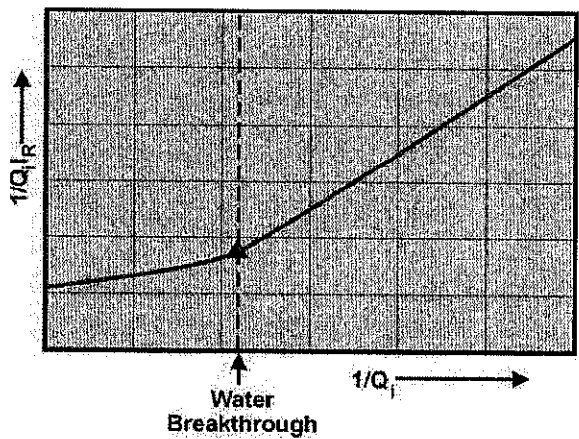


Figure 2.12: Relative injectivity as a function of pore volume injection (Paul, 2000)

A plot of $\frac{\Delta p_i}{\Delta p_p}$ against Q_i is used to obtain the injectivity ratio I_R which is shown in

Figure 2.11. According to the JBN method, the k_{ro} can be obtained by plotting

$\frac{1}{Q_i I_R}$ versus $\frac{1}{Q_i}$ as shown in Figure 2.12 and using the following relationship;

$$k_{ro} = f_{o2} \frac{1}{\frac{d(1/Q_i I_R)}{d(1/Q_i)}} \quad (2.8)$$

By knowing the ratio of oil to water relative permeability from (2.6), the value of k_{rw} then can be calculated. Thus k_{ro} and k_{rw} can be plotted against S_{w2} to give the normal relative permeability curves.

In the literature several alternative techniques have been proposed to compute relative permeability from unsteady-state experiment data. Saraf and McCaffery (1982) developed a procedure by least-squares fit of oil recovery and pressure data. Jones and Roszelle (1978) developed a graphical technique for evaluation of individual phase relative permeability from displacement experimental data which are linearly scalable. Chavent *et al.* (1975) described a method for determining two-phase relative permeability from two sets of displacement experiments, one set conducted at a high flow rate and the other at a rate representative of reservoir conditions. Barroeta and Thompson (2006) developed a method using the solution of the inverse problem (numerical regression), by modeling, through the Buckley-Leverett procedure, the observed pressure versus time data only, and dismissing the recovery measurements.

In addition to these methods, the relative permeability can be computed from the capillary pressure data and centrifuge techniques. The techniques which are used for calculating relative permeability from capillary pressure data were developed for drainage situations, where a non-wetting phase (gas) displaces a wetting phase (oil or water). Several investigators have developed equations for estimating relative permeability from capillary pressure data such as Purcell (1949) and Fatt and Dykstra (1951). The centrifuge techniques for measuring relative permeability involve

monitoring liquids produced from rock samples which were initially saturated uniformly with one or two phases. Liquids are collected in transparent tubes connected to the rock sample holders and production is monitored throughout the test. Several investigators have developed mathematical techniques for deriving relative permeability data from these measurements (Slobod *et al.*, 1951; Van Spronsen, 1982; O'Meara and Lease, 1983).

2.4.4.2 Three-Phase Relative Permeability

As previously mentioned, the three-phase relative permeability data can be computed experimentally through the steady-state or unsteady state methods. In the steady-state experiment, Darcy's law again can be used directly to calculate the effective permeability for each phase but here, the fluids saturation measurements are essential issues. In unsteady-state experiment, one fluid such as gas can be displaced the two other fluids like oil and water. There are different extensions of Welge's analysis and JBN method to estimate three-phase relative permeability from displacement data (Sarma *et al.*, 1992; Nordtvedt *et al.*, 1997; Ahmadloo *et al.*, 2009). In this study because of difficulty in experimental measurement of three-phase relative permeability, they are computed based on Stone's II model and using experimental two-phase relative permeability data.

2.4.5 Factors Affecting Relative Permeability

Relative permeability is a complicated function of fluids and rock properties. It is believed to be affected by the following factors; pore geometry, wettability, fluid distribution, saturation, saturation history, flow rate, viscosity ratio, temperature, overburden pressure, interfacial tension, density, initial wetting phase, and immobile phase saturation (Lefebvre du Prey, 1973; Anderson, 1987; Honarpour *et al.*, 1988; Ursin and Zolotukhin, 1997; Civan, 2000; Tarek, 2001; Watt, 2008). All these factors have been reviewed in relative permeability of petroleum reservoirs book which is written by Honarpour *et al.* (1988). They are pointed out that all factors which influence flow in systems containing two mobile phases can apply to three-phase

systems as well. Furthermore, they are mentioned that wettability of reservoir rock has a major impact upon relative permeability curves and subsequent reservoir performance. They are emphasized that wettability is the main factor responsible for the microscopic fluid distribution in porous media and it determines to a great extent the amount of residual oil saturation and ability of a particular phase to flow.

Moreover, many researchers have reported the effects of hysteresis and spreading coefficient on three-phase relative permeability (Kalaydjian *et al.*, 1993; Egermann *et al.*, 2000; Shahverdi and Sohrabi, 2012). The problem of hysteresis increases significantly when moving from two-phase to three-phase flow system. The three-phase hysteresis problem is significantly more advanced than that in two-phase flow for two reasons (Honarpour *et al.*, 1988). First, the number of saturation directions increases and second the definition of hysteresis becomes ambiguous.

On a macroscopic scale the number of process paths increases from two-phase flow to three-phase flow. In addition, the saturation path within ternary diagram is not predefined in three-phase systems. For the two-phase case, only unknown part of the saturation trajectory is endpoints, as compared with three-phase flow for which the whole saturation trajectory is initially unknown. On microscopic scale displacement sequences that can occur in three-phase systems are not seen in two-phase systems. These include double displacement mechanisms and spreading behavior of the intermediate wetting phase (Honarpour *et al.*, 1988). Depending on the equilibrium spreading coefficient, one or two phases can be distributed as films in the porous medium.

2.4.6 Relative Permeability Correlations

In many cases, relative permeability data on actual core samples from the reservoir under study may not be available, in which case, it is necessary to obtain desired relative permeability data in some other manner rather than the direct experimental measurement. In addition, experimental measurement of three-phase relative permeability data is extremely difficult and involves rather complex techniques to determine the fluid saturation distribution along the length of the core. For this reason,

empirical methods for determining two-phase and three-phase relative permeability data are becoming more attractive and widely used, particularly with the advent of numerical reservoir simulators (Honarpour *et al.*, 1988; Tarek, 2001).

2.4.6.1 Two-Phase Relative Permeability Correlations

Several correlations have been developed for computing two-phase relative permeability data such as Fatt and Dykstra (1951), Burdine (1953), Wyllie and Sprangler (1952), Wyllie and Gardner (1958), Corey (1954), Brooks and Corey (1964,1966), Honarpour *et al.* (1988), and Hirasaki (1975) correlations. Various parameters have been used to estimate the relative permeability data including, residual saturation values, initial saturation values, and capillary pressure data. In addition, most of the proposed correlations use the effective phase saturation as a correlating parameter. The typical shape of the two-phase relative permeability curves based on effective wetting phase saturation, S_w^* , may be approximated by the following equations;

$$S_w^* = \frac{S_w - S_{wc}}{1 - S_{wc} - S_{nw}} \quad (2.9)$$

$$k_{rw} = A \times (S_w^*)^n \quad (2.10)$$

$$k_{ro} = B \times (1 - S_w^*)^m \quad (2.11)$$

where k_{rw} and k_{ro} are water and oil relative permeability, A , B , n , and m are constants, S_{wc} and S_{nw} are critical wetting and non-wetting saturations. Honarpour *et al.* (1988) provide a comprehensive treatment and listed numerous correlations for estimating two-phase relative permeability which is recommended to refer for further details.

2.4.6.2 Three-Phase Relative Permeability Correlations

Since the experimental problems associated with three-phase flow are difficult to overcome, a mathematical model appears to be a very good alternative method. Several probability models have been developed to compute three-phase relative permeability relationships in the literature, such as Corey et al. (1956), Stone (1970), Stone (1973), Dietich and Bonder (1976), Parker et al. (1987), Lake (1987), Baker (1988), Almen and Sillatery (1988), Grader and O'Meara (1988), Delshad and Pope (1989), Kokal and Maini (1989), Hustad and Hansen (1995), Oosrom and Lenhard (1998), Balbinski *et al.* (1999), Blunt (1999). Ahmadloo *et al.* (2009) present several three-phase relative permeability models in oil and gas industry that it is recommended to refer for further details.

In a three-phase system, most probability models assume that water relative permeability is dependent only on water saturation and similarly, gas relative permeability is dependent only on gas saturation. However, oil relative permeability, varies in a more complex manner and is dependent on the both water and gas saturations. These assumptions have been confirmed in laboratory investigations for a water-wet system (Honarpour *et al.*, 1988; Ahmadloo *et al.*, 2009). They are justified that in a water-wet system, water behaves as a completely wetting phase, gas behaves as a completely non-wetting phase, but oil has an intermediate ability to wet the rock.

Therefore, in this system, the water can flow only through the smallest interconnected pores that are present in the rock and able to accommodate its volume, and its flow does not depend upon the nature of the fluids occupying the other pores, $k_{rw} = f(S_w)$. Similarly, gas can flow only through largest pores and its flow does not depend upon nature of the fluids occupying the other pores, $k_{rg} = f(S_g)$ (Leverett and Lewis, 1941; Ahmadloo *et al.*, 2009)

However, the pores available for intermediate wetting phase which is oil here, are those, that in size, are larger than pores passing only water, and smaller than pores passing only gas. The number of pores occupied by oil depends upon the particular size distribution of the pores in the rock in which the three-phase coexist and upon the oil saturation itself (Honarpour *et al.*, 1988);

$$k_{ro} = f(S_w, S_g) \quad (2.12)$$

In general, the relative permeability of oil phase in a three-phase system is rarely known and therefore, they need to be estimated. Several practical approaches are proposed based on estimating the oil relative permeability from two sets of two-phase relative permeability data. As previously explained, for oil-water system and also oil-gas system, it can be shown that:

$$k_{row} = f(S_w) \quad (2.13)$$

$$k_{rw} = f(S_w) \quad (2.14)$$

$$k_{rog} = f(S_g) \quad (2.15)$$

$$k_{rg} = f(S_g) \quad (2.16)$$

where k_{row} is defined as oil relative permeability in the water-oil system and similarly, k_{rog} is the oil relative permeability in the gas-oil system. Usually the symbol k_{ro} is reserved for oil relative permeability in three-phase system. The simplest approach to predict the relative permeability to the oil phase in a three-phase system is defined as (Tarek, 2001):

$$k_{ro} = k_{row} \times k_{rog} \quad (2.17)$$

There are several practical and more accurate correlations that have developed over the years which are listed in Honarpour *et al.* (1988), Tarek (2001), and Ahmadloo *et al.* (2009) which are recommended to study for further details.

2.4.6.3 Stone's I Model

One of very well-known probability model to estimate oil relative permeability in the three-phase system from laboratory measurement of two-phase data is developed by Stone (1970). This model is named as Stone's first (or Stone I) model. This model

combines channel flow theory in porous media with probability concepts to obtain a formula for computing the relative permeability to oil in the presence of water and gas flow. Stone introduced non-zero residual oil saturation when oil is displaced simultaneously by water and gas, which is named minimum oil saturation, S_{om} . It should be noted that the minimum oil saturation is different than the residual oil saturation in the oil-water system, i.e., S_{orw} and the residual oil saturation in the gas-oil system, i.e., S_{org} . Stone introduced the following normalized saturations, and therefore, the oil relative permeability in three-phase system is then defined as;

$$S_o^* = \frac{S_o - S_{om}}{1 - S_{wc} - S_{om}}, \text{ for } S_o \geq S_{om} \quad (2.18)$$

$$S_w^* = \frac{S_w - S_{wc}}{1 - S_{wc} - S_{om}}, \text{ for } S_w \geq S_{wc} \quad (2.19)$$

$$S_g^* = \frac{S_g}{1 - S_{wc} - S_{om}} \quad (2.20)$$

$$k_{ro} = S_o^* \times \beta_w \times \beta_g \quad (2.21)$$

The two multipliers in (2.21) are determined from following relationships:

$$\beta_w = \frac{k_{row}}{1 - S_w^*} \quad (2.22)$$

$$\beta_g = \frac{k_{rog}}{1 - S_g^*} \quad (2.23)$$

Selecting minimum oil saturation, S_{om} is a difficulty in using Stone's first model. Later an expression for determining the minimum oil saturation is suggested by Fayers and Matthews (1984). They defined a new parameter to compute the minimum oil saturation as follows;

$$S_{om} = \alpha \times S_{orw} + (1 - \alpha) \times S_{org} \quad (2.24)$$

$$\alpha = 1 - \frac{S_g}{1 - S_{wc} - S_{org}} \quad (2.25)$$

In 1979 Aziz and Settari indicated that Stone's first model could give the oil relative permeability k_{ro} values greater than unity. Therefore, they suggested an expression which is a normalized form of Stone's first model as follows (Aziz and Settari, 1979):

$$k_{ro} = \frac{S_o^*}{(1 - S_w^*)(1 - S_g^*)} \left(\frac{k_{row} \times k_{rog}}{(k_{ro})_{S_{wc}}} \right) \quad (2.26)$$

where $(k_{ro})_{S_{wc}}$ is the value of the oil relative permeability at the connate water saturation as determined from the oil-water relative permeability system. Then, Hustad and Holt (1992) modified Stone's first model as following relationship;

$$k_{ro} = \left[\frac{k_{row} \times k_{rog}}{(k_{ro})_{S_{wc}}} \right] (\beta)^n \quad (2.27)$$

$$\beta = \frac{S_o^*}{(1 - S_w^*)(1 - S_g^*)} \quad (2.28)$$

$$S_o^* = \frac{S_o - S_{om}}{1 - S_{wc} - S_{om} - S_{gc}} \quad (2.29)$$

$$S_w^* = \frac{S_w - S_{wc}}{1 - S_{wc} - S_{om} - S_{gc}} \quad (2.30)$$

$$S_g^* = \frac{S_g - S_{gc}}{1 - S_{wc} - S_{om} - S_{gc}} \quad (2.31)$$

The β term may be interpreted as a variable that varies between zero and one for low-oil saturations and high-oil saturations, respectively. If the exponent n is one, the correlation is identical to Stone's first model.

2.4.6.4 Stone's II Model

In 1973 Stone proposed another expression to overcome the difficulties in choosing the minimum oil saturation that led to the development of Stone's second (or Stone II) model. This model is more accepted by different researchers. This model gives a reasonable approximation to the oil relative permeability in three-phase system (Stone, 1973);

$$k_{ro} = (k_{ro})_{S_{wc}} \left[\left(\frac{k_{row}}{(k_{ro})_{S_{wc}}} + k_{rw} \right) \left(\frac{k_{rog}}{(k_{ro})_{S_{wc}}} + k_{rg} \right) - (k_{rw} + k_{rg}) \right] \quad (2.32)$$

2.5 Summary

In this chapter, the literature review of the topics what are relevant to this research study is provided. The review covers the literatures related to asphaltene precipitation and deposition issues, the WAG application, and relative permeability. The review also highlighted the effect of asphaltene precipitation and deposition on reservoir performance, rock and fluid properties during WAG application.

CHAPTER 3

RESEARCH METHODOLOGY

3.1 Overview

In this chapter the research methodology of this study is given. The experimental materials and apparatus preparation, the basic experiments and measurements for rock and fluid samples during this study are described. These are followed by the coreflooding experiments that have been undertaken in water-oil and gas-oil systems independently. A commercial black-oil core flow simulator is used as a one-dimensional two-phase simulation model for analyzing special core analysis experimental data and estimating two-phase relative permeability curves.

3.2 Experimental Materials and Apparatus

In this section, experimental materials and apparatus which are used during this study are given.

3.2.1 Core Samples Specification

The two one-foot long and one and half-inch diameter core samples are used for this study. They are consolidated Berea sandstone cores having almost the same porosity and absolute permeability. One of these core samples is cut into four three-inch plug pieces, and each core plug is separately used for one dynamic core flooding experiment during water-oil relative permeability measurements. Similarly, the second one is cut and used for gas-oil relative permeability measurements. In experimental work of this study, it is not considered the measurement of three-phase

relative permeability by experiments. It is only conducted two-phase flow experiments under asphaltene deposition and then, it is used the Stone's II model to come up with three-phase relative permeability that having the effect of asphaltene deposition.

3.2.2 Fluid Samples Specification

The fluids used for experimental part of this study include crude oil, brine water, n-heptane, toluene and nitrogen. The sodium chloride with more than 99.5 % purity and 58.44 g/mol molecular weight is used to make synthetic brine water with 10,000 ppm sodium chloride concentration. For this purpose, each one liter of distilled water is mixed with 10 gram of sodium chloride. The mixture is stirred around 30 minutes by using magnetic stirrer hard plate. Also, the n-heptane with purity more than 99 % and molecular weight 100.2 g/mol is used as asphaltene precipitant agent during experiments. Moreover, the toluene with 99.9 % purity and 92.14 g/mol molecular weight is applied for core and system cleaning purpose. The crude oil sample with relatively high amount of asphaltene content is chosen for this experimental approach. The general specification of crude oil sample and brine water are computed and discussed later in related sections. Table 3.1 presents the general specification of crude oil sample used during the experimental part of this study.

Table 3.1: Properties of crude oil sample

Property	API gravity	Density @20°C , g/cc	Viscosity @20°C, cp	C ₇ Asphaltene wt%
Crude Oil	29.30	0.880	15.6	2.7

To study the effect of asphaltene deposition on gas and oil relative permeability in gas-oil system nitrogen is used during gas injection process. Nitrogen (N₂) is one of the common applied gases in most laboratories and it is generally inert gas, nonmetallic, colorless, odorless and tasteless and has a molecular weight of 28.0134. Nitrogen has a density of 1.251 g/L at 0 °C and a specific gravity of 0.96737 that is slightly lighter than air. At atmospheric pressure molecular nitrogen condenses (liquefies) at -195.79 °C and freezes at -210.01 °C. At a temperature of -210.0 °C

and a pressure of 12.6 kpa, nitrogen reaches its triple point (the point an element can exist in gaseous, liquid and solid forms simultaneously).

3.2.3 Experimental Apparatuses

The main experimental apparatuses to set up complete required system for studying the effects of asphaltene precipitation and deposition on relative permeability are as follows:

1. High pressure high temperature core flooding equipment and its accessories
2. Poroperm instrument
3. Manual saturator with vacuum pump
4. Digital density meter
5. Electromagnetic viscosity meter
6. Digital balance
7. Soxhlet distillation extraction
8. Core cutter machine
9. Magnetic stirrer
10. Air forced drying oven
11. Standard laboratory equipment

3.3 Basic Experiments and Measurements

In this section, the basic experiments and measurements on the core samples and the fluids which are used during this study are given.

3.3.1 Core Samples Preparation

The core cutter machine is used to cut the long core samples to the smaller plug core samples. As shown in Figure 3.1, the versatile diamond impregnated radial blade utilized to slab core samples in two halves or to trim full diameter rock samples. The standard machine comes with a worktable, blade guard, motor to power the saw, core clamp assembly for holding core, sample trolley on ball bearing guide, coolant feeding system, coolant recovery pan and diamond impregnated saw blade. The recirculation coolant system is also available (Vinci, 2012). The one-foot long core samples are cut into four three-inch plug pieces by using this machine. The two long core samples are labeled by A and B. Therefore, the three-inch plug samples which are taken are labeled by A-1 to A-4 and B-1 to B-4, respectively.

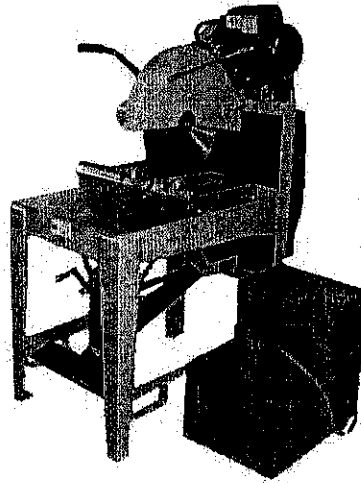


Figure 3.1: Core cutter machine (Vinci, 2012)

3.3.2 Gas Porosity and Absolute Permeability Measurements

Porosity and absolute permeability are the two major properties of a reservoir rock that may reduce due to asphaltene deposition. Porosity is a measure of storage capacity of a reservoir. Based on the porosity definition porosity of a core sample can be determined by measuring any two of the three quantities: bulk volume, pore volume or grain volume. The bulk volume can be computed from measurements of dimensions of a uniformly shaped sample. Moreover, the permeability is a property of a porous medium and is a measure of its ability to transmit fluids. The permeability is

calculated by using Darcy's Law which establishes a relationship between permeability of a porous media and potential gradient observed during flow of a fluid through core.

The Poroperm instrument is dedicated to measure gas permeability, Klinkenberg permeability, pore volume, and grain volume of plug sized core samples at room conditions. The instrument is provided with a permeameter console, a Hassler core holder, a matrix cup and a data acquisition computer station to be operated in manual and automatic mode. An optional hydrostatic core holder can be used to perform measurement at overburden pressure. The schematic of this system is shown in Figure 3.2 (Vinci, 2012).

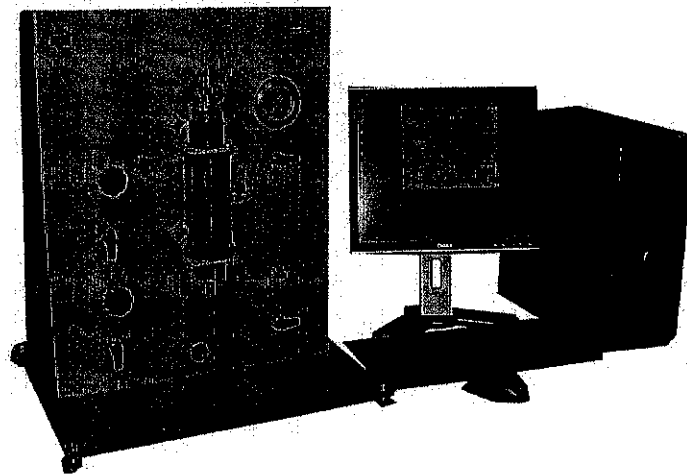


Figure 3.2: Poroperm apparatus (Vinci, 2012)

The Poroperm instrument is a permeameter and porosimeter used to determine properties of plug sized core samples at ambient confining pressure. In addition to the direct properties measurement, the instrument offers reporting and calculation facilities thanks to its user-friendly windows operated software. The gas permeability determination is based on steady-state method whereas the pore volume is determined using the Boyles law technique. Length and diameter of the core samples are measured and subsequently the bulk volumes are determined automatically. The length and diameter of the core samples are measured precisely by caliper. Each measurement of length and diameter are repeated three times and their averaged values are used for bulk volume measurement. Also, the dry core samples weight are measured carefully by digital balance.

The procedure to measure the porosity and permeability with a Poroperm is very simple. After loading the dry and clean core inside the core holder a confining pressure around 350 psi is applied. The required input data such as name of the core sample, length, diameter, and weight should fill in the software to measure the permeability and porosity for each sample. The Helium gas is used for gas injection and injection pressure is around 200 psi. Then, the measurement is started by clicking on the start button on the software. The result is saved under measured tab of the software for each core sample separately. The details of measurement and calculation of the gas porosity and absolute permeability per each core samples are presented in the analysis of data and discussion of results chapter.

3.3.3 Core Saturation and Liquid Porosity Measurement

Saturation of the core sample with brine water is the first step for conducting the coreflooding experiment. For this purpose, the manual saturator apparatus which is a rapid and efficient core sample saturation method is used. This apparatus permits to perform a sequence of vacuum and saturation cycles on core plug size samples. The standard apparatus which is shown in Figure 3.3 includes a plug sized core cell, a vacuum pump, a hand operated pressure pump (2,000 psi output), a saturate vacuum tank and necessary hand operated valves and plumbing. A larger capacity cell to accommodate full size core samples is also available. Distillated water, brine, oil or other liquid can be used to saturate the core by this apparatus (Vinci, 2012).

The procedure to saturate core samples is simple. After computing the core bulk volume from measurements of the dimensions of uniformly shaped core sample and weighting the dry core samples, all core samples are put inside the large core cell. Then, the half of the core cell is filled with brine of 10,000 ppm sodium chloride concentration which is need for core samples saturation. The core cell is connected to the two valves and two pressure gauges. One of the valve and pressure gauge is connected to vacuum pump and the other can control inside cell pressure and brine water level. In the beginning, the vacuum valve is only opened. The saturation is started by using the vacuum pump and extracting out the air inside the sample and

replacing the void pore spaces of the core samples with prepared brine water. This step takes around half an hour. Then, the vacuum pump is turned off and the related valve is closed. Then, the other valve is opened and the core cell is filled with brine water from the brine storage container by using a hand operated pressure pump. This step is continued till the brine water is come out from the valve. Then, this valve is again closed and the pumping by hand pumping is continued. The inside core cell pressure is increased and when the pressure is achieved to 2,000 psi the hand pumping is stopped. The core cell is kept for two days and the pressure is tried to keep around 2,000 psi. After this step, the pressure is released and the saturated core samples are taken off from the core cell. The weights of the core samples after saturation are measured again. The saturated core samples are immersed into brine water inside the beaker to keep the same initial brine saturation status of them for further experiments.

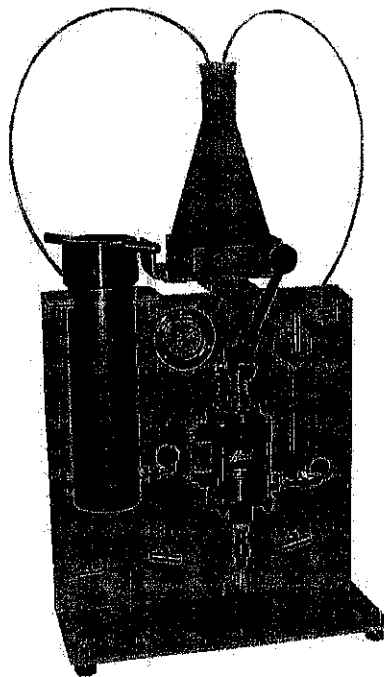


Figure 3.3: Manual saturator instrument (Vinci, 2012)

In addition, the porosity of core plug samples can be determined during core saturation by using this equipment which is called liquid porosity measurement. The values of core bulk volumes are computed from direct measurement of the length and diameter and the values of pore volume are computed from the difference between the dry and the wet weights of the rock samples and brine density. The details of

measurement and calculation of the core saturation and liquid porosity per each core sample are presented in the analysis of data and discussion of results chapter.

3.3.4 Viscosity Measurement

In this study, the viscosity of liquids is determined by an electromagnetic viscometer. The electromagnetic viscometer is a precision instrument designed to accurately measure the viscosity of high-pressure high-temperature (HPHT) fluids which is shown in Figure 3.4. The heart of the system is a sensing cell, developed in cooperation with Cambridge applied systems, capable of continuous operation to 15,000 psi and 190 °C. Performing viscosity measurements over the range of 0.02 to 10,000 cp, on very small volumes of fluid, makes this instrument a valuable component for petroleum fluid laboratory studies.

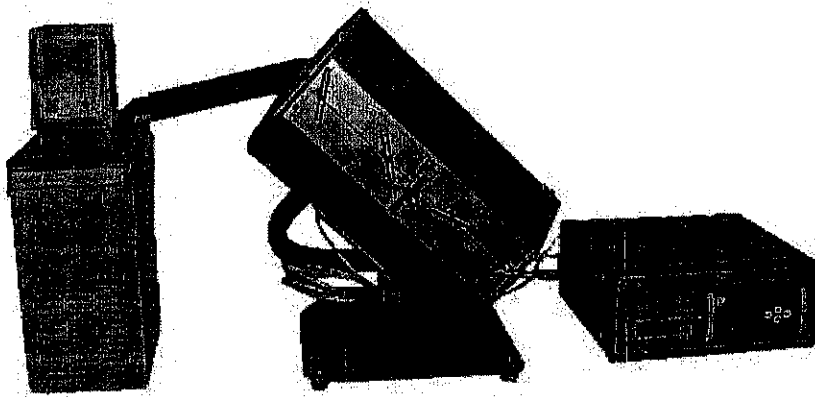


Figure 3.4: Electromagnetic viscometer instrument (Vinci, 2012)

The electromagnetic viscometer is based on a simple and reliable electromagnetic concept. Two coils move the piston back and forth magnetically at a constant force. Proprietary circuitry analyzes the piston's two-way travel time to measure absolute viscosity. An onboard electronic transducer and a resistance temperature detector (RTD) provide precise pressure and temperature measurements in the sampling chamber. The viscometer consists of a Cambridge electromagnetic viscometer SPSL 440, a set of six calibrated pistons to cover viscosity ranging from 0.02 cp to 10,000 cp, a pressure transducer with its digital display, a temperature probe and a controlled temperature air bath. The menu-driven electromagnetic viscometer electrometer provides viscosity and temperature-compensated-viscosity data of unparalleled

accuracy, auto-output in real time (Vinci, 2012). The crude oil viscosity is measured under 1500 psi pressure and different temperatures. The details of measurement of oil viscosity under reservoir conditions are presented in the analysis of data and discussion of results chapter.

3.3.5 Density Measurement

Crude oil density is measured by a digital densitometer as shown in Figure 3.5. The digital densitometer consists of a high pressure, high temperature cell made from hastelloy to cover the range of density of most reservoir fluids from 0 to 3 g/cm³. It can operate at temperature up to 200 °C and at pressure rate up to 15,000 psi. Complete system includes a density measuring cell, a control station and a thermostatic bath (Vinci, 2012). The details of measurement and calculation of crude oil density are presented in the analysis of data and discussion of results chapter.

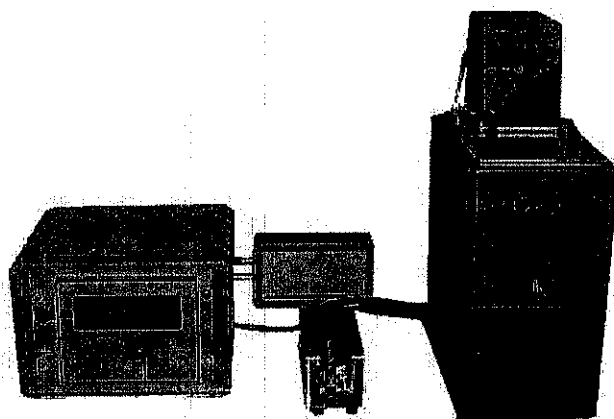


Figure 3.5: Digital densitometer instrument (Vinci, 2012)

3.3.6 Asphaltene Content Measurement

The asphaltene weight percent in crude oil sample is experimentally determined based on IP-143 (2001) standard method. The principle of this method is that a test portion of the sample is mixed with n-heptane and the mixture heated under reflux, and the precipitated asphaltenes, waxy substances and inorganic material collected on a filter paper. The waxy substances are removed by washing with hot n-heptane in an

extractor. After removal of the waxy substances, the asphaltenes are separated from the inorganic material by dissolution in hot toluene, the extraction solvent is evaporated, and the asphaltenes are weighed.

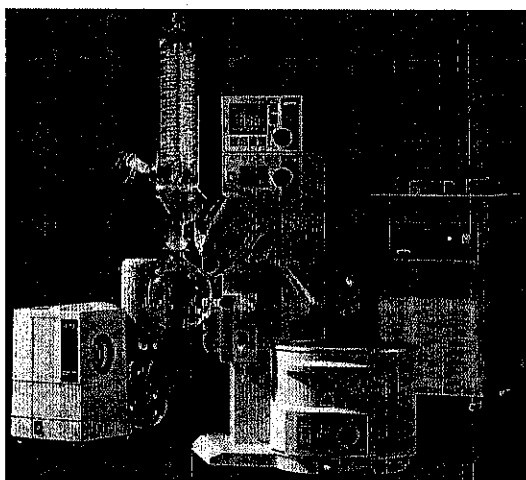


Figure 3.6: Rotary evaporator instrument (Buchi, 2011)

The measurement based on this method is started by adding n-heptane to test portion in the flask at a ratio of 30 ml to each 1 g of sample if the expected asphaltene content is below 25 % (m/m). The test portion is fully dispersed within n-heptane then the mixture is boiled under reflux for 60 ± 5 min. The flask and contents at the end of this period is removed and cooled. Then, it is closed with a stopper and stored in a dark cupboard for 90 to 150 min. The whatman filter paper grade number 42 is folded in filter funnel using forceps and residue in the flask is transferred as completely as possible with successive quantities of hot n-heptane, using stirring rod is necessary.

Thereafter, the hot n-heptane is used to rinse flask and residue rinsing is poured through the filter. The flask is kept without washing aside for use later. The filter paper and contents are removed from the funnel and placed in the reflux extractor again. Here a flask different from that used initially is used. A reflux is done with n-heptane at a rate of 2 drops/s to 4 drops/s from the end of the condenser for an extraction period of not less than 60 min, or until a few drops of heptane from the bottom of the extractor leave no residue on evaporation on a glass slide. Then, the flask which is used initially is replaced, and filled with 30 ml to 60 ml of toluene. The refluxing is continued until all the asphaltenes have been dissolved from the paper.

The contents of the flask are transferred to a clean, dry, and pre-weighted evaporating vessel. The toluene is removed by evaporation process on a boiling water bath in a rotary evaporator which is shown in Figure 3.6. Then, the dish and contents are dried in the oven, cooled and weighed. The different between two weights is related to weight of asphaltene. Based on this procedure the asphaltene weight percent of dead crude oil is measured and reported in Table 3.1. The details of measurement and calculation of the asphaltene weight percent of the crude oil samples are presented in the analysis of data and discussion of results chapter.

3.3.7 Cores Cleaning and Drying

A soxhlet extraction apparatus is the most common method for cleaning sample, and is routinely used by most laboratories. The schematic of this apparatus is given in Figure 3.7.



Figure 3.7: Soxhlet distillation extraction instrument

The soxhlet distillation extraction method is used to dissolve and extract oil and brine from rock core sample by using solvents, mostly toluene. The cleanliness of sample is determined from the color of solvent that siphons periodically from the extractor which must be clear. After each coreflooding experiment, before taking out

the core sample, the core was flushed with n-heptane to displace remaining oil and water for two pore volumes. Then, the core samples are placed in the extractor and cleaned by refluxing solvent. The solvent is heated and vaporized in boiling flasks and cooled at the top by condenser. The cooled solvent liquid falls into the sample chamber. The cleaned solvent fills chamber and soaks the core sample. When the chamber is full, dirty solvent which was used to clean the core siphons back into boiling flask and is redistilled again. The apparatus consists of a distillation/extraction glassware unit and a heating mantle with thermostatic controller. The glassware is composed of boiling flask, soxhlet extractor and condenser. Flexible plastic tubing is also used to connect condenser to the water cooling unit. All these devices are mounted on a mounting rack.

A complete extraction may take several days to several weeks in the case of low API gravity crude or presence of heavy residual hydrocarbon deposit within the core. Low permeability rock may also require a long extraction time. After that core sample is dried for the purpose of removing solvent used in cleaning the cores. Drying is commonly performed in a regular air forced drying oven or a vacuum oven at temperatures between 50 to 105 centigrade degrees. The oven is composed of a robust air forced convection air bath, a variable speed turbine, an electronic temperature regulator and a timer.

3.4 General Flowchart of Dynamic Experiments

Dynamic experiments are conducted in the coreflooding system under reservoir conditions that the pressure was 1500 psi and the temperature was 60 °C. To investigate the effect of asphaltene on relative permeability during WAG application and due to experimental difficulty of three-phase relative permeability measurements, the effect of asphaltene on relative permeability is investigated in water-oil system as well as gas-oil system separately. Then, the two sets of relative permeability data which are obtained for oil-water and gas-oil systems are combined by well-known Stone's second model to obtain the three-phase relative permeability under asphaltene

deposition. The general flowchart of these core flooding experiments in water-oil system and gas-oil system are presented in Figure 3.8 and Figure 3.9, respectively.

3.5 Dynamic Experimental Approach

Preparation of a proper oil sample is crucial step in conducting any asphaltene study. In this study, because of difficulty in preparation of down-hole sample, the surface oil sample is used. For investigation of asphaltene effect on relative permeability by this type of sampling, a synthetic dynamic procedure is used to simulate asphaltene deposition and study asphaltene problems associated with it. In this procedure, n-heptane solvent as asphaltene precipitating agent is used to create in-situ asphaltene precipitation in porous media during core flooding experiments. As reported in the literature, n-alkanes are common solvents to precipitate asphaltene from dead oil (Mullins *et al.*, 2007; Khanifar *et al.*, 2011).

In this synthetic experimental approach n-heptane and oil are injected simultaneously through different injection ports into a core sample. These fluids can be completely miscible inside porous media. The miscibility of these fluids may lead to asphaltene precipitation and then deposition depending on the core pore geometry and core pore-size distribution. During coreflooding experiments some oil samples are collected to determine their asphaltene weight presents. The reduction in asphaltene weight presents can be an indication of asphaltene deposition inside the porous media.

On the other hand, different amounts of n-heptane to oil ratio injection could lead to a creation of different amounts of asphaltene deposition. Therefore, the different ratios of simultaneously n-heptane to oil injection are chosen to obtain different degree of asphaltene deposition inside the core. This synthetic experimental setup and procedure are explained in detail for water-oil system and gas-oil system separately.

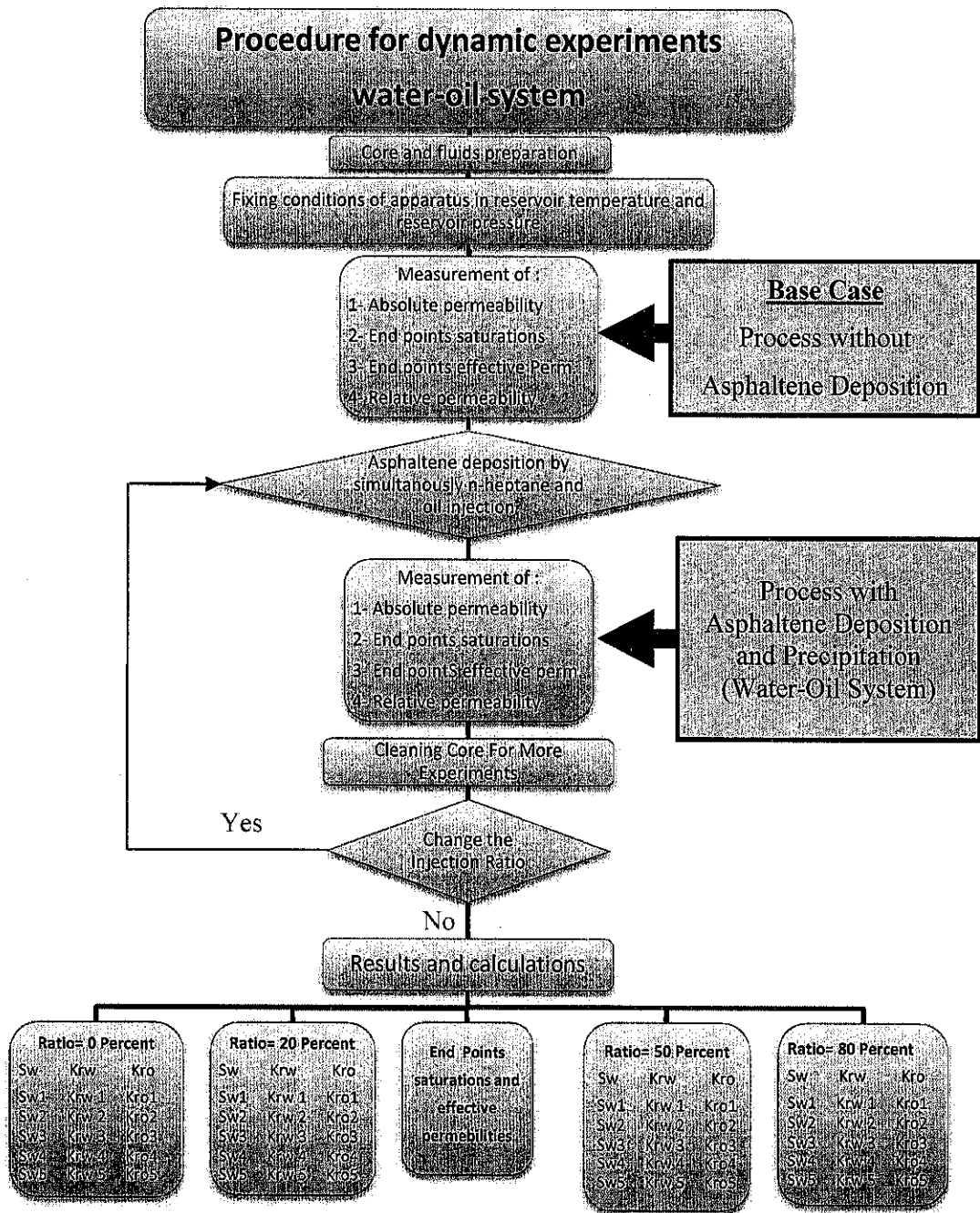


Figure 3.8: General flowchart of core flooding experiments, water-oil system

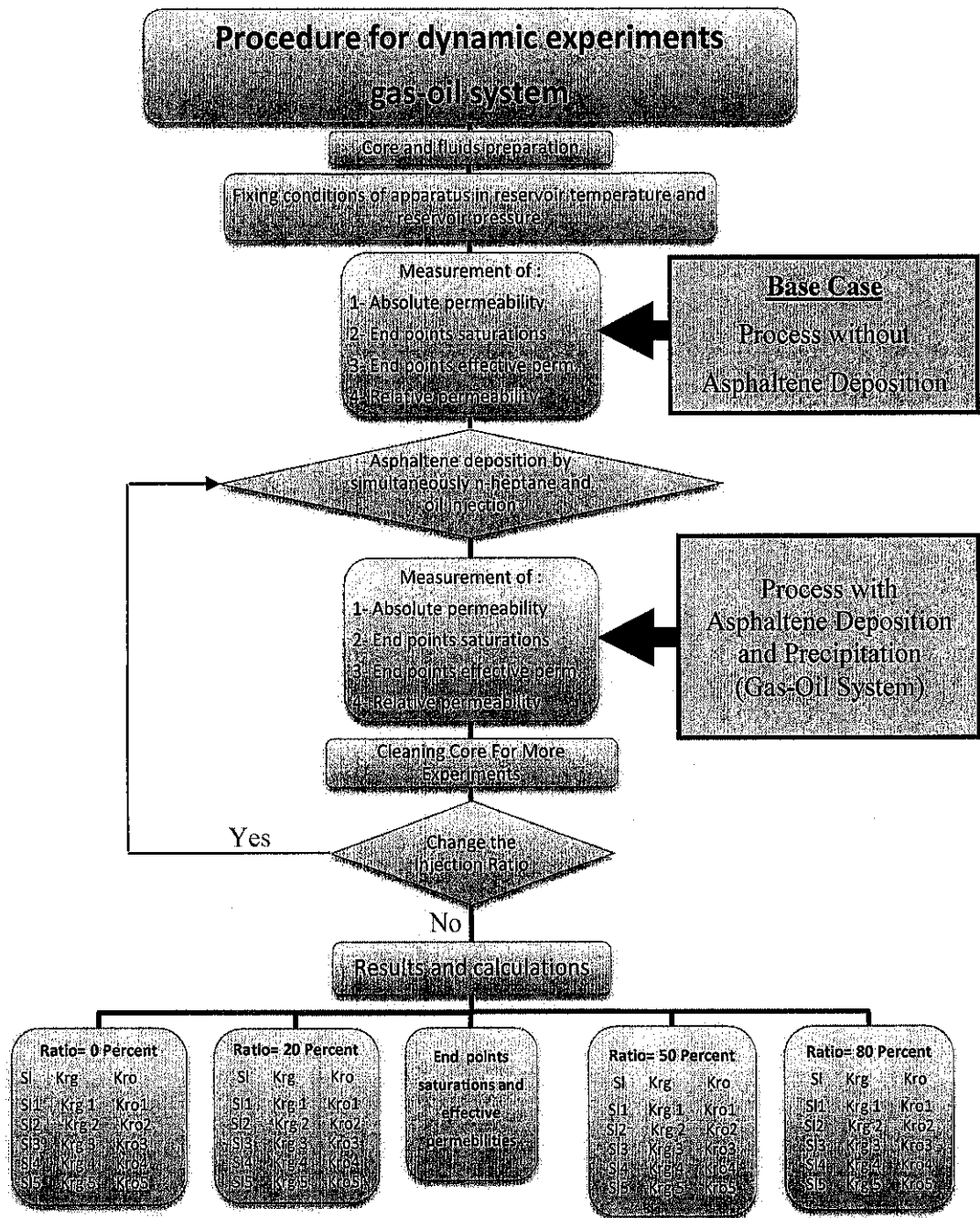


Figure 3.9: General flowchart of core flooding experiments, gas-oil system

3.6 Dynamic Experimental Set-Up and Materials

The schematic of experimental set-up used in this study to investigate effect of asphaltene deposition on relative permeability in water-oil and gas-oil systems are presented in Figure 3.10. The experimental set-up from Sanchez technologies consists

of two injection pumps, three fluid stainless steel accumulators, radial core holder, a three-phase separator and collecting pumps, an automatic fraction collector, pressure transducers, back pressure regulator, and electronic valves. The system is equipped with a powerful and user friendly data acquisition system (Sanchez, 2012).

A radial core holder which is manufactured by Sanchez technologies can accommodate cores with variable length up to 12 inches and a constant diameter of 1.5 inches. The core holder can be placed horizontally, vertically or tilted depends on the experiment objective. In this study, it is placed horizontally during all experiments, and injection is carried out from left to right hand side. There are two pressure taps in inlet and outlet of the core and four temperature taps placed at the inlet, across two sections of core, and at outlet. Also the core holder has three inlet ports; two for liquid and one for gas injection, and one outlet port for fluid production. The inlet and outlet ports of the core holder are connected to pressure and temperature transducers which can control the pressure and temperature around the core sample. The inlet ports also are connected to the three accumulators and then to injection pumps respectively.

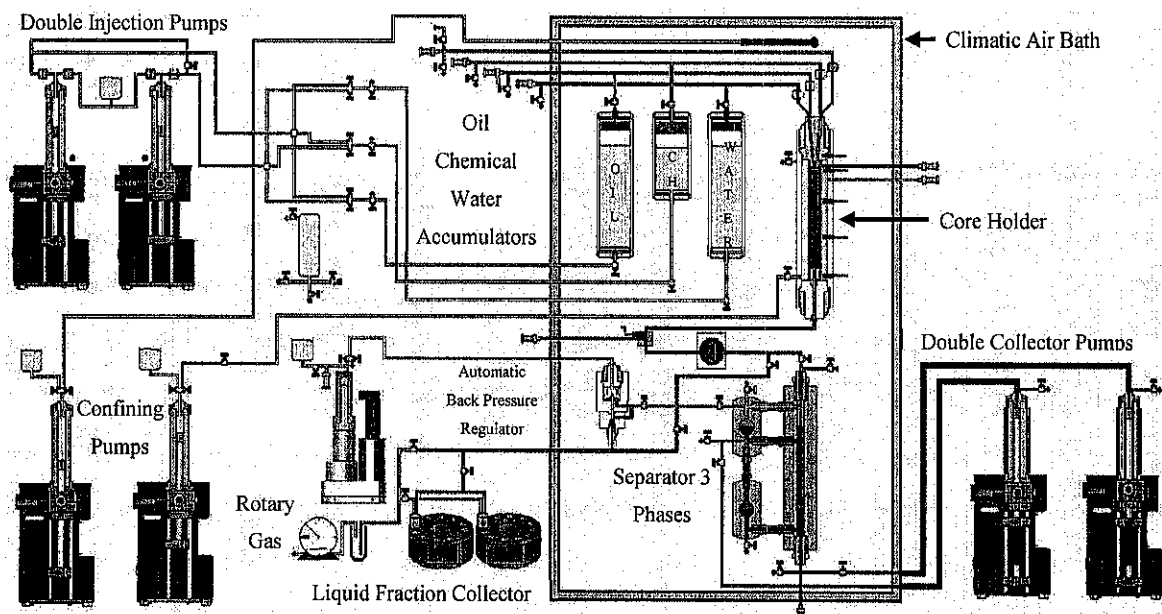


Figure 3.10: Schematic of experimental set-up used for displacement experiments

A rubber sleeve is placed inside core holder to apply confining pressure around the core sample. The confining pressure is applied around the core sleeve to prevent any fluid leakage or bypass around the core sample during the displacement

experiments the confining pressure on the core is provided by injecting distilled water in the annular space between core holder and rubber sleeve. The three accumulators are used to store oil, chemical, and water for delivery under high pressure up to 15,000 psi. The oil and water columns are from stainless steel which can hold a volume of 3000 cc. The chemical accumulator can hold a volume of 1000 cc from hastelloy materials which are resistant to corrosion. Three accumulators can work in a range of temperature from ambient to 200°C. The outlet port can connect to automatic fractional collector or three-phase separator through a back pressure regulator for collection of produced fluid from the core sample. A back pressure regulator (BPR) can maintain a constant pressure in system by blocking flow until system pressure reaches the set pressure.

The automatic fraction collector is used to collect the different fraction at the output of the differential valve continuously. It is composed with two heated trays that each tray can accommodate three different size of collecting tubes with capacity of 20, 15, and 10 cc. Each tray can hold twelve collecting tubes or collection liquid fraction. The temperature of fraction collector can be increased from ambient to 80 °C. It is worthwhile to mention that in a single experiment it is not possible to use both separator and fraction collector simultaneously.

A three-phase separator is used to measure produced oil, gas, and water from coreflooding experiments. The separator works based on infrared detection system which varies with physical properties of the phases. An infrared phase detection system includes a light source for emitting into a fluid. A detector can detect the attenuation of the infrared wavelength band as the infrared radiation passing through a fluid. Different fluids have a different but specific output signal which is used to determine the phase type. There are two infrared detection systems to determine the water-oil contact and gas-oil contact. At the beginning of experiments both contacts should exactly be adjusted in front of infrared system as shown in Figure 3.11. Any changes in fluid level can be detected by signal changes.

There are two collecting pumps and a wet rotary gas meter which can collect and measure the produced liquids and gases. A rotary gas meter which works upon the principle of positive displacement measures the cumulative volume of gas released.

The sample gas stream rotates a measuring drum within a packing fluid, usually water or low viscous "white" (clear) oil. A needle-dial and counting mechanism, coupled to the rotating drum, records the volume of gas flow as it sequentially fills and empties from the drum's rigid, fixed volume measuring chambers. The complete coreflooding system is placed inside the digital oven system therefore; the system temperature can be controlled and kept at a certain temperature. For this study, the temperature of all coreflooding experiments is kept around 60°C. Also, the back pressure regulator always is used to keep coreflooding system pressure around 1500 psi.

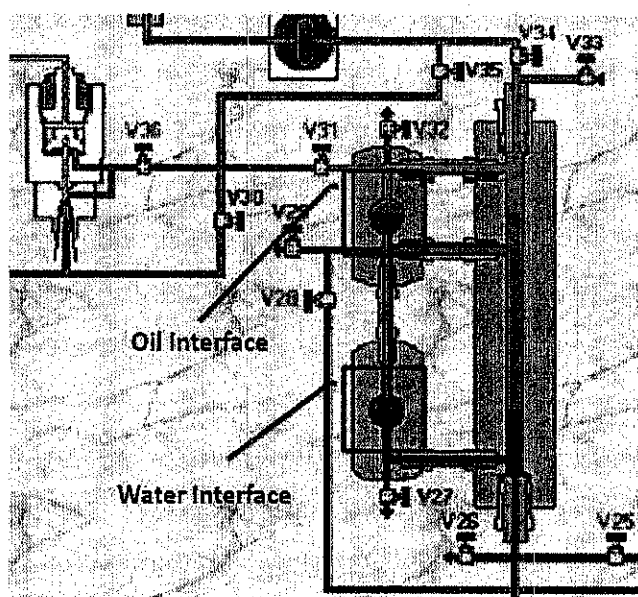


Figure 3.11: Schematic of three-phase separator in coreflooding system

3.7 Coreflooding Procedure in Water-Oil System

The unsteady-state or dynamic displacement method is most frequently applied method in reservoir analysis of strong wetting preference, and with homogeneous samples. Therefore, in this study the unsteady-state method based on Johnson *et al.* (1959) is used for determination of relative permeability data. The procedure for performing an unsteady-state displacement as previously explained in Chapter 2 is relatively simple, fast, and well-known. In the following, for each core sample, the subsequent experimental procedure is separately applied to investigate the effect of asphaltene precipitation and deposition on relative permeability and reservoir performance in the water-oil system. The details of measurement and calculation of

the relative permeability in the water-oil system which are affected by asphaltene deposition for each core sample are presented in the analysis of data and discussion of results chapter;

- a) *Determination of basic core properties*: The bulk volume of the core is computed from measurements of dimensions of uniformly shaped core sample. After weighting the dry core sample, brine of 10,000 ppm sodium chloride concentration is used for saturation of core sample. The saturation is done by using vacuum pump and extracting out the initial fluid inside the sample and replacing the void pore spaces of the sample with prepared brine. The core sample is weighed again to determine the wet weight of core sample. The value of pore volume is computed from the difference between the dry and the wet weight of the rock sample and brine density.
- b) *Preparation and setting-up system*: The saturated core sample is inserted into rubber sleeve, and carefully tightens in the core holder to insure direct contact between core sample and core holder end pieces. The three accumulators are fully filled by crude oil sample, brine water and n-heptane. The core flooding system temperature is increased to the 60 °C and the overburden pressure is applied on the rubber sleeve which is always 500 psi over than injection pressure. The back pressure regulator is used to control the coreflooding system pressure around 1500 psi
- c) *Absolute permeability, irreducible water and initial oil saturations measurements*: The brine is injected into the core at a constant flow rate of 1.0 cc/min until the pressure drop across the core is stabilized and a steady-state condition is attained. The absolute core permeability is calculated using the Darcy's law and the stabilized pressure drop. Then, the oil is injected into the core at same system injection pressure condition to displace brine water at a rate 0.5 cc/min, until the pressure drop is again stabilized and no more water could be displaced from the core. Total amount of brine production is recorded during the oil injection process. Again the stabilized pressure drop is used to calculate effective oil permeability at irreducible water saturation by using Darcy's law. This is considered to be as the original effective oil permeability without asphaltene effects at irreducible water saturation. The irreducible

water saturation and initial oil saturation are then determined from the volumetric material balance.

- d) *In-situ asphaltene precipitation and deposition*: As stated previously, the ratio of n-heptane to oil injection can control the amount of asphaltene precipitation and deposition. The three ratios 20%, 50%, and 80% are selected to create different asphaltene precipitation and deposition. The first core plug sample is used for the case without asphaltene precipitation that means with 0 % ratio n-heptane to oil injection. The three other core plug samples that are cut from long core sample and with mostly same property are used for the ratios of 20%, 50%, and 80% respectively. All steps from (a) to (f) are separately done for all core plug samples except for first core plug sample, the step (d) is excluded. The n-heptane is injected simultaneously along with oil injection but separately port injection with pre-selected ratio. During this process the injection pressure and pressure drop are recorded and monitored. Increase in the injection pressure is an indication of asphaltene deposition. Some oil samples are collected for asphaltene weight percent determination during the simultaneously injection. This simultaneous injection is stopped after several hours and continued by only oil injection until the pressure drop once again stabilized and the core is saturated fully with oil. The material balance for asphaltene weight percent between the collected oil samples and injected oil is done to determine the amount of asphaltene that can be deposited inside the core for this simultaneously ratio injection.
- e) *Relative permeability measurements*: The oil injection is stopped after the core is fully saturated with oil at irreducible water saturation. The brine injection is again started to displace oil out at a rate 0.5 cc/min and the same system injection pressure condition. Time, pore volume injection, pressure drop across core, and oil and water production are measured continuously until pressure drop is again stabilized and no more oil could be displaced from the core. Effective water permeability at irreducible oil saturation is again calculated based on the stabilized pressure drop and using Darcy's law. Irreducible oil saturation and final water saturation are then determined from volumetric material balance which is explained by details later. The

commercial core flow simulator Sendra (2011), a black-oil simulation model, is used to determine the oil and water relative permeability. This simulator performs history matching of the experimental data (e.g. differential pressure, oil production, and water production) obtained in the lab to estimate the relative permeability data.

- f) *Cleaning*: After measurements of relative permeability by dynamic displacement of oil by water, core and coreflooding system are flashed again with n-heptane, and core is cleaned with toluene to extract the residual crude oil with its asphaltene and water. Then, the core is dried.

3.8 Coreflooding Procedure in Gas-Oil System

The unsteady-state or dynamic displacement method is again used to investigate the effect of asphaltene on relative permeability in the gas-oil system. In the following, for each core sample, similar subsequent experimental procedure as have been explained for water-oil system except the step one before the last indeed, step (e) is separately applied to investigate the effect of asphaltene precipitation and deposition on relative permeability and reservoir performance in the gas-oil system.

During dynamic experiments in gas-oil system instead of using brine injection in step (e) the gas injection should be used. Nitrogen is used for gas injection process. For this purpose after drain out the all brine from brine accumulator the nitrogen is transferred carefully from high pressure cylinder into accumulator at pressure less than 1500 psi. After heating up the nitrogen to the system temperature, indeed 60°C, the accumulator pressure reached to the 1500 psi exactly.

Therefore, in these experiments gas injection pressure is adjusted around 1500 psi similar to oil injection pressure during oil-water system. The gas is injected by setting a rate 0.5 cc/min for injection pump. Actually injection pump can inject water at a rate 0.5 cc/min and this injection can move the piston in bottom of accumulator and in result gas can be injected into core sample. Because of gas compressibility, the pressure inside this accumulator should be constant and around 1500 till it can be

assumed that this is the same as gas injection rate. The gas rate during gas injection should represent the typical reservoir gas velocities and pressure drops of 1 to 5 psi/ft.

For this purpose after stopping oil injection and when the core is fully saturated with oil at irreducible water saturation, gas injection is started to displace oil out at a rate 0.5 cc/min and the same system injection pressure condition. Again here the time, the pore volume injection, the pressure drop across the core, and the oil and gas production are measured continuously until pressure drop is again stabilized and no more oil could be displaced from the core. Effective gas permeability at irreducible liquid saturation is again calculated based on the stabilized pressure drop and using Darcy's law. Irreducible liquid saturation and final gas saturation are then determined from volumetric material balance.

The commercial core flow simulator Sendra (2011) is used to determine oil and gas relative permeability in presence of irreducible water saturation again here. The simulator performs history matching of the experimental data (e.g. differential pressure, oil production, water production) obtained in the lab to estimate the relative permeability data in gas-oil system. The details of measurement and calculation of the relative permeability in the gas-oil system which are affected by asphaltene deposition for each core sample are presented in the analysis of data and discussion of results chapter.

3.9 Core Flow Simulator

A commercial black-oil core flow simulator, Sendra (2011) is used as a one dimensional two-phase simulation model for analyzing special core analysis experimental data. The simulator uses a history matching procedure to reconcile the experimental data, e.g. for water-oil system differential pressure across the core, oil production and water production which obtained in the lab during the experimental performance. This simulator is useful for analysis experimental data in the water-oil system as well as gas-oil system; also the two processes drainage and imbibition can be considered. It is worth noting that the software is equipped with some correlations

for estimation of the relative permeability curves such as Corey and LET (Lomeland-Ebeltoft-Thomas) correlations (Corey, 1954; Lomeland *et al.*, 2008).

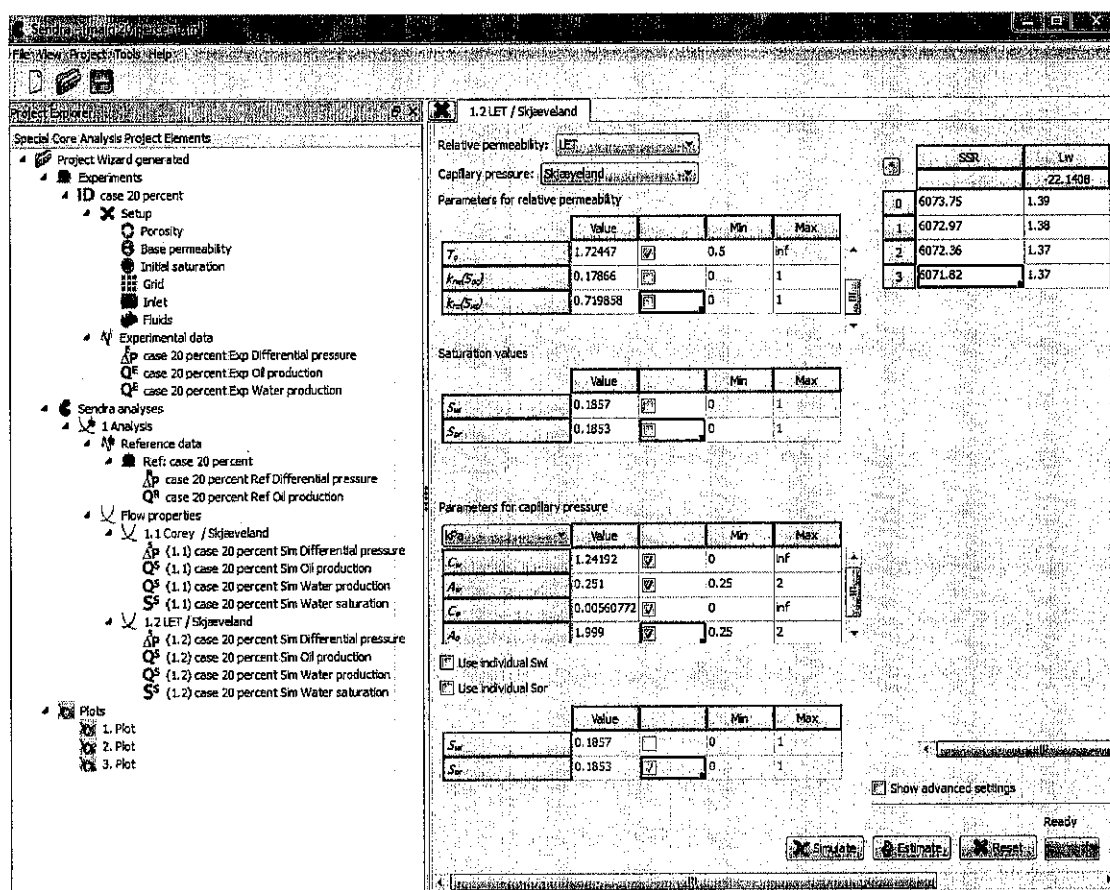


Figure 3.12: Main functionalities of main window of Sendra at start up

The main window of Sendra at start up is shown in Figure 3.12. In first step of using this simulator, the water-oil system or the gas-oil system and also the drainage process or the imbibition process should be chosen. Then, general core specifications are introduced into simulator such as length, diameter, porosity, absolute permeability, injection rate, and initial water saturation.

In the next step, experimental data vs. time are introduced into software such as differential pressure across the core, oil production and water production for water-oil system and differential pressure across the core, oil production and gas production for gas-oil system which obtained in the lab during the experimental performance. Then, one correlation such as Corey correlation is chosen and fourth endpoints of relative permeability curves are introduced. These fourth endpoints of relative permeability curves which are computed during experiments and explained in the analysis of data

and discussion of results chapter, are known parameters and can be directly used into the simulator.

For water-oil system they are effective oil permeability at irreducible water saturation which is an endpoint in oil relative permeability curve, effective water permeability at residual oil saturation which is an endpoint in water relative permeability curve, irreducible water saturation which means zero effective water saturation and residual oil saturation which means zero effective oil saturation. In addition, for gas-oil system they are effective oil permeability at irreducible gas saturation which is an end-point in the oil relative permeability curve, effective water permeability at residual liquid saturation which is an end-point in the gas relative permeability curve, irreducible gas saturation which means zero effective gas saturation and residual liquid saturation which means zero effective oil saturation.

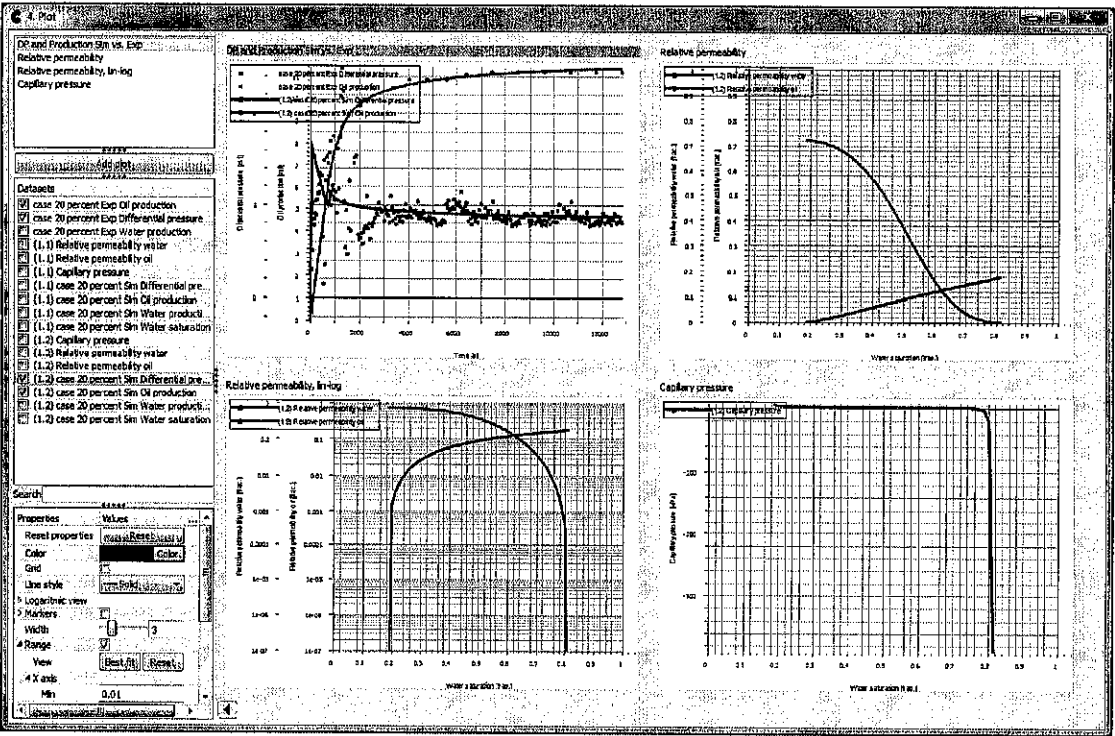


Figure 3.13: Plot window with several plots after matching process

Typically, an estimation step should preferably be initiated with one correlation and then proceed with more other correlations until an adequate history match of the experimental data are obtained. The experimental data which are used during history matching of this study are pressure drop across the core sample, oil cumulative production, and water cumulative production data. Figure 3.13 shows a plot window

with several plots after matching process. The reader is referred to user's manual of this simulator for further details (Sendra, 2011). The details of computation of the relative permeability in the water-oil system and gas-oil system which are affected by asphaltene deposition for each core sample are presented in the analysis of data and discussion of results chapter.

3.10 Relative Permeability Correlations

In many cases, relative permeability data on actual samples from reservoir under study may not be available. Hence, for such cases it is necessary to have the desired relative permeability data based on correlations so that it can be used such relative permeability data for prediction purposes. To the best of the author's knowledge, there exists no correlation available in the literature that can be used to predict the relative permeability alteration due to asphaltene deposition which considers amount of asphaltene as an independent variable. It has been reported (Kalantari *et al.*, 2008; Alizadeh *et al.*, 2009) that some of its effect may be captured by wettability change and relative permeability shift from a water-wet to an oil-wet (or a mixed-wet) system.

In this research, new experimental correlations are obtained and presented to predict the effect of asphaltene deposition on irreducible water saturation, residual oil saturation, and water-oil relative permeability, and gas-oil relative permeability. The correlations are obtained by history matching experimental data from several dynamic displacement experiments (conducted on the different core-plug samples, but having the same rock properties under reservoir conditions) with corresponding data from a one-dimensional two-phase black-oil simulation model. Here, based on dynamic experimental data, some correlations for relative permeability having effects of asphaltene deposition are developed.

Like most of the relative permeability correlations, obtained correlations use the normalized water saturation as one of the correlating parameters. In addition to this parameter the amount of asphaltene deposition per pore volume apply as a new independent variable. Moreover, the three-phase relative permeability data which

altered with asphaltene deposition are obtained from well-known three-phase model such as the Stone's II model. The details of the developments of these correlations for water-oil relative permeability and gas-oil relative permeability and three-phase relative permeability which are affected by asphaltene deposition are presented in the analysis of data and discussions of results chapter.

3.11 Summary

In this chapter, a methodology to investigate the effect of asphaltene deposition on relative permeability data is given. It includes some descriptions for the equipment and materials preparation, basic experiments measurements for rock and fluid samples, coreflooding experiments procedures in water-oil and gas-oil systems. Also a one-dimensional two-phase simulation model for estimating two-phase relative permeability curves is given.

CHAPTER 4

ANALYSIS OF DATA AND DISCUSSION OF RESULTS

4.1 Overview

In this chapter, first, the experimental data which are obtained during the basic core and fluid analysis process and coreflooding experiments in water-oil and gas-oil system are presented together with some analyses and discussions for them. These data mostly include pressure drop across the core, oil production, and water production versus time for coreflooding experiments. The end-point saturations during coreflooding experiments for water, oil and gas are computed based on material balance calculation. The end-point effective and relative permeability for water, oil, and gas are computed based on the amount of pressure drop data during steady-state conditions, rock and fluid properties, and using the Darcy law.

The entire curves of relative permeability for water-oil and gas-oil systems are estimated during history matching processes of experimental data and using a one-dimensional two-phase black-oil simulation model. The Stone's II model is used to compute three-phase relative permeability for oil phase. The non-linear multi-regression analysis based on matching process results is used to develop the appropriate correlations for irreducible water saturation, residual oil saturation, water relative permeability, gas relative permeability, and oil relative permeability in as a function of asphaltene deposition.

4.2 Experimental Results

In this section, all experimental results during this study are given. The fluid and core samples properties measurement follows by asphaltene weight percent determination are presented and the results of all coreflooding experiments are all described.

4.2.1 Fluid Properties Measurements

As previously explained, sodium chloride with more than 99.5 % purity and 58.44 g/mol molecular weight is used to make synthetic brine water with 10,000 ppm or 0.1 percent sodium chloride concentration in both water-oil and gas-oil systems. For this purpose each one liter of distilled water is mixed with 10 gram of sodium chloride. The mixture is stirred around 30 minute by using magnetic stirrer hard plate.

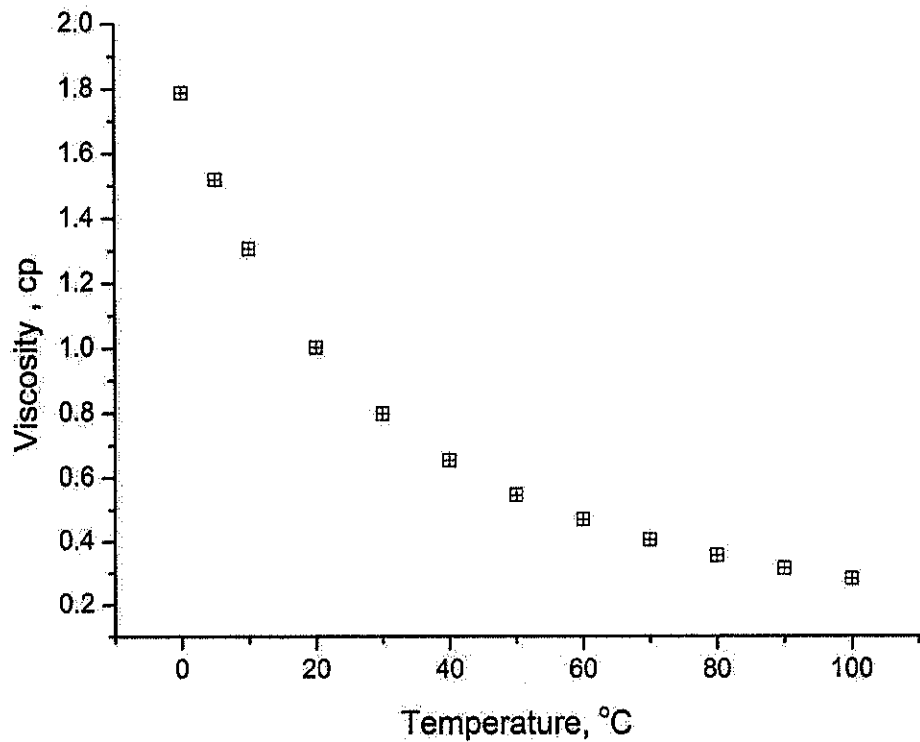


Figure 4.1: Calculated brine viscosity versus different temperatures (Ozbek, 2010)

The brine water density is measured in a digital densitometer. The amount of brine density at 20 °C, is measured 1.005 g/cc. Also the brine water viscosity at different temperature is calculated from the report given by Ozbek (2010). The Ozbek’s report includes a summary of selected analytical expressions and correlations

which describe the change in viscosity of sodium chloride solutions as a function of concentration, temperature, and pressure (Ozbek, 2010). Figure 4.1 shows the calculated values of brine water viscosity for a brine solution with 10,000 ppm sodium chloride concentration as a function of different temperatures at experimental pressure of 1500 psi.

Moreover, the crude oil density is also measured in a digital densitometer, and its viscosity is also measured in an electromagnetic viscometer at different temperatures. Table 4.1 presents the general specification of crude oil sample used for this experimental study. Shown in Figure 4.2 is the variation of viscosity of this crude oil sample as a function of temperature and experimental pressure of 1500 psi.

Table 4.1: General properties of crude oil sample

Property	API gravity	Density @20°C , g/cc	Viscosity @20°C, cp	C ₇ Asphaltene wt%
Crude Oil	29.30	0.880	15.6	2.7

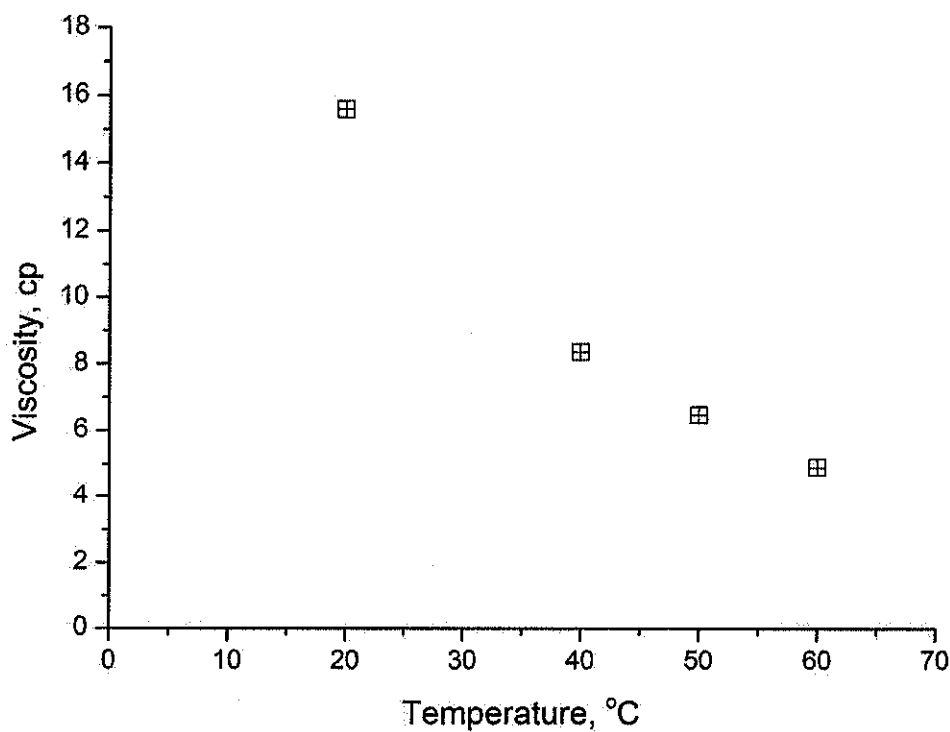


Figure 4.2: Crude oil viscosity versus different temperature

The gas viscosity is not commonly measured in laboratory because it can be estimated from empirical correlations. However the gas viscosity correlations have

been derived from experimental measuring which were done at low to moderate pressures (less than 10,000 psi) and temperature (less than 150 °C) and cannot confidently extrapolated to high pressure and high temperature gas reservoir conditions (Ling *et al.*, 2009). As has been approved by Ling *et al.* (2009) through the laboratory investigation the experimental nitrogen viscosity values are lower than the values which obtained from some empirical correlations at high pressure high and temperature conditions. They observed that the difference increase as temperature decrease, and it increase as pressure increase. In this study the experiments conditions are less that these criteria, therefore, the empirical correlation which is given in Ling *et al.* (2009) study can be used. Figure 4.3 shows the variation of nitrogen viscosity at different temperatures versus pressure from Ling *et al.* (2009) experimental data.

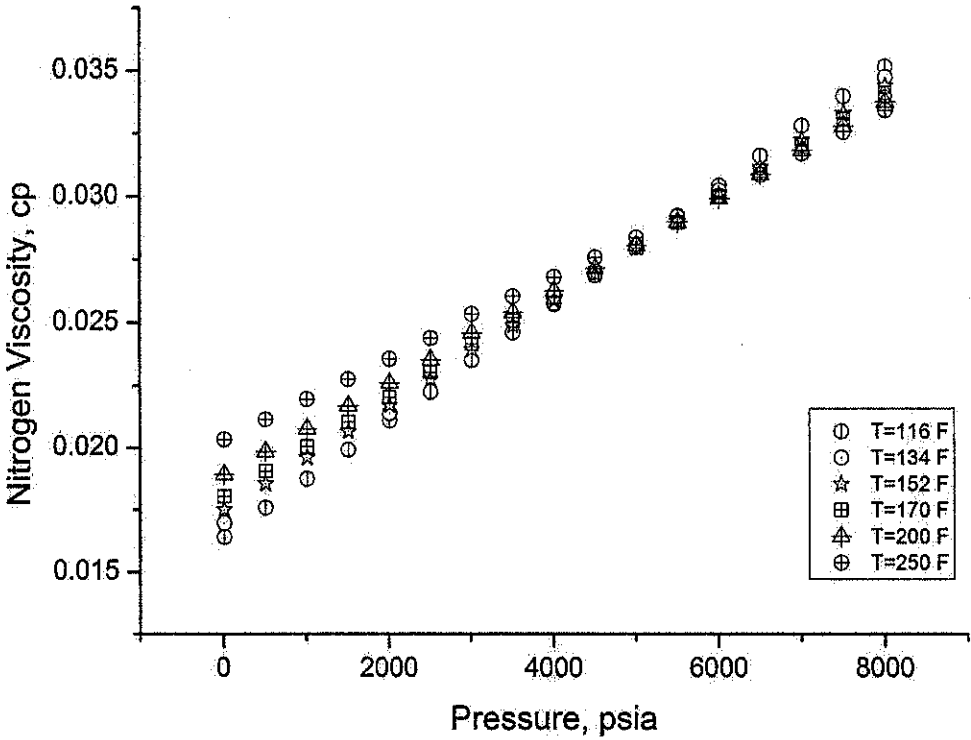


Figure 4.3: Nitrogen viscosity vs. pressure at different temperatures (Ling *et al.*, 2009)

4.2.2 Core Properties Measurements

The basic rock properties measurements such as the pore volume, the bulk volume, the porosity, and the absolute permeability are necessary to characterize the core samples before starting any coreflooding experiment. As previously mentioned the

two one-foot long core samples is cut into four three-inch plug pieces by using core cutter machine. The core plug samples have regular cylindrical shape and therefore, the bulk volumes can be calculated by measuring diameter and length of each core plug sample according to the cylinder volume equation;

$$BV = \frac{\pi}{4}(D)^2(L) \quad (4.1)$$

where;

BV is bulk volume of core plug sample, cm³

D is core plug diameter, cm

L is core plug length, cm

Also the porosity for each core plug sample can be calculated by considering the ratio of pore volume of the core plug sample to the bulk volume of the core plug sample;

$$\phi = \frac{PV}{BV} \times 100 = \frac{(BV - GV)}{BV} \times 100 \quad (4.2)$$

where;

ϕ is the porosity, percent

PV is pore volume, cm³

GV is grain volume, cm³

In this study the porosity values have been measured by using two methods. In the first method Poroperm was used and the second method was during core saturation process with brine water. The dry weights of core plug samples are measured by digital balance carefully before stating any measurements. The Boyle-Mariotte's Law is used to determine grain and pores volume from the expansion of a known mass of helium into a matrix cup in Poroperm experiments, whereas pore volume can be computed based on the difference between dry weight of core plug sample and wet

weight of core plug sample and knowing density of saturated fluid during the saturation method. The brine density is measured by digital density meter at lab temperature. Therefore, after saturating the core plug samples with brine water it is necessary to measure the weight of the core samples. The pore volume of core plug samples is calculated according to following equation;

$$PV = \frac{W_{Sat} - W_{Dry}}{\rho_{Brine}} \quad (4.3)$$

where;

W_{Sat} is weight of wet or saturated core, g

W_{Dry} is weight of dry core, g

ρ_{Brine} is brine density at room temperature, g/cm³

In addition, the Poroperm can be measured the gas permeability determination based on steady-state method (pressure falloff) and using Darcy's Law. The basic core properties which are computed during these experiments for all core plug samples are given in Table 4.2 and Table 4.3. As can be seen the porosity values of core samples almost same from two methods.

Table 4.2 shows the basic core properties calculation from Poroperm experiments. The length, the diameter, the bulk volume, the grain volume, the pore volume, the porosity, and the permeability of each core plug sample are given in different columns, respectively. The infinity permeability in the last column indicates a Klinkenberg correction for air permeability. In petroleum engineering, a Klinkenberg correction is a procedure for calibration of permeability data obtained from a Poroperm instrument. When using nitrogen or helium gas for core plug measurements, the Klinkenberg correction is usually necessary due to the so called Klinkenberg gas slippage effect (Klinkenberg, 1941).

Moreover, Table 4.3 shows the basic core properties calculation from saturation method. The length, the diameter, the bulk volume, the brine density, the dry weight,

the wet weight, the pore volume, and the porosity of each core plug sample are given in different columns, respectively.

Table 4.2: Basic core properties from Poroperm instrument

Core sample	Length, cm	Diameter, cm	Bulk volume, cubic cm	Grain volume, cubic cm	Pore volume, cubic cm	Porosity, %	Air permeability, md	Infinity permeability, md
A-1	7.62	3.81	86.831	68.339	18.492	21.297	301.081	280.214
A-2	7.65	3.81	87.173	68.556	18.613	21.352	312.255	275.478
A-3	7.62	3.81	86.831	67.708	19.123	22.023	308.325	284.325
A-4	7.60	3.81	86.603	68.371	18.232	21.052	307.284	288.328
B-1	7.65	3.81	87.173	67.974	19.199	22.024	420.052	390.524
B-2	7.62	3.81	86.831	68.121	18.710	21.548	411.265	385.358
B-3	7.62	3.81	86.831	66.926	19.905	22.924	402.884	374.455
B-4	7.60	3.81	86.603	67.043	19.559	22.585	416.258	387.145

Table 4.3: Basic core properties from saturation method

Core sample	Length, cm	Diameter, cm	Bulk volume cubic cm	Brine density, g/cubic cm	Dry weight, g	Wet weight, g	Pore volume, cubic cm	Porosity, %
A-1	7.62	3.81	86.831	1.0074	166.197	185.321	17.806	21.863
A-2	7.65	3.81	87.173	1.0074	167.012	186.128	17.799	21.768
A-3	7.62	3.81	86.831	1.0074	166.052	185.192	17.821	21.881
A-4	7.60	3.81	86.603	1.0074	165.885	185.022	17.818	21.935
B-1	7.65	3.81	87.173	1.0074	167.107	186.224	18.731	21.769
B-2	7.62	3.81	86.831	1.0074	166.255	185.365	18.724	21.845
B-3	7.62	3.81	86.831	1.0074	166.108	185.221	19.286	21.850
B-4	7.60	3.81	86.603	1.0074	165.325	184.515	18.797	21.996

4.2.3 Asphaltene Weight Percent

The displacement experiments were conducted for all core plugs in two water-oil and gas-oil systems where the ratios of n-heptane to oil injection were varied from 0%, 20%, 50%, and 80%. The amount of deposition for each ratio of injection in each system is determined based on measurements of asphaltene weight percent in the collected samples and material balance calculation. As mentioned previously, the asphaltene weight percent in the crude oil sample is experimentally computed by using the IP143 standard method. As can be seen in Table 4.1, the initial amount of asphaltene weight percent in dead crude oil sample which is used during each displacement experiment was found approximately 2.7 weight percent.

The material balance equation given below is used to compute the equivalent values of asphaltene deposition inside the core samples;

$$Asphaltene\ deposition = \frac{2.70000 - Asphaltene\ in\ Collected\ Sample}{2.70000} \times 100 \tag{4.4}$$

where the values of asphaltene in collected sample in the right-hand side of (4.4) are experimental measured values of asphaltene weight percent in collected oil samples that obtained from the displacement experiments. These values are given in Table 4.4 as a function of the ratios of n-heptane to oil injection together with the computed values for the equivalent amount of asphaltene deposition inside the core from (4.4). Figure 4.4 shows the equivalent values of asphaltene deposition at various ratios of n-heptane crude oil injections for water-oil system.

Table 4.4: Equivalent values of asphaltene deposition inside core samples

Ratio of n-heptane to oil injection, %	Asphaltene weight percent in collected samples, wt %	Equivalent values of asphaltene deposition, %
0	2.70000	0.0000
20	2.62441	2.79963
50	2.58256	4.34963
80	2.46376	8.74963

During experiments of gas-oil system the same simultaneously injection times and rates are applied. Due to all core plug samples have sandstone lithology and almost identical properties, it is assumed that same amount of deposition is occurred. As shown the amount of asphaltene deposition increases as well as amount of n-heptane increases. The amount of deposition should be directly related to pores geometry, pores size distribution, surface area, amount of solvent pore volume injection, rate injection, and absolute permeability (Leontaritis *et al.*, 1994; Civan, 2000; Shedid, 2001; Sim *et al.*, 2005).

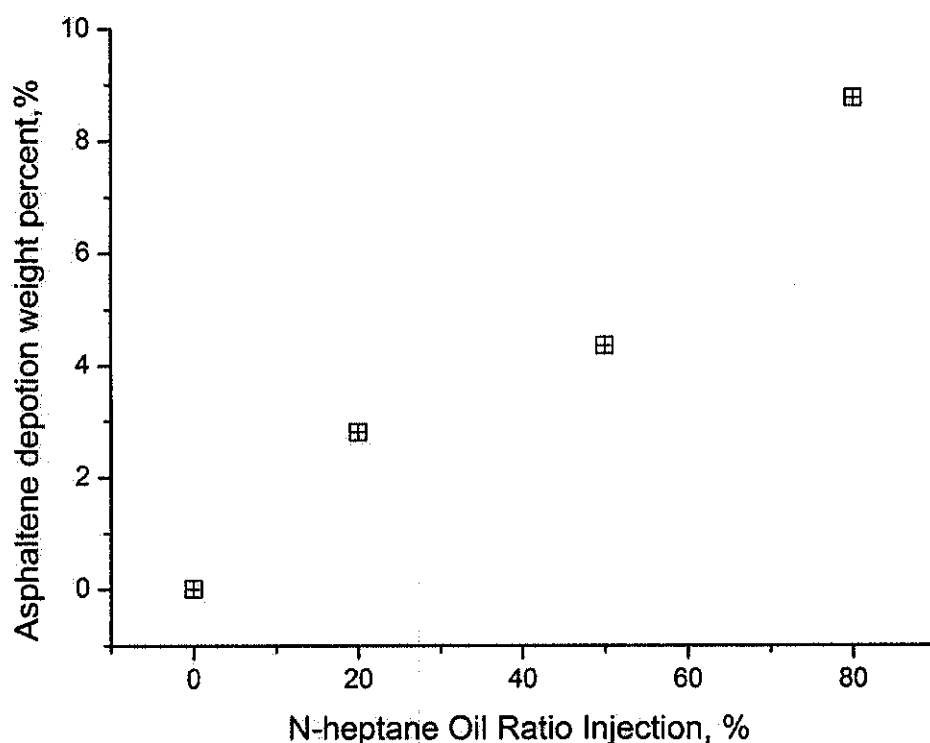


Figure 4.4: Amount of asphaltene deposition at various ratios of n-heptane crude oil injections

4.2.4 Brine Permeability and Fluid Saturation

In water-oil and gas-oil systems after saturating the core plug samples with brine and before each coreflooding experiment, the saturated core plug sample is loaded into core holder of coreflooding system separately and then, confining pressure is applied by pumping distilled water in the annular space between rubber sleeve and core holder. During core flooding experiments, it should be ensured that the confining

pressure is at least 500 psi higher than injection fluid pressure in the core; otherwise, flow of fluids from the curved surface of the core will occur. After confining pressure is applied, core holder is placed in the oven, and the oven is set to experimental temperature. All flow tubing connections are made and the system is checked for leakages. Typically, the saturated core is first flooded with same brine which is used for core saturation to obtain the absolute permeability of the core sample. The brine injection continues until a steady-state condition which means a constant pressure drop during injection. The brine absolute permeability of core is calculated according to Darcy's law which is the following equation:

$$k = \frac{14700 \times \mu \times Q \times L}{A \times \Delta P} \quad (4.5)$$

where;

k is liquid permeability, md

μ is viscosity of flowing liquid (brine), cp

Q is liquid (brine) flow rate, cc/sec

L is length of core sample, cm

A is area of core sample, cm²

ΔP is differential pressure across core sample, psi

14700 is a conversion factor

The experimental values of all required parameters in the right-hand side of equation (4.5) during brine injection in both water-oil system and gas-oil system are given in Table 4.5 and Table 4.6 with the computed values for absolute permeability of core samples respectively. The values of brine absolute permeability that are calculated based on this method are a little less than the values that have been obtained from Poroperm experiments. In addition, as can be seen in Table 4.5 the brine permeability values are close to each other in all experiments except for 50%

experiment. Also in Table 4.6 the brine permeability values are close to each other in all experiments except for 20% experiment. These values are a bit lower than other values which it may be caused by some errors during reading the pressure drop.

Table 4.5: Brine absolute permeability of core samples (water-oil system)

Brine permeability, md	Pressure drop, psi	Brine rate, cc/min	Brine viscosity, cp	Diameter, cm	Length, cm	Ratio of n-heptane to oil injection, %
273.250	0.14	0.50	0.467	3.81	7.62	0
274.326	0.14	0.50	0.467	3.81	7.65	20
255.033	0.15	0.50	0.467	3.81	7.62	50
272.533	0.14	0.50	0.467	3.81	7.60	80

Table 4.6: Brine absolute permeability of core samples (gas-oil system)

Brine permeability, md	Pressure drop, psi	Brine rate, cc/min	Brine Viscosity, cp	Diameter, cm	Length, cm	Ratio of n-heptane to oil injection, %
320.047	0.12	0.50	0.467	3.81	7.65	0
294.269	0.13	0.50	0.467	3.81	7.62	20
318.792	0.12	0.50	0.467	3.81	7.62	50
317.955	0.12	0.50	0.467	3.81	7.60	80

The brine injection is then stopped and crude oil injection is again started. The crude oil injection is continued till the core saturation reaches to the irreducible brine saturation and constant pressure drop should obtain again across core sample. In the next step, n-heptane is allowed to inject simultaneously along with oil injection with pre-selected ratio. As previously stated, ratios 0%, 20%, 50%, and 80% are chosen to produce different asphaltene deposition inside the core samples. During this step it was observed that the oil injection pressure is sharply increased and then drastically decreased. This phenomenon is observed periodically for different coreflooding

experiments. The similar trend for oil injection pressure values almost have been observed during all core flooding experiments. Figure 4.5 shows an example of the oil injection pressure values for the case with 50 % ratio injection in water-oil system. It seems that the simultaneously injection of oil and n-heptane has created some asphaltene particles which it could seal the pores in injection points and it causes increasing in the injection pressure. However, after increasing the injection pressure to some values the asphaltene can be moved and the injection pressure has decreased. These phenomena can be considered an indication of occurring asphaltene deposition inside the core sample.

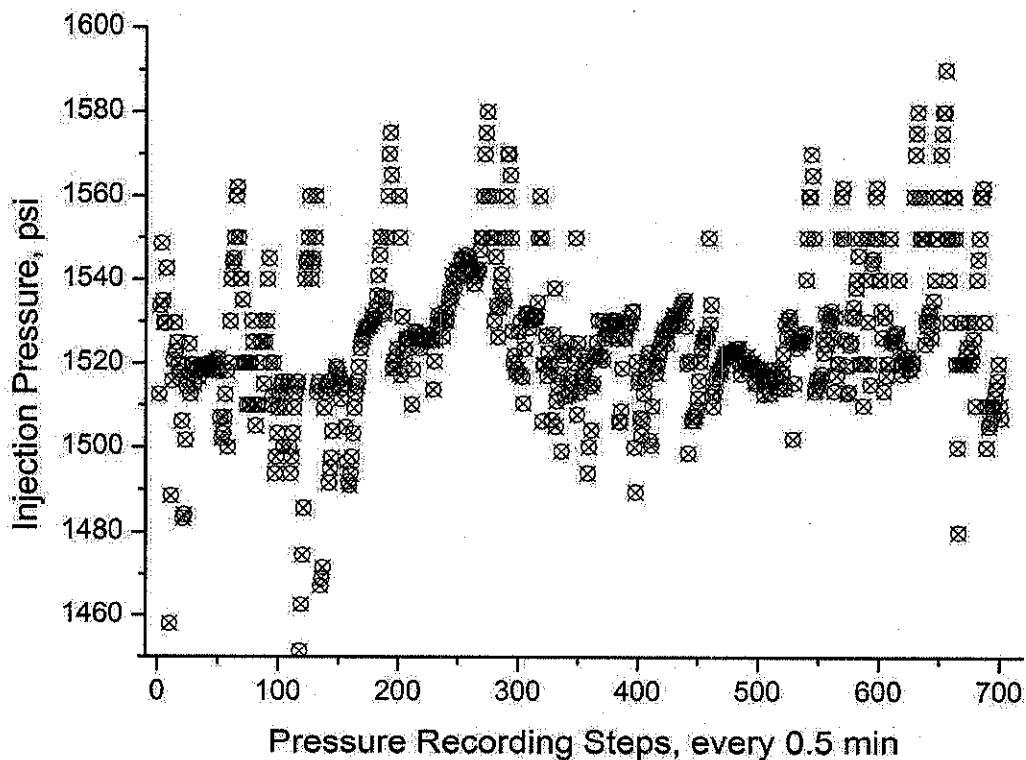


Figure 4.5: Oil injection pressure during simultaneously n-heptane and oil injection (50%, water-oil system)

The simultaneous injection of n-heptane and oil after several pore volume injections are then stopped, however, oil injection is still continued until the pressure drop once again stabilized. Once more by using Darcy's law (Equation 4.5) and stabilize pressure drop across the core, effective oil permeability can be calculated at irreducible brine saturation. Also oil relative permeability at this step can be defined as the ratio of the effective oil permeability at irreducible brine saturation to the brine permeability which is measured previously at 100 percent brine saturation. The

experimental values of all required parameters to compute the effective and relative oil permeability during the oil injection for both water-oil and gas-oil systems are given in Table 4.7 and Table 4.8, respectively. Also the computed values for effective oil permeability and relative oil permeability of core samples based on this method can be seen in two last columns.

Table 4.7: Effective and relative oil permeability (water-oil system)

Ratio of n-heptane to oil injection, %	Length, cm	Diameter, cm	Oil viscosity, cp	Oil rate, cc/min	Pressure drop, psi	$k_{eo}(S_{wi})$, md	$k_{ro}(S_{wi})$, fraction
0	7.62	3.81	4.70	0.50	1.50	256.67	0.9589
20	7.65	3.81	4.70	0.50	2.00	192.67	0.7198
50	7.62	3.81	4.70	0.50	2.25	171.11	0.6393
80	7.60	3.81	4.70	0.50	2.51	153.39	0.5731

Table 4.8: Effective and relative oil permeability (gas-oil system)

Ratio of n-heptane to oil injection, %	Length, cm	Diameter, cm	Oil viscosity, cp	Oil rate, cc/min	Pressure drop, psi	$k_{eo}(S_{wi})$, md	$k_{ro}(S_{wi})$, fraction
0	7.65	3.81	4.70	0.50	1.3	297.33	0.9506
20	7.62	3.81	4.70	0.50	1.5	256.67	0.8207
50	7.62	3.81	4.70	0.50	1.8	213.89	0.6839
80	7.60	3.81	4.70	0.50	1.9	202.10	0.6462

In addition the volume of produced water during oil injection can be used to calculate the initial oil saturation and irreducible water saturation. Indeed, the produced water volume is replaced by oil in the core sample, and represents the amount of the oil volume that saturates the core. Therefore, the initial oil saturation is the ratio of recovered water to core plug sample pore volume and remaining brine inside the core is irreducible water saturation as given by following equations;

$$S_{oi} = \frac{V_{water}}{PV} \quad (4.6)$$

$$S_{wi} = 1 - S_{oi} \quad (4.7)$$

where;

V_{water} is recovered water during oilflooding, cc

S_{oi} is initial oil saturation, fraction

S_{wi} is irreducible water saturation, fraction

The experimental recovered water volume and computed values for initial oil saturation and irreducible water saturation parameters in water-oil and gas-oil systems are given in Table 4.9 and Table 4.10, respectively.

Table 4.9: Initial oil saturation and irreducible water saturation (water-oil system)

Ratio of n-heptane to oil injection, %	V_{water} , cc	S_{oi} , %	S_{wi} , %
0	14.20	79.75	20.25
20	14.50	81.43	18.57
50	14.75	82.85	17.15
80	15.00	84.24	15.76

Table 4.10: Initial oil saturation and irreducible water saturation (gas-oil system)

Ratio of n-heptane to oil injection, %	V_{water} , cc	S_{oi} , %	S_{wi} , %
0	15.00	79.43	20.57
20	15.10	79.96	20.04
50	15.20	80.49	19.51
80	15.15	80.23	19.77

4.2.4.1 Water-Oil System

In water-oil system brine is injected again to simulate waterflooding process. The brine injection is continued until no more oil can be produced which means reaching to residual oil saturation into the core sample. Once more, in this step the effective brine permeability at residual oil saturation, the relative brine permeability, the oil saturation and the brine saturation parameters can be calculated. The effective brine permeability at residual oil saturation and the brine relative permeability are computed as same method as previously mentioned for oil. The all experimental required parameters and computed values for effective brine permeability at residual oil saturation and relative brine permeability are given in Table 4.11.

Table 4.11: Effective and relative water permeability (water-oil system)

Ratio of n-heptane to oil injection, %	Length, cm	Diameter, cm	Brine viscosity, cp	Brine rate, cc/min	Pressure drop, psi	$k_{ew}(S_{or})$, md	$k_{rw}(S_{or})$, fraction
0	7.62	3.81	0.467	0.5	1.35	28.34	0.1059
20	7.65	3.81	0.467	0.5	0.80	47.82	0.1787
50	7.62	3.81	0.467	0.5	0.65	58.85	0.2199
80	7.60	3.81	0.467	0.5	0.50	76.51	0.2859

The residual oil saturation after waterflooding can be very easily calculated based on subtraction of recovered oil from the initial oil as following;

$$S_{or} = \frac{V_{water} - V_{oil-w}}{PV} \quad (4.8)$$

$$S_{wf} = 1 - S_{or} \quad (4.9)$$

where;

S_{or} is residual oil saturation, fraction

S_{wf} is final brine saturation, fraction

V_{oil-w} is recovered oil during waterflooding, cc

The experimental values for recovered oil volume during waterflooding and computed values for residual oil saturation and final water saturation are given in Table 4.12.

Table 4.12: Residual oil saturation and final water saturation (water-oil system)

Ratio of n-heptane to oil injection, %	V_{oil-w} , cc	S_{or} , %	S_{wf} , %
0	10.85	18.81	81.19
20	11.20	18.53	81.47
50	11.65	17.41	82.59
80	12.10	16.27	83.73

The calculating these residual fluid saturation and related effective permeability values are important for computing relative permeability curves, and for determining recoverable oil for any EOR process. The values of these parameters are showed in the next subsection which has been entitled end-points of the relative permeability curves.

4.2.4.2 Gas-Oil System

In gas-oil system nitrogen gas is injected after stopping the oil injection instead of brine injection. The gas injection is continued until no more oil can be produced which means reaching to residual oil saturation into core sample. Once more, in this step the effective gas permeability at residual liquid saturation, the relative gas permeability, the oil saturation and the gas saturation parameters can be calculated similar procedure to the water-oil system. All experimental parameters and computed values for the effective gas permeability at residual liquid saturation and the relative gas permeability are given in Table 4.13. The residual liquid saturation, S_{lr} , is used for gas-oil system since the residual liquid saturation in this system includes the residual oil saturation plus irreducible brine saturation.

Table 4.13: Effective and relative gas permeability (gas-oil system)

Ratio of n-heptane to oil injection, %	Length, cm	Diameter, cm	Gas viscosity, cp	Gas rate, cc/min	Pressure drop, psi	$k_{eg}(S_{lr})$, md	$k_{rg}(S_{lr})$, fraction
0	7.65	3.81	0.02066	0.50	0.01*	169.91	0.5432
20	7.62	3.81	0.02066	0.50	0.01*	169.24	0.5411
50	7.62	3.81	0.02066	0.50	0.01*	169.24	0.5411
80	7.60	3.81	0.02066	0.50	0.01*	168.80	0.5397

The '*' symbol in sixth column of the Table 4.13 indicates that these values are under some uncertainty. The pressure drop values during coreflooding experiments are computed from difference between pressure inlet and pressure outlet sensors. Each pressure sensor can detect a minimum pressure change of 0.01 psi. Whereas, during gas injection, pressure drop values across a three-inch length core should be around some small values between 0.01 to 0.1 psi. For example the pressure drop values fluctuate and show some negative values in the 50% n-heptane to oil injection experiment as shown in Figure 4.6.

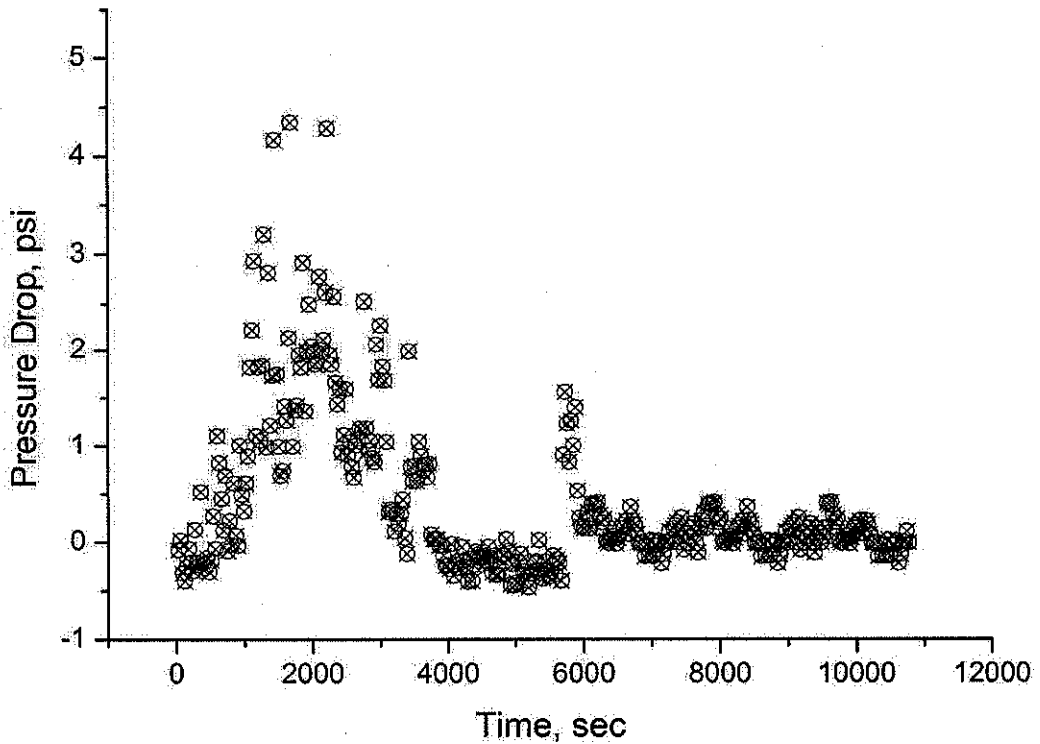


Figure 4.6: Pressure drop during gas injection (50%, gas-oil system)

Furthermore, it can be seen that they could not stabilize during steady-state period of gas injection. Therefore, it can be concluded that the obtained pressure drop data during all gas injection experiments are under some uncertainty. These may be related to gas injection technique which is used during these experiments and also limitation of reading accuracy of pressure sensors in this coreflooding system. To overcome this, a method for computation for the effective gas permeability at residual liquid saturation is proposed as explained in Section 4.2.5.2.

The residual liquid saturation after gas injection can be calculated by subtraction of recovered oil volume from the initial oil as following;

$$S_{lr} = \frac{V_{water} - V_{oil-g}}{PV} \tag{4.10}$$

$$S_{gf} = 1 - S_{lr} \tag{4.11}$$

where;

S_{lr} is residual liquid saturation, fraction

S_{gf} is final gas saturation, fraction

V_{oil-g} is recovered oil during gas injection, cc

Table 4.14: Residual liquid saturation and final gas saturation (gas-oil system)

Ratio of n-heptane to oil injection, %	V_{oil-g} , cc	S_{lr} , %	S_{gf} , %
0	7.10	41.83	58.17
20	7.00	41.30	58.70
50	7.15	41.57	58.43
80	7.10*	42.36	57.64

The experimental values for recovered oil volume during gas injection, computed values for residual liquid saturation, and final gas saturation are given in Table 4.14. The values of these parameters are used in the next subsection which has been entitled

end points of the relative permeability curves. The '*' symbol in last row of the second column in Table 4.14 indicates that this value is not obtained experimentally. During this experiment, for the 80% injection case, the back pressure value of coreflooding system faced some problems and it caused the experiment to be terminated. Therefore, 7.10 cc is considered as most probable value for recovered oil during gas injection based on other experiments.

4.2.5 End-Point of Relative Permeability Curves

In this section, the end-point of relative permeability curves for water-oil and gas-oil systems are shown in different graphs. The comparisons between these experimental results follows by detailed description are given.

4.2.5.1 Water-Oil System

As above mentioned, the irreducible water saturation, S_{wi} and the initial oil saturation, S_{oi} , are determined from the volumetric material balance during oil injection step. The computed values of these saturations for different ratios of n-heptane to oil injection are shown in Figure 4.7. Similarly, the residual oil saturation, S_{or} , and final water saturation, S_{wf} , during water injection step are computed again through the volumetric material balance (see Figure 4.8).

As can be seen from Figure 4.7, the initial oil saturation increased and hence, the irreducible water saturation decreased as the asphaltene deposition increased. These results indicate that some portions of the original irreducible water saturation become mobile as the asphaltene deposition increases. The residual oil saturation is also slightly decreased (Figure 4.8) with the asphaltene deposition. Shown in Figure 4.9 are the computed values of the end-point effective water, $k_{ew}(S_{or})$, and the end-point oil, $k_{eo}(S_{wi})$, permeabilities which are computed based on method has been explained above. As is seen from Figure 4.9, $k_{eo}(S_{wi})$ is decreased, while $k_{ew}(S_{or})$ is increased. In fact, all these results indicate the complex mechanisms leading to wettability

alterations and interfacial tension change in porous media due to asphaltene precipitation and deposition.

Similar and consistent results to these results shown in Figure 4.7, Figure 4.8, and Figure 4.9 have also been reported in the literature previously by some researchers such as Kim *et al.* (1990) and Kamath *et al.* (1993). These researchers attribute these results to wettability alteration, change of relative permeability curves, and interfacial tension (IFT) reductions between oil and asphaltene as a result of complex mechanisms of asphaltene precipitation and deposition in porous media.

However, as it is discussed later, based on experimental results of this study to be given in Section 4.2.7 entitled as oil recovery and sweep efficiency performance, to observe the improvement in sweep efficiency and oil recovery as a result of asphaltene deposition requires at least two pore volumes of water injection, which may not be feasible for example in real EOR applications.

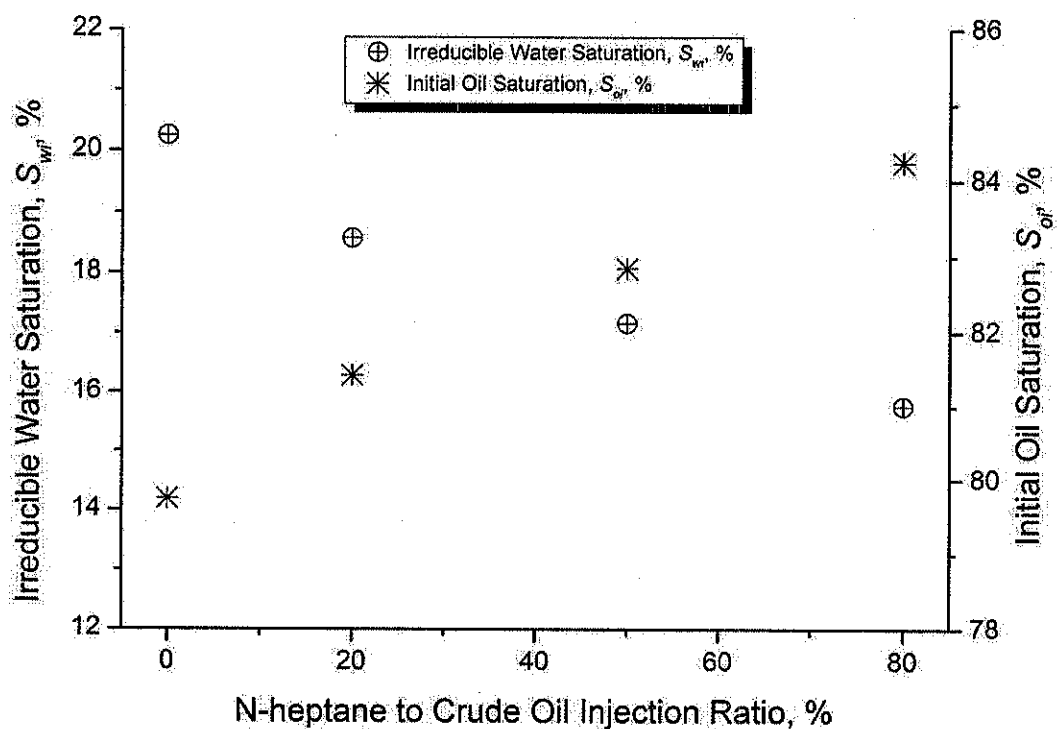


Figure 4.7: Irreducible water and initial oil saturation at various ratios of n-heptane–crude oil injections (water-oil system)

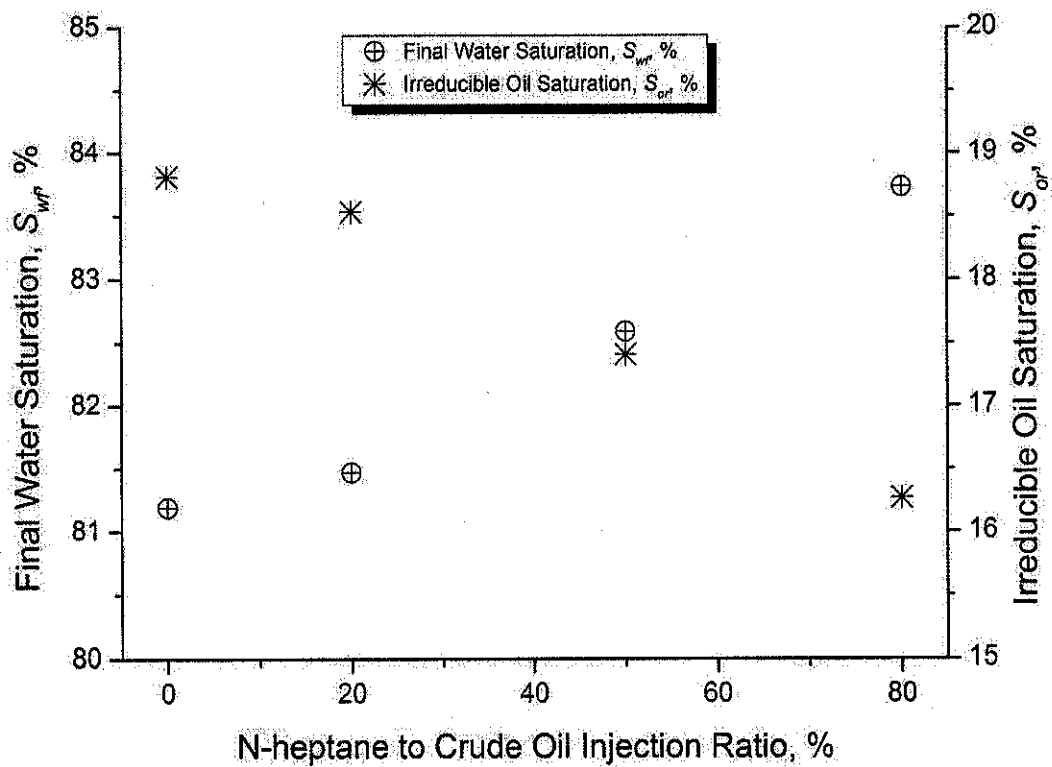


Figure 4.8: Residual oil and final water saturation at various ratios of n-heptane–crude oil injections (water-oil system)

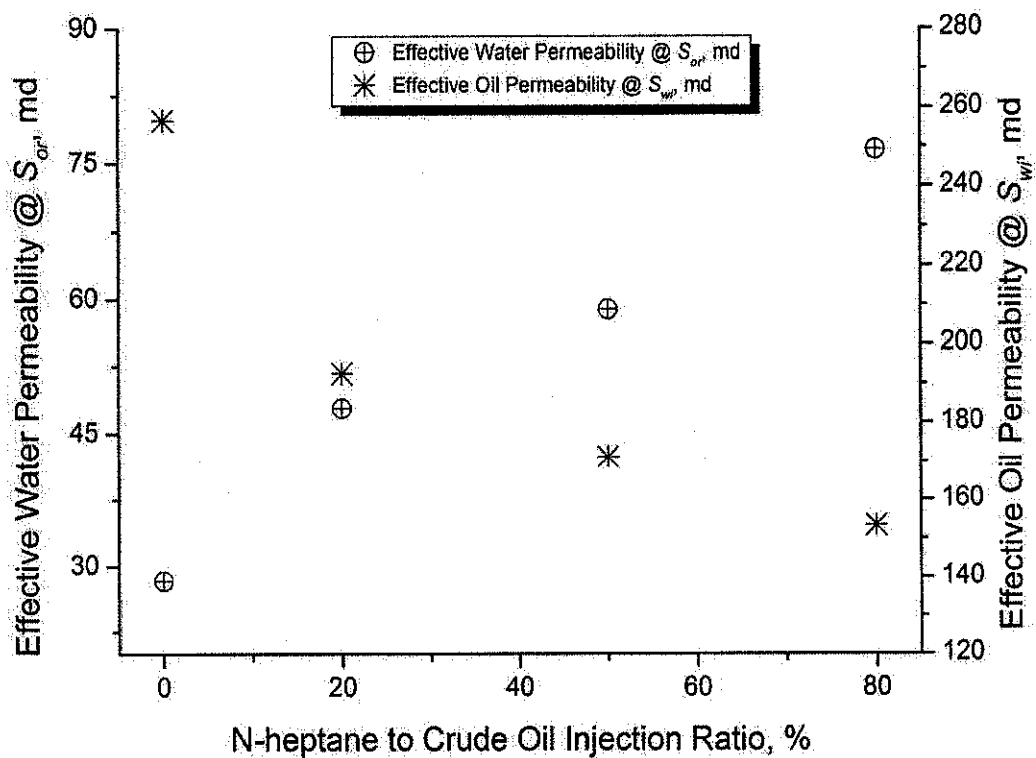


Figure 4.9: Effective water and oil permeability at various ratios of n-heptane–crude oil injections (water-oil system)

4.2.5.2 Gas-Oil System

During gas-oil system experiments, irreducible water saturation, S_{wi} and initial oil saturation, S_{oi} , are determined from the volumetric material balance during oil injection step. The computed values of these saturations for different ratios of n-heptane to oil injection are shown in Figure 4.10. The initial oil saturation increased and hence, the irreducible water saturation decreased (except for the 80 % case) as the asphaltene deposition increased.

Similarly, the residual liquid saturation, S_{lr} , and final gas saturation, S_{gf} , during gas injection step are computed again through the volumetric material balance and can be shown in Figure 4.11. As shown, there are not significant changes in these saturations and it can be assumed they are almost at their same values at zero injection ratio. It can be concluded that the asphaltene deposition during gas injection may not have a significant effect on the residual liquid saturation.

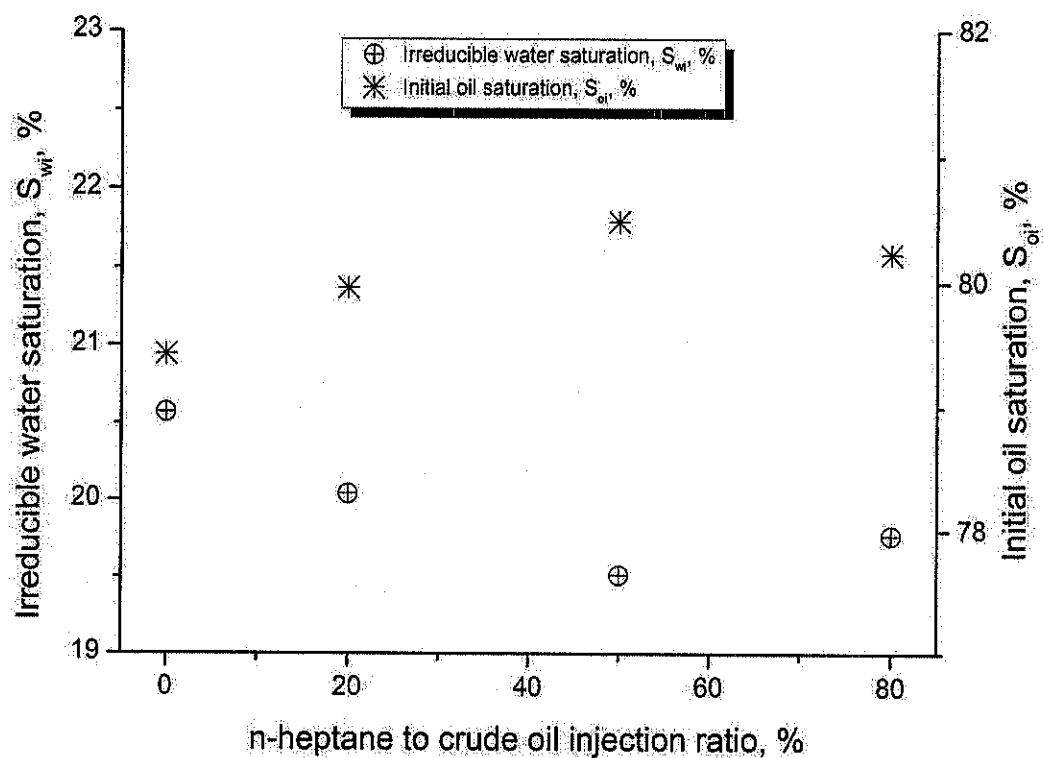


Figure 4.10: Irreducible water and initial oil saturation at various ratios of n-heptane–crude oil injections (gas-oil system)

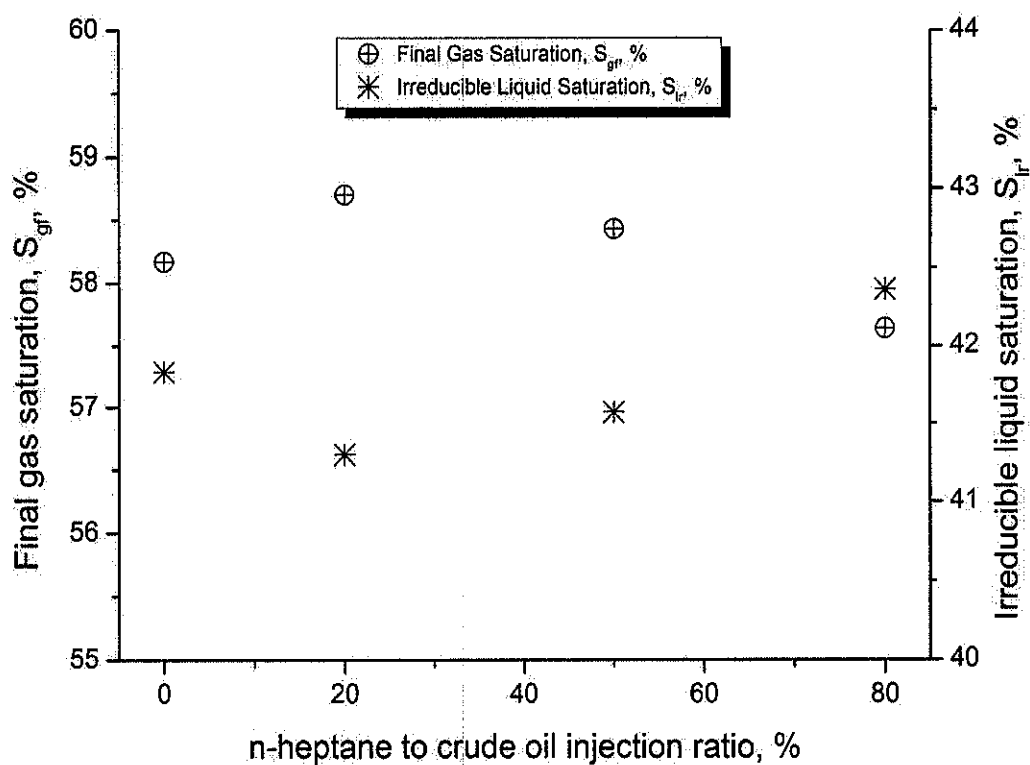


Figure 4.11: Residual liquid and final gas saturation at various ratios of n-heptane–crude oil injections (gas-oil system)

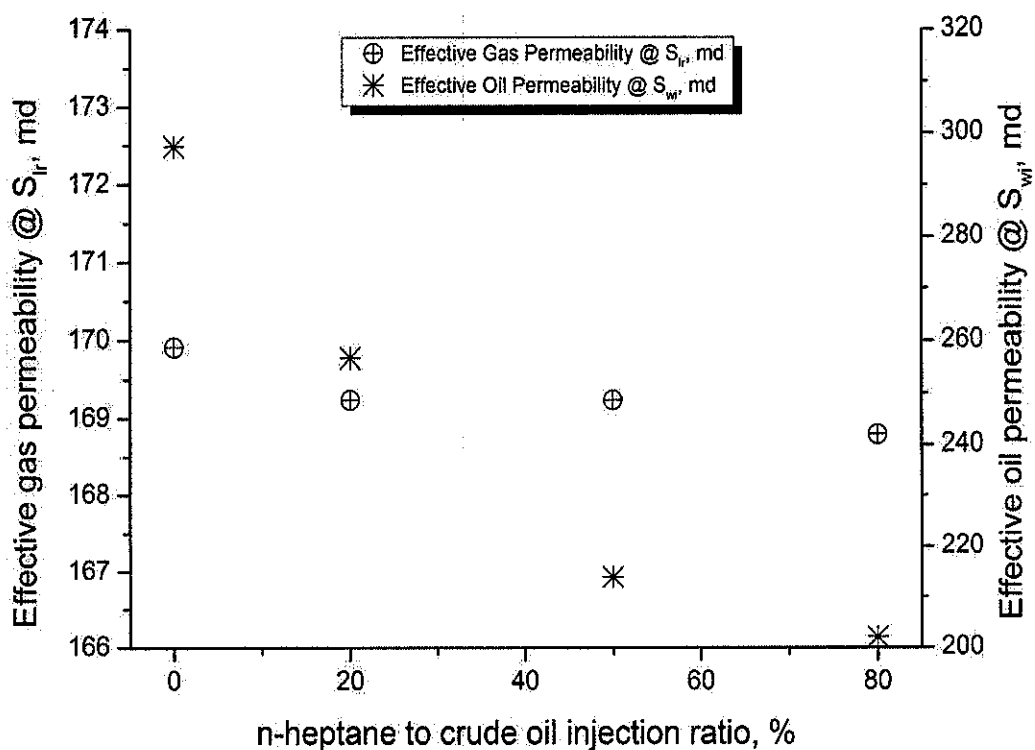


Figure 4.12: Effective gas and oil permeability at various ratios of n-heptane–crude oil injections (gas-oil system)

Again shown in Figure 4.12 are the computed values of the endpoint effective gas, $k_{eg}(S_{lr})$, and the endpoint oil, $k_{eo}(S_{wi})$, permeability which are computed based on method has been explained above. As is seen in Figure 4.12, $k_{eo}(S_{wi})$ is decreased as same as water-oil system. While as previously explained, the $k_{eg}(S_{lr})$ values are under some uncertainty and they do not follow any trend.

Standing (1974) presented a correlation for computing the effective non-wetting phase permeability at residual wetting phase saturation. He emphasized that the results of many testes he made lead to a general relationship between effective non-wetting phase permeability and residual wetting phase saturation. Based on his results, he presented the following relationship;

$$\frac{k_{e-nwt}(S_{wtr})}{k} = 1.08 - 1.11(S_{wtr}) - 0.73(S_{wtr})^2 \tag{4.12}$$

where $k_{e-nwt}(S_{wtr})$ is effective non-wetting phase permeability at residual wetting phase saturation.

Table 4.15: Effective and relative gas permeability, Standing (gas-oil system)

Ratio of n-heptane to oil injection, %	S_{lr} , %	$k_{eg}(S_{lr})$, md	$k_{rg}(S_{lr})$, fraction
0	41.83	152.62	0.4880
20	41.30	155.46	0.4970
50	41.57	154.01	0.4924
80	42.36	149.76	0.4788

Table 4.15 presents the equivalent values of effective and relative gas permeability at the residual liquid saturation based on Standing relationship, Equation 4.12. As can be compared typically these values are very close to each other and less than values computed from pressure drop data and using the Darcy law in Table 4.13. It can be concluded that the effective gas permeability under different amounts of asphaltene deposition do not change significantly.

4.2.6 Reduction in Effective Oil Permeability at Irreducible Water Saturation

Here, the effect of asphaltene deposition on the reduction of effective oil permeability at irreducible water saturation is investigated. Note, that this value is typically very close to (actually slightly smaller than) the absolute permeability and determines the performance of any injection procedure into porous media.

The ratio of effective oil permeability at irreducible water saturation at various percentages of asphaltene deposition; 20%, 50%, and 80%, $k_{eo}(S_{wi})_{Asphaltene}$, to the effective oil permeability at irreducible water saturation for the first core without asphaltene; i.e., the permeability at 0% simultaneously injection, $k_{eo}(S_{wi})_{Basic}$, is shown in Figure 4.13. These values previously are given in Table 4.7 for water-oil system.

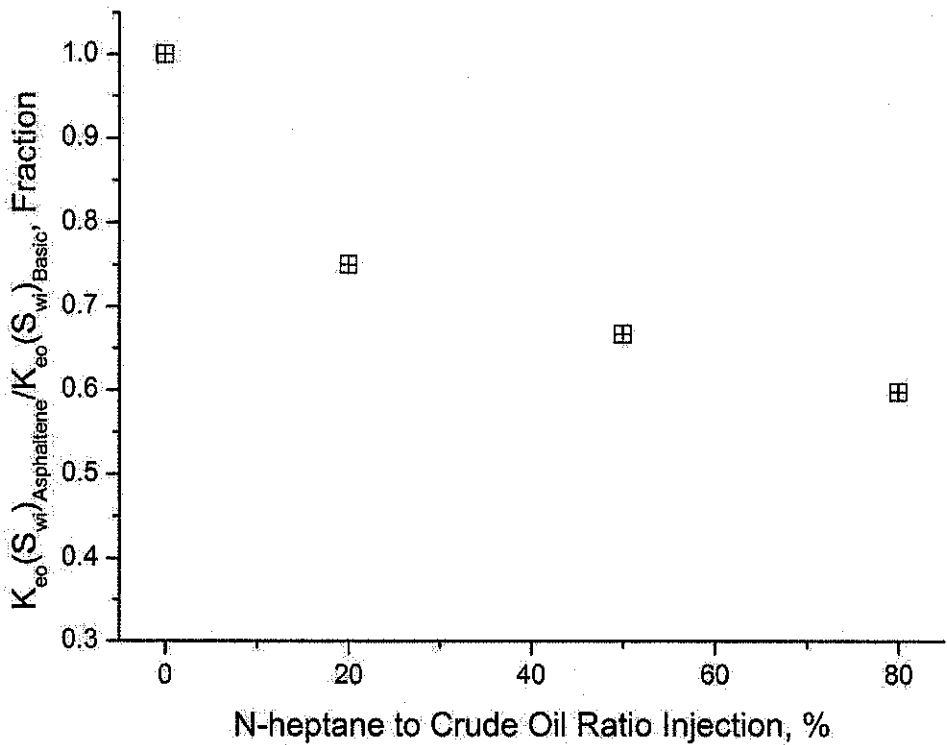


Figure 4.13: Ratio of effective oil permeability at irreducible water saturation at various ratios of n-heptane–crude oil injections (water-oil system)

As shown in Figure 4.13, the oil effective permeability decreases with increasing asphaltene deposition for all cores. The oil effective permeability reduction is related directly to the pore-size distribution. This phenomenon can be explained in terms of the different pore size distributions that the asphaltene molecules are blocked more in

the pore spaces and also they are adsorbed more on the pore surfaces because of the lower absolute permeability.

During the gas-oil system experiments, similar results for the reduction in oil effective permeability are obtained as previously given in Table 4.8 and shown in Figure 4.14.

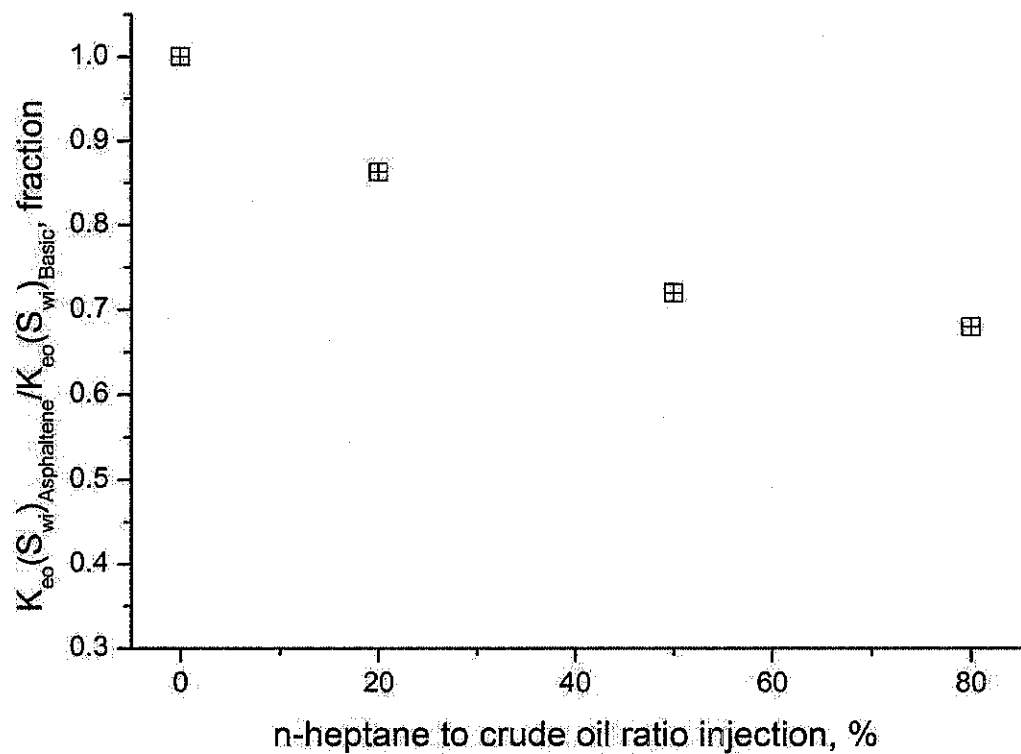


Figure 4.14: Ratio of effective oil permeability at irreducible water saturation at various ratios of n-heptane–crude oil injections (gas-oil system)

4.2.7 Oil Recovery and Sweep Efficiency Performance

In this section, the oil recovery results and sweep efficiency performance of different coreflooding experiments for water-oil and gas-oil systems are shown in different graphs. The comparisons between these experimental results follows by some description are given.

4.2.7.1 Water-Oil System

The observation experimental values for pressure drop across the core samples which are obtained during waterflooding experiments for all cases of 0%, 20 %, 50 %, and 80% injection ratios are given in Figure A.1 to Figure A.4 in Appendix A, respectively. Also the oil and water productions obtained from these experiments are given in Figure A.5 to Figure A.8 for oil production and in Figure A.9 to Figure A.12 for water production in Appendix A.

Based on these observation experimental data, the cumulative pore volumes of oil production, N_p , versus the cumulative pore volume of water injection, Q_i , at various ratios of n-heptane to crude oil injections are computed and are plotted in Figure 4.15. As expected, the cumulative oil production during the one and half pore volume injection is decreased due to increase the amount of asphaltene deposition but after that is increased which is absolutely different what is expected from asphaltene formation damage. This means that the additional water pore volume injection with increasing asphaltene deposition can lead to extra oil production and can improve the sweep efficiency and reaching to higher oil recovery factors. Also as shown in this figure, the ultimate oil recovery for the cases with 0 %, 20 %, 50 % and 80 % injection ratios are almost achieved after the one and half, three and half, four and half and six water pore volume injections, respectively. The oil recovery factor at various n-heptanes to crude oil ratios injections at end of the first pore volume injection is shown in Figure 4.16. Moreover, the ultimate oil recovery after extra pore volume injection is shown in Figure 4.17. As shown the oil recovery is decreased during the first pore volume injection but increased during the extra pore volume injection.

There are several mechanisms such as wettability alteration, surface film oil drainage, changes in end-points, and interfacial tension, etc. that may play simultaneously roles on the asphaltene deposition that leads to improvement of oil recovery (Morrow, 1990). Nevertheless, it is very difficult to identify which of them is the most dominant mechanism for improvement in oil recovery observed in the experimental results. For instance, during the desaturation of initially water-wet core with oil, water is displaced from the larger pores while capillary forces retain water in small capillaries and at grain contacts. Then, if some organic materials from the oil

are deposited onto those rock surfaces that are in direct contact with oil, thus this makes those surfaces strongly oil-wet. This condition can develop and lead to non-uniform wettability which is named mixed wettability conditions (Salathiel, 1973).

Under mixed wettability conditions, the fine pores and grain contacts are preferentially water-wet and the larger pores surfaces are strongly oil-wet. As explained by Salathiel (1973) the oil-wet surfaces may connect to each other and create continuous paths for oil inside porous media. In this condition water could displace oil from the large pores and small or no oil seize by capillary forces in fine pores or at grain contacts. Therefore, this type of mixed wettability condition could create paths for oil phase to flow even at very low saturations which is explained by surface film oil drainage mechanism. In this mechanism it is postulated that the flow of oil (surface drainage) occurs in films over strongly oil-wetted pore surfaces, forming continuous oil wet paths extending through the pore structure. Similar observations has been noted in the classical paper of Morrow (1990) on wettability.

Therefore, as it is expected and also shown in Figure 4.15 for water-wet core which is zero percent ratio of n-heptane–crude oil injection experiment, most of recoverable oil is displaced before water breakthrough, and almost little oil could be produced after breakthrough. Therefore, oil saturation almost is reached a constant value. The residual oil is remained trapped by capillary forces as discontinuous droplets or irregular bodies of oil separated by continuous water.

For the mixed wet cores which are 20, 50, 80 percent ratios of n-heptane–crude oil injection experiments on the other hand, oil production is continued for many pore volumes after water breakthrough and resulted in lower oil saturation than could be reached in water-wet core. Therefore, the oil saturation continued to decline as long as water was injected.

However, as mentioned previously, the question of how practical it is to inject fluid volumes of more than two pore volumes of reservoir to achieve improvement in oil recovery in the presence of asphaltene precipitation and deposition remains as an important question to answer.

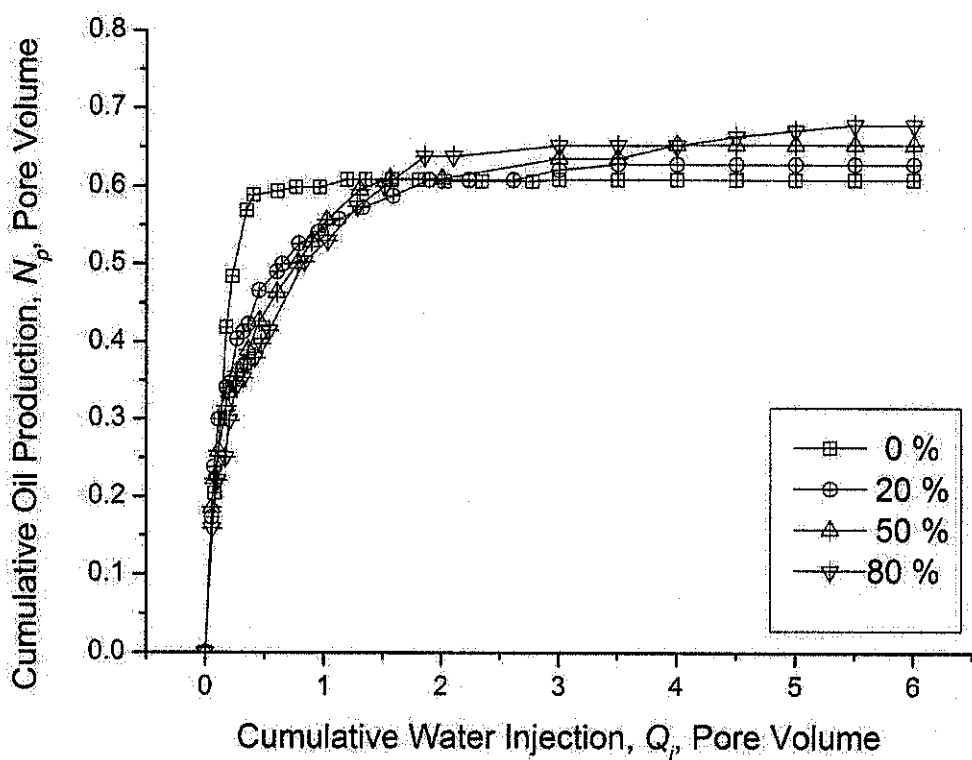


Figure 4.15: Cumulative oil production versus cumulative water injection at various ratios of n-heptane-crude oil injections (water-oil system)

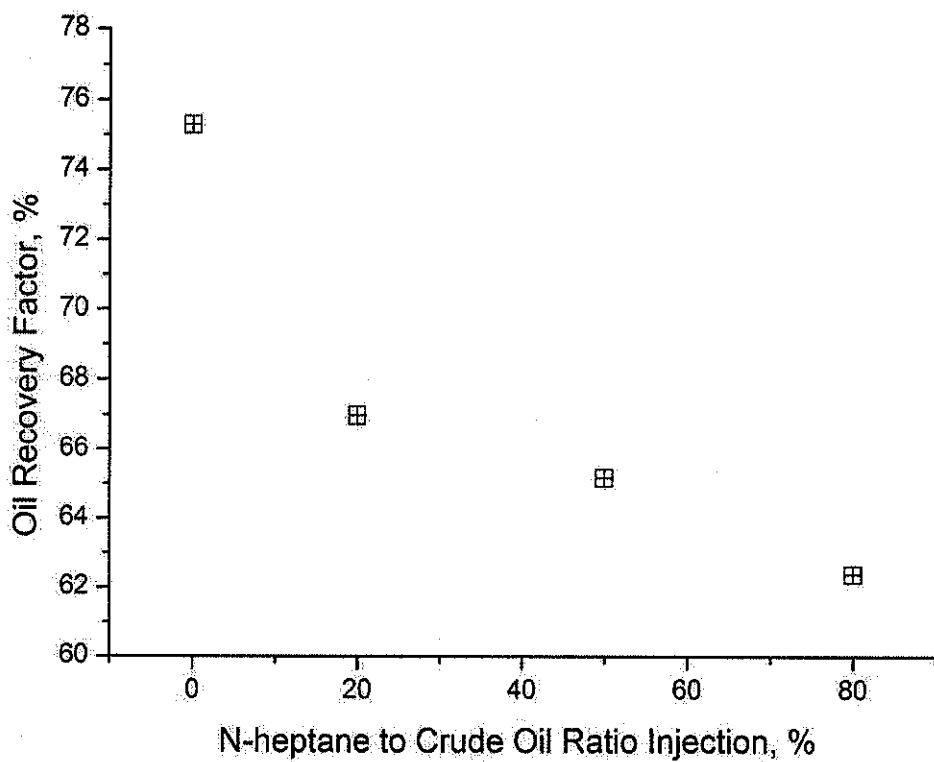


Figure 4.16: Oil recovery factor for first pore volume injection at various n-heptane-crude oil ratios injections (water-oil system)

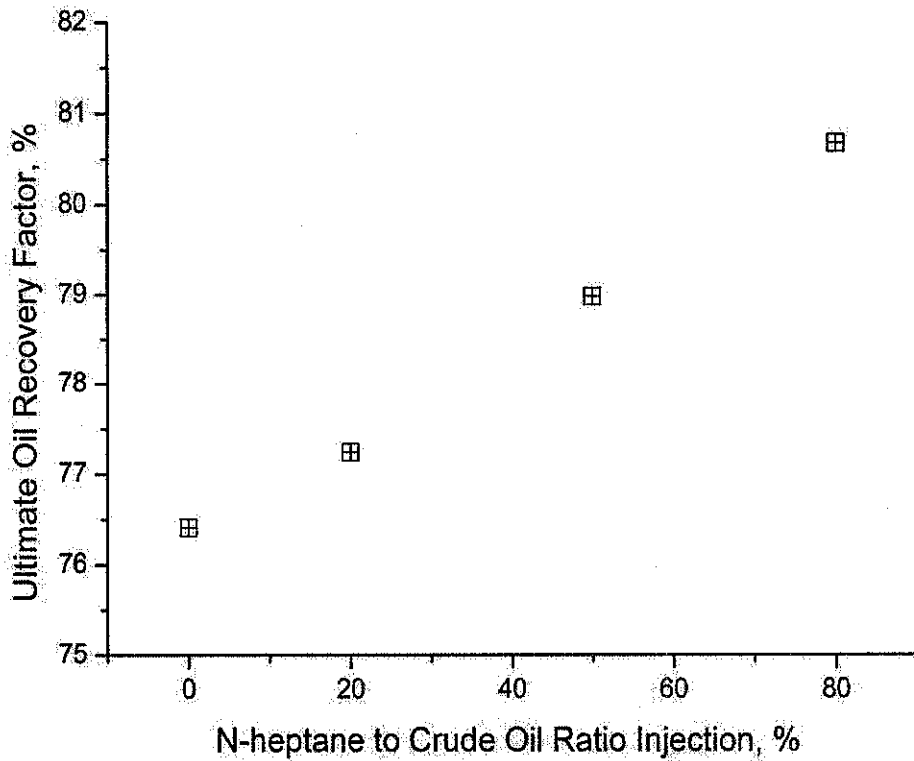


Figure 4.17: Ultimate oil recovery factor at various n-heptane–crude oil ratios injections (water-oil system)

4.2.7.2 Gas-Oil System

The observed experimental values for pressure drop across the core samples which are obtained during gas injection experiments for all cases 0%, 20%, 50% are given in Figure A.46 to Figure A.48 in Appendix A, respectively. As previously explained the last experiment which is 80% case was terminated because of some setup issues. The experimental values of oil production for these experiments are given in the Appendix A and in Figure A.49 to Figure A.51.

Based on these observed experimental data the cumulative pore volumes of oil production, N_p , versus the cumulative pore volume of gas injection, Q_i , at various ratios of n-heptane to crude oil injections are computed and can be shown in Figure 4.18. For case 80% in lack of experimental data as previously explained an average trend similar to 20% and 50% cases is considered.

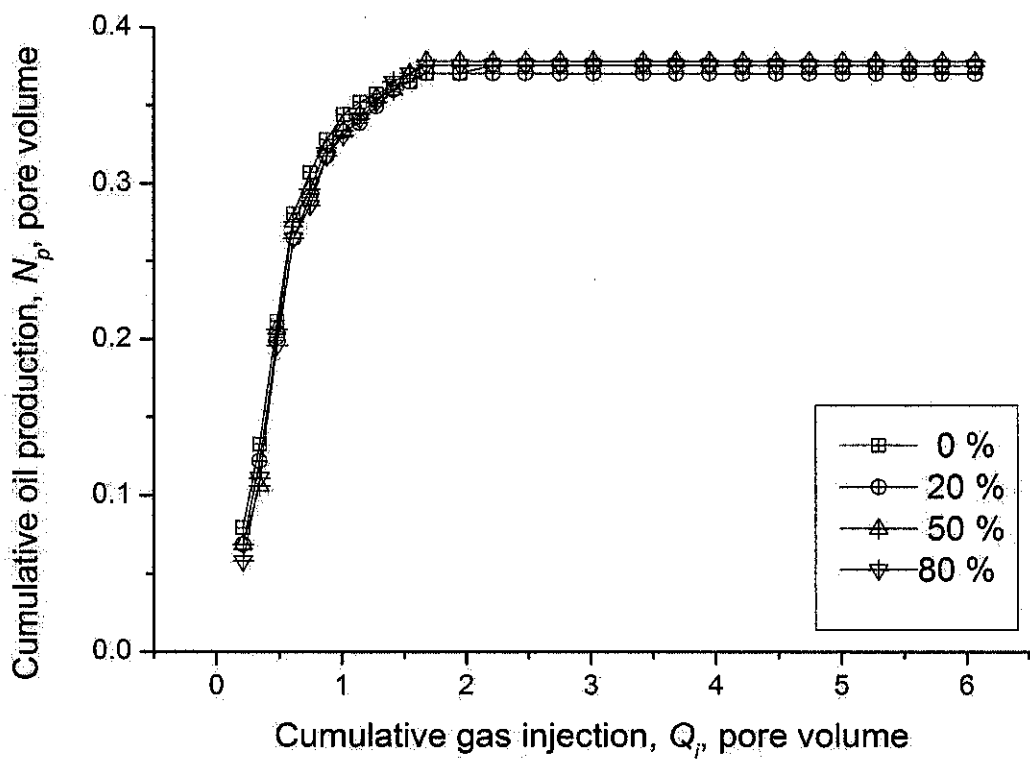


Figure 4.18: Cumulative oil production versus cumulative gas injection at various ratios of n-heptane–crude oil injections (gas-oil system)

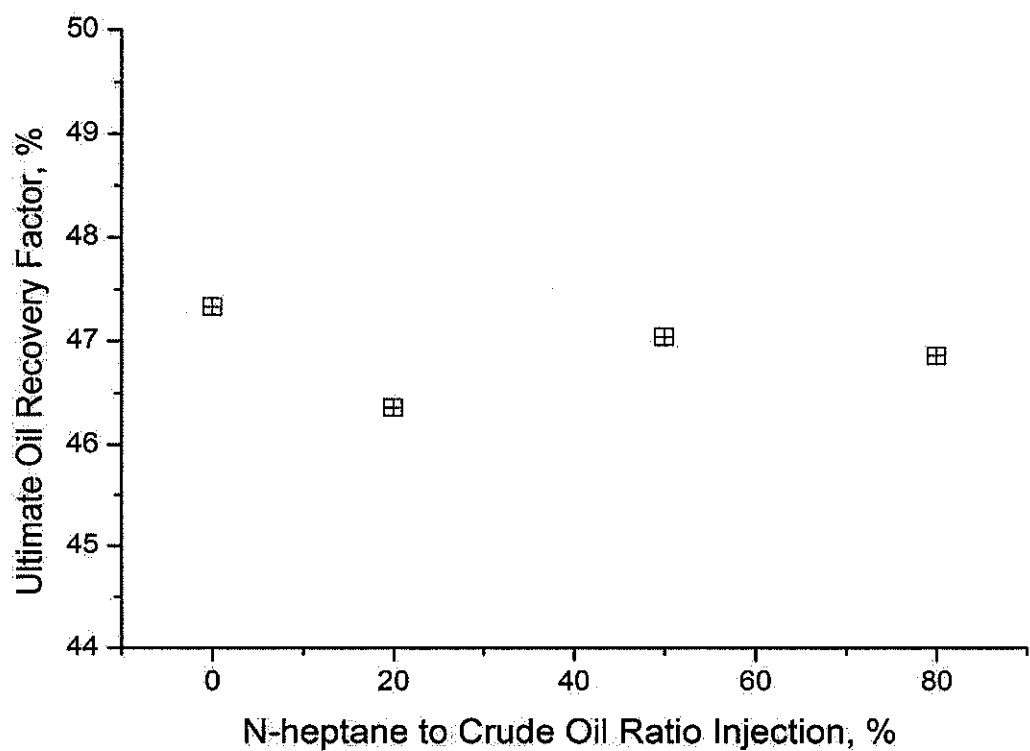


Figure 4.19: Ultimate oil recovery factor at various n-heptane–crude oil ratios injections (gas-oil system)

As shown asphaltene deposition does not have significant effects on oil production curve during gas injection. This may be related to the behavior of gas in sweep up the oil. Indeed, in the most systems gas can play a non-wetting phase rule compared to oil and water. Whereas gas can enter the large pore spaces and can sweep up the oil better than water. The ultimate oil recovery factor at various n-heptanes to crude oil ratios injections at end of the sixth pore volume injection is shown in Figure 4.19. As shown and it can be expected the oil recovery is not following any trend and it can be considered as almost constant. It can be concluded that the ultimate oil recovery factor under different amounts of asphaltene deposition do not change significantly.

4.3 Estimation of Relative Permeability Curves

In this section, estimating the water-oil and gas-oil relative permeability curves from a one-dimensional two-phase black-oil simulator based on history matching process is given.

4.3.1 Oil-Water Relative Permeability

The oil and water relative permeability data are computed based on history matching of the all experimental displacement data, e.g. pressure drop, oil cumulative production, and water cumulative production data by using a one dimensional two-phase black oil simulator (Sendra, 2011). This simulator is equipped with well-known correlations of relative permeability such as Corey, LET, Burdine, Chierici, and Sigmund & McCaffery (Sendra, 2011) for estimation purposes.

During the history matching processes the Corey and LET correlations are found to be the best ones providing very good matches for the relative permeability curves. The history matching results between experimental data and Corey correlation or LET correlation for all ratios of n-heptane to oil injection are given in Appendix A. The history matching of pressure drop, water cumulative production, and oil cumulative production by Corey correlation are given in Figure A.13 to Figure A.24, respectively.

Also the history matching of pressure drop, water production, and oil production by LET correlation are given in Figure A.29 to Figure A.40, respectively. For instance, the history match of pressure drop for 20 % ratio n-heptane to oil injection experiment is shown in Figure 4.20. Similarly, Figure 4.21 and Figure 4.22 show the history matches of oil and water cumulative production data for this experiment, respectively.

The predicted simulation results for oil and water relative permeability curves based on these history matching and different asphaltene deposition percentages are shown in Appendix A. Figure A.25 to Figure A.28 show the predicted oil and water relative permeability curves from the simulation results and Corey correlation and Figure A.41 to Figure A.45 show the predicted oil and water relative permeability curves from LET correlation.

Figure 4.23 shows the all predicted oil and water relative permeability curves from simulation results and Corey correlation. As can be seen the asphaltene deposition increases the water relative permeability, reduces the oil relative permeability, and changes the position of crossover point.

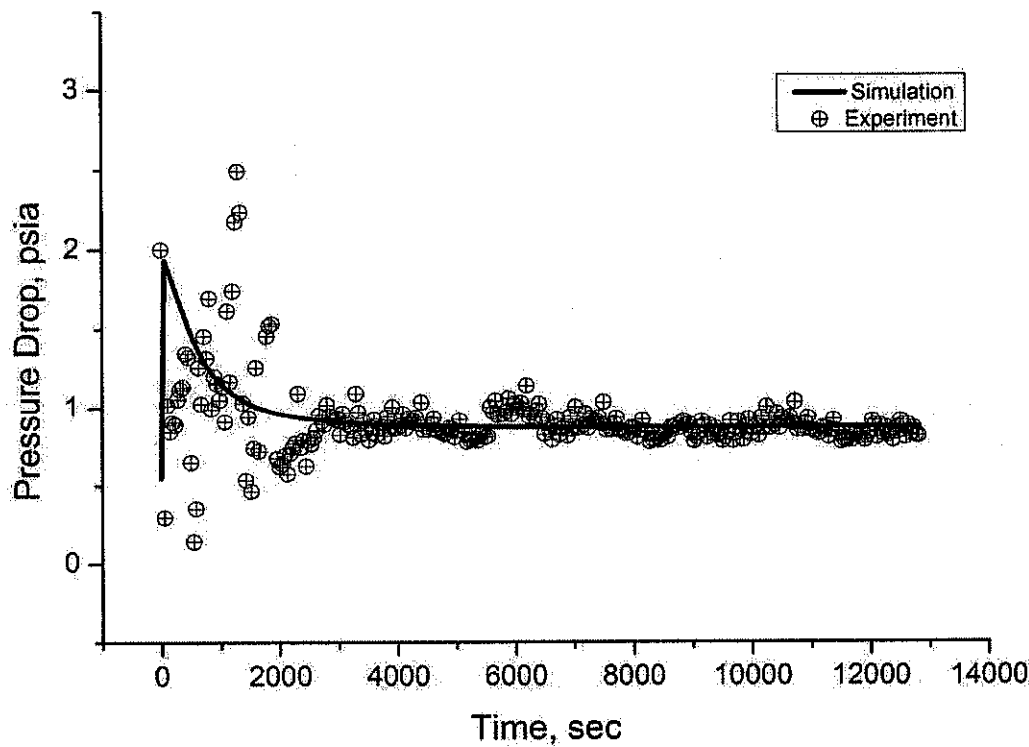


Figure 4.20: Pressure drop history match of 20% case, Corey (water-oil system)

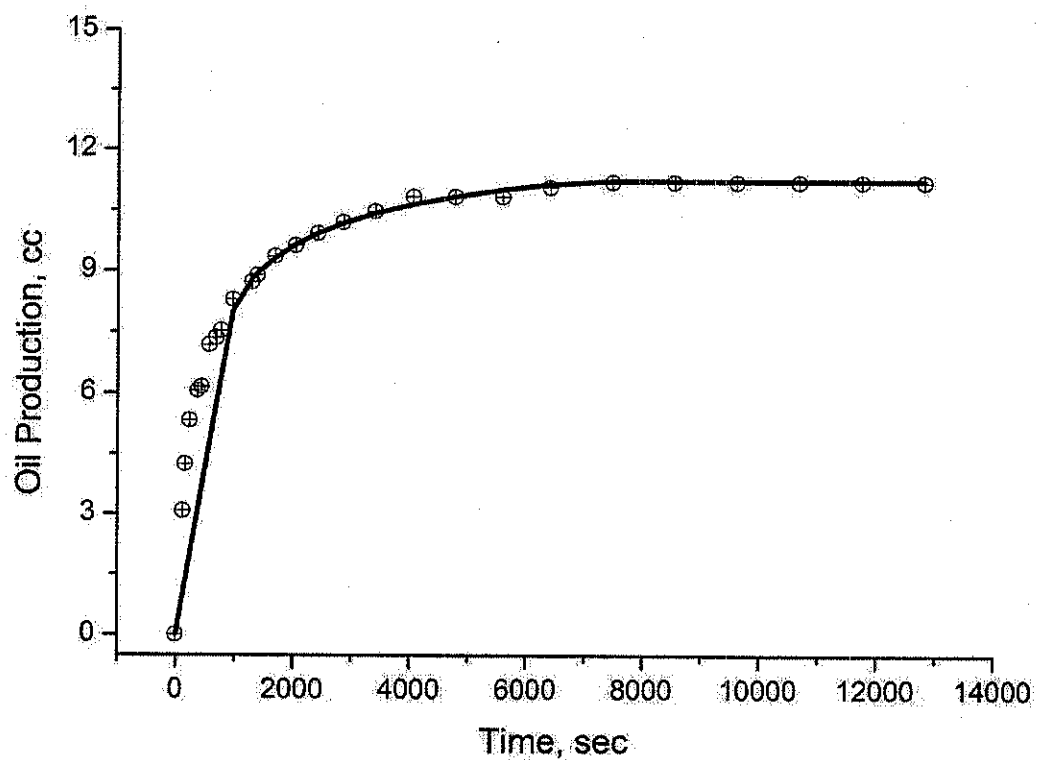


Figure 4.21: Oil production history match of 20% case, Corey (water-oil system)

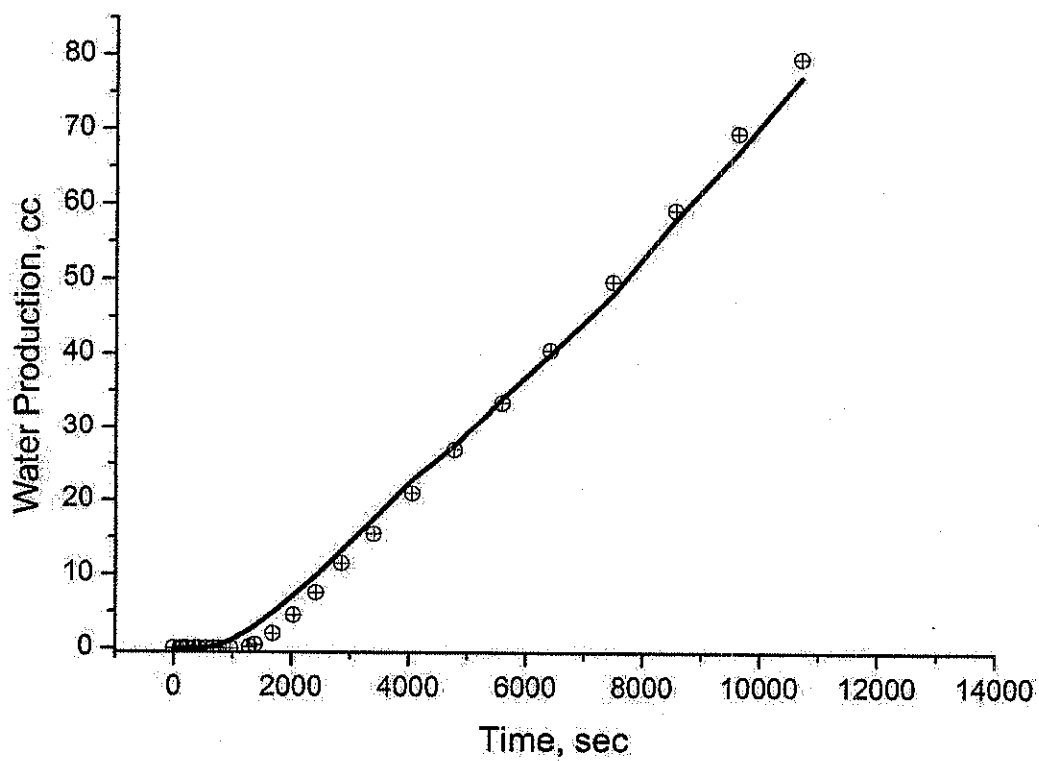


Figure 4.22: Water production history match of 20% case, Corey (water-oil)

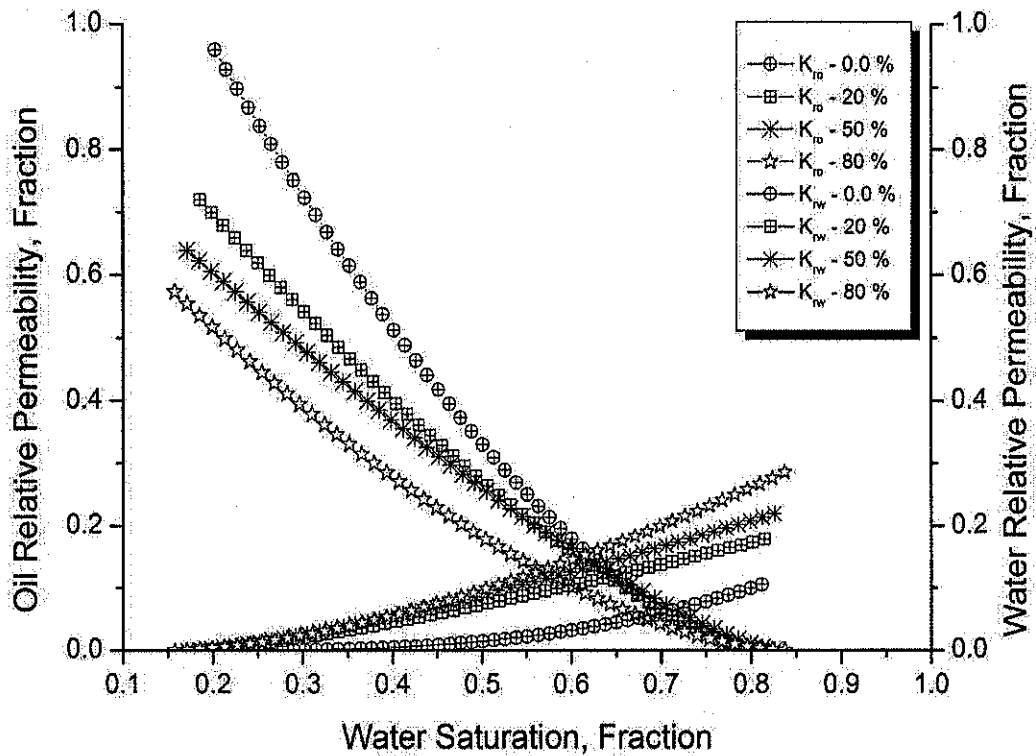


Figure 4.23: Effect of asphaltene on relative permeability at various n-heptane–crude oil ratios injections, Corey correlation (water-oil system)

As previously mentioned and reported in the literature the shape of relative permeability curves of each rock can be an indication for wettability of that rock. There are several rules of thumb, as presented by Craig (1971), that identify the differences in the relative permeability characteristics of strongly water-wet and strongly oil-wet cores (Craig, 1971; Anderson, 1987). The Craig's rules of thumb regarding the water relative permeability generally give an indication of the rock wettability. Based on the rules of Craig, it may be stated that the results given in Figure 4.23 show that the wettability is changing from a water-wet rock towards an oil-wet or mixed-wet rock. However, to be certain whether the rock becomes oil or mixed-wet, some contact angle measurements needs to be done, though such measurements were not done during the course of this study.

4.3.2 Gas-Oil Relative Permeability

The same methodology is used to compute the oil and gas relative permeability data by history matching of the experimental displacement data by using a one-

dimensional two-phase black oil simulator (Sendra, 2011). During the history matching processes again the Corey and LET correlations are used. The history matching results between experimental data and Corey correlation for all ratios of n-heptane to oil injections are only done for oil production data and given in Appendix A. The pressure drop and gas production data were not used during matching process because as previously explained these experimental data were under some uncertainty. The history matching process of oil cumulative production data for various injection ratios is shown in Figure A.52 to Figure A.54. For instance, the history match of oil production for 20 % ratio n-heptane to oil injection experiment is shown in Figure 4.24.

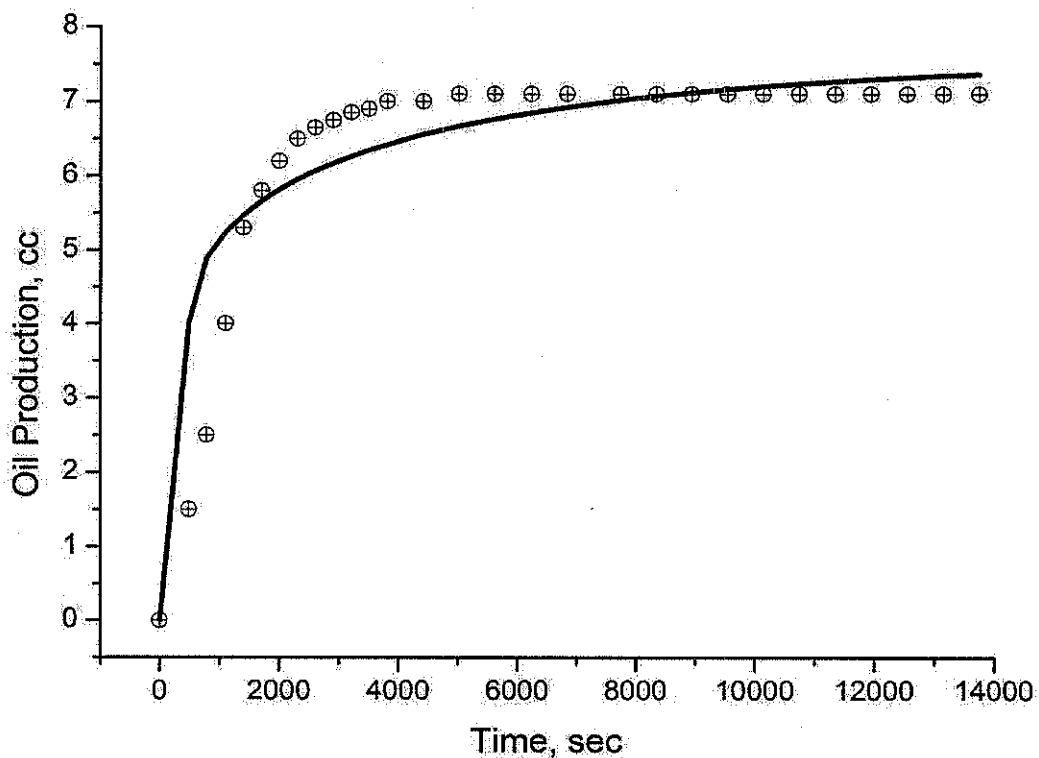


Figure 4.24: Oil production history match of 20% case, Corey (gas-oil system)

Figure 4.25 shows the all predicted oil and gas relative permeability curves from simulation results and Corey correlation. As can be seen the asphaltene deposition does not seem to have significant effect on gas relative permeability curves. It is also expected that the relative permeability curves for all cases should be close to each other graphically. Since almost the identical experimental results for oil productions for all coreflooding experiments have been obtained and also the close residual liquid saturation values for all cases have been computed.

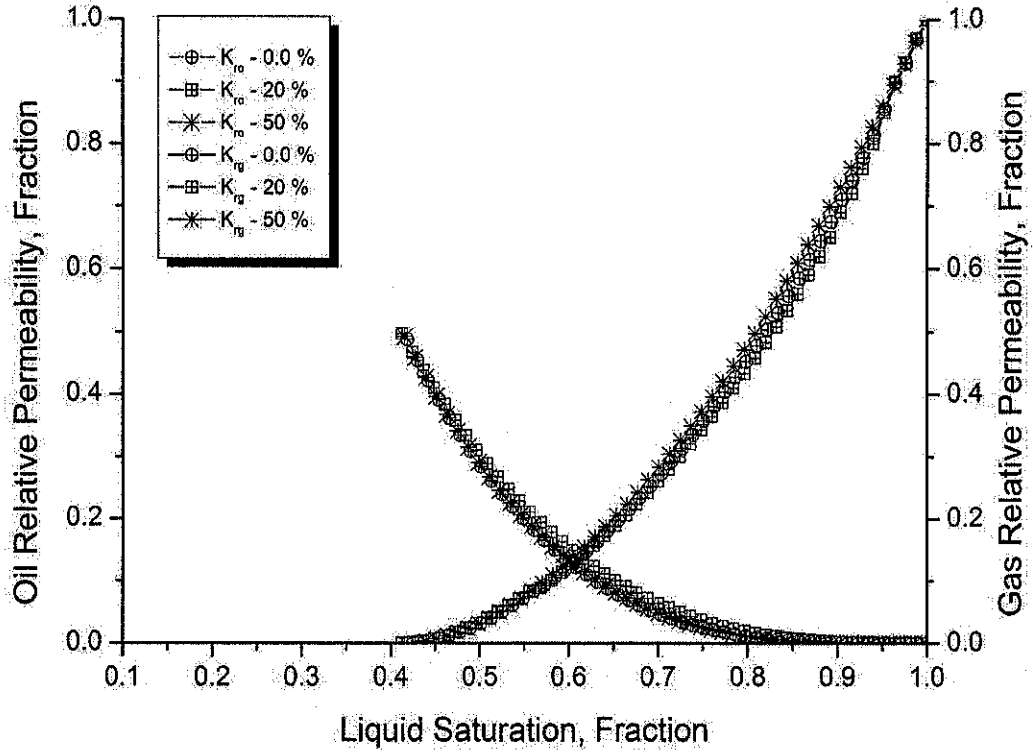


Figure 4.25: Effect of asphaltene on relative permeability at various n-heptane–crude oil ratios injections, Corey (gas-oil system)

4.4 Three-Phase Relative Permeability

The Stone's II model is used to compute the oil relative permeability in a three-phase system based on the two sets of two-phase relative permeability data. The relative permeability data in water-oil system and gas-oil system are previously presented in Figure 4.23 and Figure 4.25, respectively. As explained in Chapter II, the second model of Stone is given by the following equation:

$$k_{ro} = (k_{ro})_{S_{wc}} \left[\left(\frac{k_{row}}{(k_{ro})_{S_{wc}}} + k_{rw} \right) \left(\frac{k_{rog}}{(k_{ro})_{S_{wc}}} + k_{rg} \right) - (k_{rw} + k_{rg}) \right] \quad (4.13)$$

To compute the oil relative permeability by (4.13) the values of $(k_{ro})_{S_{wc}}$, k_{row} and k_{rw} as function of S_w are taken from water-oil system data and the values of k_{rog} and k_{rg} as function of S_g are taken from gas-oil system data. Also the oil saturation

values are computed simply by subtracting the water and gas saturations from one ($S_o = 1 - S_w - S_g$).

The ternary diagram with fluids saturation points and iso-perm curves are commonly used to illustrate changes in the oil relative permeability values in three-phase system. The computed values for oil relative permeability for different n-heptane–crude oil ratios injection experiments (0%, 20%, 50%, and 80%) based on Stone's II model are shown by oil iso-perm curves in Figure 4.26 through Figure 4.29, respectively. In these figures the wide range of oil relative permeability from 0.1 to 0.9 are shown by different and separate trend line points. To investigate the effect of asphaltene deposition on oil iso-perm curve, the comparison of oil relative permeability values from different experiments and for different oil iso-perm values 0.1, 0.2, and 0.3 are shown in Figure 4.30 to Figure 4.32, respectively. Moreover, the comparison for other oil iso-perm values are presented in Figure A.55 through Figure A.59 in Appendix A.

As can be seen in all figures, the effect of asphaltene deposition on oil relative permeability is related to the amount of gas saturation. The oil iso-perm in three-phase system show different trajectories with different levels of asphaltene deposition until a certain gas saturation. For gas saturations above this saturation all oil iso-perm trajectories merge, indicating no significant effect of asphaltene deposition. Figure 4.30 shows this level of gas saturation close to 0.3 for oil iso-perm equal to 0.1. As can be seen in this figure, there are two different behaviors for oil iso-perm trajectories around this gas saturation. Above the 0.3 gas saturation that all oil iso-perm trajectories merge to each other and there is no significant effect of asphaltene deposition and below of this level of gas saturation that different oil iso-perm trajectories can occur and significant effect of asphaltene deposition can happen. Moreover, this criterion for level of gas saturation in Figure 4.31 and Figure 4.32 can be obtained equal to 0.25 and 0.2 for oil iso-perm equal to 0.2 and 0.3, respectively. In addition, as can be seen in higher values of oil relative permeability such as 0.6, 0.7, and 0.8 (Figure A.55 through Figure A.59 in Appendix A) the difference between the oil iso-perm curves from different asphaltene deposition experiments is significantly reduced.

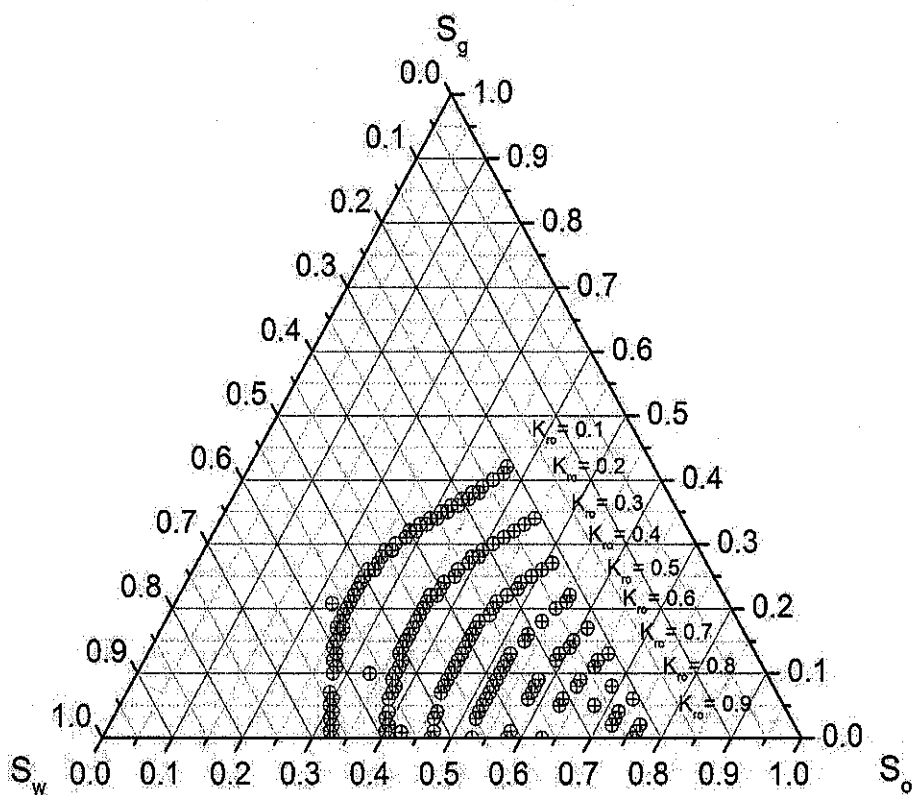


Figure 4.26: Oil relative permeability at zero % ratio of n-heptane-crude oil injection

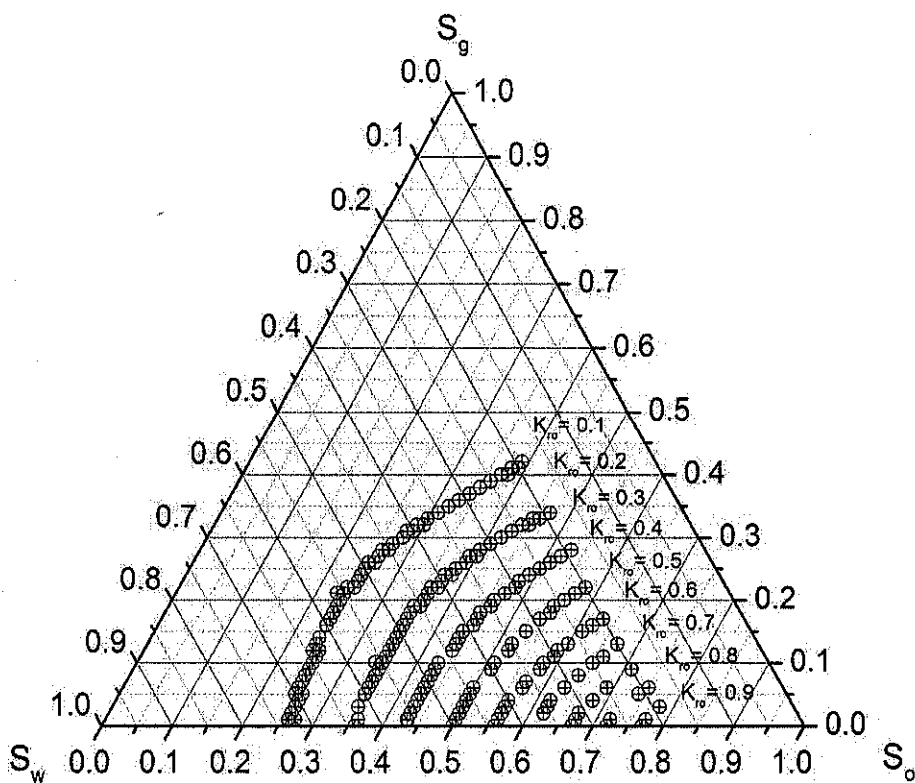


Figure 4.27: Oil relative permeability at 20 % ratio of n-heptane-crude oil injection

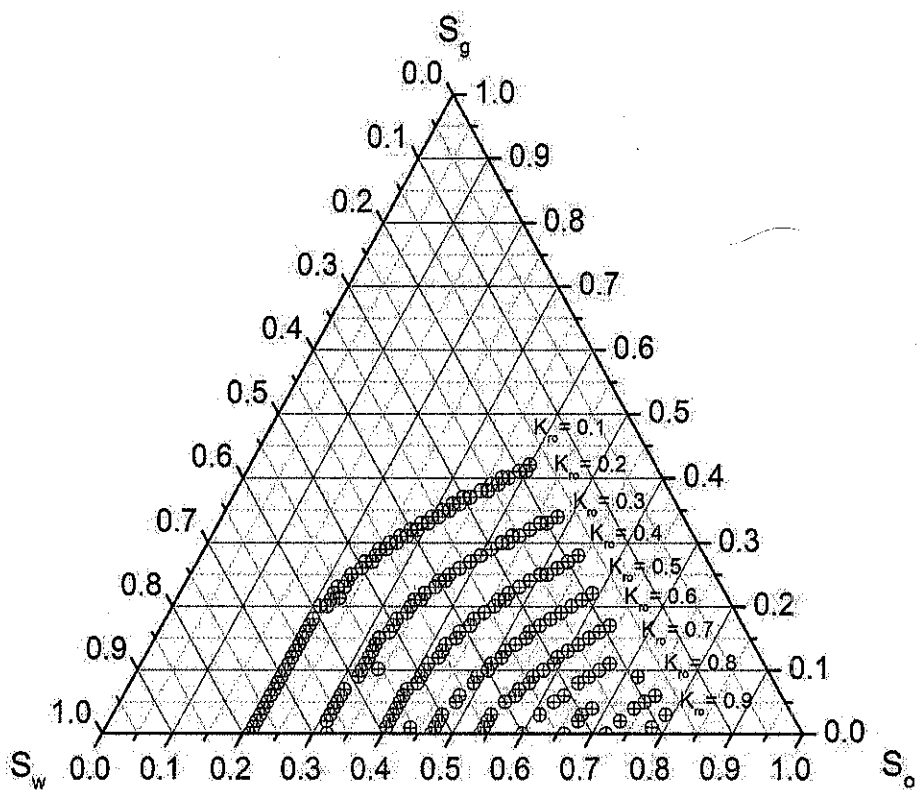


Figure 4.28: Oil relative permeability at 50 % ratio of n-heptane–crude oil injection

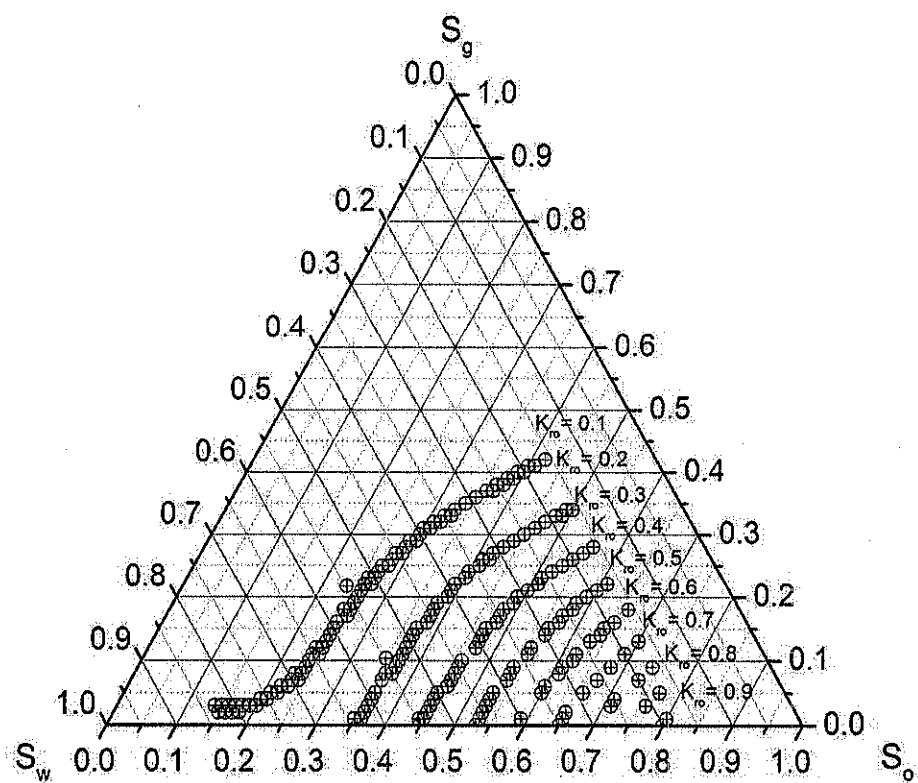


Figure 4.29: Oil relative permeability at 80 % ratio of n-heptane–crude oil injection

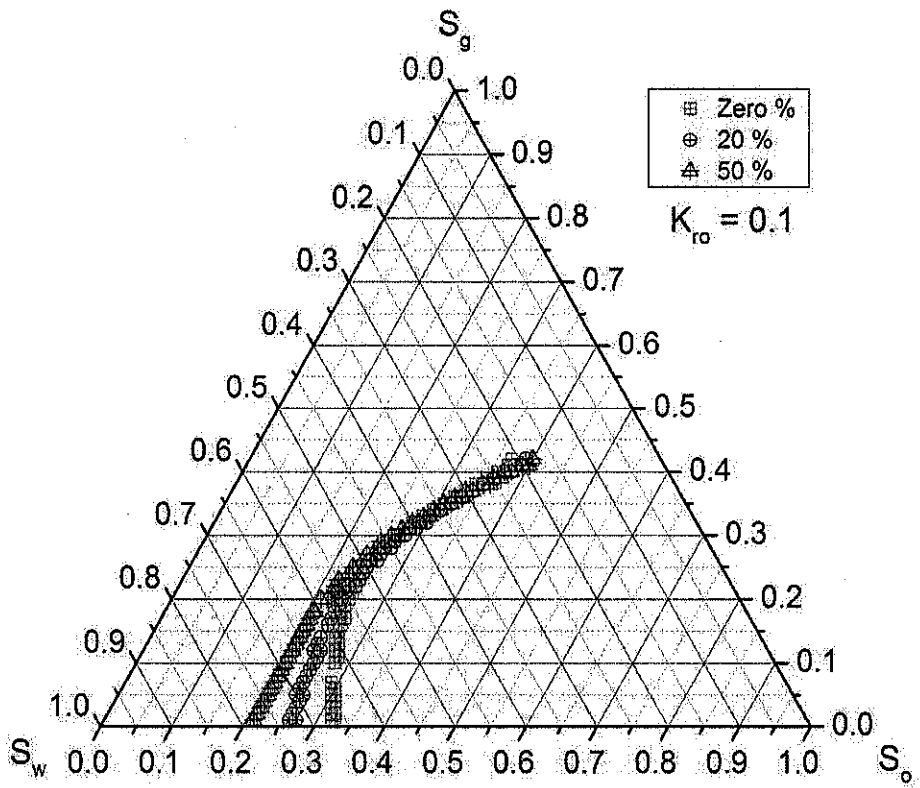


Figure 4.30: Comparison of oil relative permeability 0.1 for all cases

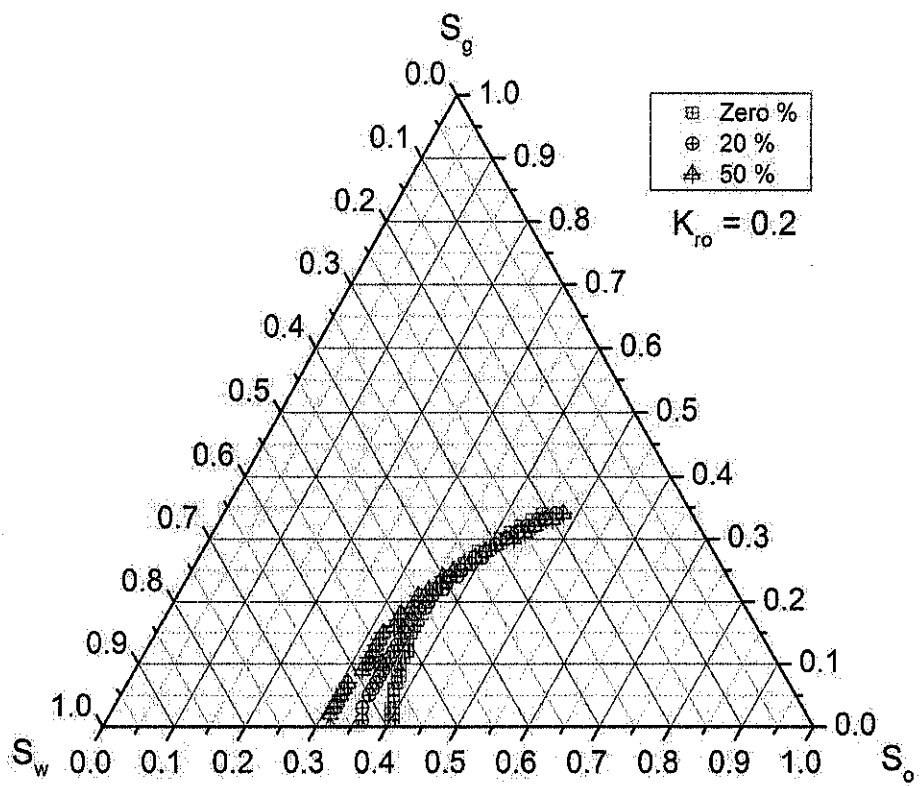


Figure 4.31: Comparison of oil relative permeability 0.2 for all cases

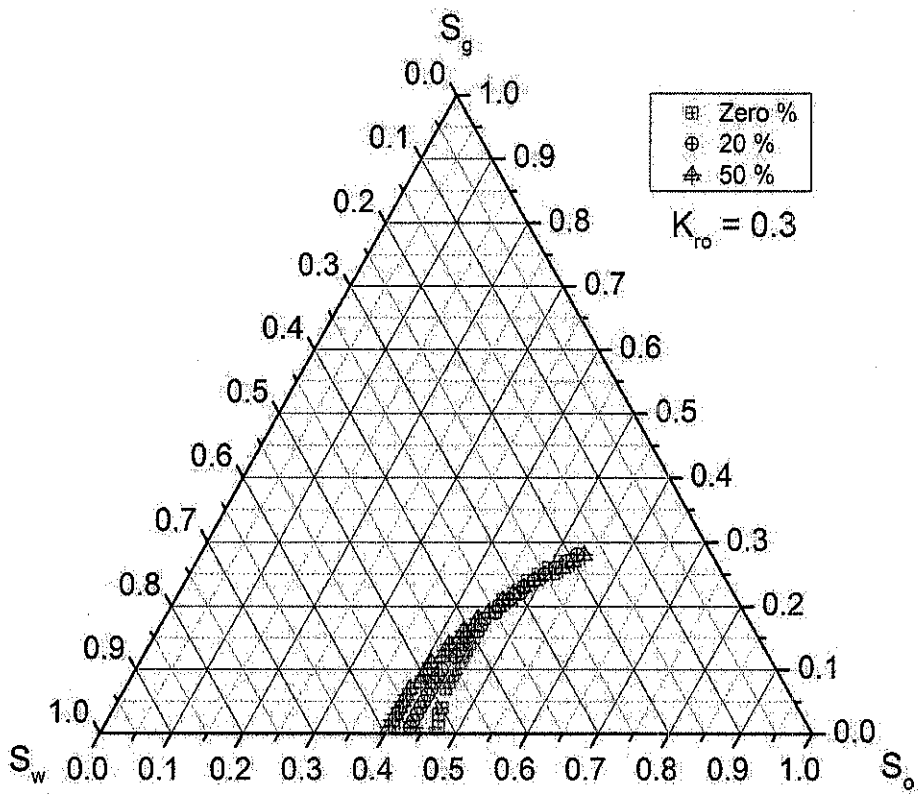


Figure 4.32: Comparison of oil relative permeability 0.3 for all cases

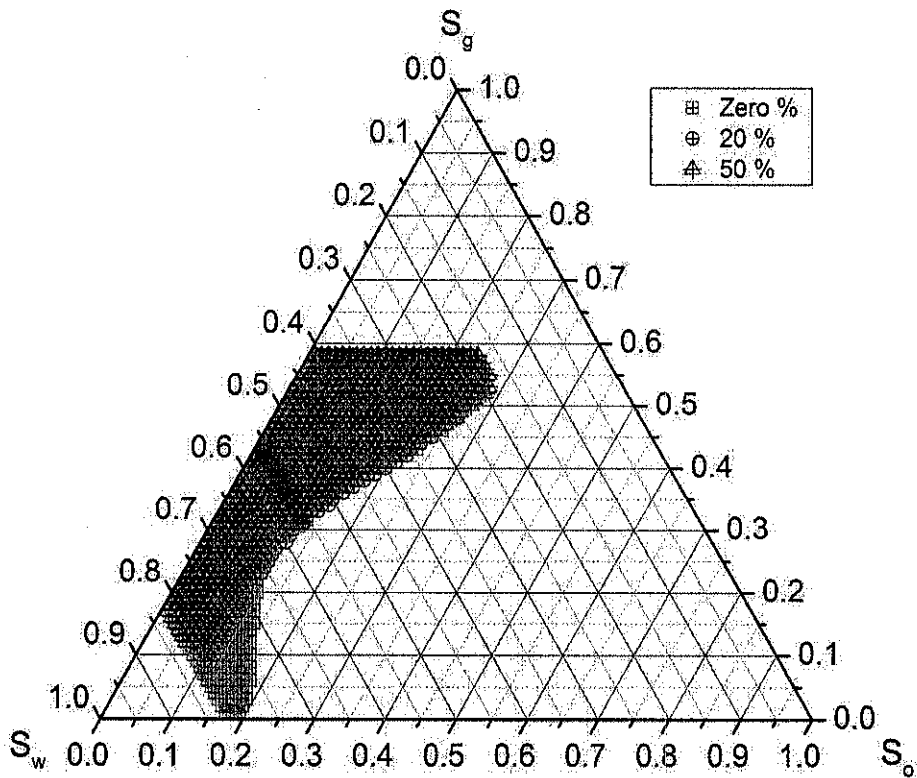


Figure 4.33: Comparison of fluid saturation distribution for oil relative permeability equal to zero for all cases

One of the interesting results is the triangular diagrams for location of the fluid saturation points in oil relative permeability equal to zero that are shown in Figure A.60 to Figure A.63 in Appendix A for different ratios of n-heptane to crude oil injection experiments. Indeed, in these water, oil, and gas saturations points the oil phase cannot move and seize to flow. Furthermore, a comparison of these fluid saturation points for zero %, 20 %, and 50 % experiments is shown in Figure 4.33. The 80 % n-heptane–crude oil ratios injection experiment is excluded from this comparison. As can be seen in Figure 4.33 due to asphaltene deposition the area for fluid saturation points is reduced with increasing of asphaltene deposition. It means that the oil can move in some saturation points due to asphaltene deposition which cannot move in zero % n-heptane–crude oil injection experiment.

4.5 Water-Oil Relative Permeability Correlations

Some correlations for relative permeability having the effect of asphaltene deposition are developed based on the obtained dynamic experimental data. Like most of relative permeability correlations, these correlations use normalized water saturation as one of correlating parameter. However, in these correlations the amount of asphaltene deposition per pore volume as a new independent variable is introduced. As mentioned previously, among several efforts to match experimental data and simulation results during history matching process it is found that the Corey and LET correlations can match the experimental results acceptably. The mathematical formulations of Corey and LET relative permeability correlations are shown in following equations as a function of normalized water saturation. Moreover, the definition of the normalized water saturation is given as following:

$$S_w^* = \frac{S_w - S_{wi}}{1 - S_{wi} - S_{or}} \quad (4.14)$$

The oil and water relative permeability from Corey correlations are given by;

$$k_{rw}(S_w^*) = k_{rw}^0 \times (S_w^*)^{N_w} \quad (4.15)$$

$$k_{ro}(S_w^*) = k_{ro}^0 \times (1 - S_w^*)^{N_o} \quad (4.16)$$

where, k_{rw}^0 and k_{ro}^0 are effective permeability at the irreducible water saturation (S_{wi}) and reducible oil saturation (S_{or}), N_w and N_o are exponents on water and oil relative permeability curves respectively.

Indeed, in (4.15) and (4.16) the curvatures of relative permeability curves are defined by parameters N_w and N_o for water relative permeability and oil relative permeability, respectively. Figure 4.34 shows behavior of oil relative permeability with Corey parameter N_o (Corey, 1954; Sendra, 2011).

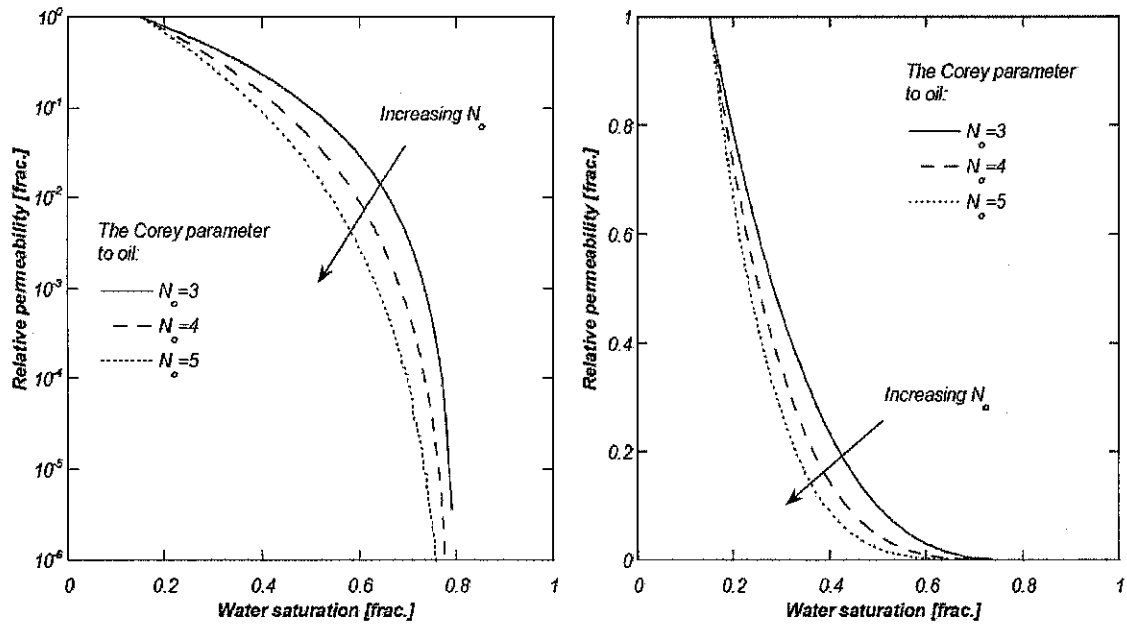


Figure 4.34: Behavior of oil relative permeability, Corey-parameter (Sendra, 2011)

Also the oil and water relative permeability from LET correlations are given by;

$$k_{rw}(S_w^*) = k_{rw}^0 \times \frac{(S_w^*)^{L_w}}{(S_w^*)^{L_w} + E_w(1 - S_w^*)^{T_w}} \quad (4.17)$$

$$k_{ro}(S_w^*) = k_{ro}^0 \times \frac{(1 - S_w^*)^{L_o}}{(1 - S_w^*)^{L_o} + E_o(S_w^*)^{T_o}} \quad (4.18)$$

where L_w and T_w are constant exponents on water relative permeability curve, and L_o and T_o are constant exponents on oil relative permeability curve. Once more, in (4.17) and (4.18) the curvatures of relative permeability curves are defined by these

empirical parameters. Figure 4.35 shows the behavior of oil relative permeability with LET correlation (Sendra, 2011). The parameter L describes lower part of the curve, and by similarity and experience L -values are comparable to the appropriate Corey parameter. The parameter T describes upper part (or the top part) of the curve in a similar way that the L -parameter describes the lower part of the curve. The parameter E describes position of the slope (or the elevation) of the curve. A value of one is a neutral value, and the position of the slope is governed by the L - and T -parameters. Increasing the value of the E -parameter pushes the slope towards the high end of the curve. Decreasing the value of the E -parameter pushes the slope towards the lower end of the curve (Sendra, 2011).

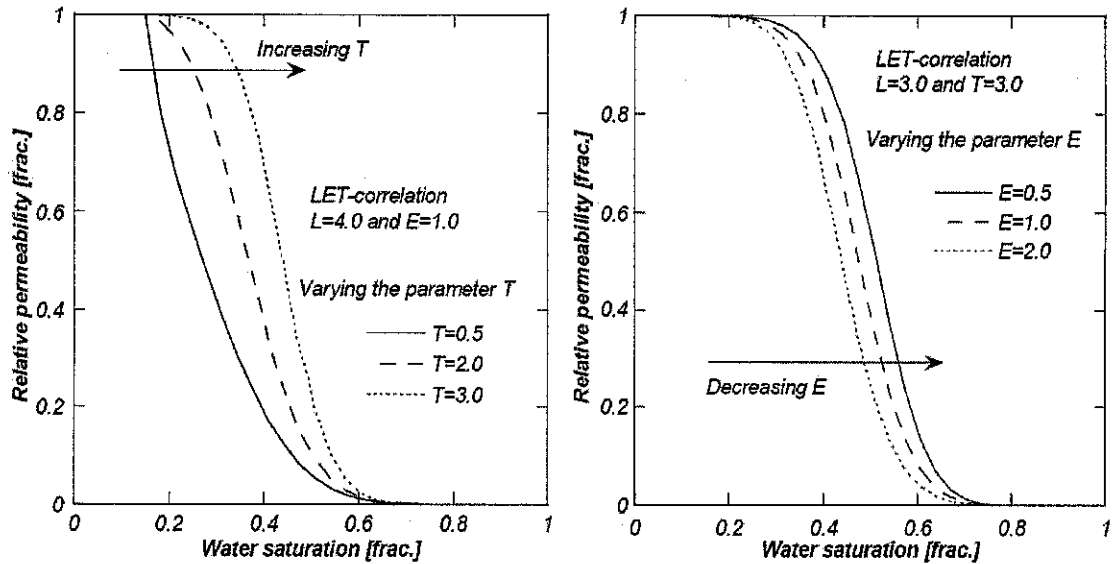


Figure 4.35: Behavior of oil relative permeability, LET correlation (Sendra, 2011)

The most frequently used functional forms for expressing relative permeability data are given in the power law relationship and Corey and LET correlations were the best ones for providing the best history match of the experimental data. Therefore, the new correlations are developed similar to the form of Corey type correlations which it has less empirical parameters compare to LET correlation by introducing some more supplementary parameters related to asphaltene deposition. For this purpose, the non-linear multi-regression analysis based on experimental results is used to develop the appropriate correlations for irreducible water saturation, residual oil saturation, water relative permeability, and oil relative permeability in as a function of the average amount of asphaltene deposition per pore volume, denoted by α .

Table 4.16: Average amount of asphaltene deposition during coreflooding experiment

Ratio of n-heptane to oil injection, %	Asphaltene deposition, g/pore vol	Asphaltene deposition, vol/bulk vol
0	0.00000000000	0.00000000000
20	0.03588026966	0.0067539328
50	0.05225865168	0.0098367168
80	0.08409438202	0.0158303845

Here, α is defined as the ratio of average amount of asphaltene deposition in gram to the pore volume of core sample in cubic cm, g/cm³. Table 4.16 shows the obtained values for α during coreflooding experiments as function of amount of asphaltene deposition.

Based on the results of non-linear multi-regression analysis, the following relationships, among various forms tried, for the irreducible water saturation and the residual oil saturation as a function of α , provided the best match of the experimental data, respectively;

$$S_{wi} = A_1 + A_2 \times \alpha^{2.5} + A_3 \times \alpha^{3.0} \quad (4.19)$$

$$S_{or} = B_1 + B_2 \times \alpha^{0.5} + B_3 \times \exp(-\alpha) \quad (4.20)$$

where, the coefficients A_1 , A_2 , A_3 , B_1 , B_2 , and B_3 are given by;

$$A_1 = 0.202399336827508$$

$$A_2 = -111.679140690674$$

$$A_3 = 309.96168267463$$

$$B_1 = -0.449937033913859$$

$$B_2 = 0.103124261863403$$

$$B_3 = 0.638133880573715$$

Moreover, the water and oil relative permeability as a function of normalized water saturation and average amount of asphaltene deposition per pore volume are given by;

$$k_{rw}(S_w^*) = C_1 \times (S_w^*)^{C_2} + \alpha \times C_3 \times (S_w^*)^{(\alpha \times C_4)} \quad (4.21)$$

$$k_{ro}(S_w^*) = D_1 \times (1 - S_w^*)^{D_2} + \alpha \times D_3 \times (1 - S_w^*)^{(\alpha + D_4)} \quad (4.22)$$

where the coefficients C_1 , C_2 , C_3 , C_4 , D_1 , D_2 , D_3 , and D_4 are given by;

$$C_1 = 9.95921868622281\text{E-}02$$

$$C_2 = 2.30478548350005$$

$$C_3 = 2.04663411338869$$

$$C_4 = 15.079810820436$$

$$D_1 = 0.922625545986362$$

$$D_2 = 1.49343481064284$$

$$D_3 = -4.10276846678706$$

$$D_4 = 1.49275414055384$$

The exponents and coefficients in (4.19) through (4.20) are determined by the least-squares method to match the experimental irreducible water saturation, experimental residual oil saturation, and experimental relative permeability data. In addition, these proposed correlations use only the normalized water saturation and the amount of asphaltene deposition per pore volume as correlating parameters.

The agreements between oil and water relative permeability values predicted from the history matching process, indeed experiments, and from proposed correlations (4.19-4.20) for different values of α that related to the different ratios of simultaneously n-heptane to oil injection, 0%, 20%, 50% and 80% experiments, are shown in Figure 4.36 to Figure 4.39. As can be seen, the agreements are quite good

just for the oil relative permeability values in saturations close to irreducible water saturation.

As reported in the literature amount of asphaltene deposition in the porous media is related to the pore size distribution (Shedid, 2001). Therefore, the pore size distribution should be considered as additional independent parameter into these correlations too. As previously explained, all displacement experiments in this study were conducted for the sandstone cores having almost same properties. Further research and experimental works may be needed to investigate the effect of pore size distribution on asphaltene deposition and to relate the parameter α into pore size distribution.

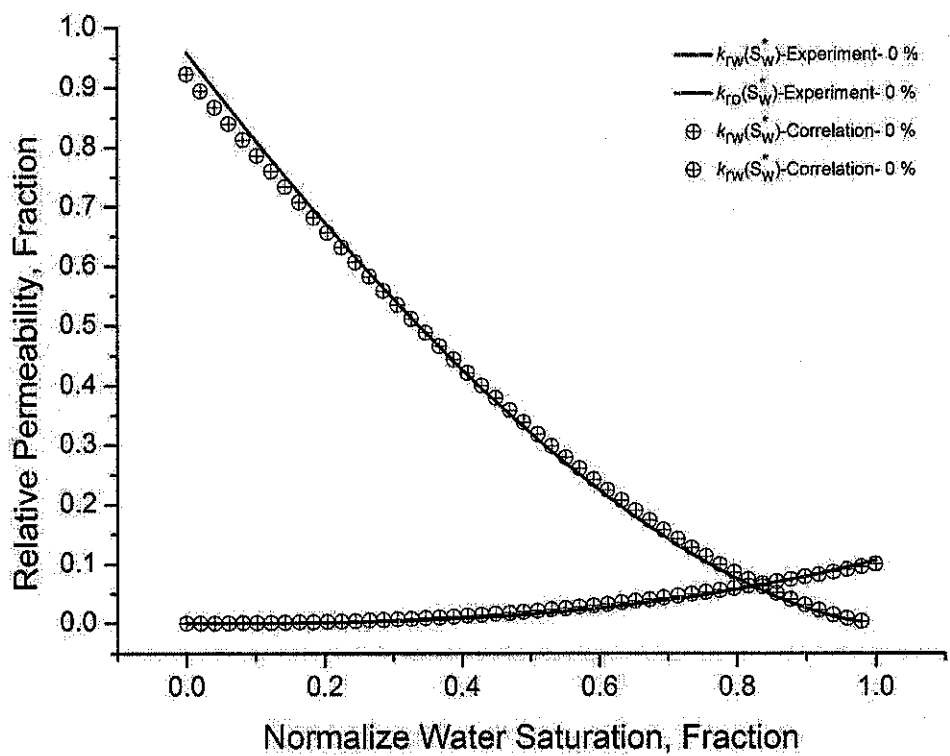


Figure 4.36: Oil-water relative permeability matching between Corey Correlation and this study correlation (zero % ratio of n-heptane–crude oil injection)

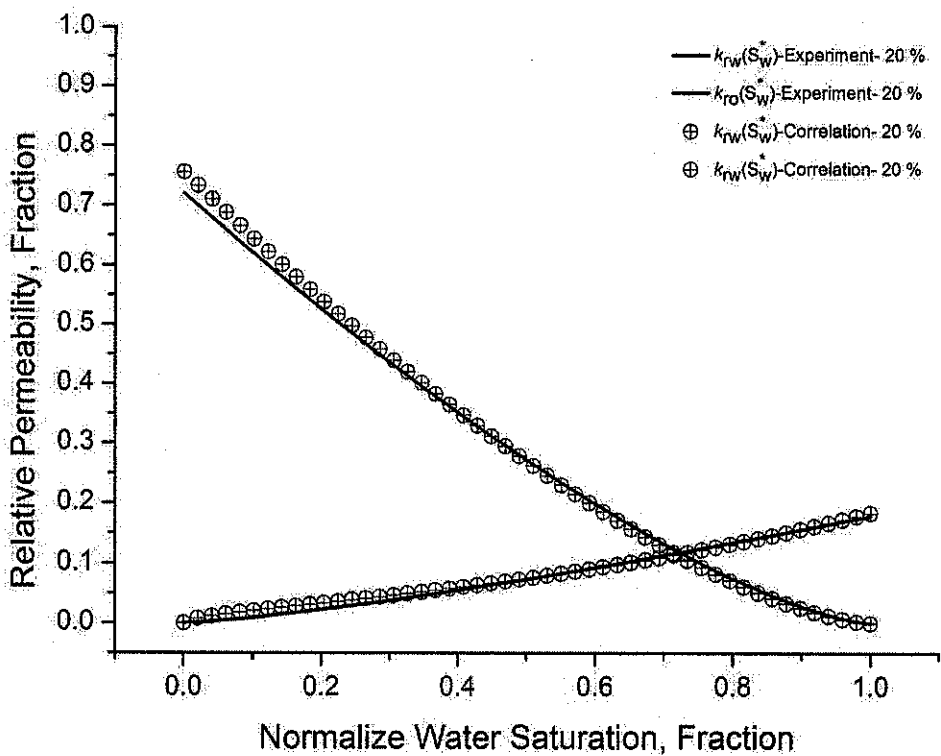


Figure 4.37: Oil-water relative permeability matching between Corey Correlation and this study correlation (20 % ratio of n-heptane–crude oil injection)

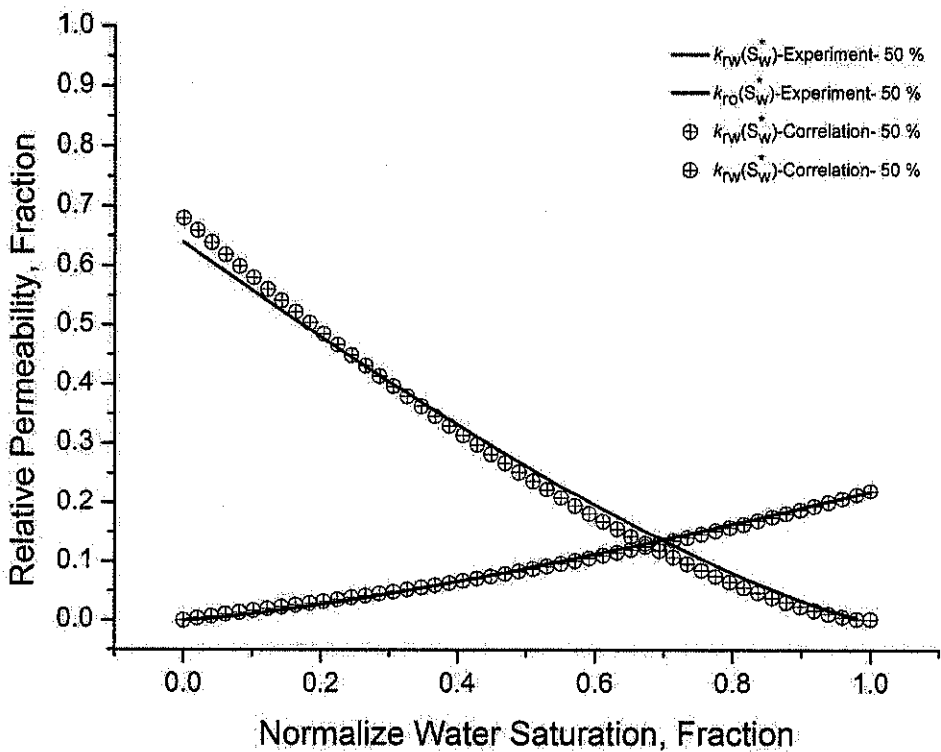


Figure 4.38: Oil-water relative permeability matching between Corey Correlation and this study correlation (50 % ratio of n-heptane–crude oil injection)

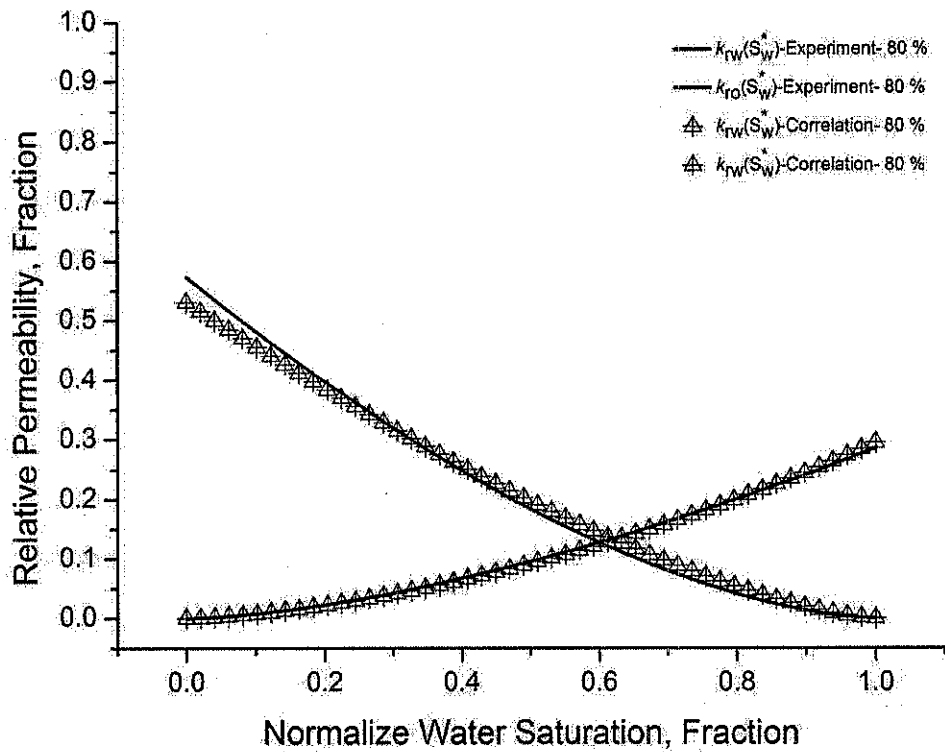


Figure 4.39: Oil-water relative permeability matching between Corey Correlation and this study correlation (80 % ratio of n-heptane–crude oil injection)

4.6 Summary

In this chapter the experimental results which are obtained during this study have been presented. The relative permeability curves for water-oil and gas-oil systems have been computed by the history matching of experimental data and simulation results. Three-phase relative permeability for oil phase is computed based on the Stone's II model. Correlations to predict the behavior of two-phase oil and water relative permeability under asphaltene deposition (as a function of the parameter α , defined as the ratio of average amount of asphaltene deposition to volume of core sample) have been proposed.

CHAPTER 5

ASPHALTENE MODELING AND SIMULATION

5.1 Overview

In this chapter, a workflow to use the coreflooding results given in the previous chapter for simulation of asphaltene deposition during WAG process is proposed. Within this the workflow, the technique of asphaltene modeling and simulation by using a compositional simulator (Eclipse 300) is investigated. A fluid model based on fluid properties and asphaltene experimental data is constructed. The asphaltene control parameters are adjusted by using the coreflooding data. Moreover, the required weight factors for relative permeability alteration as function of asphaltene deposition are obtained based on dynamic displacement experiments results and non-linear multi-regression analysis. In addition, the simulation results for two different cases, asphaltene and without asphaltene causes are presented.

5.2 Asphaltene Modeling and Simulation

Reservoir simulation has become a standard predictive tool in the oil industry. It can be used to obtain accurate performance predictions for a hydrocarbon reservoir under different operating conditions. A hydrocarbon recovery project usually involves a capital investment of hundreds of millions of dollars, and the risk associated with its selected development and production strategies must be assessed and minimized (Ma, 2006; Chen, 2007). This risk includes such important factors as complexity of a petroleum reservoir and fluids filling it, complexity of hydrocarbon recovery mechanisms, and applicability of predictive methods. These complexities can be taken into account in reservoir simulation through data input into simulation model, and this

applicability can be estimated through sound engineering practices and accurate reservoir simulation. Reservoir simulators based on classification of type of reservoir fluids include black oil and compositional simulators. The black oil simulators are conventional simulators, and are used in cases where recovery processes are not sensitive to compositional changes in the reservoir fluids. Compositional simulators are used when recovery processes are sensitive to compositional changes, such as asphaltene precipitation and deposition.

There are a number of asphaltene models currently in use by the simulators, but, there is still no consensus about the characterization of asphaltene behavior (Schlumberger, 2011). Basically, asphaltene modeling and simulation processes are decomposed into different stages in each simulator. Precipitation triggers sequence of flocculation, deposition and formation damage, including porosity and absolute permeability reduction, viscosity changes, and relative permeability alteration, as shown in Figure 5.1. The double arrow indicates partial or total reversibility (Schlumberger, 2011).

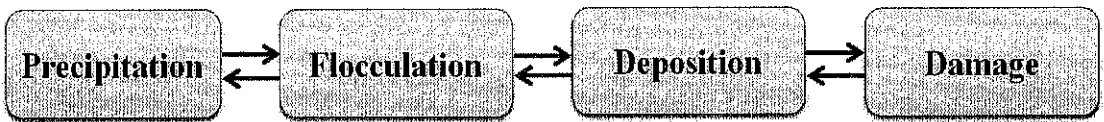


Figure 5.1: Asphaltene modeling and simulation processes

There are several conventional and in-house compositional simulators that can be used to model the asphaltene. Three of very popular compositional simulators are Eclipse 300 from Schlumberger Company, CMG/GEM from Computer Modeling Group Ltd., and UTCOMP which is produced by the Petroleum Engineering Department at the University of Texas, Austin.

However, there are some differences between the methods of these simulators to model asphaltene precipitation, flocculation, deposition, porosity reduction, permeability reduction, viscosity changes, and wettability, and relative permeability alteration. For instance, Eclipse 300 and UTCOMP have some models to consider relative permeability alteration however CMG/GEM does not proposed any model for that. In this study initially the fluid modeling utility of CMG which is called WinProp

has been used to obtain a proper equation of state then Eclipse 300 with asphaltene option has been applied.

5.3 Fluid Modeling

Typically, asphaltene modeling and simulation start with introduction a fluid model. The fluid model can be an equation of state to describe the behavior of fluid components including asphaltene which it can be obtained by performing a PVT data analysis.

A solid model is used for fluid modeling in WinProp simulator. The approach for modeling asphaltene precipitation based on the solid model is described in detail by Nghiem *et al.* (1993, 1996) and Kohse *et al.* (2000). The solid model is adopted to represent the asphaltene behavior while, phase behavior of oil and gas is modeled with one of equation of states. Precipitation of asphaltene can be modeled by using a multiphase flash calculation in which fluids phases are described with an equation of state and fugacity of components in the solid phase are predicted using the solid model.

The precipitated phase is represented as an ideal mixture of solid components. The crucial step in modeling asphaltene precipitation is characterization of solid forming components, both in solution and in the solid phase. The heaviest pseudo component in the fluid model should be split into two components, a non-precipitating and a precipitating fraction. These two components have same critical properties and acentric factors, but may have different binary interaction parameters and different volume shift parameters. The mole fractions of these two pseudo components can be calculated by using the experimental value of weight percent asphaltene in the dead oil sample. Typically, this fluid model with asphaltene component should tune based on the experimental fluid properties and the solid model given in fugacity equation should use to predict the amount of solid precipitate. To use fugacity equation a reference fugacity at a reference pressure and a solid molar volume must be known. Usually, the reference fugacity is set equal to the fugacity of asphaltene component in liquid phase predicted by equation of state. Moreover, the

solid molar volume is normally set slightly higher than molar volume of the asphaltene component predicted by equation of state. Therefore, after these steps, the asphaltene precipitation values at different reservoir conditions can be predicted by this fluid model.

5.4 Asphaltene Simulation and Control Parameters

Currently, the conventional simulation package (Eclipse 300) considers asphaltene modeling base on the description of asphaltene control parameters. These parameters should use to model the asphaltene precipitation, the flocculation-dissociation, the deposition, the porosity reduction, the absolute permeability reduction, the viscosity changes, and the relative permeability alteration processes. These parameters mostly should be obtained and adjusted by the experimental results and should be defined by user.

5.4.1 Asphaltene Precipitation

Asphaltene is defined as a set of component(s) that can precipitate depending on their percentage molar weight in the solution. The percentage molar weight limit is defined by the user as a function of pressure, temperature or molar fraction of a specified component. The amount of precipitate corresponds to the excess of a specified component in oil phase with respect to limit defined by the user. The amount of asphaltene precipitation versus pressure at constant temperature can be calculated based on this percentage limit or the corresponding percentage of asphaltene dissolved in the oil phase. These values should be between zero and one hundred. A value of zero means that all asphaltene component(s) have precipitated, whereas a value of one hundred means that all asphaltene component(s) remain(s) dissolved in the oil phase (Schlumberger, 2011).

5.4.2 Asphaltene Flocculation-Dissociation

As described earlier in the fluid modeling section, a pseudo component is represented the asphaltene precipitating component in the oil phase. The flocculation process can be modeled by considering this component as a floc component. The flocculation-dissociation process which lets asphaltene can flocculate from precipitated status is modeled by a set of two kinetic reactions parameters. These two parameters allow reversibility (partial or total) between aggregation and dissociation processes. The first process is aggregation of the precipitated fines asphaltene into precipitated flocs asphaltene and the second one is dissociation of the flocs precipitated asphaltene into fines. Let C_i denote the concentration of the precipitated fines asphaltene that is coming from component i and C_a the concentration of the precipitated flocs asphaltene. Once precipitation occurs, the aggregations rate of the fines i into flocs a is modeled by;

$$R_a = \frac{\partial C_a}{\partial t} = r_{ia} \times C_i - r_{ai} \times C_a \quad (5.1)$$

where R_a is aggregation rate, r_{ia} is flocculation rate coefficient of the fines and r_{ai} is dissociation rate coefficient of flocs. In the case where asphaltene is seen as a single pure component, this flocculation reduces to two kinetic reactions only (Schlumberger, 2011).

5.4.3 Asphaltene Deposition

Wang and Civan (2001) model uses to simulate the asphaltene deposition. In this model precipitated flocs asphaltene can be deposited in three mechanisms which are adsorbing on the rock surface, plugging in the porous media, and entraining the deposited asphaltene. Therefore, the deposition process is modeled with incorporating three coefficients which are represented process that precipitated flocs asphaltene can be adsorbed on the rock surface, can be trapped within the porous media because of their size or can be entrained and returned to the oil phase because of high, local velocity, respectively.

Wang and Civan's (2001) model in the flow direction i is given as follows;

$$\frac{\partial \varepsilon_i}{\partial t} = \frac{\alpha}{d} \phi C_a + \gamma |F_{oi}| C_a - \beta (|U_{oi}| - |U_{cr}|)^+ \varepsilon_i \quad (5.2)$$

where;

d is the dimension of the problem (1, 2 or 3)

ε_i is volume fraction of deposit in the i direction of the flow

α is adsorption or static deposition coefficient

ϕ is current porosity (at time t)

C_a is volumetric concentration of the flocs in the oil phase (flowing flocs)

F_{oi} is oil Darcy flux

γ is plugging coefficient

β is entrainment coefficient

U_{oi} is oil phase velocity ($F_{oi} / A\phi$), A is the section area between connecting cells

U_{cr} is user input critical velocity.

The “+” sign around the bracket for the entrainment part means that the entrainment will be zero if the velocity $|F_{oi}|$ is smaller than the critical value, U_{cr} .

The overall volume fraction deposit is sum of the deposits in each direction I which ε is the cumulative volume of asphaltene deposition (Schlumberger, 2011);

$$\varepsilon = \sum_{i=1}^{i=d} \varepsilon_i \quad (5.3)$$

5.4.4 Porosity and Absolute Permeability Reduction

The porosity reduction associated with asphaltene deposition is defined as a reduction of pore spaces which is resided in with deposited asphaltene, indeed, instantaneous or local porosity, ϕ , during asphaltene deposition is equal to the difference between initial porosity, ϕ_0 , and fractional pore volume occupied by asphaltene deposits, ε which can be written as (Wang and Civan, 2001; Schlumberger, 2011);

$$\phi = \phi_0 - \int_0^t \frac{\partial \varepsilon}{\partial t} dt \quad (5.4)$$

Typically, the absolute permeability can be correlated to the porosity. Therefore, the reduction in absolute permeability due to asphaltene deposition can also be taken into account using a parameterized power law relationship given the ratio of the instantaneous permeability, k , at time t with respect to the initial permeability, k_o , which can be written as:

$$\frac{k}{k_o} = \left(1 - \frac{\varepsilon}{\phi_0} \right)^\delta \quad (5.5)$$

where δ is a user input around 3 that it should be based on core experiment data and ϕ_0 is initial porosity, ε is volume fraction of asphaltene deposit from Wang and Civan's (2001) model. Alternatively, if rock permeability is independent of porosity, or data giving a relationship between the permeability and the amount of asphaltene deposit are available, this can be directly used (Schlumberger, 2011).

5.4.5 Viscosity Changes

The viscosity of oil phase can change during asphaltene precipitation process. Indeed, when precipitation process occurs, asphaltene components which are considered as colloids in the oil phase can precipitate from bulk flow. This precipitation can be caused oil phase properties change and in result can alter the viscosity oil phase. Currently, the viscosity changes can be modeled in three different ways (Schlumberger, 2011). First if data that gives oil viscosity multiplier as a function of

volume fraction of asphaltene precipitate are available. Second using the generalized Einstein model (one parameter) where the default value for constant parameter, a is 2.5, and C_p is the volume concentration of asphaltene precipitate, and μ_o is oil viscosity at $C_p=0$;

$$\frac{\mu}{\mu_o} = 1 + aC_p \quad (5.6)$$

The third model is Krieger and Dougherty (1959) model (two parameters) where, η is intrinsic viscosity, $\eta=2.5$ for spherical colloids, C_{po} is volumetric concentration for maximum packing, equal to 0.65 for spheres packing;

$$\frac{\mu}{\mu_o} = \left(1 - \frac{C_p}{C_{po}}\right)^{-\eta C_{po}} \quad (5.7)$$

5.4.6 Relative Permeability Alteration

As reported by Schlumberger (2011), the asphaltene deposition can change the rock wettability and its effects can be considered with a shifting of relative permeability data from a water-wet system to an oil-wet system. The weight factor, F , as a function of volume fraction of asphaltene deposit is only proposed method to model relative permeability alteration. The main relative permeability data which are considered as water-wet data are modified with oil-wet relative permeability data which entered by user . To perform this method, the amount of asphaltene deposition is computed, a proper F -factor is found from the user input data, and the residual oil and irreducible water saturations are scaled based on this F -factor. Moreover, a look-up for relative permeability data is carried out on the scaled saturations from previous step, followed by a linear interpolation between the water-wet and oil-wet relative permeability data as follow;

$$S_{ora} = FS_{oro} + (1-F)S_{orw} \quad (5.8)$$

$$S_{wia} = FS_{wio} + (1-F)S_{wiw} \quad (5.9)$$

$$k_{rwa} = Fk_{rwo} + (1 - F)k_{rww} \quad (5.10)$$

$$k_{roa} = Fk_{roo} + (1 - F)k_{row} \quad (5.11)$$

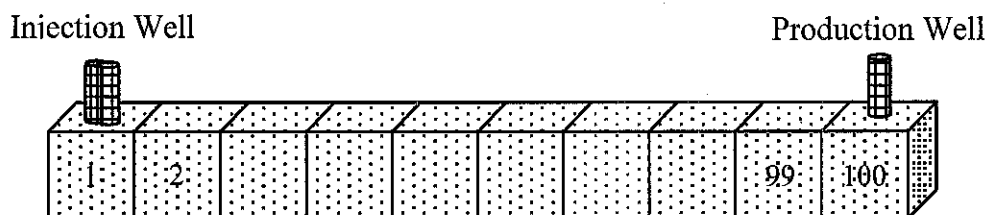
where S_{oro} , S_{wio} , k_{rwo} , and k_{roo} are residual oil saturations, irreducible water saturation, water relative permeability, and oil relative permeability in oil-wet relative permeability data, respectively. In the same definition S_{orw} , S_{wiw} , k_{rww} , and k_{row} are parameters in water-wet relative permeability data.

5.5 Workflow for Asphaltene Modeling and Simulation

The proposed workflow in this study starts with building a compositional simulation input data file with asphaltene facilities. Then, a fluid model with asphaltene facility is constructed based on fluid experimental data. The asphaltene control parameters are adjusted based on coreflooding experiments. Moreover, the required weight factors for relative permeability alteration as function of asphaltene deposition are obtained based on dynamic displacement experiments results and multi-regression analysis. The simulation results for asphaltene and without asphaltene causes are given. Of course, a geologic model should be given to start with modeling. Here, to illustrate the workflow proposed here a simple synthetic model given below is considered.

5.5.1 Synthetic Model

One dimensional model with a grid dimension of $100 \times 1 \times 1$ is chosen. The widths of each grid block in the x and y direction is a uniform 80 ft with a uniform vertical grid block thickness of 20 ft. The porosity is considered 22.4 percent and same for all grid blocks. The absolute permeability in x direction is 260 md. The porosity and absolute permeability values are considered as the same as those for the core sample properties.



The water injector and CO₂ injector wells are located at block 1 which is left edge of the reservoir and the producer well is located at block 100 which is right edge of the reservoir. Figure 5.2 shows a schematic of the simulation model for this reservoir. The injection and production plan is included five hundred days natural depletion, five hundred days water injection, and two-thousand days cycle of WAG injection. The total recovery period is more than eight years. The producer operates under a constant bottomhole pressure (BHP) of 500 psi. The water injection and gas injection wells are commenced at a constant surface rate of 100 STB/day and 500 MSCF/day, respectively.

In lack of using the live oil sample for this study, the fluid properties and the experimental asphaltene precipitation data which are required for building the fluid model are taken from Burke *et al.* (1990). The composition of this oil is given in Table 5.1. The oil contains 16.08% (weight) asphaltene at stock tank condition, a reported bubble point pressure of 2,950 psi, and a stock tank oil API gravity of 19.0. Moreover, the experimental data of asphaltene precipitation have been reported for oil sample at 212 °F as a function of pressure and are shown in Table 5.2.

Table 5.1: Experimental fluid properties

Component	Mole Fraction
Nitrogen	0.57
Carbon Dioxide	2.46
Methane	36.37
Ethane	3.47
Propane	4.05
i-Butane	0.59
n-Butane	1.34
i-Pentane	0.74
n-Pentane	0.83

Hexanes	1.62
Heptane plus	47.96
Total	100.00
C ₇₊ molecular weight	329
C ₇₊ specific gravity	0.9594
Live oil molecular weight	171.4
Stock tank oil API gravity	19.0
Asphaltene content in stock tank oil	16.8 wt%
Reservoir temperature	212 °F
Saturation pressure	2950 psi

Table 5.2: Experimental asphaltene precipitation at 212 °F

Test pressure, psi	Precipitates live oil, wt%	Precipitates residual STO, wt%
1014.7	0.403	15.73
2014.7	1.037	14.98
3034.7	0.742	15.06
4014.7	0.402	14.86

5.5.2 Fluid Modeling

The most important step in numerical compositional simulation is fluid modeling. Typically, an equation of state (EOS) should introduce into simulation model and its parameters should tune based on available experimental fluid properties data. The steps required to develop a fluid model are: fluid characterization, regression and tuning of equation of state, specification of solid model parameters, and adjusting the prediction of asphaltene precipitation behavior (CMG, 2011).

In this study the Peng-Robinson (1976) equation of state has been chosen to predict the state of oil and gas phases. A data set which is taken from Burke *et al.* (1990) has been prepared to characterize the fluid by defining the compositions of components up to C₆ and pseudo-components describing the C₇₊ fraction. The composition data to C₆ has been used, and a plus fraction splitting calculation has been specified with the C₇₊ molecular weight and specific gravity. The plus fraction is split from C₇ to C₃₁₊ and then, they are lumped into four pseudo components, and Lee and Kesler (1975) correlations are used to predict the critical properties of these pseudo-components.

After splitting, lumping, and updating the components to reflect the results of the splitting calculation, the equation of state model is tuned to any available PVT data via regression. The observed data that have been provided from lab experiments are bubble point pressure, API gravity, and live oil molecular weight. Regression is conducted on these experimental data by tuning the regression variables. The hydrocarbon interaction coefficient exponent and the critical properties of heavy components are selected as regression variables. Several runs to tune the equation of state have been done until the regression summary table at the end of the output file has showed a good match to the saturation pressure and stock tank oil API gravity. In this step the model needs to be modified for asphaltene precipitation option by introducing the asphaltene component and its properties.

To define the asphaltene component, the heaviest component of the oil should split into two parts, non-precipitating component C_{31A+} and precipitating component, C_{31B+} . The precipitating component is assumed to be asphaltene which is later called as the “floc” component in Eclipse 300. To split the heaviest component, C_{31+} into two components C_{31A+} and C_{31B+} a new component is added to end of the component list. All properties of C_{31+} are copied and pasted onto the newly added component. The two last components which have same name (C_{31+}) and same properties should be renamed as C_{31A+} and C_{31B+} respectively. To specify the binary interaction coefficients of C_{31B+} with the light components up to about C_5 as opposed to calculating them with the hydrocarbon (HC) interaction coefficient exponent, the HC flag in the column next to the C_{31B+} component name should be set to zero. The binary interaction coefficients for the precipitating component must be considered higher than those for the non-precipitating component to give the correct shape of the precipitation curve below the bubble point. Typically, the binary interaction coefficients between C_{31B+} - CO_2 and C_{31B+} - N_2 should be considered as the same as those between C_{31A+} - CO_2 and C_{31A+} - N_2 , respectively. Moreover, the values of binary interaction coefficients between C_{31B+} and heavier components than C_5 should be entered as zero. The remaining values are changed on the order 0.2 which is expected to give good match.

In addition, the mole fraction of newly added asphaltene component should specify in this step. The mole fraction of C_{31B+} as asphaltene component is computed from following relation;

$$x_{Asphaltene} = w_{Asphaltene} \times \frac{\overline{MW}_{Oil}}{MW_{Asphaltene}} \quad (5.12)$$

$$\overline{MW}_{Oil} = \sum x_i MW_i \quad (5.13)$$

where;

$x_{Asphaltene}$ is mole fraction of asphaltene component, fraction

x_i is mole fraction of oil components, fraction

$MW_{Asphaltene}$ is molecular weight of asphaltene, kg/kmol

$w_{Asphaltene}$ is weight percent of asphaltene in oil, wt%

\overline{MW}_{Oil} is average molecular weight of oil, kg/kmol

MW_i is molecular weight of each oil components, kg/kmol

By subtracting the amount of mole fraction of C_{31B+} from the original mole fraction of C₃₁₊, the mole fraction for C_{31A+} can be obtained. These results are given in Table 5.3.

Table 5.3: Splitting heaviest component to obtain asphaltene mole percent

Before Splitting		MW _{Oil}	171.4	After Splitting	
C ₃₁₊	0.11749267	MW _{Asphaltene}	665.625	C _{31A+}	0.07424660
		Weight % of Asphaltene	16.8	C _{31B+} or floc	0.04324607

The splitting heaviest component process, the entering the mole fractions step, and the adjusting the binaries interaction coefficients for the precipitating asphaltene

component, may affect the previous match of equation of state that has been achieved. For this reason, regression step must be performed once more to ensure that the equation of state can again achieve a good match.

In this model fluid phases are described with an equation of state and solid model can predict the fugacity of components in the solid phase. Usually, the equation of state cannot compute correctly the fugacity of asphaltene in the solid phase. Consequently, the following fugacity equation which can describe the fugacity of solid component (asphaltene) in the solid phase under isothermal conditions should be used. In this equation asphaltene fugacity is depends on its solid molar volume and reference fugacity that are the most critical terms in computing the asphaltene precipitation.

$$\ln f_s = \ln f_s^* + v_s \frac{(P - P_0)}{RT_0} \quad (5.14)$$

where;

f_s^* is referred to as the reference (asphaltene) fugacity, psi

P_0 is reference conditions for pressure, psi

T_0 is reference conditions for temperature, °R

v_s is molar volume of the solid (asphaltene), L/mol

R is gas constant, ft³ psi R⁻¹ lb-mol⁻¹

The reference fugacity is usually set equal to the fugacity of the precipitating component calculated by the equation of state at an experimentally determined asphaltene precipitation onset pressure for a given temperature. Therefore, at least amount of asphaltene precipitation in one creation condition (pressure and temperature) should be determined experimentally. Typically, the amount of asphaltene precipitation is reported in the asphaltene onset point conditions.

As shown in Table 5.1 an exact onset pressure is not reported. Moreover, the amounts of asphaltene precipitation are reported at pressure below and above the bubble point pressure as shown in Table 5.2. For this reason the data of 0.402 wt% asphaltene precipitated at 4014.7 psi and 212 °F is used supplementary to compute the solid molar volume and set the reference fugacity.

Once more the model is run to check the regression on the fluid properties data and to find the solid molar volume which is predicted by equation of state. This solid molar volume should be set to a value slightly higher than the molar volume for the precipitating component predicted by the equation of state. The output regression summary file shows that both the saturation pressure and stock tank API are exactly matched and the solid molar volume is given as 0.65883 L/mol. Therefore, an initial value of the solid molar volume can be entered equal to 0.67000 L/mol. In this step the predictions of asphaltene precipitation curve can be drawn by using the asphaltene/wax modeling option of simulator. The asphaltene prediction curve based on this initial solid molar volume value and those are obtained from experiment are shown in Figure 5.3.

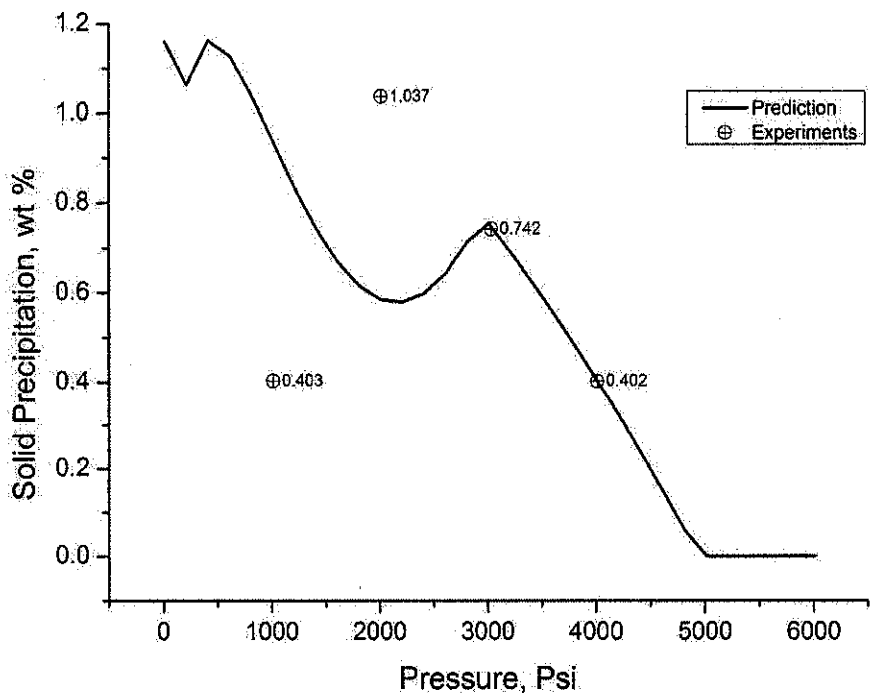


Figure 5.3: Initial asphaltene precipitation curve

As shown in this figure the shape of asphaltene precipitation curve for the pressure higher than saturation pressure shows an expected trend of decreasing precipitation with increasing pressure. The predicted amount of asphaltene at the reference pressure of 4014.7 psi is exactly equal to the experimental value of 0.402 wt%. However, the shape of the curve at lower pressures than saturation pressure is incorrect. Therefore, the solid model parameters should be adjusted to achieve the correct shape of the precipitation curve. The parameters that control the reversibility behavior of asphaltene precipitation in the solid model are solid molar volume and interaction parameter. It is assumed that the precipitation of asphaltene from the oil is reversible process and the maximum amount of precipitation can be obtained around the saturation pressure. When the gas liberates from the oil in pressures lower than saturation pressure, the solubility of the crude oil change and the precipitated asphaltene go back into the oil. As it is recommended, increasing the value of solid molar volume can increase the maximum amount of asphaltene precipitation at saturation pressure. Moreover, increasing the values of the interaction coefficient parameters between heavy components (i.e., asphaltene) and light components (i.e., C_1 - nC_5) induce the re-dissolution of the precipitated asphaltene.

The experimental data shown in Table 5.2 indicate that the maximum amount of precipitation from crude oil is 1.037 wt% and from the initial run results in Figure 5.3 is 0.8 wt% that is lower than the experimental value. Therefore, to increase this maximum amount of asphaltene precipitation from 0.8 to 1.037 wt% the solid molar volume of the asphaltene should be slightly increased. Typically, first the value of the solid molar volume should be adjusted to achieve the desired maximum amount of precipitation then, the binary interaction coefficients should be changed. In this case, a value of 0.675 L/mol for solid molar volume and value of 0.224 wt% for all of binary interaction coefficients were found to give good shape to the asphaltene precipitation curve as shown in Figure 5.4.

Figure 5.4 shows that the predicted asphaltene data do not match exactly the experimental data and also the maximum asphaltene precipitate always occurs at pressure of 2950 psi rather than 2014.7. It can be concluded that experimental data may have some errors either in the asphaltene precipitation data or the bubble point

pressure value. Burke *et al.* (1990) also noticed this error, but they did not offer an explanation. Table 5.2 shows that the values of asphaltene precipitation increase with the decreasing in pressure; they reach a maximum value 1.037 wt % at a pressure above the 2014.7 psi, and then decrease rapidly with further decreasing in pressure. Therefore, it may be concluded that value of the reported bubble point is inaccurate and should be a value between 2014.7 and 2950 psi. Based on this argument, the two values of 2500 and 2050 psi have been chosen for bubble point value and all above mentioned procedures have been repeated.

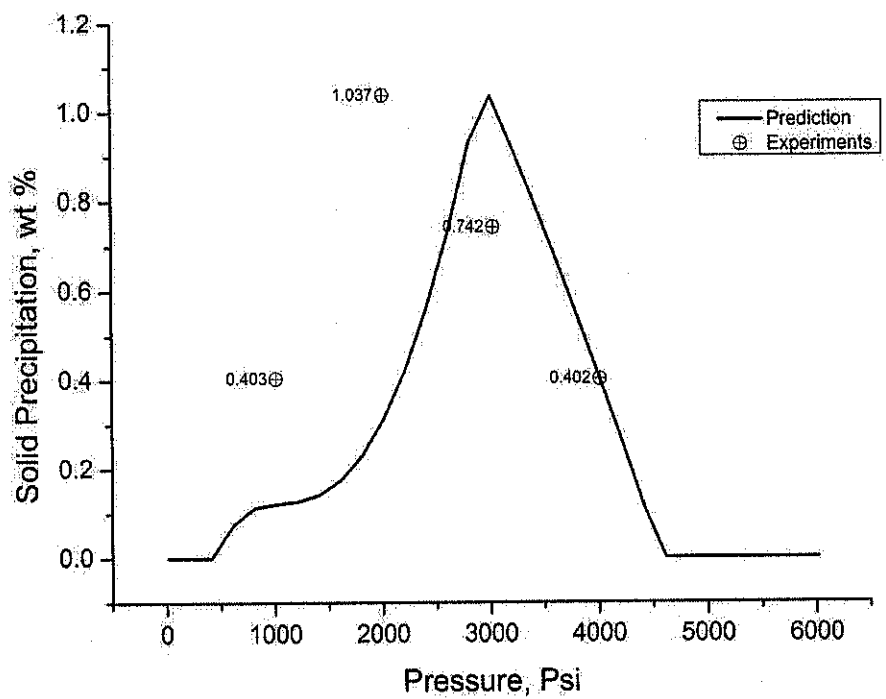


Figure 5.4: Asphaltene precipitation curve after adjusting related parameters

Figure 5.5 and Figure 5.6 show the prediction of asphaltene precipitation curves based on these bubble point pressures. Figure 5.5 shows that the maximum asphaltene precipitation has been obtained 1.04637 wt % that is very close to the experimental value. However, only the two points of four experimental data are matched. Moreover, Figure 5.6 shows the maximum asphaltene precipitation 1.15791 wt % and three points of the four experimental data are matched. It can be concluded that the most possible value for the saturation pressure is around 2050 psi.

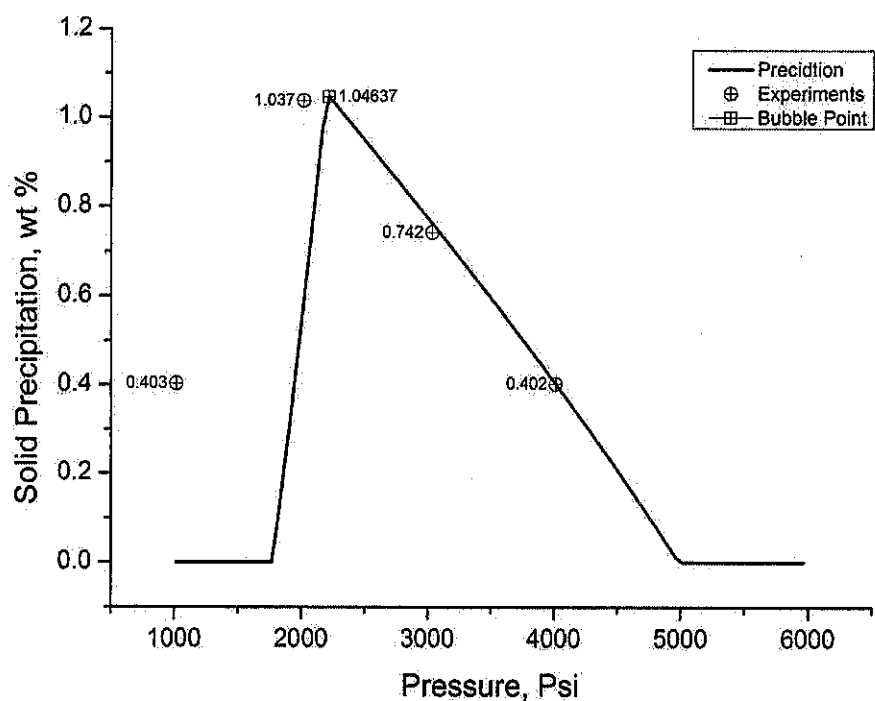


Figure 5.5: Asphaltene precipitation curve for saturation pressure 2500 psi

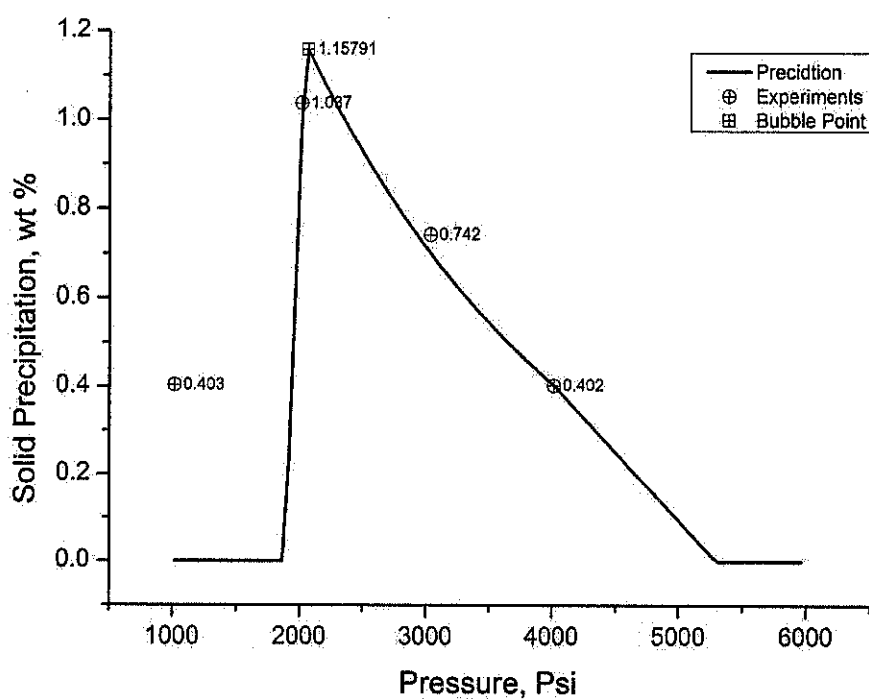


Figure 5.6: Asphaltene precipitation curve for saturation pressure 2050 psi

5.5.3 Asphaltene Control Parameters

One of the important steps for building a simulation model with asphaltene option is introduction values for asphaltene control parameters. Typically, they should be

adjusted based on coreflooding experiments data. The sensitivity studies on the asphaltene control parameters by using the numerical study in two conventional simulators have been done (Khanifar *et al.*, 2011; Khanifar *et al.*, 2012). They have shown that all asphaltene control parameters have been affected the reservoir performance during natural depletion, water injection, and WAG application. Moreover, in the literature, there are only a few published coreflooding experimental data related to asphaltene deposition and a few studies are presented procedures for adjusting the asphaltene control parameters (Burke *et al.*, 1990; Minssieux, 1997; Wang and Civan, 2001; Yi *et al.*, 2009; Figuera *et al.*, 2010).

In this study the asphaltene control parameters are adjusted based on evaluation of values of absolute permeability reduction as a function of asphaltene deposition data from coreflooding experiments and simulation. The equivalent values for asphaltene deposition during coreflooding experiments are computed based on injection rate, total time of simultaneously injection, and average asphaltene weight present in collected oil samples. These values are shown in Figure 5.7 by scatter points as denoted from experiment.

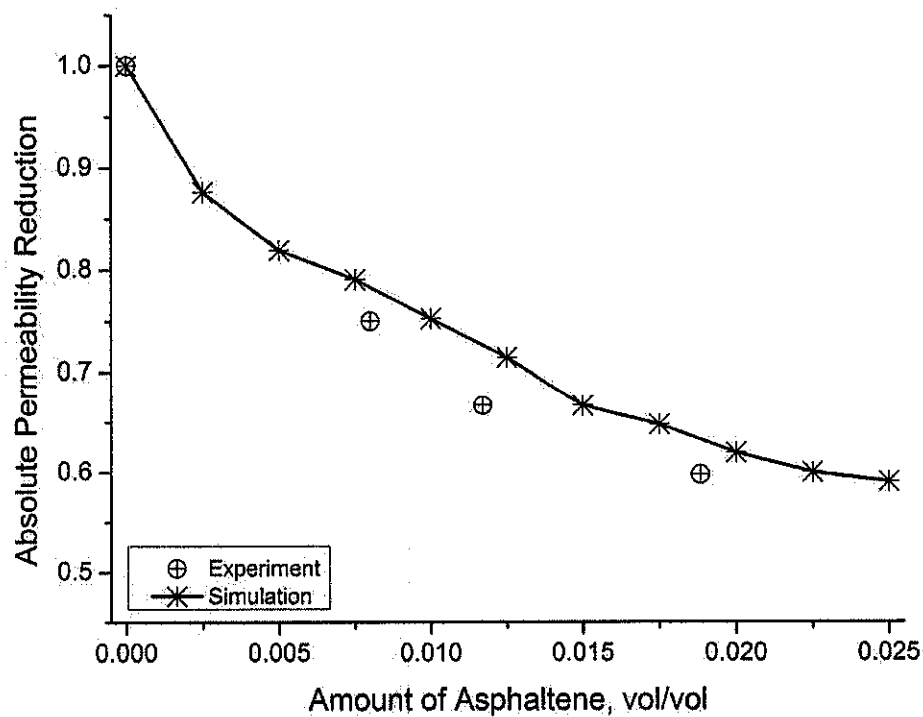


Figure 5.7: Absolute permeability reduction matching between experiments and simulation

Table 5.4: Adjusted asphaltene control parameters

Asphaltene Control Parameters	Value
Flocculation Rate Coefficient (day^{-1})	0.150
Dissociation Rate Coefficient (day^{-1})	0.001
Adsorption Coefficient (day^{-1})	0.100
Plugging Coefficient (ft^{-1})	0.100
Critical Deposition Fraction	0.0
Critical Flocs Concentration	0.0
Permeability Reduction Exponential Index	3
Entrainment Coefficient (ft^{-1})	0.0
Critical Velocity for Entrainment (ft/day)	2500
Constant of Generalized Einstein Model for Viscosity(Schlumberger, 2011)	2.5

Therefore, the asphaltene control parameters have been adjusted during a history matching process of the experimental data with those predicated from the numerical simulation. During this attempt the related values for asphaltene control parameters are changed until an acceptable match between experimental and simulation results are obtained. The comparison between the predicted values from simulation and experimental results of permeability reduction due to asphaltene deposition are shown in Figure 5.7. Moreover, the obtained values for the asphaltene control parameters by this attempt are shown in Table 5.4 and used for further asphaltene simulation.

5.5.4 Relative Permeability Alteration

The relative permeability alteration during simulation can be considered by using the approach of weight factor F as a function of asphaltene deposit. To use this approach a table of weight factor F as function of asphaltene deposition (α^*) and a set oil-wet relative permeability data should be introduced into simulation file data.

The simulator computes the amount of asphaltene deposition in each time step and it uses Equations 5.15 to 5.18 to obtain the corresponding relative permeability data for the obtained amount of asphaltene deposition.

$$S_{ora}(\alpha^*) = F S_{oro}(\text{oil} - \text{wet}) + (1 - F) S_{orw}(\text{water} - \text{wet}) \quad (5.15)$$

$$S_{wia}(\alpha^*) = F S_{wio}(\text{oil} - \text{wet}) + (1 - F) S_{wiw}(\text{water} - \text{wet}) \quad (5.16)$$

$$k_{rwa}(\alpha^*) = F k_{rwo}(\text{oil} - \text{wet}) + (1 - F) k_{rww}(\text{water} - \text{wet}) \quad (5.17)$$

$$k_{roa}(\alpha^*) = F k_{roo}(\text{oil} - \text{wet}) + (1 - F) k_{row}(\text{water} - \text{wet}) \quad (5.18)$$

In this study, to find the suitable data for this approach based on the available experimental results some assumptions need to be considered. It is assumed that the relative permeability data which are obtained during zero% n-heptane-oil injection coreflooding experiment are considered as water-wet relative permeability data. Therefore, the corresponding value for weight factor F for this case is considered equal to zero ($F_1 = 0.0$). Furthermore, the relative permeability data which are obtained during 80% n-heptane-oil injection coreflooding experiment are considered as oil-wet relative permeability data and consequently, the corresponding values for weight factor F is considered equal one ($F_4 = 1.0$).

As a result, the values of weight factor F for other two coreflooding experiments (20% and 50% n-heptane-oil injection) which amounts of their asphaltene deposition are expected between these two cases, should be between zero and one. To obtain the corresponding value for weight factor F for 20% n-heptane-oil injection coreflooding experiment the Equations 5.15 to 5.18 can be modified as following relations;

$$S_{ora}(20\%) = F_2 S_{oro}(80\%) + (1 - F_2) S_{orw}(0\%) \quad (5.19)$$

$$S_{wia}(20\%) = F_2 S_{wio}(80\%) + (1 - F_2) S_{wiw}(0\%) \quad (5.20)$$

$$k_{rwa}(20\%) = F_2 k_{rwo}(80\%) + (1 - F_2) k_{rww}(0\%) \quad (5.21)$$

$$k_{roa}(20\%) = F_2 k_{roo}(80\%) + (1 - F_2) k_{row}(0\%) \quad (5.22)$$

where F_2 is corresponding value for weight factor F in this experiment. As can be seen the only unknown in these equations is F_2 and it can be found by performing the non-linear multi-regression analysis. Similarly, to obtain the weight factor value for

50% n-heptane-oil injection coreflooding experiment once more the Equations 5.15 to 5.18 can be modified as following relations;

$$S_{ora}(50\%) = F_3 S_{oro}(80\%) + (1 - F_3) S_{orw}(0\%) \quad (5.23)$$

$$S_{wia}(50\%) = F_3 S_{wio}(80\%) + (1 - F_3) S_{wiw}(0\%) \quad (5.24)$$

$$k_{rwa}(50\%) = F_3 k_{rwo}(80\%) + (1 - F_3) k_{rww}(0\%) \quad (5.25)$$

$$k_{roa}(50\%) = F_3 k_{roo}(80\%) + (1 - F_3) k_{row}(0\%) \quad (5.26)$$

where F_3 is corresponding value for weight factor F in this experiment. Once more, the only unknown in these equations is F_3 and it can be again found through the non-linear multi-regression analysis. Table 5.5 shows the obtained values for weight factor F as function of amount of asphaltene deposition.

Table 5.5: Weight factor as function of asphaltene deposition

Ratio of n-heptane to oil injection, %	Asphaltene deposition, α^* Asphaltene vol/bulk vol	(Weight Factor, F), fraction
0	0.0000000000	$F_1 = 0.00000$
20	0.0067539328	$F_2 = 0.53230$
50	0.0098367168	$F_3 = 0.70496$
80	0.0158303845	$F_4 = 1.00000$

By using the non-linear multi-regression analysis for values of weight factor F as function of amount of asphaltene deposition in Table 5.5 the following correlation can be provided to predict the other values for F ;

$$F(\alpha^*) = \frac{\alpha^*}{A + B\alpha^* + C\sqrt{\alpha^*}} \quad (5.27)$$

$$A = 0.00582525930049594$$

$$B = -0.0914083050003412$$

$$C = 0.0910209660724414$$

where α^* is the amount of asphaltene deposition and it varies from zero to 0.0158303845 vol/vol and $F(\alpha^*)$ is weight factor F as function of α^* that changes from zero to one. The maximum value of α can be less or equal to 0.0158303845 vol/vol which are obtained during this study coreflooding experiments. For asphaltene deposition more than this value this correlation is not valid and it needs some modification based on new experimental data.

5.5.5 Simulation Results

The injection pattern that has been conducted during this simulation is shown in Figure 5.8. The waterflooding is started after five hundred days of natural depletion. The two cycles of WAG implementation with five hundred days of slugs as EOR method are considered after waterflooding process. In this simulation study two different simulation cases are run to investigate the effect of asphaltene on reservoir performance during WAG implementation. The first case is without considering the asphaltene option and the second case is with activating the asphaltene option. The compositional simulation input file data in asphaltene mode and in Eclipse 300 format is given in Appendix C.

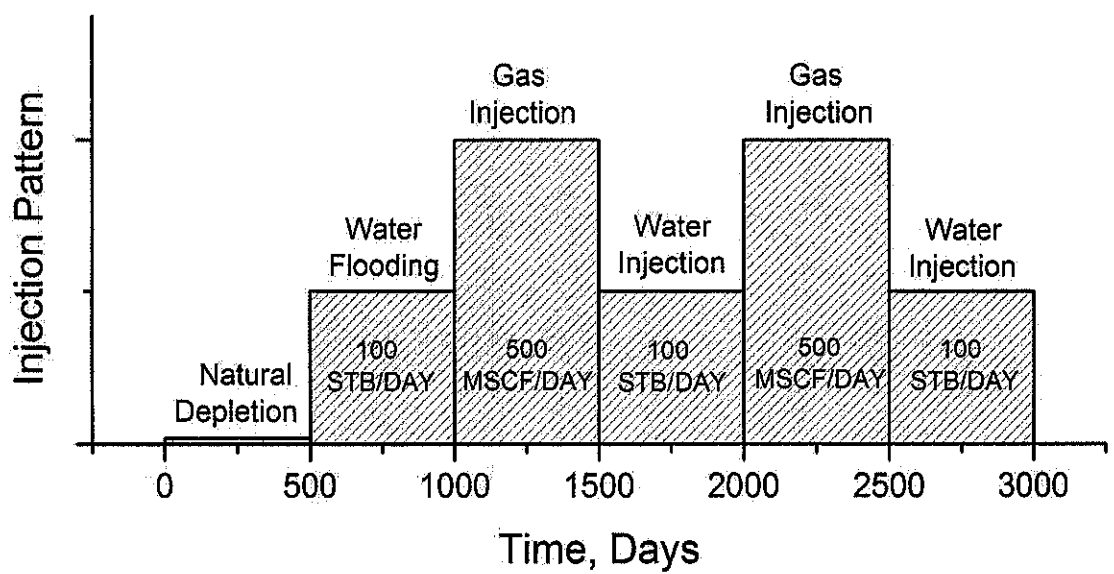


Figure 5.8: Injection pattern during this study simulation

The field oil efficiency based on production well, the field average pressure, the field oil production rate, and well gas oil ratio (GOR) for these two cases are shown in Figure 5.9, Figure 5.10, Figure 5.11, and Figure 5.12, respectively. The dash lines in these figures indicate the parameters for asphaltene case and the solid lines indicate the parameters for case of without asphaltene. As shown using asphaltene facility has been affected these parameters and reservoir performance that some explanations are given as following.

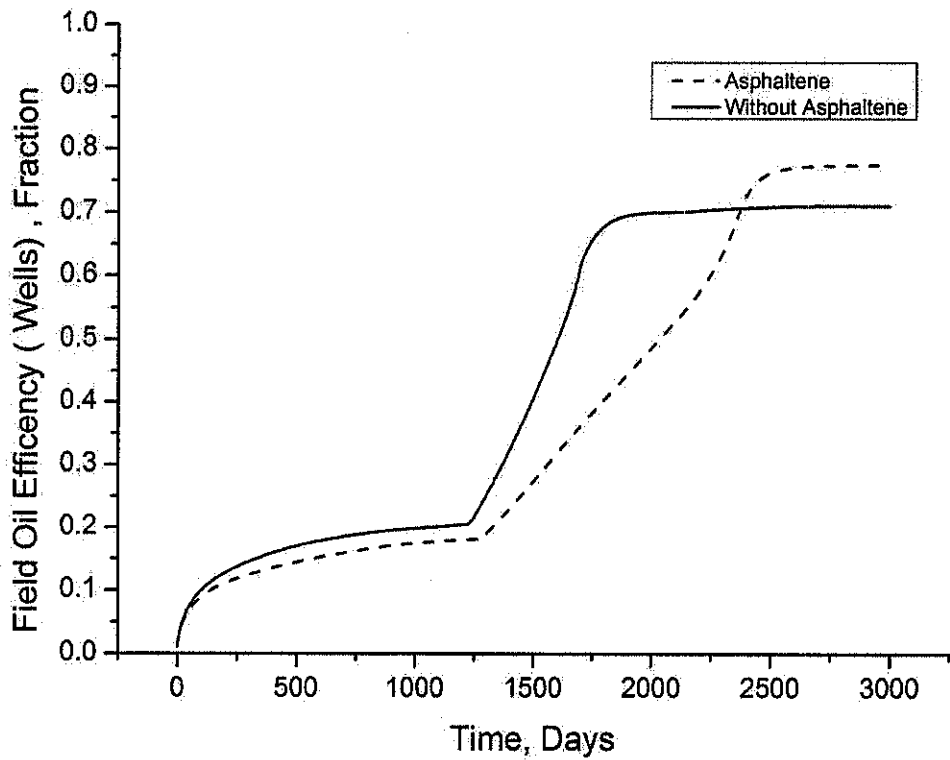


Figure 5.9: Field oil efficiency factors, asphaltene and without asphaltene cases

Figure 5.9 shows the effect of alteration of relative permeability data from water-wet to more oil-wet system due to asphaltene deposition on the field oil efficiency based on production well. As expected and can be seen in this figure, the field oil recovery factor for asphaltene case is almost lower than without asphaltene case. However, the ultimate oil recovery factor for asphaltene case is higher than case of without asphaltene. It should note that this amount of the ultimate oil recovery factor is achieved by more than three pore volume injection. Furthermore, the coreflooding results for oil recovery are in compliance with these simulation results. However, the question of how practical it is to inject fluid volumes of more than two pore volumes

to achieve improvement in oil recovery in the presence of asphaltene deposition remains again as an important question to answer.

Figure 5.10 shows that the field average pressure values for asphaltene case are higher than the without asphaltene case. It can be noted that the asphaltene deposition by reduction in porosity and absolute permeability can cause increasing in average oil reservoir pressure. Moreover, as can be seen, the most increasing in the average reservoir pressure values are obtained during CO₂ gas injection slugs during WAG implementation periods. These can be related to increase in the amount of asphaltene deposition due to CO₂ gas injection periods. Figure 5.11 demonstrate that the maximum field oil production rate is obtained for case of without asphaltene. However, as can be seen the asphaltene case can produce in lower rates compared to without asphaltene case but in longer production period which it has improved the ultimate oil recovery.

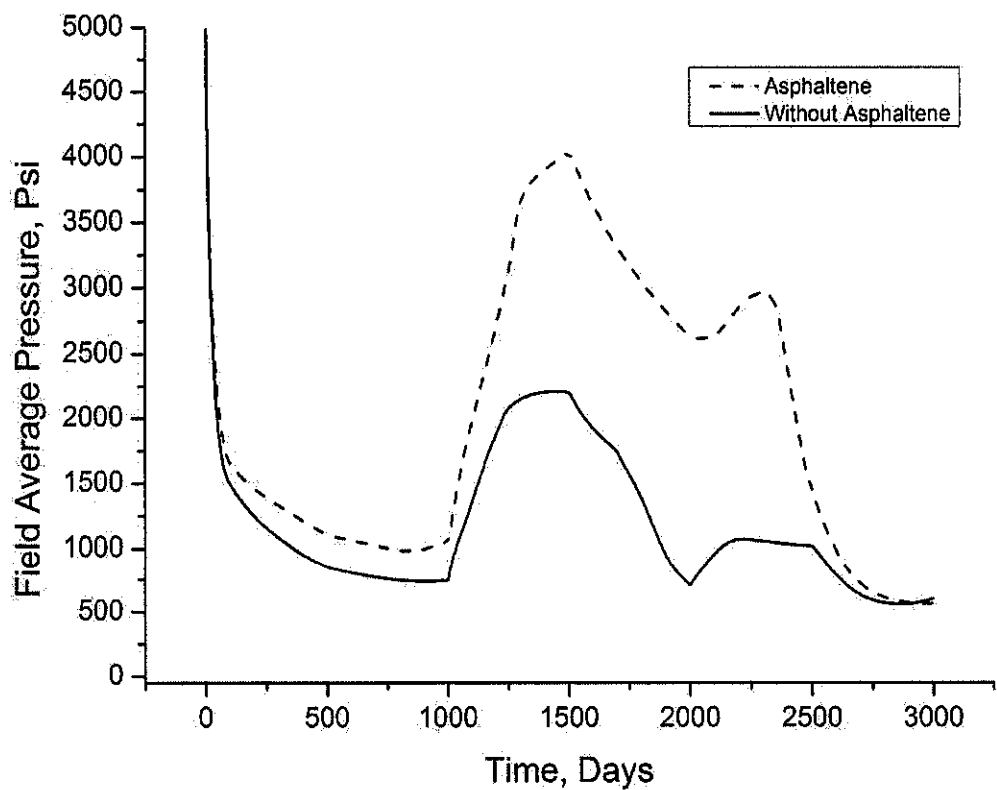


Figure 5.10: Field average pressure, asphaltene and without asphaltene cases

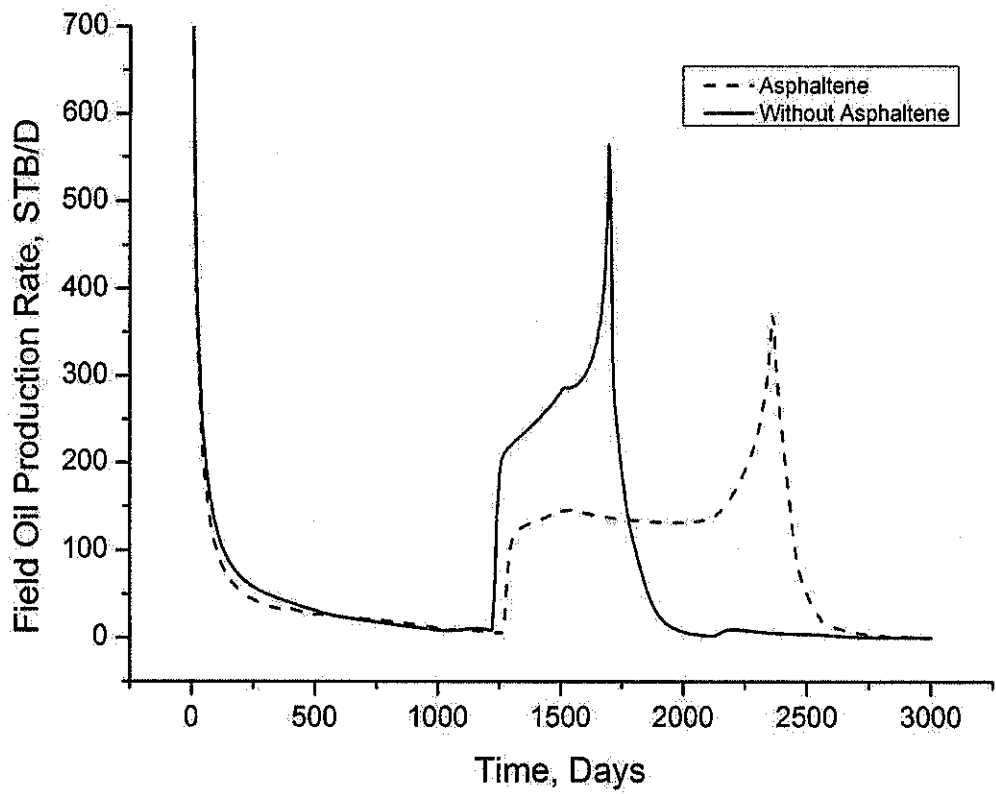


Figure 5.11: Field oil production rate, asphaltene and without asphaltene cases

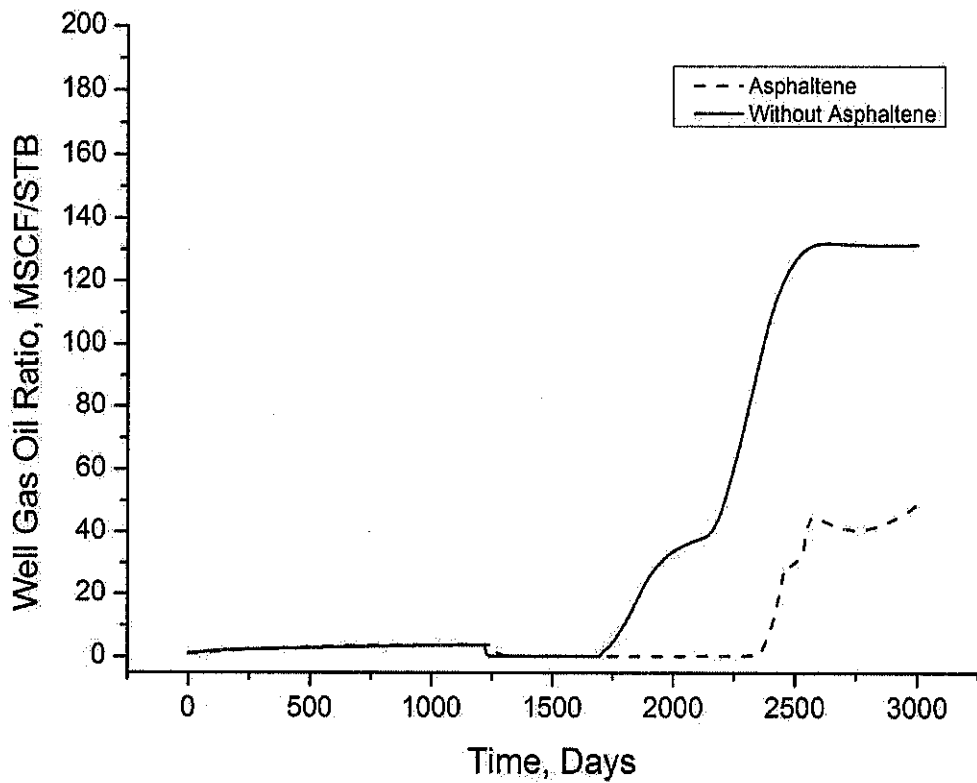


Figure 5.12: Well gas oil ratio (GOR) for production well

Moreover, as can be seen in this figure there are two pick points in field oil production curves for both cases. In each case the field oil production increases during gas injection but sharply decreases in the pick point. This can be explained in term of early gas breakthrough time in case of without asphaltene and increasing the gas oil ratio in production well that is shown in Figure 5.12

The well bottomhole pressure values for water injection and gas injection wells are given in Figure 5.13 and Figure 5.14, respectively. However, it should be mentioned that the production well in both cases is controlled with a bottomhole pressure mode of 500 psi. As shown in these figures, the asphaltene deposition has increased the well bottomhole pressure values. This can be caused because of flow issues due to asphaltene deposition which caused some difficulty in term of injectivity of these wells in term of porosity and absolute permeability reduction.

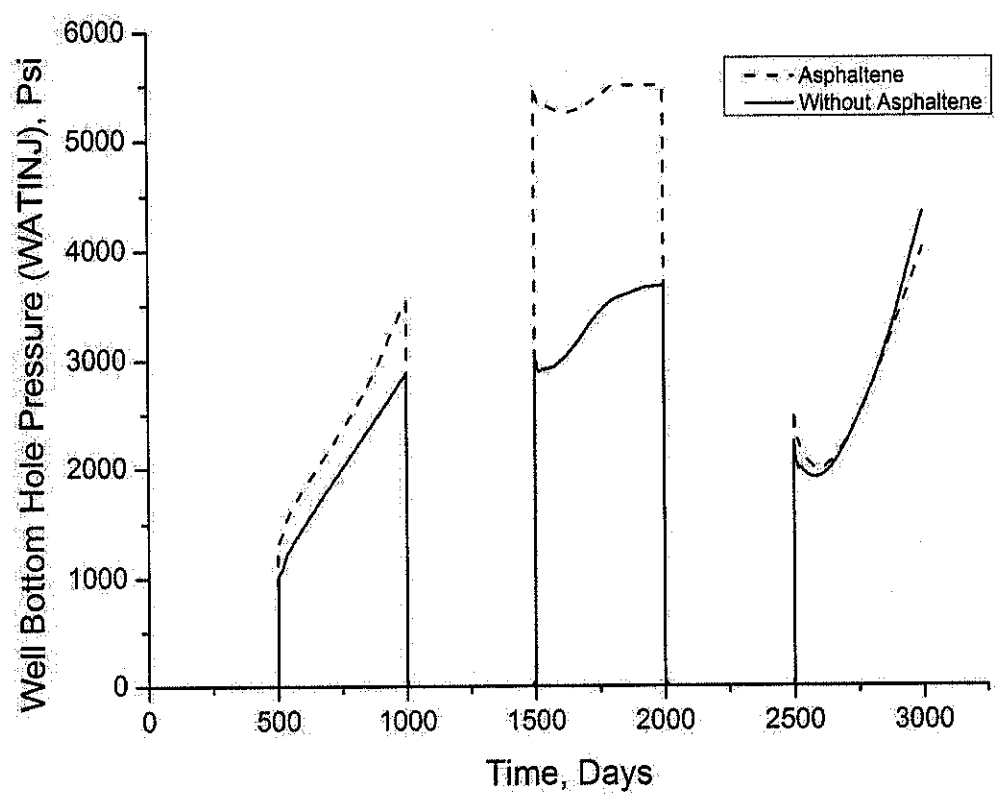


Figure 5.13: Well bottomhole pressure for water injection well

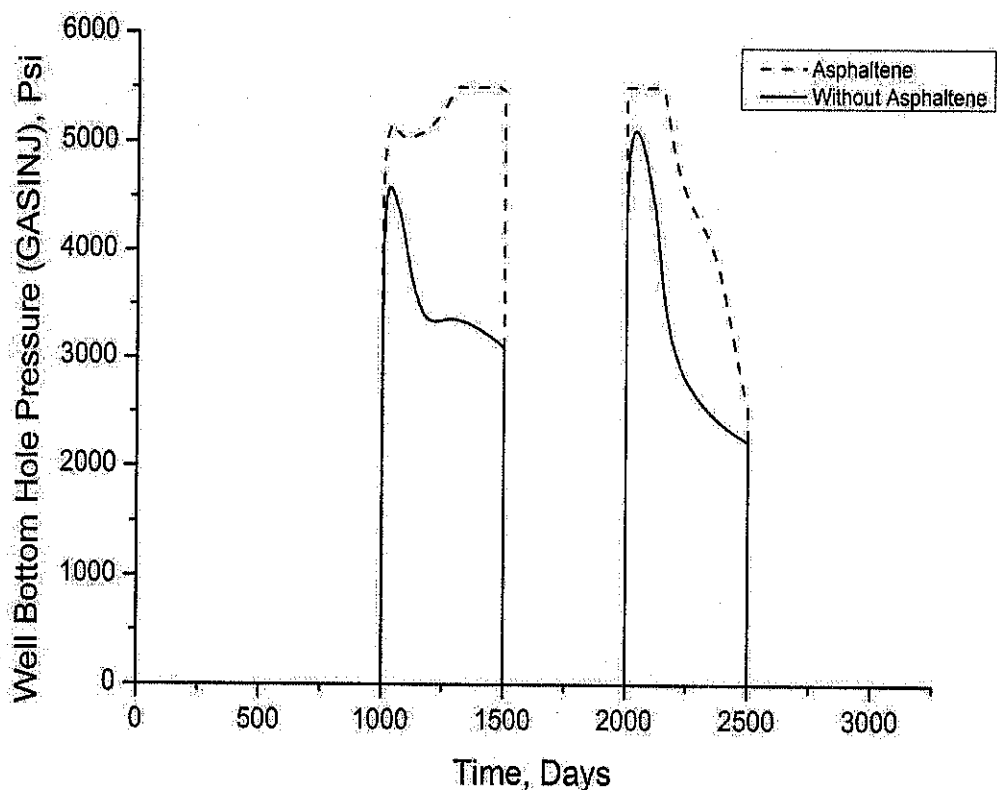


Figure 5.14: Well bottomhole pressure for gas injection well

5.6 Summary

In this chapter the modeling and simulation of the asphaltene in a conventional composition simulator and all relevant topics are reviewed. A workflow to use the coreflooding results into simulation of asphaltene deposition during WAG process is proposed. A fluid model based on fluid properties and asphaltene experimental data is constructed. The asphaltene control parameters are adjusted based on dynamic displacement experiments results. The values of weight factors F for relative permeability alteration as function of asphaltene deposition are obtained by non-linear multi-regression analysis. The simulation results for asphaltene and without asphaltene causes are given. These results show that the asphaltene deposition has affected the field oil recovery factor, the average reservoir pressure, gas oil ratio, and bottomhole pressure in injection wells.

CHAPTER 6

CONCLUSIONS AND RECOMENDATIONS

6.1 Overview

In this chapter, first, the main conclusions which are drawn by this research are given. Then, some recommendations are presented for an extension of this research into a future work.

6.2 Conclusions

Based on the results of this study, the following conclusions can be warranted:

- The oil relative permeability values in three-phase system under WAG process show different trajectories for oil iso-perm with different levels of asphaltene deposition until a certain gas saturation is achieved. For gas saturations above this level of gas saturation all oil relative permeability trajectories merge together indicating no significant effect of asphaltene deposition. The coreflooding experiment results during water-oil experiments show that the asphaltene deposition changes the wettability of the rock. Specifically, it increases the water relative permeability value at residual oil saturation increases, the oil relative permeability value at irreducible water saturation decrease, and the cross point of the oil and water relative permeability curves change to lower water saturation. To the best of the author's knowledge, these can be indications for changing the wettability of system from water-wet to more oil-wet or mixed-wet system. Also, the coreflooding experiment results during gas-oil system show that the asphaltene deposition does not have a

significant effect on gas-oil relative permeability and the cumulative oil production.

- The cumulative oil production in less than two pore volumes injection is decreased due to increasing the amount of asphaltene deposition during coreflooding experiments in water-oil system. However, the ultimate cumulative oil production during the six pore volumes injection is increased due to increasing the amount of asphaltene deposition. There could be several mechanisms such as wettability alteration, surface film oil drainage, changes in end-points, and interfacial tension which may play simultaneous roles on the asphaltene deposition result in improvement of oil recovery. Nevertheless, it is very difficult to identify which one is the most dominant mechanism for improvement in the oil recovery observed in the experimental results. However, in this study the wettability alteration from water-wet to more oil wet or mixed-wet is experimentally identified as an essential mechanism. Moreover, the question of how practical it is to inject fluid volumes of more than two pore volumes to achieve improvement in oil recovery in the presence of asphaltene precipitation and deposition remains as an important question to answer from point of economy.
- The non-linear multi-regression analysis based on experimental results are used to develop the appropriate correlations for water relative permeability and oil relative permeability as a function of the average amount of asphaltene deposition per pore volume in water-oil system. These correlations are developed similar to the Corey correlation which is found to be the best for history match of the experimental results during history-matching process in estimating step the relative permeability curves in water-oil and gas-oil systems.
- The modeling and simulation of asphaltene process during WAG process in conventional compositional simulators is investigated and a workflow based on coreflooding experiments data is established. Asphaltene control parameters are adjusted based on the absolute permeability reduction data which are obtained during coreflooding experiments. The required weight factors values for relative permeability alteration as function of asphaltene

deposition are obtained based on dynamic displacement experiments results and non-linear multi-regression analysis. The simulation results with and without asphaltene show that the ultimate field oil recovery factor for asphaltene case is higher than without asphaltene case. This amount of oil recovery is achieved by more than three pore volume injections that are in compliance with the observation coreflooding results, however, it is still questionable from practical view. Moreover, the maximum field oil production rate is obtained for case of without asphaltene deposition. The asphaltene case can produce in lower rate values compare to the case of without asphaltene but in longer production period which it has improved the ultimate oil recovery. Furthermore, the asphaltene deposition has increased the well bottomhole pressure values in water injection and gas injection wells that it can cause because of flow insurance issues due to asphaltene deposition around the wellbores. Experimental results indicate that more than one value for weight factor F should be used for certain amount of asphaltene deposition to account for the alteration of the relative permeability data. Unfortunately, currently the same value of weight factor F for certain amount of asphaltene deposition uses into conventional simulator.

6.3 Recommendations for Future Work

Based on the results of this study, the following recommendations are suggested to take into account for a future work:

- This study focused on high permeability sandstone core samples but according to the literature the carbonate core samples has different behavior. Therefore, it is recommended that the similar coreflooding experiments but for carbonate core samples should be conducted.
- It is believed that the properties of the porous medium such as pore size distribution, wettability, and absolute permeability can significant effects on the asphaltene deposition. Experimental investigations concerning the effects of these crucial factors on asphaltene deposition are strongly recommended.

- Flow visualization experiments are recommended in high pressure heterogeneous micro models. Furthermore, the mechanisms of asphaltene deposition should be studied under miscible and immiscible displacements.
- Three-phase relative permeability data should be obtained from other available methods and should be compared with Stone's II model which is used in this research.
- The comprehensive asphaltene laboratory testing under static conditions on the characterization and phase behavior studies of typical crude oil samples, dynamic coreflooding experiments, and simulation study should be conducted before implementing EOR project.

6.4 Summary

This chapter summarizes the conclusions of the entire research along with recommendations for a future work.

REFERENCES

- Abdallah, D. (2012). Impact of Asphaltenes Deposition on Completion Design for CO₂ Pilot in an Onshore Abu Dhabi Field. Abu Dhabi International Petroleum Conference and Exhibition. Abu Dhabi, UAE, Society of Petroleum Engineers.
- Abeyasinghe, K. P., I. Fjelde and A. Lohne (2012). Acceleration of Oil Production in Mixed-wet Reservoirs by Alteration of Relative Permeability Curves using Surfactants. SPE EOR Conference at Oil and Gas West Asia. Muscat, Oman, Society of Petroleum Engineers.
- Agbalaka, C. C., A. Y. Dandekar, S. L. Patil, S. Khataniar and J. Hemsath (2008). The Effect of Wettability on Oil Recovery : A Review. SPE Asia Pacific Oil and Gas Conference and Exhibition. Perth, Australia.
- Ahmadloo, F., K. Asghari and B. Y. Jamaloei (2009). Experimental and Theoretical Studies of Three Phase Relative Permeability. SPE Annual Technical Conference and Exhibition. New Orleans, Louisiana, Society of Petroleum Engineers.
- Akervoll, I., M. S. Talukdar, S. H. Midtlyng, J. A. Stensen and O. Torsaeter (2000). WAG Injection Experiments With In-Situ Saturation Measurements at Reservoir Conditions and Simulations. SPE/DOE Improved Oil Recovery Symposium. Tulsa, Oklahoma, Copyright 2000, Society of Petroleum Engineers Inc.
- Al-Maamari, R. S. H. and J. S. Buckley (2000). Asphaltene Precipitation and Alteration of Wetting: Can Wettability Change during Oil Production? SPE/DOE Improved Oil Recovery Symposium. Tulsa, Oklahoma, 2000,. Society of Petroleum Engineers Inc.
- Alizadeh, N., A. K. Manshad, A. Fadili, E. Leung and S. Ashoori (2009). Simulating the Permeability Reduction due to Asphaltene Deposition in Porous Media. International Petroleum Technology Conference. Doha, Qatar, 2009, International Petroleum Technology Conference.
- Anderson, W. G. (1987). "Wettability Literature Survey Part 5: The Effects of Wettability on Relative Permeability." SPE Journal of Petroleum Technology(11): 1453-1468.
- Aziz, K. and A. Settari (1979). "Petroleum Reservoir Simulation." London: Applied Science Publishers Ltd.

- Barroeta, R. and L. G. Thompson (2006). Estimation of Relative Permeability From Displacement Pressure Data. SPE/DOE Symposium on Improved Oil Recovery. Tulsa, Oklahoma, USA, Society of Petroleum Engineers.
- Boer, R. B. d., K. Leerlooyer, M. R. P. Eigner and A. R. D. v. Bergen (1995). "Screening of Crude Oils for Asphalt Precipitation: Theory, Practice, and the Selection of Inhibitors." SPE Production & Operations.
- Buchi (2011). "Rotary Evaporator." http://www.buchi.com/rotary-evaporator_rotavapor.4695.0.html.
- Buckley, S. E. and M. C. Leverett (1942). Mechanism of Fluid Displacement in Sands. The American Institute of Mining, Metallurgical, and Petroleum Engineers Inc.
- Burke, N. E., R. E. Hobbs and S. F. Kashou (1990). "Measurement and Modeling of Asphaltene Precipitation (includes associated paper 23831)." SPE Journal of Petroleum Technology.
- Cenegy, L. M. (2001). Survey Of Successful World-wide Asphaltene Inhibitor Treatments In Oil Production Fields. SPE Annual Technical Conference and Exhibition. New Orleans, Louisiana, Copyright 2001, Society of Petroleum Engineers Inc.
- Chavent, G., M. Dupuy and P. Lemonnier (1975). "History Matching by Use of Optimal Control Theory." SPEJ, 7486; Trans. AIME.
- Chen, Z. (2007). "Reservoir Simulation, Mathematical Tecniques in Oil Recovery." University of Calgary, Alberta, Canada.
- Christensen, J. R., E. H. Stenby and A. Skauge (2001). "Review of WAG Field Experience." SPE Reservoir Evaluation & Engineering.
- Civan, F. (2000). "Reservoir Formation Damage." University of Oklahoma, Houston, Texas, Book.
- Civan, F. (2007). Formation Damage Mechanisms and Their Phenomenological Modeling- An Overview. European Formation Damage Conference. Scheveningen, The Netherlands, Society of Petroleum Engineers.
- CMG (2011). "User Guide WinProp, Phase Property Program." Computer Modelling Group Ltd., Canada.
- Corey, A. T. (1954). "The Interrelation Between Gas and Oil Relative Permeabilities." Prod. Monthly.
- Craig, F. F. (1971). "The Reservoir Engineering Aspects of Waterflooding." Monograph Series, SPE, Richarson, TX, USA.

D2007-93, A. (1993). "Standard Test Method for Characteristic Groups in Rubber Extender and Processing Oils by the Clay-Gel Adsorption Chromatographic Method." ASTM.

Dong, L., H. Xie and F. Zhang (2001). Chemical Control Techniques for the Paraffin and Asphaltene Deposition. SPE International Symposium on Oilfield Chemistry. Houston, Texas, Copyright 2001, Society of Petroleum Engineers Inc.

Egermann, P., O. Vizika, L. Dallet, C. Requin and F. Sonier (2000). Hysteresis in Three-Phase Flow: Experiments, Modeling and Reservoir Simulations. SPE European Petroleum Conference. Paris, France, Copyright 2000, Society of Petroleum Engineers Inc.

Fan, T., J. Wang and J. S. Buckley (2002). Evaluating Crude Oils by SARA Analysis. SPE/DOE Improved Oil Recovery Symposium. Tulsa, Oklahoma, Copyright 2002, Society of Petroleum Engineers Inc.

Fatt, I. and H. Dykstra (1951). Relative Permeability Studies. The American Institute of Mining, Metallurgical, and Petroleum Engineers Inc.

Fayers, F. J. and J. D. Matthews (1984). "Evaluation of Normalized Stone's Methods for Estimating Three-Phase Relative Permeabilities." Society of Petroleum Engineers Journal.

Fazelipour, W. (2007). "Development of a Fully Implicit, Parallel, Equation-of-State Compositional Simulator to Model Asphaltene Precipitation in Petroleum Reservoirs." Presented to the Faculty of the Graduate School of The University of Texas at Austin.

Figuera, L., M. Marin, L. R. L. G., E. Marin, A. Gammiero and C. GRANADO (2010). Characterization and Modelling of Asphaltene Precipitation and Deposition in a Compositional Reservoir. SPE Annual Technical Conference and Exhibition. Florence, Italy, Society of Petroleum Engineers.

Friedel, T., G. J. Sanza, M. I. Ali, E. Kasap, A. Embong, S. B. Yusoff and A. J. Cuauero (2006). Identifying the Improved Oil Recovery Potential for a Depleted Reservoir in the Betty Field, Offshore Malaysia. SPE Asia Pacific Oil & Gas Conference and Exhibition. Adelaide, Australia, Society of Petroleum Engineers.

Grader, A. S. and D. J. O'Meara (1988). Dynamic Displacement Measurements of Three-Phase Relative Permeabilities Using Three Immiscible Liquids. SPE Annual Technical Conference and Exhibition. Houston, Texas, 1988.

Hamdan, M. K., N. B. Darman, D. Husain and Z. B. Ibrahim (2005). Enhanced Oil Recovery in Malaysia: Making It a Reality. SPE Asia Pacific Oil and Gas Conference and Exhibition. Jakarta, Indonesia, Society of Petroleum Engineers.

- Hirschberg, A., L. N. J. deJong, B. A. Schipper and J. G. Meijer (1984). "Influence of Temperature and Pressure on Asphaltene Flocculation." Society of Petroleum Engineers Journal.
- Honarpour, M., L. Koederitz and A. H. Harvey (1988). "Relative Permeability of Petroleum Reservoirs." Boca Raton, Florida, Book.
- Hun, O. S. (2012). "A Study of CO₂ and WAG Injection Induced Asphaltene Precipitation." University Technology Petronas.
- Hustad, O. S. and T. Holt (1992). Gravity Stable Displacement of Oil by Hydrocarbon Gas After Waterflooding. SPE/DOE Enhanced Oil Recovery Symposium. Tulsa, Oklahoma, 1992 Copyright 1992, Society of Petroleum Engineers Inc.
- IP-143 (2001). "Determination of asphaltene(heptane insolubles) in crude petroleum and petroleum products."
- Jamaluddin, A. K. M., J. Creek, C. S. Kabir, J. D. Mcfadden, D. D'Cruz, J. Manakalathil, N. Joshi and B. Ross (2002). "Laboratory Techniques to Measure Thermodynamic Asphaltene Instability."
- Jamshidnezhad, M. (2005). Prediction of Asphaltene Precipitation in an Iranian South Oil Field. Canadian International Petroleum Conference. Calgary, Alberta.
- Jewell, D. M., Weber, J.H., Bungler, J.W., Plancher, H., Latham, D.R. (1972). "Ion-Exchange, Coordination, and Adsorption Chromatographic Separation of Heavy-End Petroleum Distillates."
- Johnson, E. F., D. P. Bossler and V. O. Naumann (1959). Calculation of Relative Permeability from Displacement Experiments, Society of Petroleum Engineers of AIME.
- Jones, S. C. and W. O. Roszelle (1978). "Graphical Techniques for Determining Relative Permeability From Displacement Experiments." SPE Journal of Petroleum Technology.
- Ju, B., Z. Luan, Z. Wu and G. Lu (2001). A Study of Removal of Organic Formation Damage by Experiments and Modeling Approaches. SPE Asia Pacific Oil and Gas Conference and Exhibition. Jakarta, Indonesia, Copyright 2001, Society of Petroleum Engineers Inc.
- Kabir, C. S. and A. K. M. Jamaluddin (1999). Asphaltene Characterization and Mitigation in South Kuwait's Marrat Reservoir. Middle East Oil Show and Conference. Bahrain, Copyright 1999, Society of Petroleum Engineers Inc.
- Kalantari, Gholami, Moghadasi and R. Abdi (2008). "Formation Damage Through Asphaltene Precipitation Resulting From CO₂ Gas Injection in Iranian Carbonate Reservoirs." SPE Production & Operations.

- Kalaydjian, F. J.-M., J.-C. Moulu, O. Vizika and P. K. Munkerdud (1993). Three-Phase Flow in Water-Wet Porous Media: Determination of Gas/Oil Relative Permeabilities Under Various Spreading Conditions. SPE Annual Technical Conference and Exhibition. Houston, Texas, 1993 Copyright 1993, Society of Petroleum Engineers, Inc.
- Kamath, V. A., J. Yang and G. D. Sharma (1993). Effect of Asphaltene Deposition on Dynamic Displacements of Oil by Water. SPE Western Regional Meeting. Anchorage, Alaska, 1993 Copyright 1993, Society of Petroleum Engineers, Inc. This paper was prepared for presentation at the Western Regional Meeting held in Anchorage, Alaska, U.S.A. 26-28 May.
- Kantas, A., B. Nikakhtar and M. Pow (1995). Principles of Three-phase Capillary Pressures. Annual Technical Meeting. Calgary, Alberta, Petroleum Society of Canada.
- Kawanaka, S., S. J. Park and G. A. Mansoori (1991). "Organic Deposition From Reservoir Fluids: A Thermodynamic Predictive Technique." SPE Reservoir Engineering.
- Kechut, N. I., Mustapah, M.F., Razak, I.A. (2001). "IOR/EOR Screening for Malaysia's Oil Producing Fields." PRSS Report.
- Khanifar, A., S. S. Alian, B. Demiral and N. B. Darman (2011). Study of Asphaltene Precipitation and Deposition Phenomenon during WAG Application. SPE Enhanced Oil Recovery Conference. Kuala Lumpur, Malaysia, Society of Petroleum Engineers.
- Khanifar, A., B. Demiral and N. Darman (2012). "Numerical Study of Asphaltene Control Parameters Effects on Reservoir Performance." ICIPEG 2012, Kuala Lumpur, Malaysia.
- Khanifar, A., B. Demiral and N. B. Darman (2011). Modelling of Asphaltene Precipitation and Deposition during WAG Application. International Petroleum Technology Conference. Bangkok, Thailand, International Petroleum Technology Conference.
- Kim, S. T., M.-E. Boudh-Hir and G. A. Mansoori (1990). The Role of Asphaltene in Wettability Reversal. SPE Annual Technical Conference and Exhibition. New Orleans, Louisiana, 1990 Copyright 1990, Society of Petroleum Engineer Inc.
- Klinkenberg, L. J. (1941). "The permeability of porous media to liquids and gases." Drilling and Production Practice, American Petroleum Inst., pp. 200-213.
- Kocabas, I. (2003). Characterization of Asphaltene Precipitation Effect on Reducing Carbonate Rock Permeability. Middle East Oil Show. Bahrain, Society of Petroleum Engineers.

- Kokal, S. L. and S. G. Sayegh (1995). *Asphaltenes: The Cholesterol of Petroleum*. Middle East Oil Show. Bahrain, 1995 Copyright 1995, Society of Petroleum Engineers, Inc.
- Krieger, I. M. and T. J. Dougherty (1959). "A Mechanism For Non-Newtonian Flow in Suspensions of Rigid Spheres." *Trans., Soc. Rheol.*
- Lee, B. I. and M. G. Kesler (1975). "A Generalized Thermodynamic Correlation Based on Three-Parameter Corresponding States." *Aiche J.*, 21(3), 510-527.
- Lefebvre du Prey, E. J. (1973). "Factors Affecting Liquid-Liquid Relative Permeabilities of a Consolidated Porous Medium."
- Leontaritis, K. J. (1989). *Asphaltene Deposition: A Comprehensive Description of Problem Manifestations and Modeling Approaches*. SPE Production Operations Symposium. Oklahoma City, Oklahoma.
- Leontaritis, K. J., J. O. Amaefule and R. E. Charles (1994). "A Systematic Approach for the Prevention and Treatment of Formation Damage Caused by Asphaltene Deposition." *SPE Production & Operations*.
- Leontaritis, K. J. and G. A. Mansoori (1987). *Asphaltene Flocculation During Oil Production and Processing: A Thermodynamic Colloidal Model*. SPE International Symposium on Oilfield Chemistry. San Antonio, Texas.
- Leverett, M. C. and W. B. Lewis (1941). *Steady Flow of Gas-oil-water Mixtures through Unconsolidated Sands*.
- Ling, K., W. D. McCain, E. Davani and G. Falcone (2009). *Measurement of Gas Viscosity at High Pressures and High Temperatures*. International Petroleum Technology Conference. Doha, Qatar, 2009, International Petroleum Technology Conference.
- Lomeland, F., E. Ebeltoft and W. H. Thomas (2008). "A New Versatile Relative Permeability Correlation." *International Symposium of the SCA*, Abu Dhabi, UAE, .
- Long, R. B. (1981). "The Concept of Asphaltenes," *Chemistry of Asphaltenes*., J.W. Bunger and N.C. Li (eds.), ACS, Washington, DC 17-27.
- Ma, T. D., J. A. Rugen, R. F. Stoisits and G. K. Voungren (1995). *Simultaneous Water and Gas Injection Pilot at the Kuparuk River Field, Reservoir Impact*. SPE Annual Technical Conference and Exhibition. Dallas, Texas, 1995 Copyright 1995, Society of Petroleum Engineers, Inc.
- Ma, Z. C. G. H. Y. (2006). *Computational Methods for Multiphase Flows in Porous Media*. Southern Methodist University Dallas, Texas.

- Maeda, H. and K. Okatsu (2008). EOR Using Thin Oil Film Drainage Mechanism in Water Wet Oil Reservoir. SPE Asia Pacific Oil and Gas Conference and Exhibition. Perth, Australia, Society of Petroleum Engineers.
- Majidaie, S., A. Khanifar, M. Onur and I. M. Tan (2012). A Simulation Study of Chemically Enhanced Water Alternating Gas (CWAG) Injection. SPE EOR Conference at Oil and Gas West Asia. Muscat, Oman, Society of Petroleum Engineers.
- Mansoori, G. A. (2010). "Remediation of Asphaltene and Heavy Organic Deposits in Oil Wells and in Pipelines." University of Illinois.
- Minssieux, L. (1997). Core Damage From Crude Asphaltene Deposition. International Symposium on Oilfield Chemistry. Houston, Texas, 1997 Copyright 1997, Society of Petroleum Engineers, Inc.
- Misra, S., D. Abdullah, M. K. Bazuhair, A. A. Aboukshem, B. A. Stenger and A. B. Al-katheeri (2011). Management of Asphaltenes Deposition in a Giant Carbonate Onshore Oil Field, Abu Dhabi, U.A.E. SPE Middle East Oil and Gas Show and Conference. Manama, Bahrain, Society of Petroleum Engineers.
- Moffitt, P. D. and D. R. Zornes (1992). Postmortem Analysis: Lick Creek Meakin Sand Unit Immiscible CO₂ Waterflood Project. SPE Annual Technical Conference and Exhibition. Washington, D.C., 1992 Copyright 1992, Society of Petroleum Engineers Inc.
- Morrow, N. R. (1990). "Wettability and Its Effect on Oil Recovery." SPE Journal of Petroleum Technology.
- Mullins, O. C. (2008). "Review of the Molecular Structure and Aggregation of Asphaltenes and Petroleomics." SPE Journal.
- Mullins, O. C., E. Y. Sheu, A. Hammami and A. G. Marshall (2007). "Asphaltene, Heavy Oils, and Petroleomics.", Book.
- Nabzar, L., M. E. Aguilera and Y. Rajoub (2005). Experimental Study on Asphaltene-Induced Formation Damage. SPE International Symposium on Oilfield Chemistry. The Woodlands, Texas, 2005,. Society of Petroleum Engineers Inc.
- Nadeson, G., N. A. B. Anua, D. A. Singhal and R. B. Ibrahim (2004). Water-Alternating-Gas (WAG) Pilot Implementation, A First EOR Development Project in Dulang Field, Offshore Peninsular Malaysia. SPE Asia Pacific Oil and Gas Conference and Exhibition. Perth, Australia, Society of Petroleum Engineers.
- Nadeson, G., Z. M. Zain, S. G. Sayegh and M. Girard (2001). Assessment of Dulang Field Immiscible Water-Alternating-Gas (WAG) Injection Through Composite Core Displacement Studies. SPE Asia Pacific Improved Oil

- Negahban, S., J. N. M. Bahamaish, N. Joshi, J. Nighswander and A. K. M. Jamaluddin (2005). "An Experimental Study at an Abu Dhabi Reservoir of Asphaltene Precipitation Caused By Gas Injection." SPE Production & Operations.
- Negahban, S., N. Joshi, A. K. M. Jamaluddin and J. Nighswander (2003). A Systematic Approach for Experimental Study of Asphaltene Deposition for an Abu Dhabi Reservoir Under WAG Development Plan. International Symposium on Oilfield Chemistry. Houston, Texas, Society of Petroleum Engineers.
- Nghiem, L. X. and D. A. Coombe (1997). "Modelling Asphaltene Precipitation During Primary Depletion." SPE Journal.
- Nghiem, L. X., M. S. Hassam, R. Nutakki and A. E. D. George (1993). Efficient Modelling of Asphaltene Precipitation. SPE Annual Technical Conference and Exhibition. Houston, Texas, 1993 Copyright 1993, Society of Petroleum Engineers, Inc.
- Nordtvedt, J. E., E. Ebeltoft, J. E. Iversen, A. Sylte, H. Urkedal, K. O. Vatne and A. T. Watson (1997). "Determination of Three-Phase Relative Permeabilities From Displacement Experiments." SPE Formation Evaluation.
- Nutting, P. G. (1934). "Some Physical and Chemical Properties of Reservoir Rocks Bearing on the Accumulation and Discharge of Oil." Problems of Petroleum Geology, W.E. Wrather and F.H. Lahee, AAPG, Tulsa.
- O'Meara , D. J. and W. O. Lease (1983). Multiphase Relative Permeability Measurements Using an Automated Centrifuge. SPE Annual Technical Conference and Exhibition. San Francisco, California, 1983 Copyright 1983 Society of Petroleum Engineers.
- Okwen, R. T. (2006). Formation Damage by CO₂ Asphaltene Precipitation. International Symposium and Exhibition on Formation Damage Control. Lafayette, Louisiana U.S.A., Society of Petroleum Engineers.
- Oskui, G.-R. P., M. A. Jumaa and W. Abuhained (2009). Laboratory Investigation of Asphaltene Precipitation problems during CO₂/Hydrocarbon Injection Project for EOR Application in Kuwaiti Reservoirs. Kuwait International Petroleum Conference and Exhibition. Kuwait City, Kuwait, Society of Petroleum Engineers.
- Oskui, G. P., M. Salman, E. F. Gholoum, A. Rashed, B. S. A. Matar, M. Al-Bahar and K. Kahali (2006). Laboratory Technique for Screening Asphaltene Inhibitors for Kuwaiti Reservoirs. SPE Technical Symposium of Saudi Arabia Section. Dhahran, Saudi Arabia, Society of Petroleum Engineers.

- Ozbek, H. (2010). "Viscosity of Aqueous Sodium Chloride Solutions From 0 - 150 °C." Lawrence Berkeley National Laboratory.
- Paul, G. (2000). "Formation Evaluation MSc Course Notes." <http://www2.ggl.ulaval.ca/personnel/paglover/CD%20Contents/Formation%20Evaluation%20English/Chapter%2010.PDF>.
- Prieditis, J., C. R. Wolle and P. K. Notz (1991). A Laboratory and Field Injectivity Study: CO₂ WAG in the San Andres Formation of West Texas. SPE Annual Technical Conference and Exhibition. Dallas, Texas, 1991 Copyright 1991 Society of Petroleum Engineers, Inc.
- Purcell, W. R. (1949). Capillary Pressures - Their Measurement Using Mercury and the Calculation of Permeability Therefrom, Shell Oil Co.
- Rao, D. N., S. C. Ayirala, M. M. Kulkarni and A. P. Sharma (2004). Development of Gas Assisted Gravity Drainage (GAGD) Process for Improved Light Oil Recovery. SPE/DOE Symposium on Improved Oil Recovery. Tulsa, Oklahoma, Society of Petroleum Engineers.
- Rezaian, A., A. Kordestany, M. Jamialahmadi, J. Moghadasi, M. Y. Khoshdaregi, M. Alipanah and M. H. Sefat (2010). Experimental and Theoretical Studies of Flocculated Asphaltene Deposition From Oil in Porous Media. Trinidad and Tobago Energy Resources Conference. Port of Spain, Trinidad, Society of Petroleum Engineers.
- Righi, E. F., J. Royo, P. Gentil, R. Castelo, A. D. Monte and S. Bosco (2004). Experimental Study of Tertiary Immiscible WAG Injection. SPE/DOE Symposium on Improved Oil Recovery. Tulsa, Oklahoma, Society of Petroleum Engineers.
- Robie, J., D.R., J. W. Roedell and R. K. Wackowski (1995). Field Trial of Simultaneous Injection of CO₂ and Water, Rangely Weber Sand Unit, Colorado. SPE Production Operations Symposium. Oklahoma City, Oklahoma, 1995 Copyright 1995, Society of Petroleum Engineers, Inc.
- Roper, M. K., C. T. Cheng, J. E. Varnon, G. A. Pope and K. Sepehrnoori (1992). Interpretation of a CO₂ WAG Injectivity Test in the San Andres Formation Using a Compositional Simulator. SPE/DOE Enhanced Oil Recovery Symposium. Tulsa, Oklahoma, 1992 Copyright 1992, Society of Petroleum Engineers Inc.
- Salathiel, R. A. (1973). "Oil Recovery by Surface Film Drainage In Mixed-Wettability Rocks." SPE Journal of Petroleum Technology(10): 1216-1224.
- Samsudin, Y., N. Darman, D. Husain and M. K. Hamdan (2005). Enhanced Oil Recovery in Malaysia: Making It a Reality (Part II). SPE International Improved Oil Recovery Conference in Asia Pacific. Kuala Lumpur, Malaysia, 2005, Society of Petroleum Engineers.

- Sanada, A. and Y. Miyagawa (2006). A Case Study of a Successful Chemical Treatment to Mitigate Asphaltene Precipitation and Deposition in Light Crude Oil Field. SPE Asia Pacific Oil & Gas Conference and Exhibition. Adelaide, Australia, Society of Petroleum Engineers.
- Sanchez, N. L. (2007). A General Approach for Asphaltene Modeling. Latin American & Caribbean Petroleum Engineering Conference. Buenos Aires, Argentina, Society of Petroleum Engineers.
- Sanchez, T. (2012). "Coreflooding Equipment." <http://www.stfrance.com>.
- Saraf, D. N. and F. G. McCaffery (1982). "Two- and Three-Phase Relative Permeabilities: A Review." Petroleum Recovery Institute Report #81-8, Calgary, Alberta, Canada.
- Sarma, H. K. (2003). Can We Ignore Asphaltene in a Gas Injection Project for Light-Oils? SPE International Improved Oil Recovery Conference in Asia Pacific. Kuala Lumpur, Malaysia, Society of Petroleum Engineers.
- Sarma, H. K., B. B. Maini and K. N. Jha (1992). An Unsteady-State Technique For Three-Phase Relative Permeability Measurements. Technical Meeting / Petroleum Conference Of The South Saskatchewan Section. Regina, Petroleum Society of Canada.
- Schlumberger (2011). "Eclipse Technical Description, The Asphaltene Option." Schlumberger Company.
- Sendra (2011). "Sendra User Guide." Weatherford Petroleum Consultants, Norway.
- Shahverdi, H. and M. Sohrabi (2012). Three-Phase Relative Permeability and Hysteresis Model for Simulation of Water Alternating Gas (WAG) Injection. SPE Improved Oil Recovery Symposium. Tulsa, Oklahoma, USA, Society of Petroleum Engineers.
- Shedid, S. A. (2001). Influences of Asphaltene Deposition on Rock/Fluid Properties of Low Permeability Carbonate Reservoirs. SPE Middle East Oil Show. Bahrain, Copyright 2001, Society of Petroleum Engineers Inc.
- Shedid, S. A. and E. A. A. Abbas (2005). An Experimental Approach of the Reversibility of Asphaltene Deposition under Dynamic Flow Conditions. SPE Middle East Oil and Gas Show and Conference. Kingdom of Bahrain, Society of Petroleum Engineers.
- Sim, S. S.-K., K. Okatsu, K. Takabayashi and D. B. Fisher (2005). Asphaltene-Induced Formation Damage: Effect of Asphaltene Particle Size and Core Permeability. SPE Annual Technical Conference and Exhibition. Dallas, Texas, Society of Petroleum Engineers.
- Sirota, E. B. (2005). "Physical Structure of Asphaltenes." Energy & Fuels 19, 1290-1296.

- Slobod, R. L., A. Chambers and W. L. P. Jr. (1951). Use of Centrifuge for Determining Connate Water, Residual Oil, and Capillary Pressure Curves of Small Core Samples.
- Srivastava, R. K., S. S. Huang and M. Dong (1999). "Asphaltene Deposition During CO₂ Flooding." SPE Production & Operations.
- Stalkup, F. I. (1980). "Miscible Displacement." Monograph Series, SPE, Richardson, Texas.
- Standing, M. B. (1974). "Notes on Relative Permeability Relationships." The Norgian Institute of Technology, The University of Trondheim.
- Stone, H. L. (1970). "Probability Model for Estimating Three-Phase Relative Permeability." SPE Journal of Petroleum Technology.
- Stone, H. L. (1973). "Estimation of Three-Phase Relative Permeability And Residual Oil Data." Journal of Canadian Petroleum Technology.
- Surguchev, L. M., R. Korbol and O. S. Krakstad (1992). Optimum Water Alternate Gas Injection Schemes for Stratified Reservoirs. SPE Annual Technical Conference and Exhibition. Washington, D.C., 1992 Copyright 1992, Society of Petroleum Engineers Inc.
- Takahashi, S., Y. Hayashi, S. Takahashi, N. Yazawa and H. Sarma (2003). Characteristics and Impact of Asphaltene Precipitation During CO₂ Injection in Sandstone and Carbonate Cores: An Investigative Analysis Through Laboratory Tests and Compositional Simulation. SPE International Improved Oil Recovery Conference in Asia Pacific. Kuala Lumpur, Malaysia, Society of Petroleum Engineers.
- Tarek, A. (2001). "Reservoir Engineering Handbook." Gulf Professional Publishing, Book, Second Edition.
- Ursin, J. R. and A. B. Zolotukhin (1997). "Reservoir Engineering." Stavanger University.
- Van Spronsen, E. (1982). Three-Phase Relative Permeability Measurements Using the Centrifuge Method. SPE Enhanced Oil Recovery Symposium. Tulsa, Oklahoma, 1982 Copyright 1982, Society of Petroleum Engineers of AIME.
- Venkatesan, R. and J. L. Creek (2007). Wax Deposition During Production Operations: SOTA.
- Vinci, T. (2012). <http://www.vinci-technologies.com/products>, Vinci Company.
- Wang, J. X. and J. S. Buckley (2003). "Asphaltene Stability in Crude Oil and Aromatic Solvents The Influence of Oil Composition." Energy & Fuels 17, 1445-1451.

- Wang, S. and F. Civan (2001). Productivity Decline of Vertical and Horizontal Wells by Asphaltene Deposition in Petroleum Reservoirs. SPE International Symposium on Oilfield Chemistry. Houston, Texas, 2001,. Society of Petroleum Engineers Inc.
- Wang, S. and F. Civan (2005). Preventing Asphaltene Deposition in Oil Reservoirs by Early Water Injection. SPE Production Operations Symposium. Oklahoma City, Oklahoma, Society of Petroleum Engineers.
- Watt, U. H. (2008). "Reservoir Simulation Handnotes." Institute of Petroleum Engineering, Heriot-Watt University
- Watts, R. J., W. D. Conner, J. A. Wasson and A. B. Yost II (1982). CO₂ Injection for Tertiary Oil Recovery, Granny's Creek Field, Clay County, West Virginia. SPE Enhanced Oil Recovery Symposium. Tulsa, Oklahoma, Not subject to copyright. This document was prepared by government employees or with government funding that places it in the public domain.
- Welge, H. J. (1952). A Simplified Method for Computing Oil Recovery by Gas or Water Drive.
- Wolcott, J. M., T. G. Monger, R. Sassen and E. W. Chinn (1989). The Effects Of CO Flooding on Reservoir Mineral Properties. SPE International Symposium on Oilfield Chemistry. Houston, Texas, 198 Copyright 1989, Society of Petroleum Engineers.
- Yi, T., A. Fadili, M. N. Ibrahim and B. S. Al-Matar (2009). Modeling The Effect Of Asphaltene on the Development of the Marrat Field. 8th European Formation Damage Conference. Scheveningen, The Netherlands, Society of Petroleum Engineers.
- Zain, Z. M., N. I. Kechut, G. Nadeson, N. Ahmad and D. A. Raja (2001). Evaluation of CO₂ Gas Injection For Major Oil Production Fields in Malaysia - Experimental Approach Case Study: Dulang Field. SPE Asia Pacific Improved Oil Recovery Conference. Kuala Lumpur, Malaysia, Copyright 2001, Society of Petroleum Engineers Inc.
- Zarrin Nasri , B. D. (2009). "Effects of Asphaltene Deposition on Oil Reservoir Characteristics Including Two-Phase Flow." Journal of the Japan Petroleum Institute.

APPENDIX A

EXPERIMENTS AND SIMULATION RESULTS

In this appendix the experimental results which are obtained during coreflooding experiments in water-oil and gas oil systems are given. This data includes the pressure drop across the core, oil production, and water production data for each coreflooding experiment individually. The history matching of these parameters with Corey and LET correlations follow by obtained water-oil relative permeability and gas-oil relative permeability are presented. In addition the oil relative permeability in three-phase system in triangular diagram for different oil iso-perm values are shown. Moreover, the comparisons of oil relative permeability in three-phase system due to asphaltene deposition are also given.

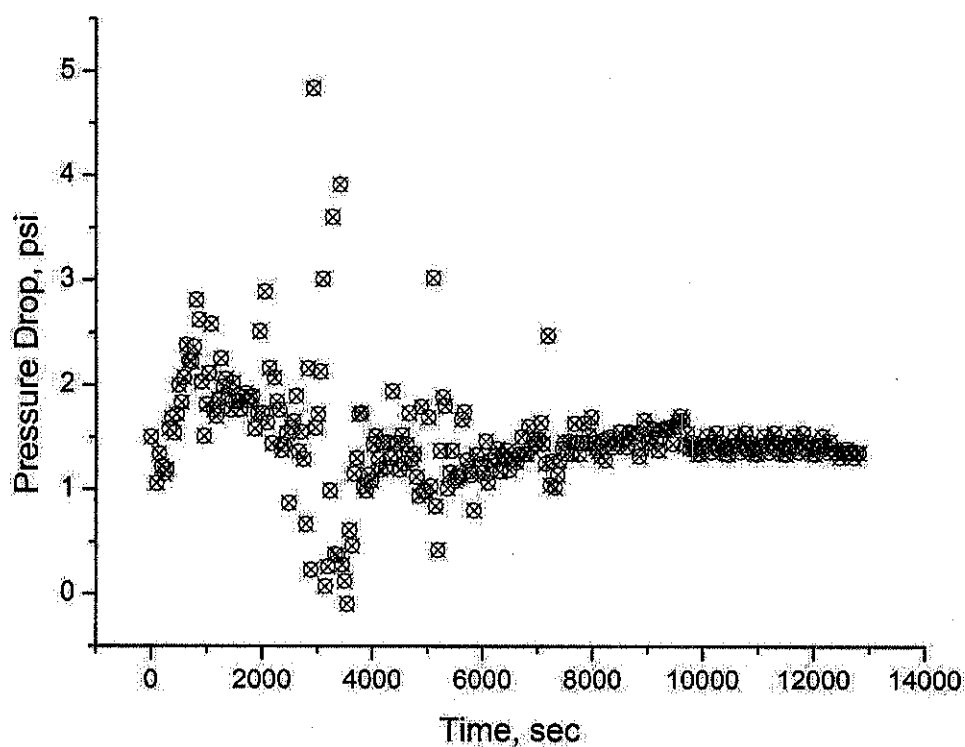


Figure A.1: Pressure drop across core sample during water injection (zero % ratio of n-heptane–crude oil injection, water-oil system)

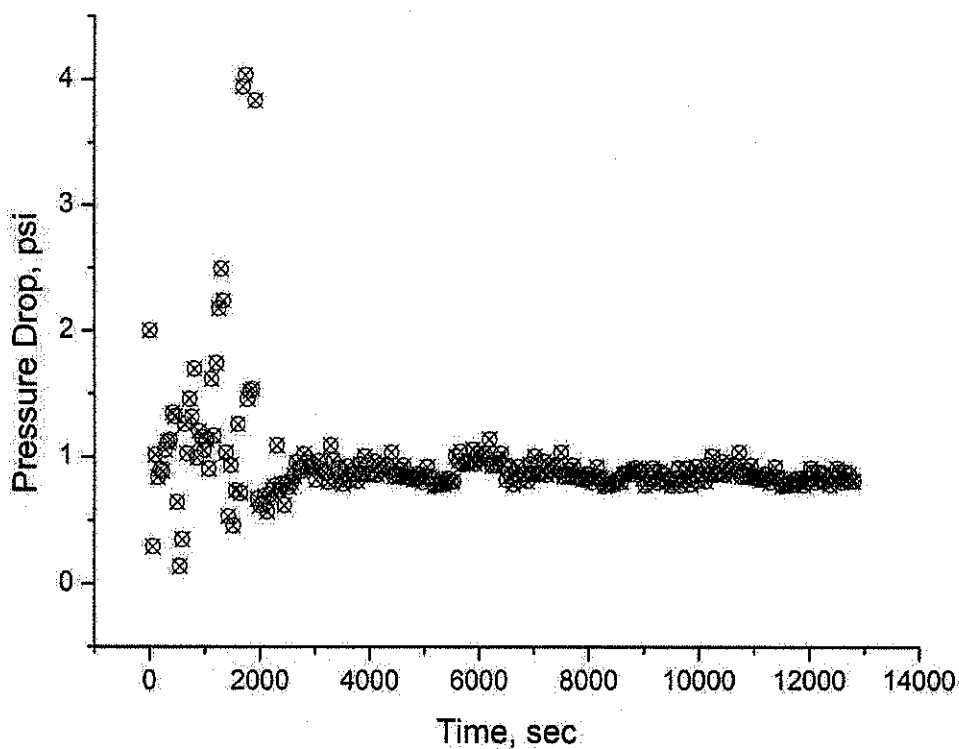


Figure A.2: Pressure drop across core sample during water injection (20 % ratio of n-heptane-crude oil injection, water-oil system)

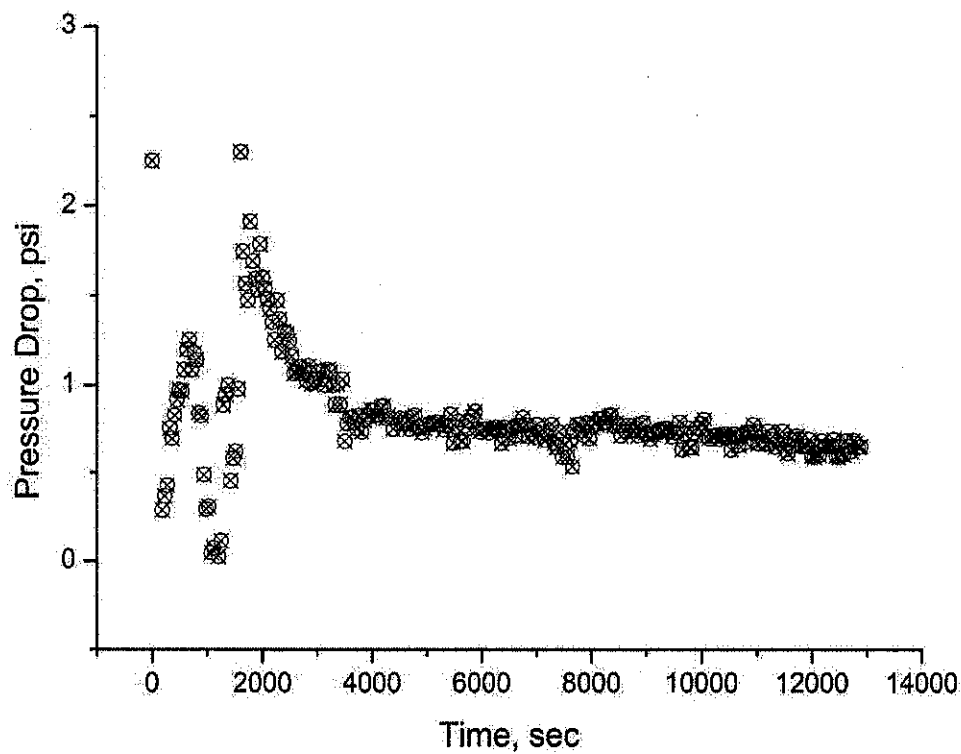


Figure A.3: Pressure drop across core sample during water injection (50 % ratio of n-heptane-crude oil injection, water-oil system)

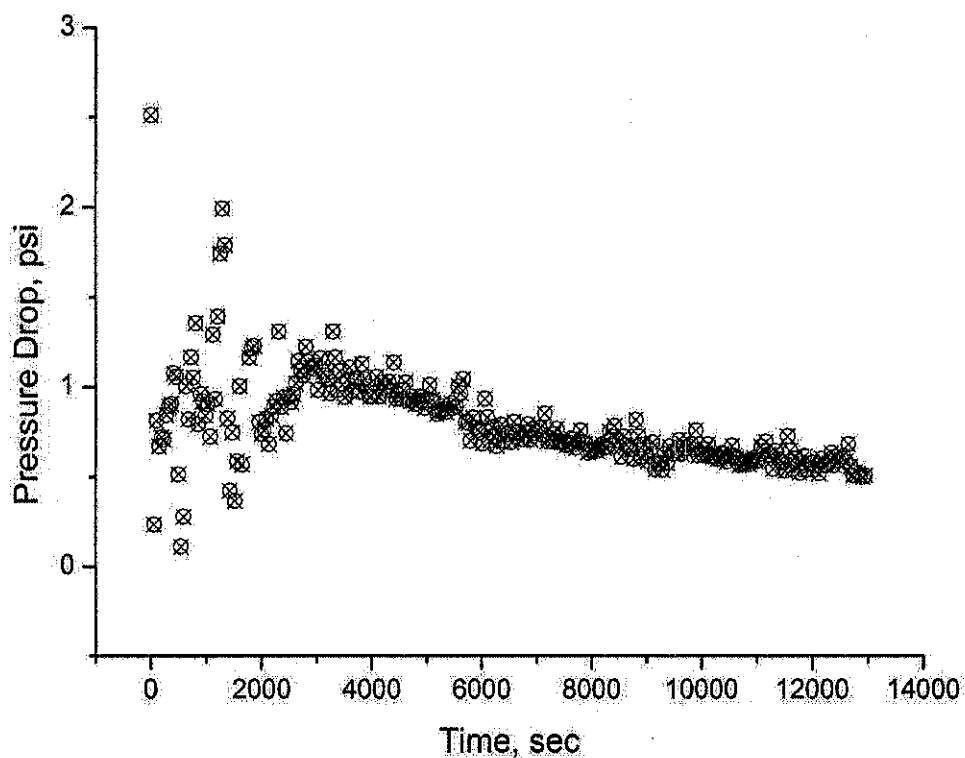


Figure A.4: Pressure drop across core sample during water injection (80 % ratio of n-heptane–crude oil injection, water-oil system)

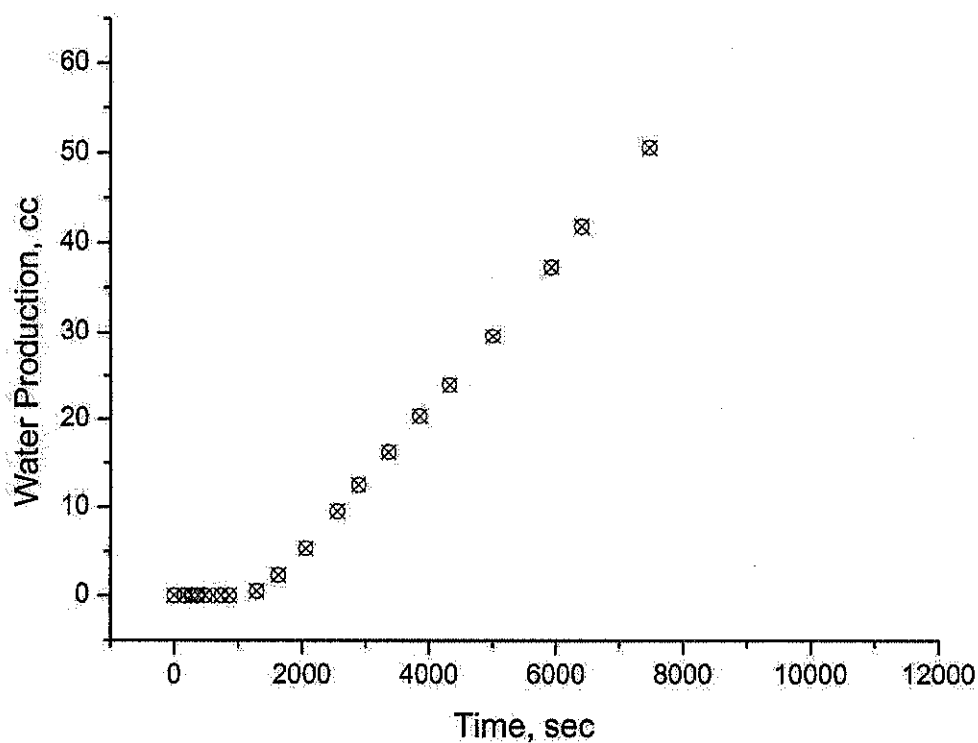


Figure A.5: Water production from core sample during water injection (zero % ratio of n-heptane–crude oil injection, water-oil system)

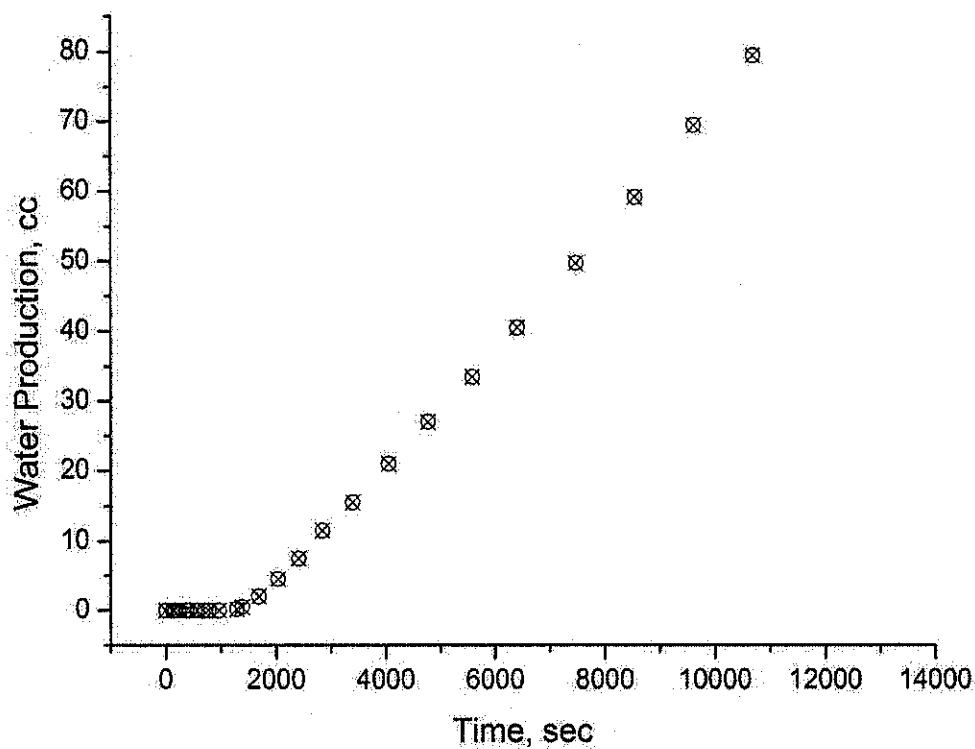


Figure A.6: Water production from core sample during water injection (20 % ratio of n-heptane–crude oil injection, water-oil system)

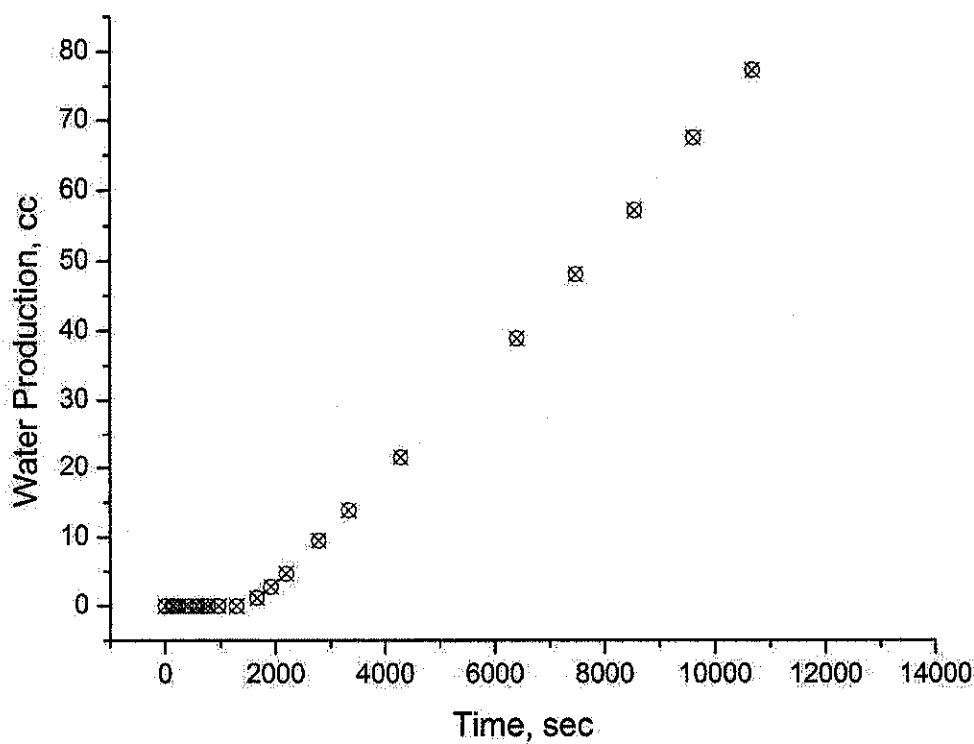


Figure A.7: Water production from core sample during water injection (50 % ratio of n-heptane–crude oil injection, water-oil system)

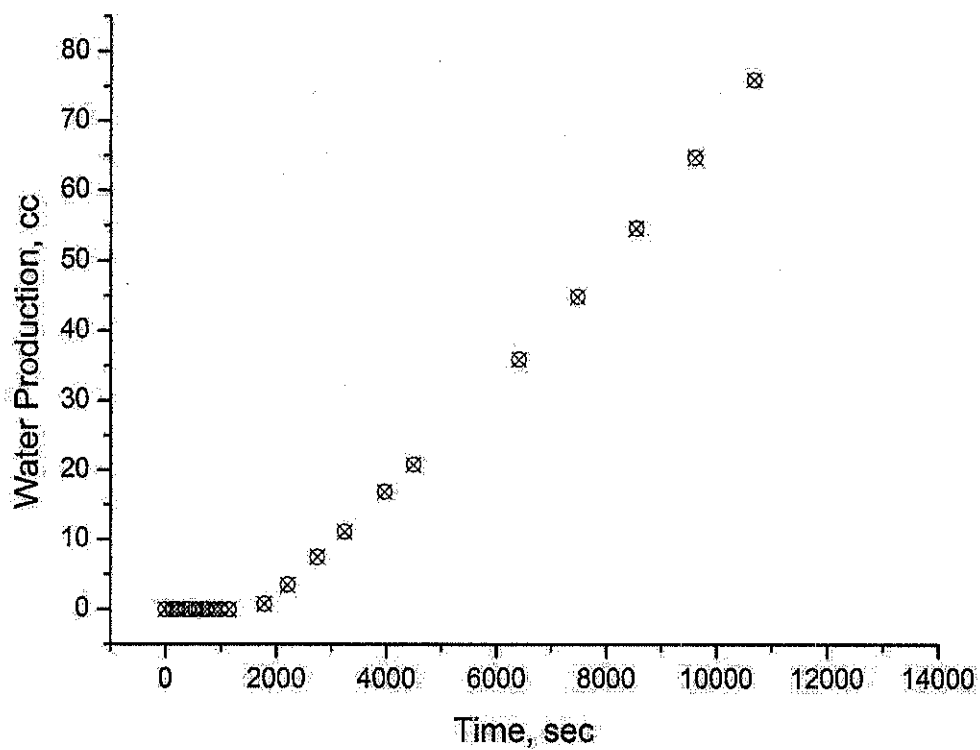


Figure A.8: Water production from core sample during water injection (80 % ratio of n-heptane–crude oil injection, water-oil system)

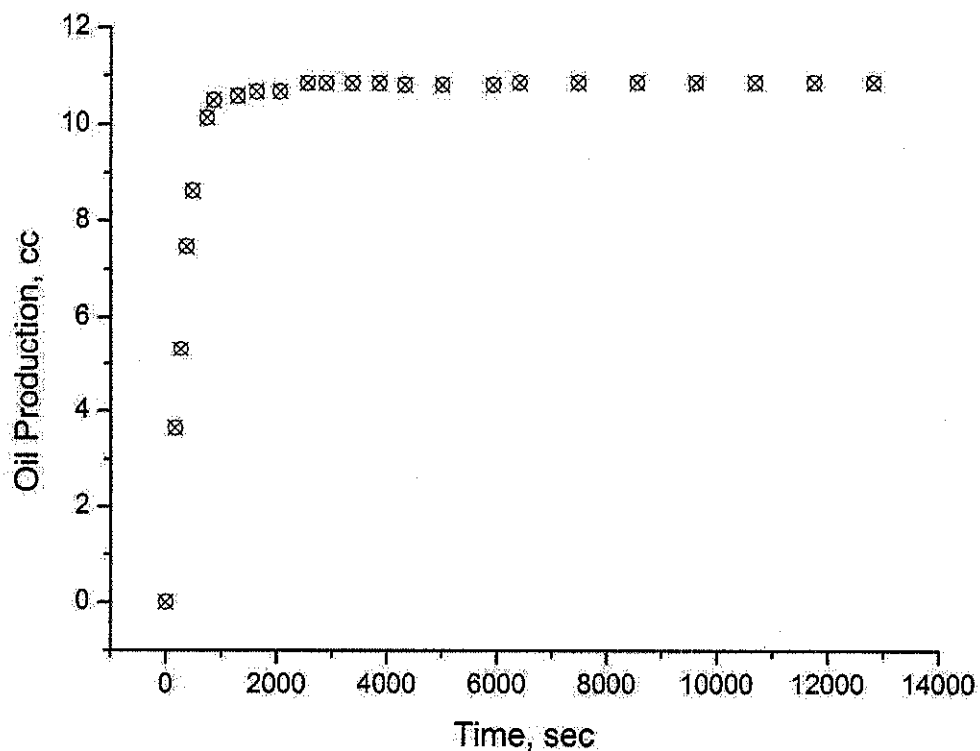


Figure A.9: Oil production from core sample during water injection (zero % ratio of n-heptane–crude oil injection, water-oil system)

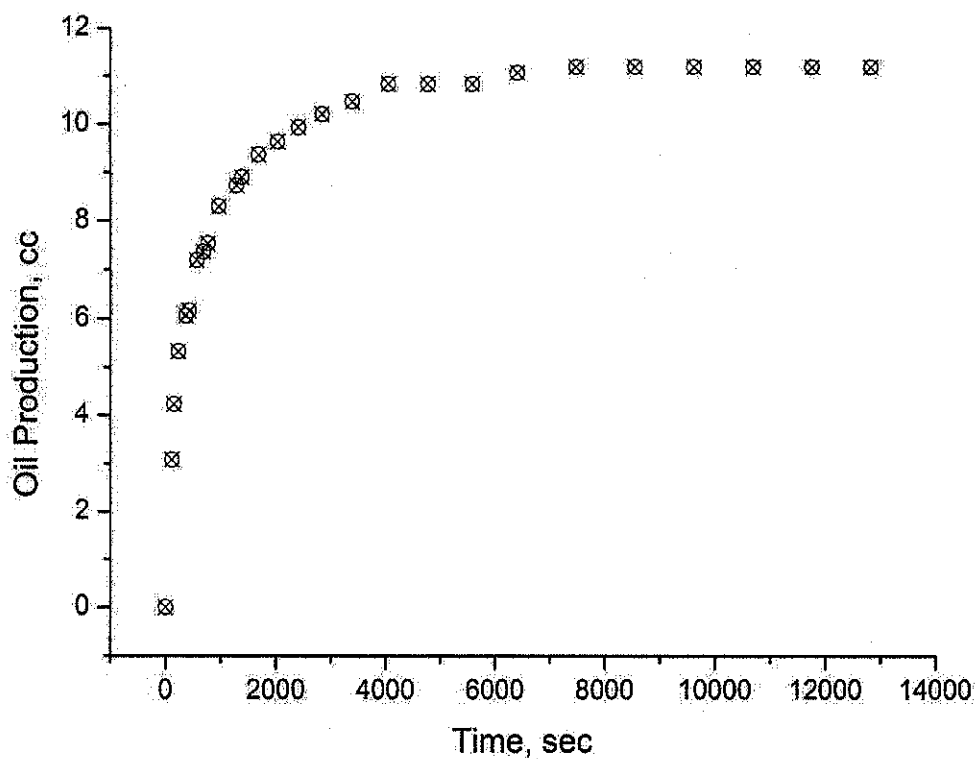


Figure A.10: Oil production from core sample during water injection (20 % ratio of n-heptane–crude oil injection, water-oil system)

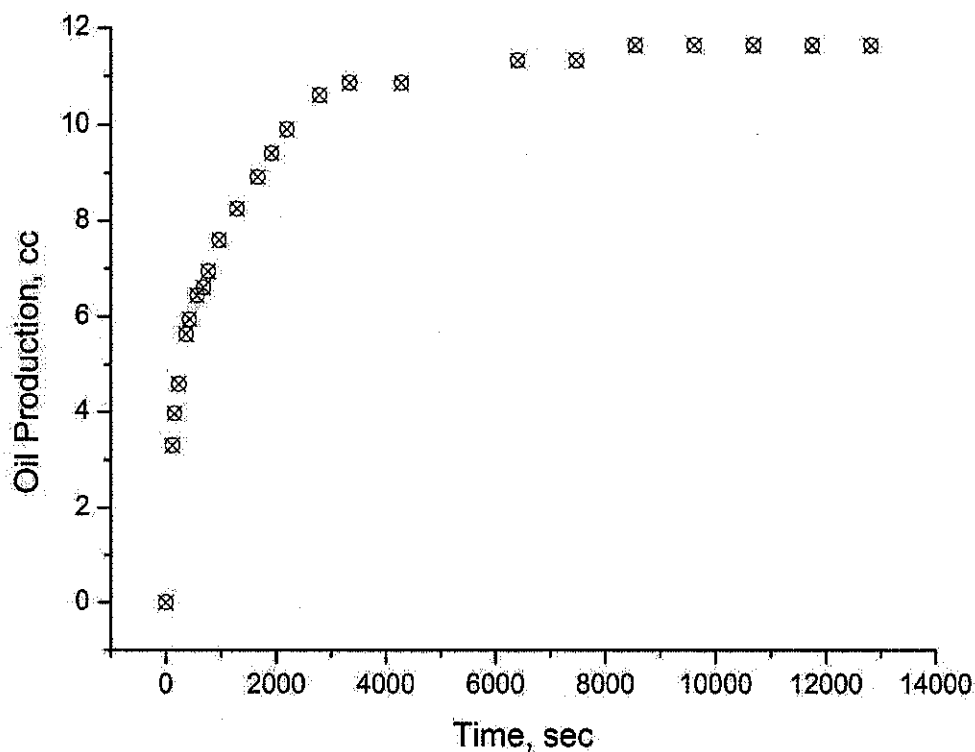


Figure A.11: Oil production from core sample during water injection (50 % ratio of n-heptane–crude oil injection, water-oil system)

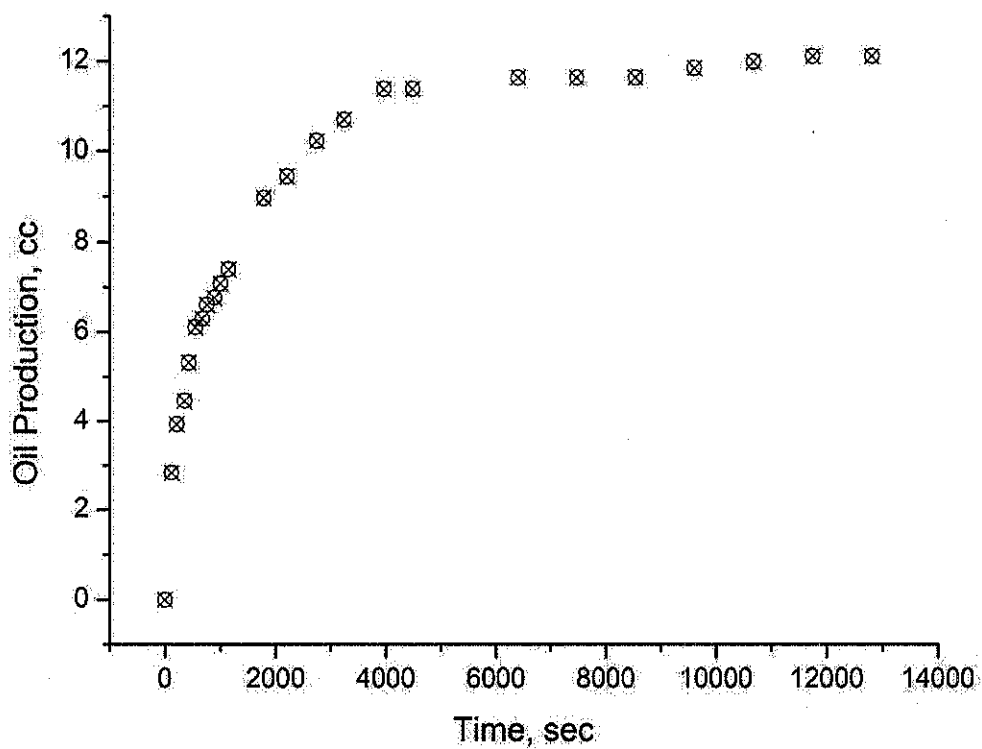


Figure A.12: Oil production from core sample during water injection (80 % ratio of n-heptane-crude oil injection, water-oil system)

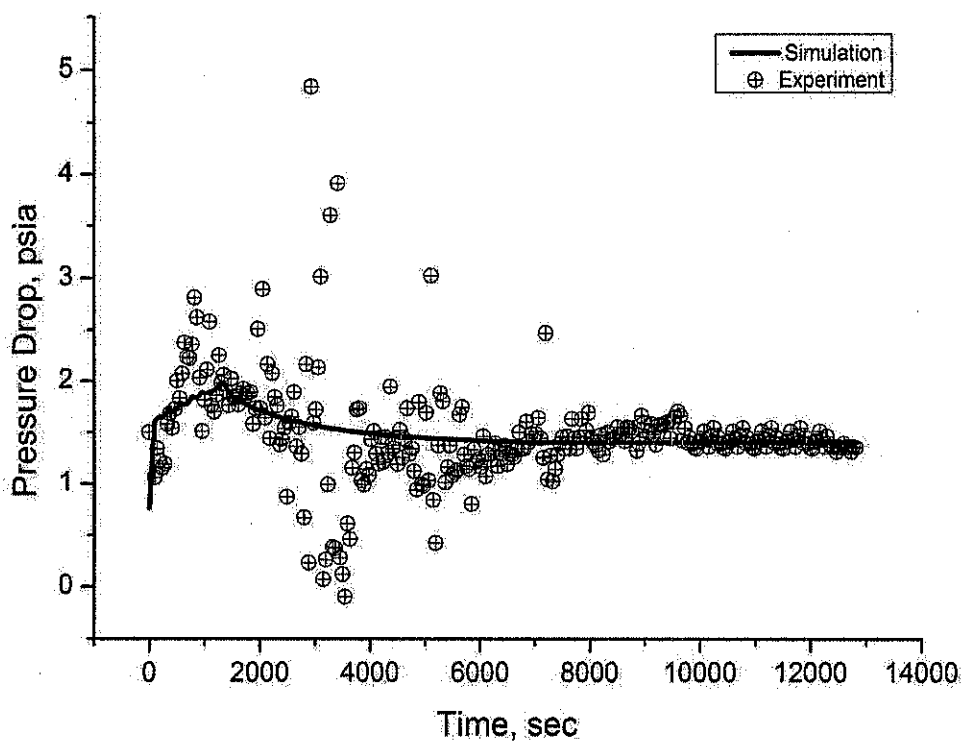


Figure A.13: Pressure drop history matching for zero % ratio of n-heptane-crude oil injection (Corey correlation, water-oil system)

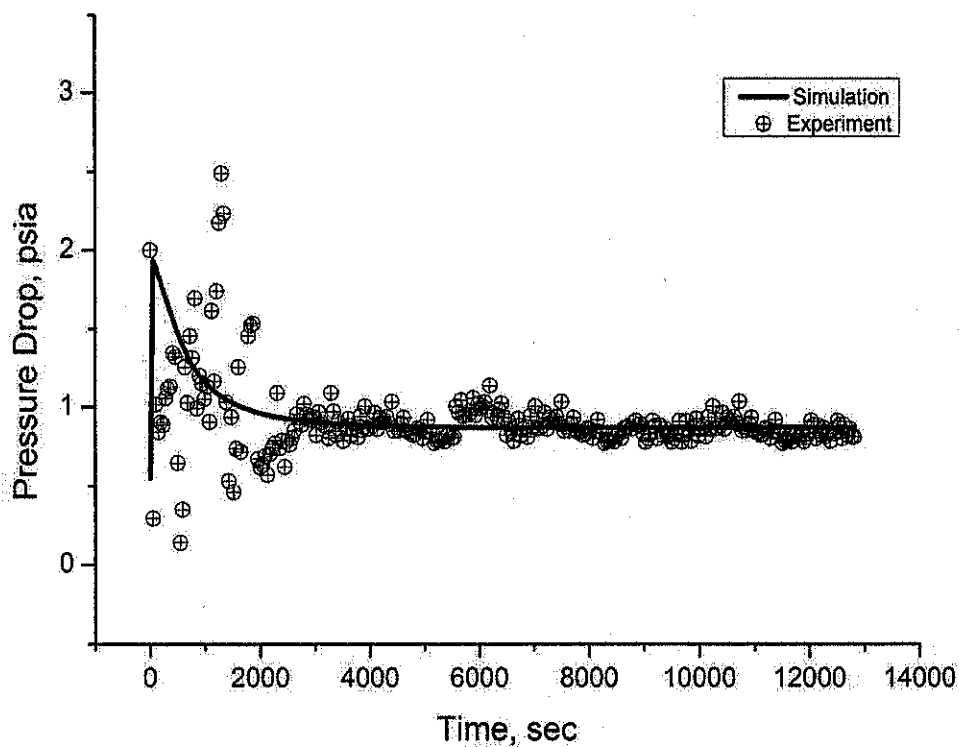


Figure A.14: Pressure drop history matching for 20 % ratio of n-heptane–crude oil injection (Corey correlation, water-oil system)

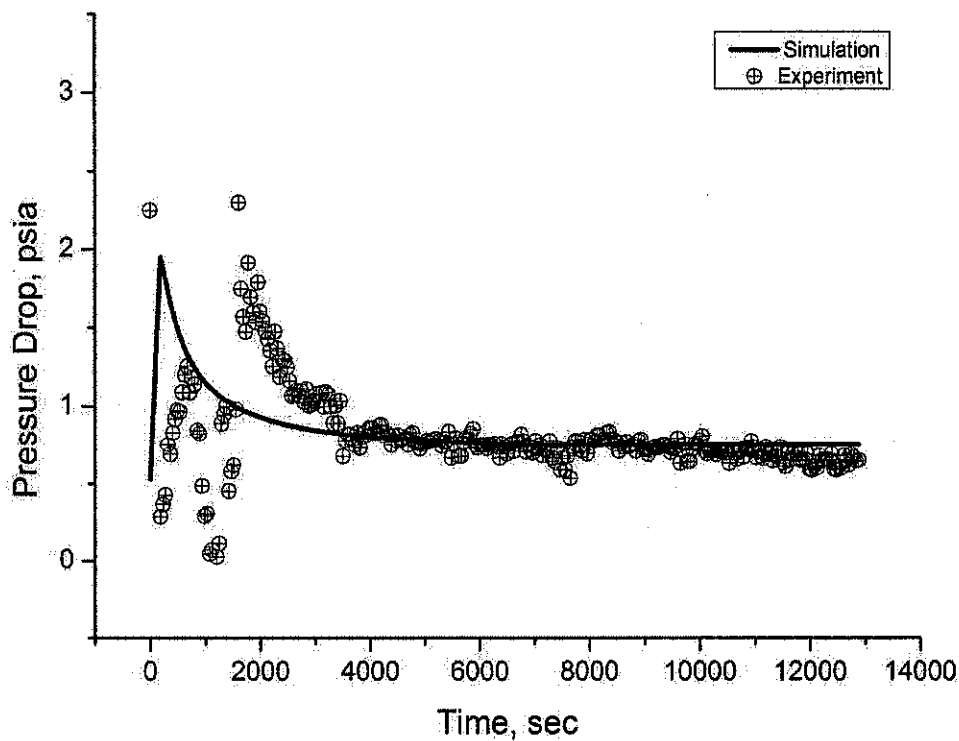


Figure A.15: Pressure drop history matching for 50 % ratio of n-heptane–crude oil injection (Corey correlation, water-oil system)

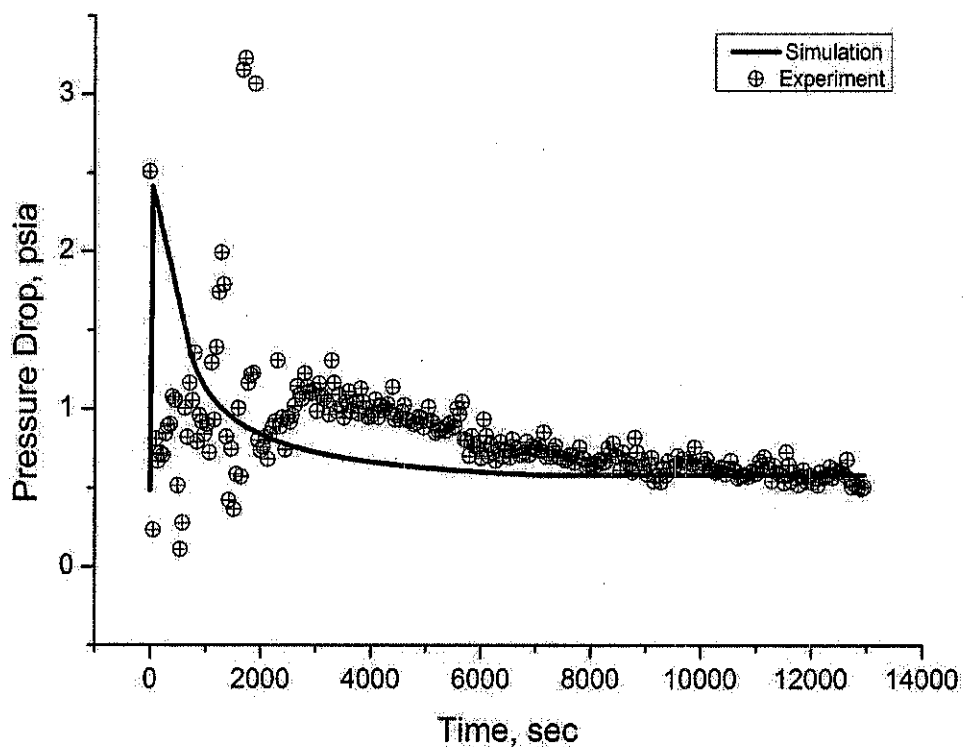


Figure A.16: Pressure drop history matching for 80 % ratio of n-heptane–crude oil injection (Corey correlation, water-oil system)

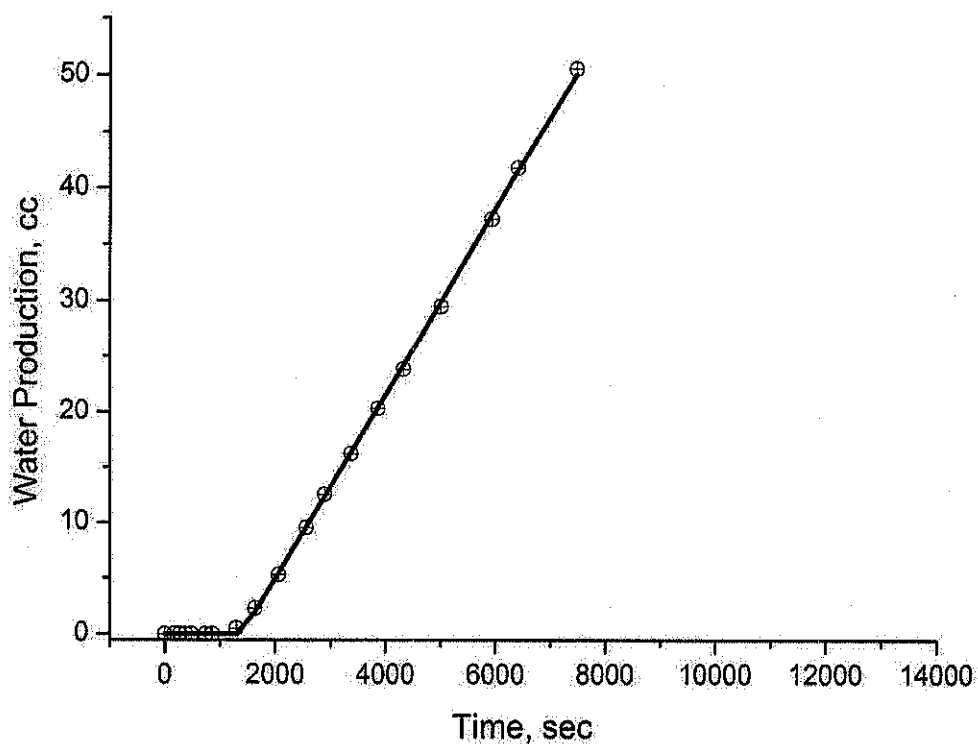


Figure A.17: Water production history matching for zero % ratio of n-heptane–crude oil injection (Corey correlation, water-oil system)

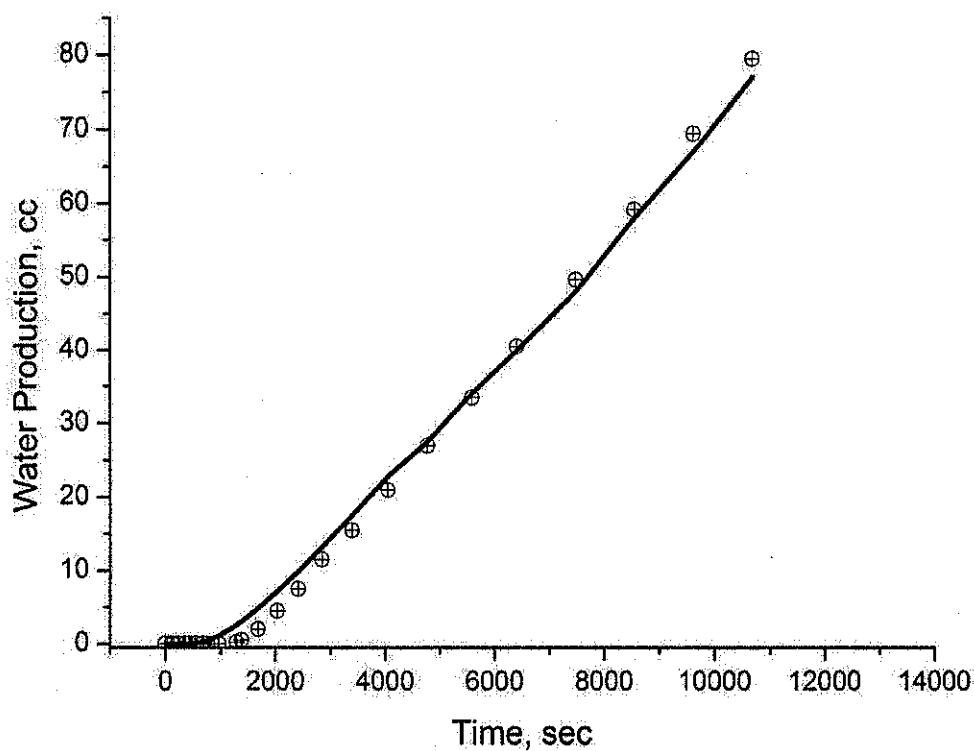


Figure A.18: Water production history matching for 20 % ratio of n-heptane–crude oil injection (Corey correlation, water-oil system)

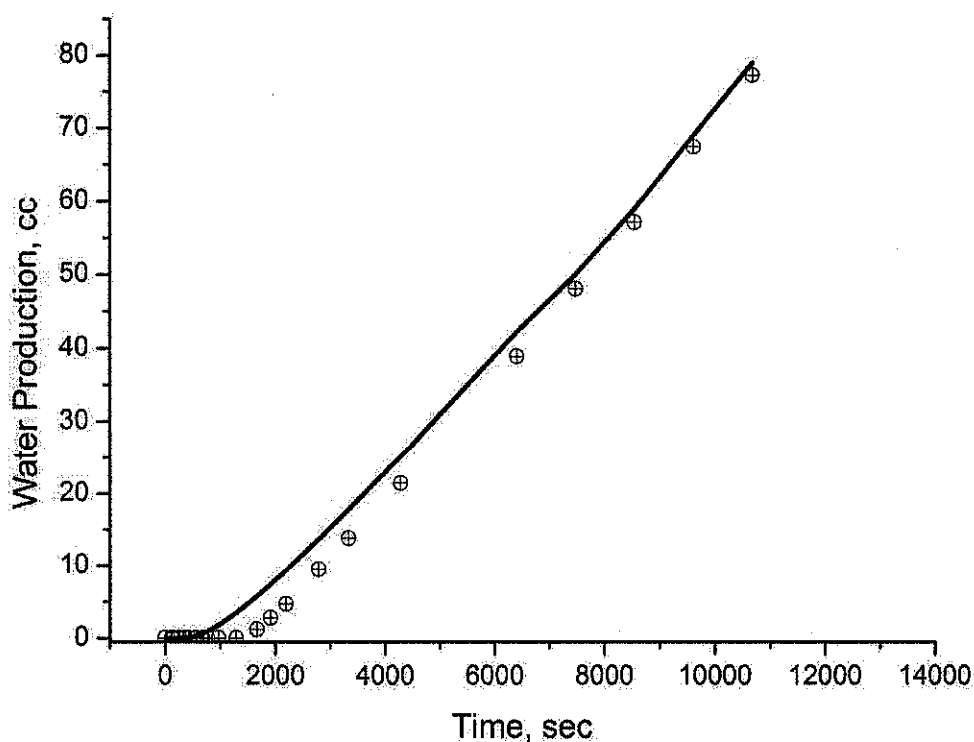


Figure A.19: Water production history matching for 50 % ratio of n-heptane–crude oil injection (Corey correlation, water-oil system)

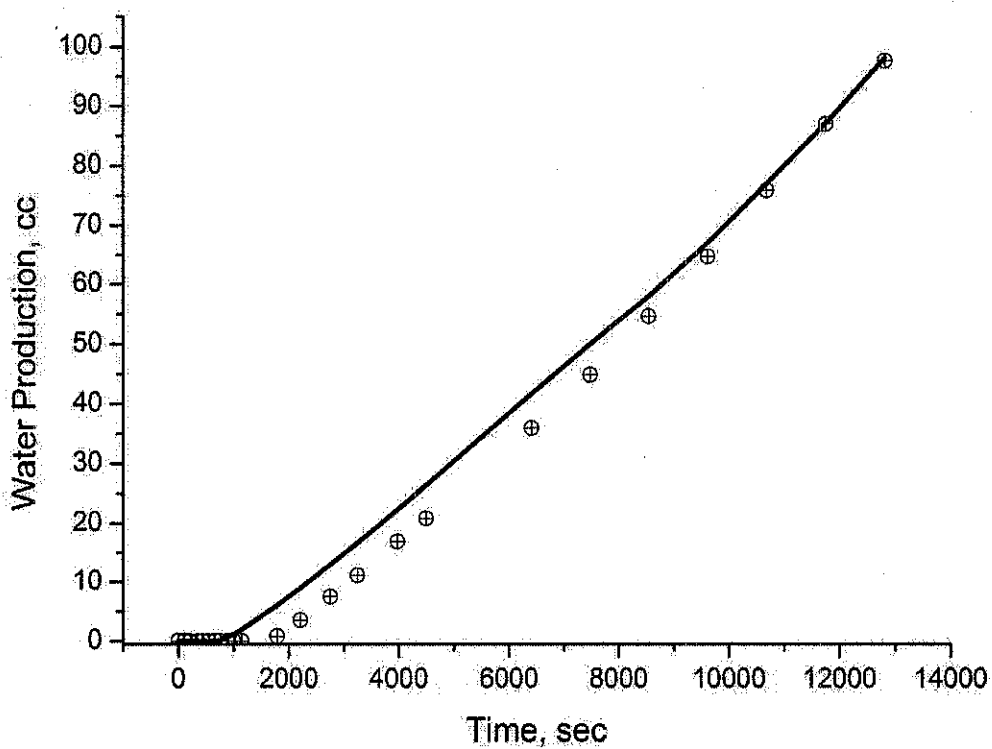


Figure A.20: Water production history matching for 80 % ratio of n-heptane–crude oil injection (Corey correlation, water-oil system)

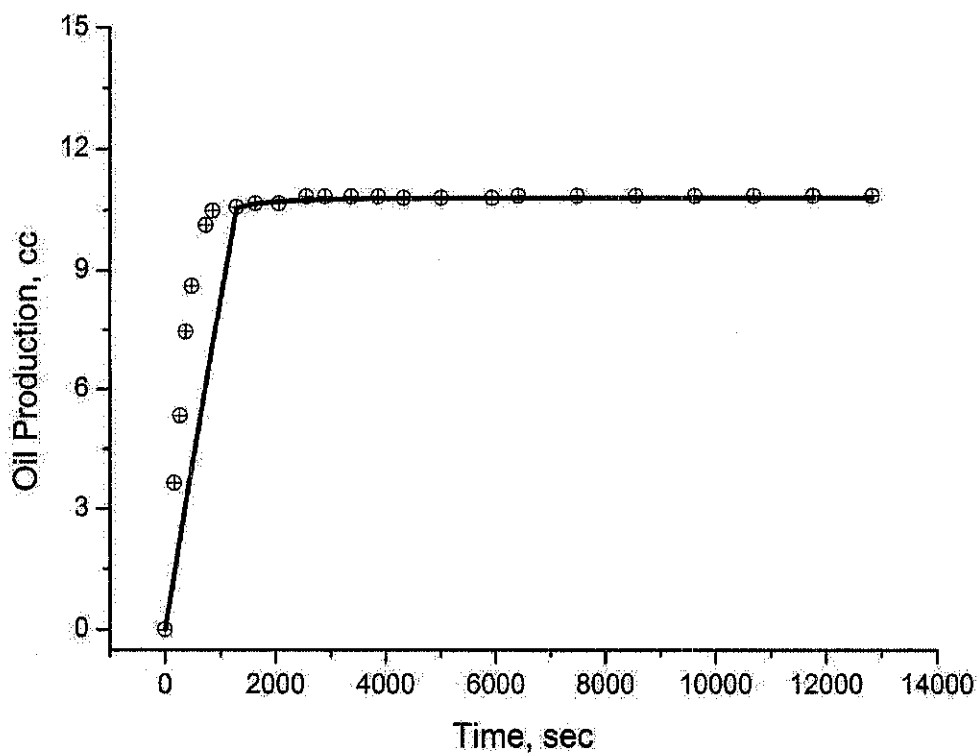


Figure A.21: Oil production history matching for zero % ratio of n-heptane–crude oil injection (Corey correlation, water-oil system)

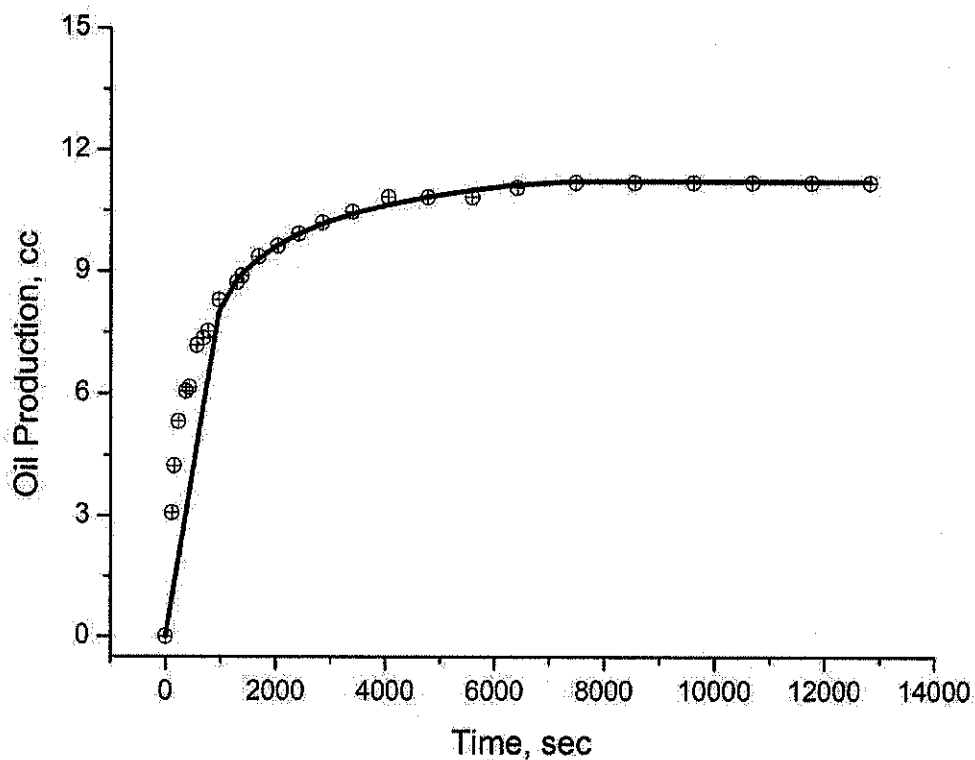


Figure A.22: Oil production history matching for 20 % ratio of n-heptane–crude oil injection (Corey correlation, water-oil system)

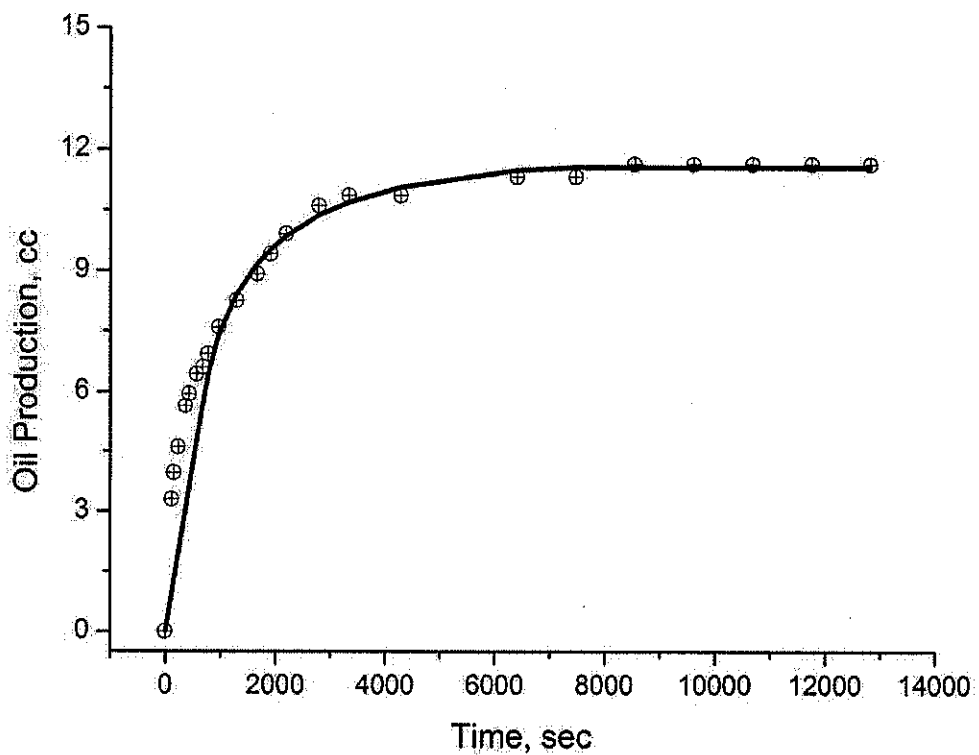


Figure A.23: Oil production history matching for 50 % ratio of n-heptane–crude oil injection (Corey correlation, water-oil system)

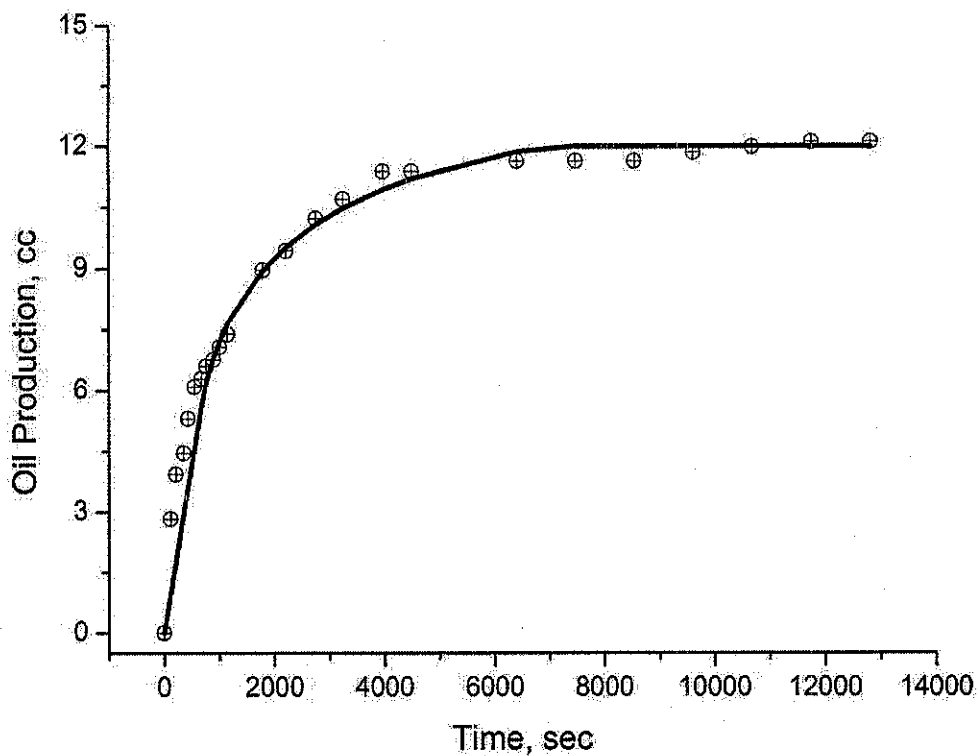


Figure A.24: Oil production history matching for 80 % ratio of n-heptane–crude oil injection (Corey correlation, water-oil system)

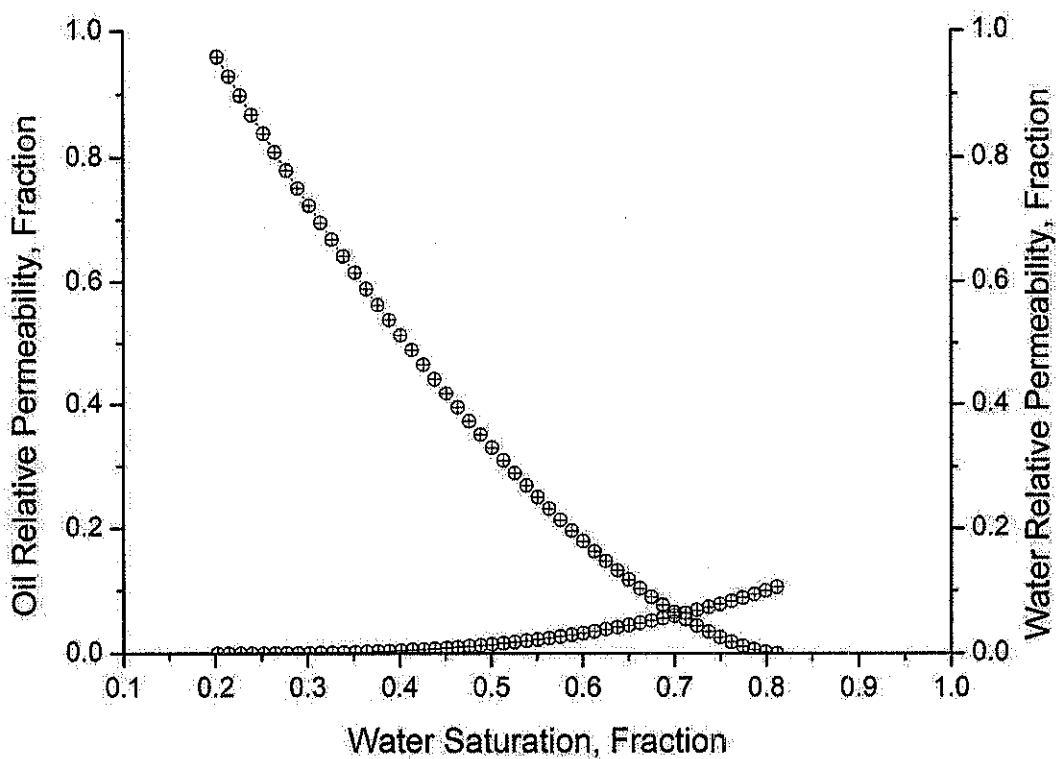


Figure A.25: Oil-water relative permeability for zero % ratio of n-heptane–crude oil injection, (Corey correlation, water-oil system)

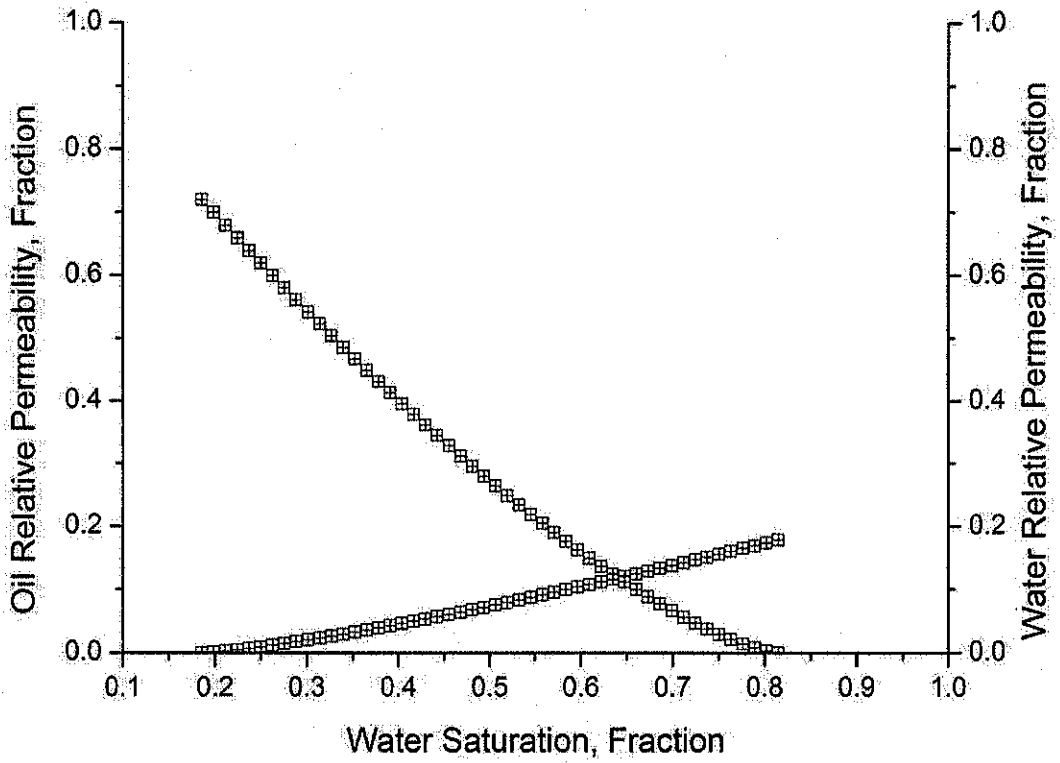


Figure A.26: Oil-water relative permeability for 20 % ratio of n-heptane–crude oil injection, (Corey correlation, water-oil system)

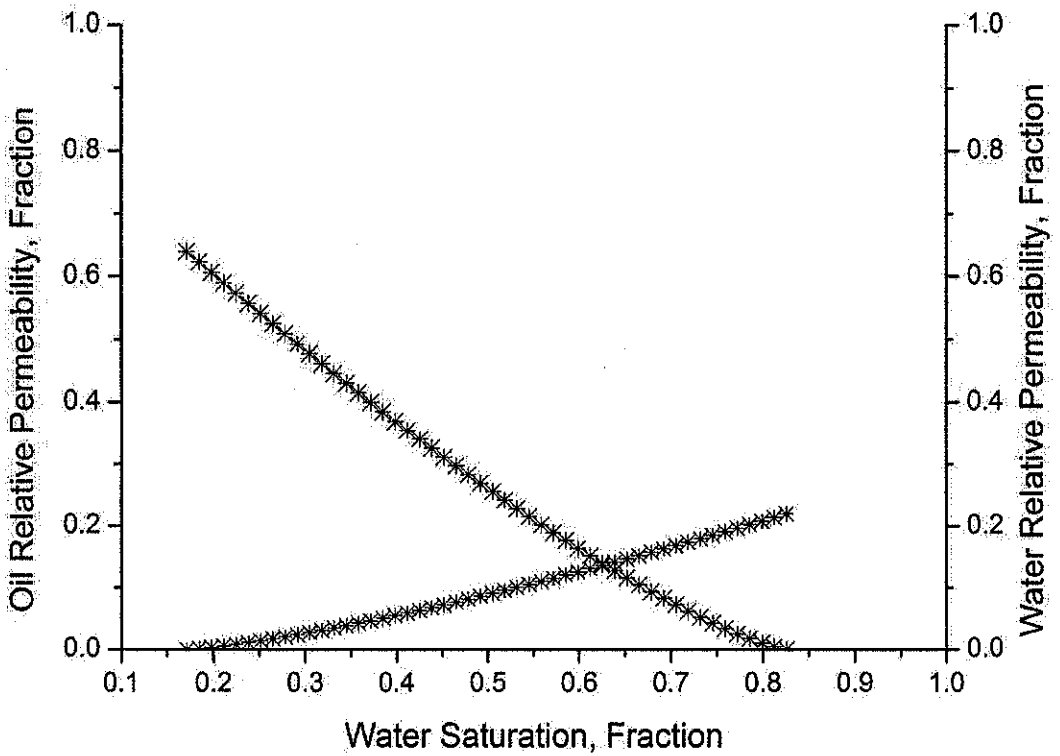


Figure A.27: Oil-water relative permeability for 50 % ratio of n-heptane–crude oil injection, (Corey correlation, water-oil system)

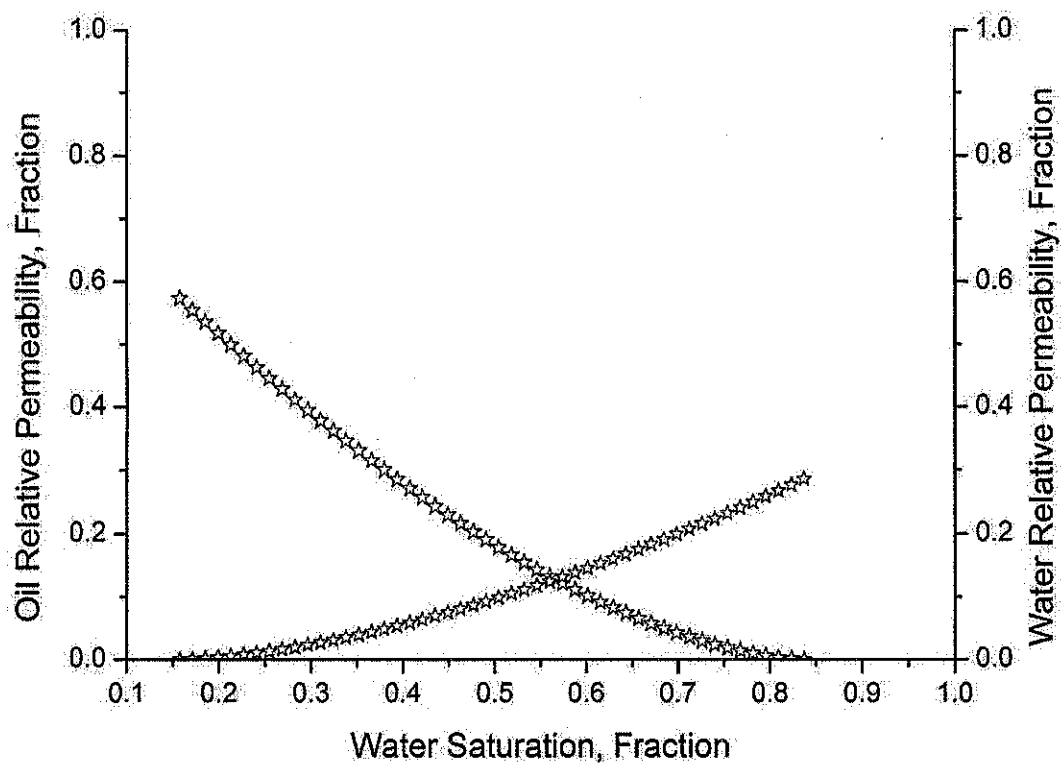


Figure A.28: Oil-water relative permeability for 80 % ratio of n-heptane-crude oil injection, (Corey correlation, water-oil system)

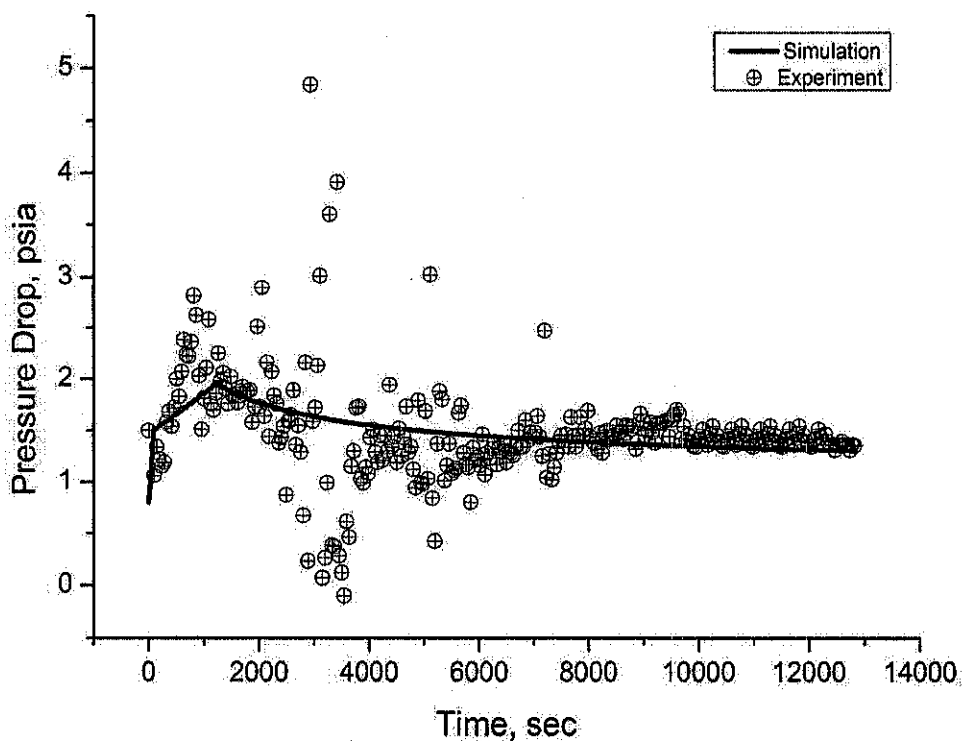


Figure A.29: Pressure drop history matching for zero % ratio of n-heptane-crude oil injection (LET correlation, water-oil system)

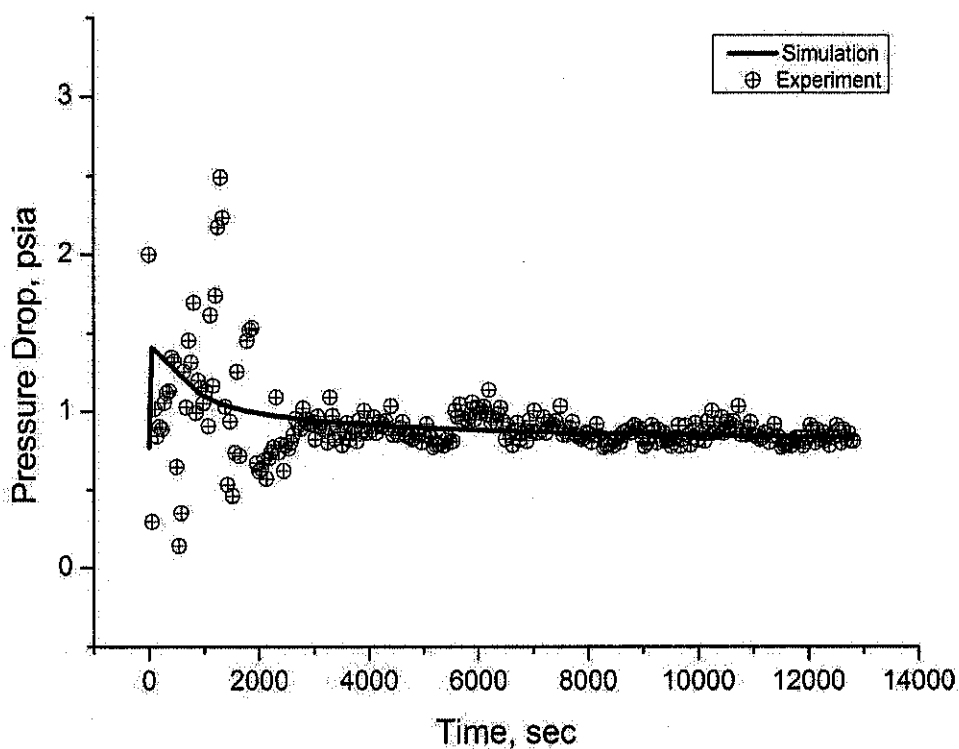


Figure A.30: Pressure drop history matching for 20 % ratio of n-heptane–crude oil injection (LET correlation, water-oil system)

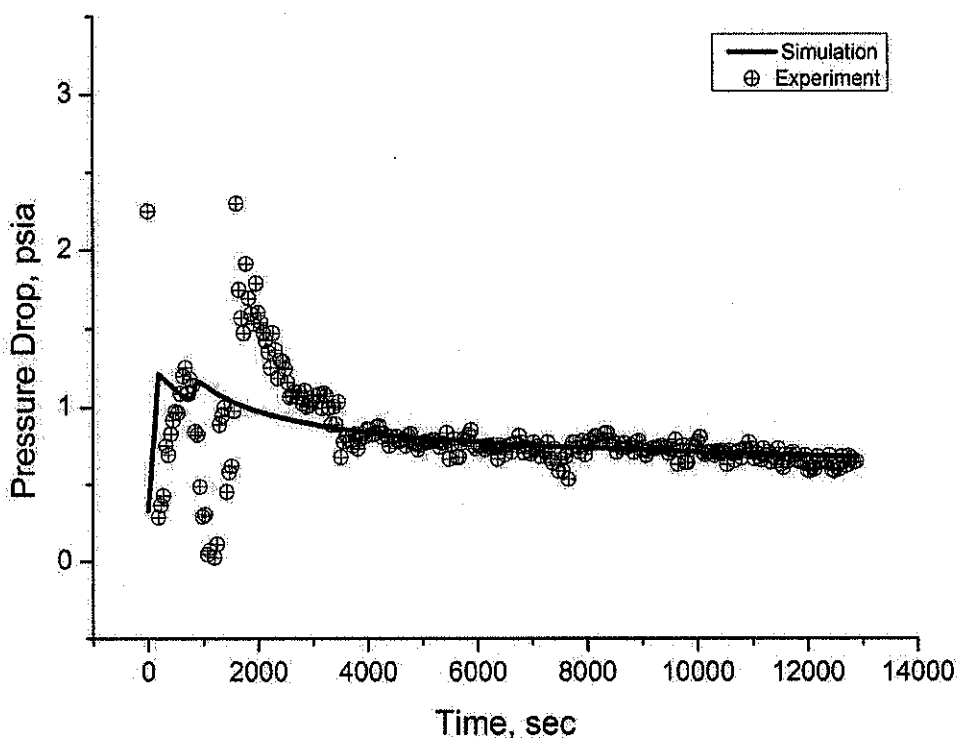


Figure A.31: Pressure drop history matching for 50 % ratio of n-heptane–crude oil injection (LET correlation, water-oil system)

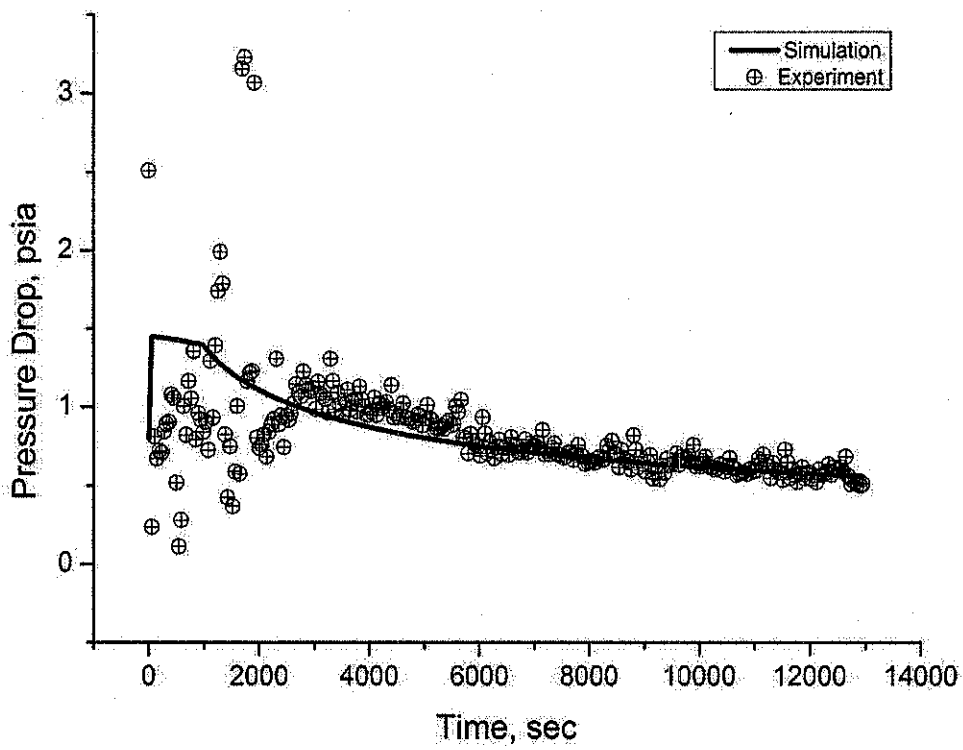


Figure A.32: Pressure drop history matching for 80 % ratio of n-heptane–crude oil injection (LET correlation, water-oil system)

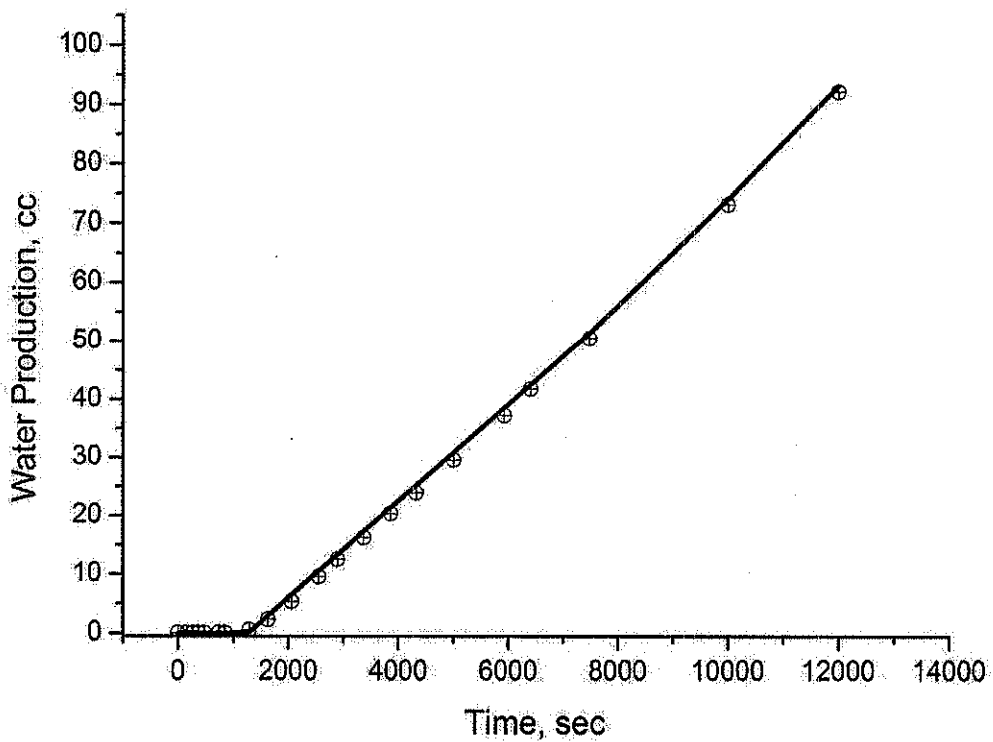


Figure A.33: Water production history matching for zero % ratio of n-heptane–crude oil injection (LET correlation, water-oil system)

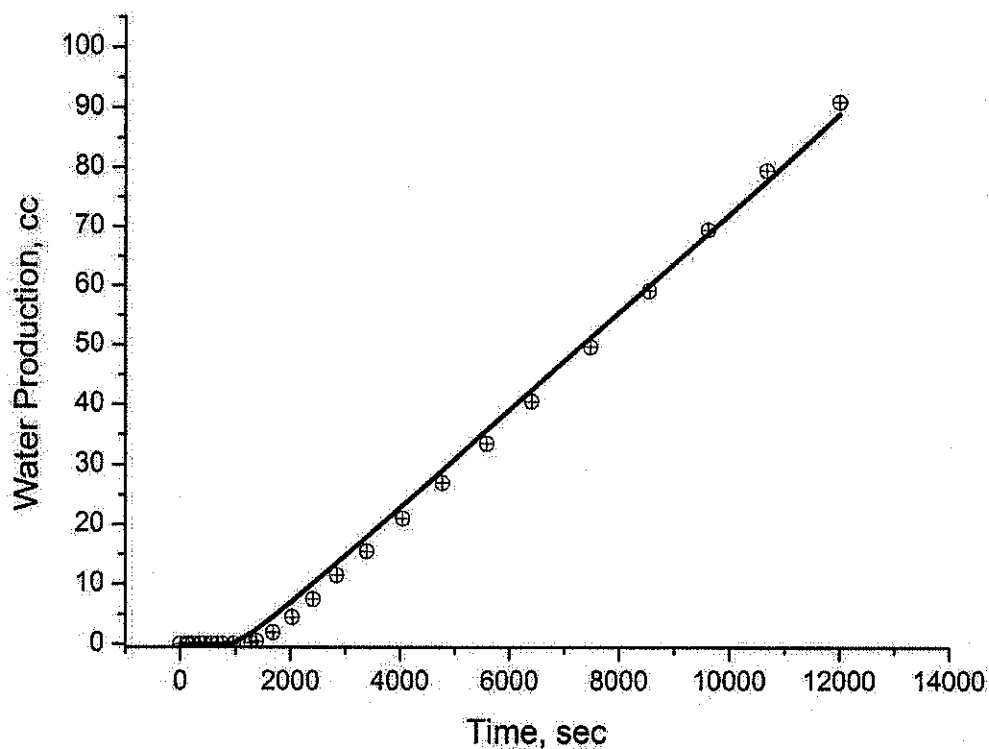


Figure A.34: Water production history matching for 20 % ratio of n-heptane–crude oil injection (LET correlation, water-oil system)

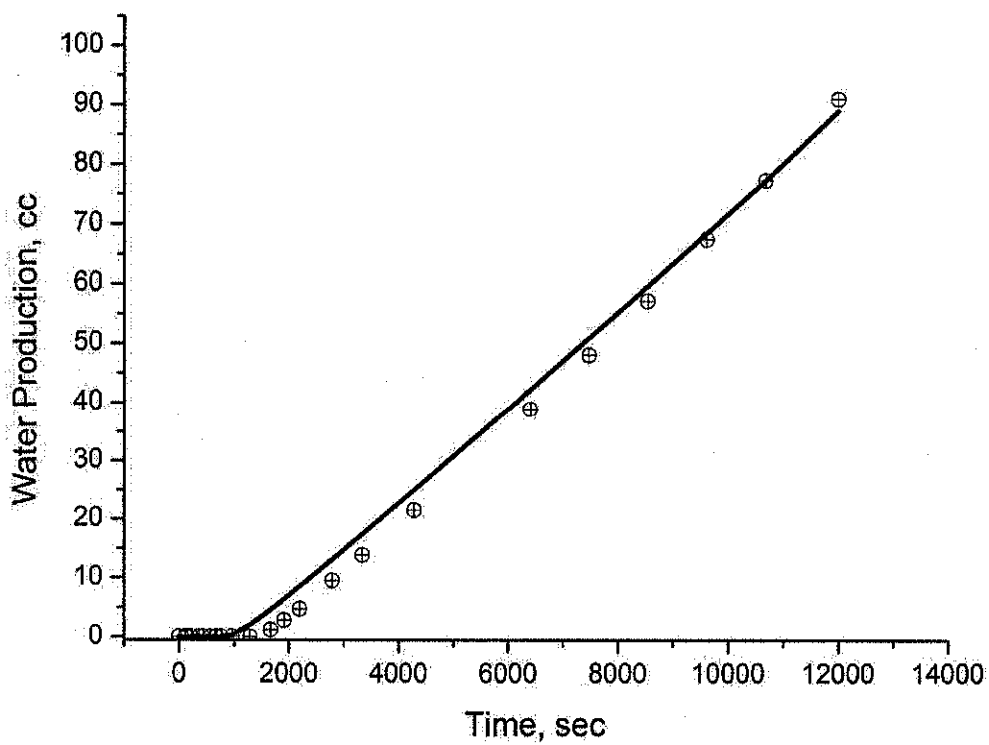


Figure A.35: Water production history matching for 50 % ratio of n-heptane–crude oil injection (LET correlation, water-oil system)

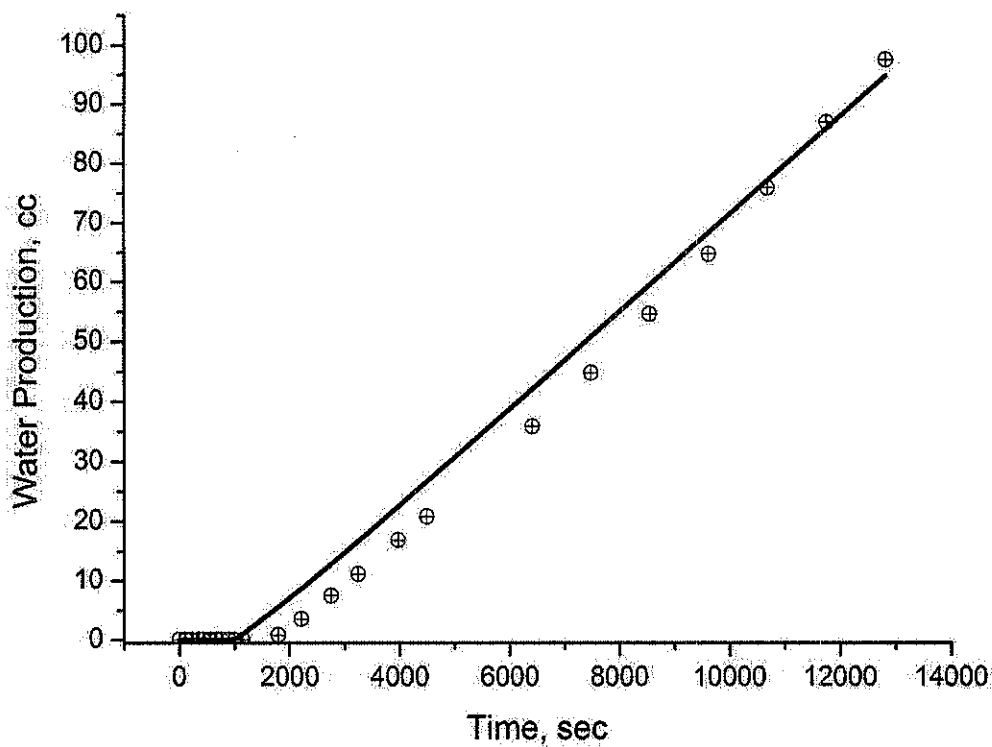


Figure A.36: Water production history matching for 80 % ratio of n-heptane-crude oil injection (LET correlation, water-oil system)

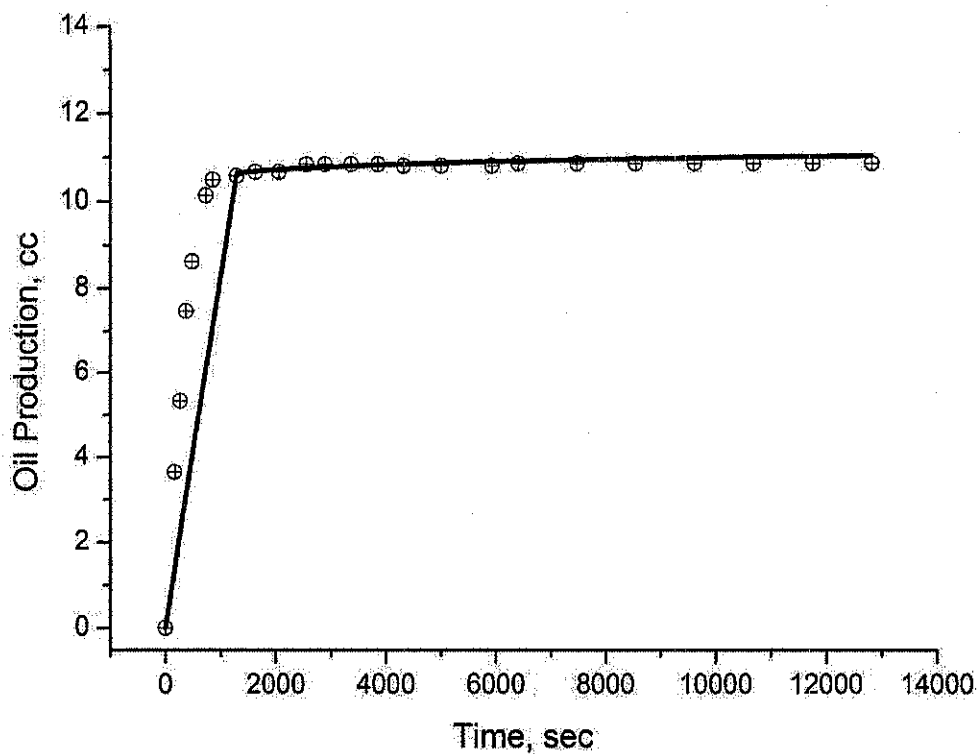


Figure A.37: Oil production history matching for zero % ratio of n-heptane-crude oil injection (LET correlation, water-oil system)

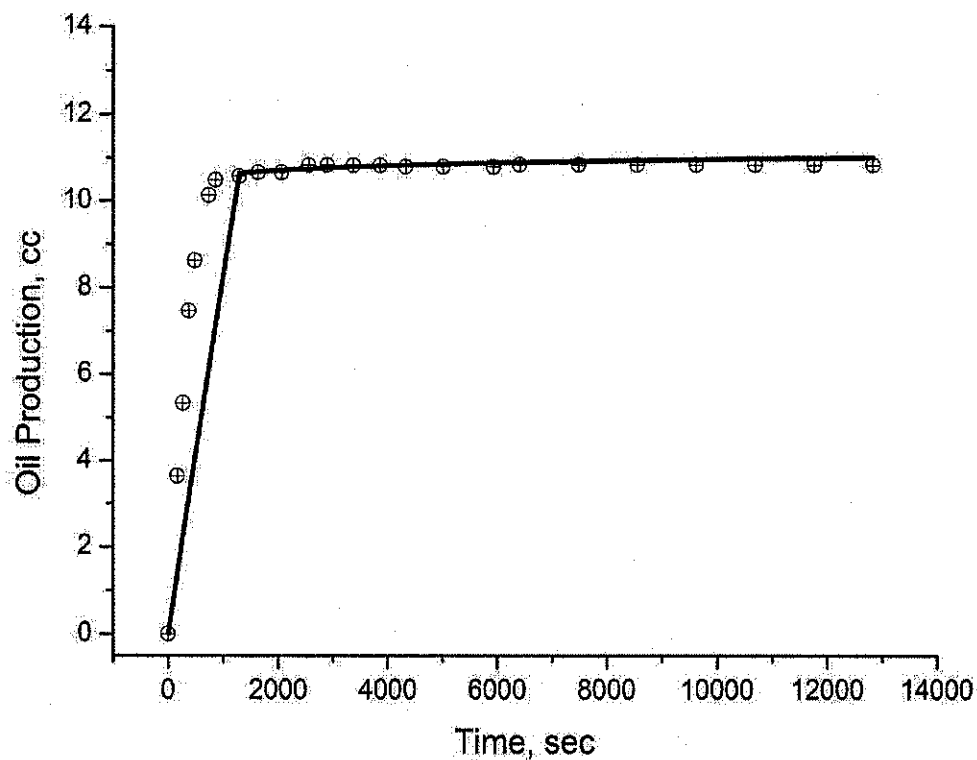


Figure A.38: Oil production history matching for 20 % ratio of n-heptane–crude oil injection (LET correlation, water-oil system)

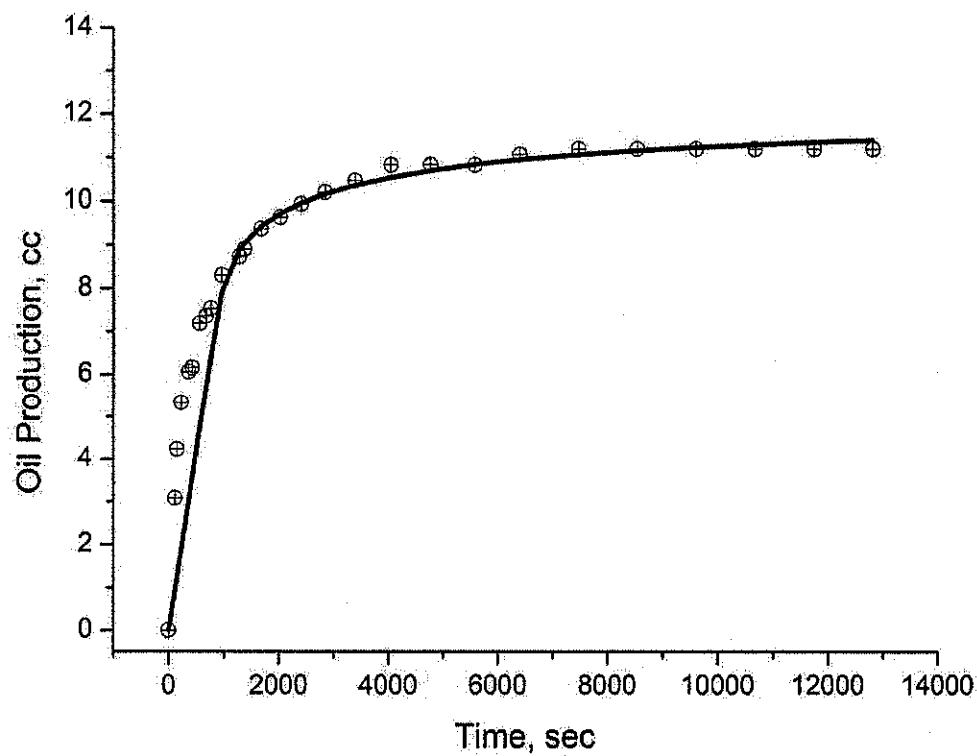


Figure A.39: Oil production history matching for 50 % ratio of n-heptane–crude oil injection (LET correlation, water-oil system)

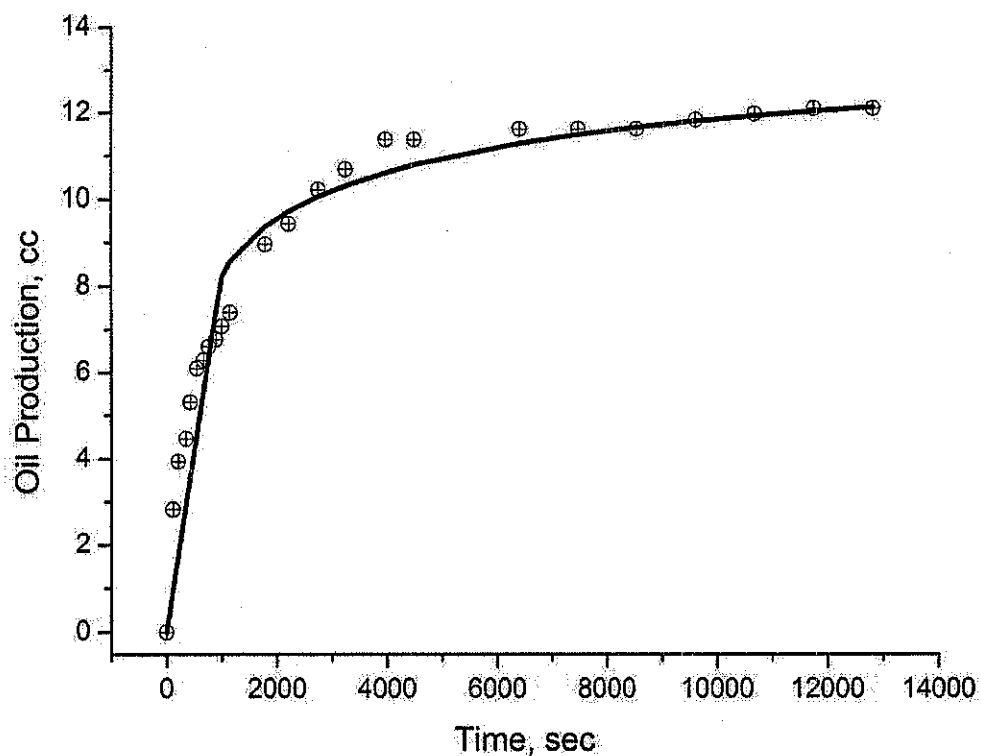


Figure A.40: Oil production history matching for 80 % ratio of n-heptane–crude oil injection (LET correlation, water-oil system)

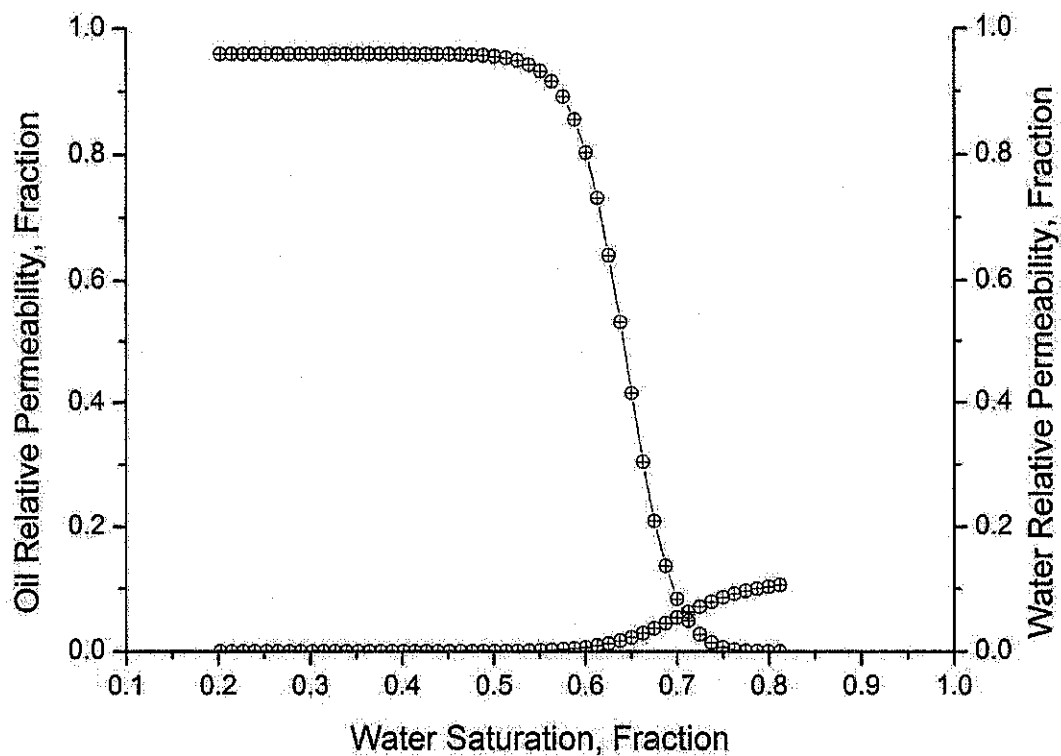


Figure A.41: Oil-water relative permeability for zero % ratio of n-heptane–crude oil injection, (LET correlation, water-oil system)

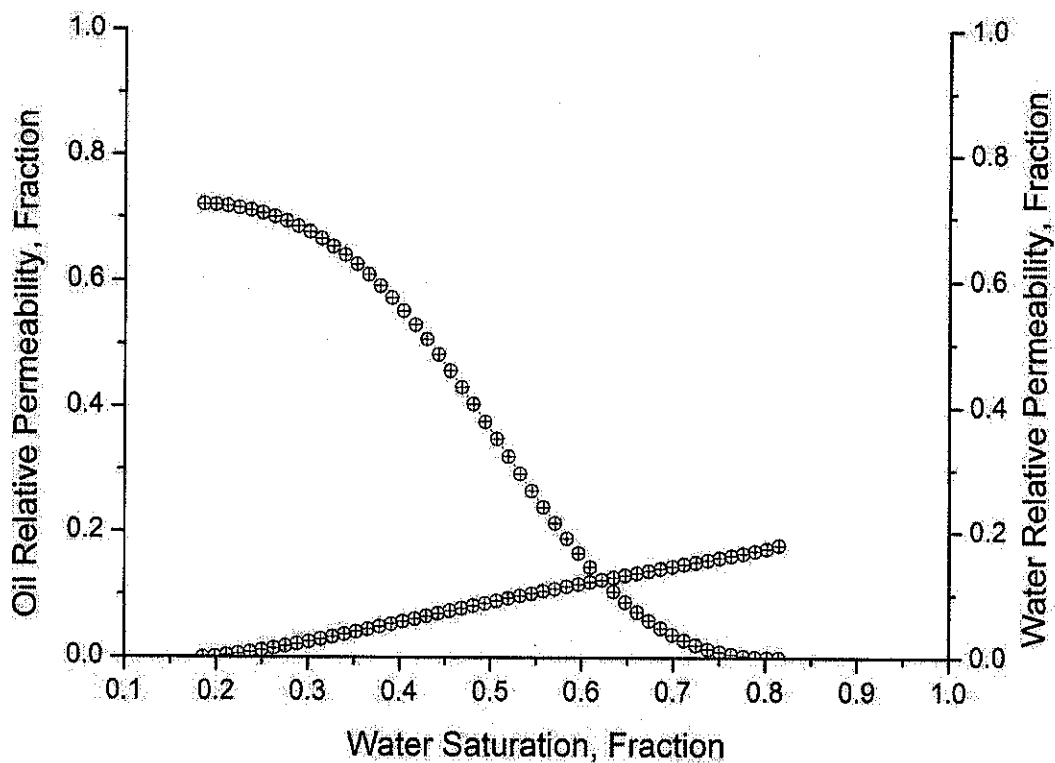


Figure A.42: Oil-water relative permeability for 20 % ratio of n-heptane–crude oil injection, (LET correlation, water-oil system)

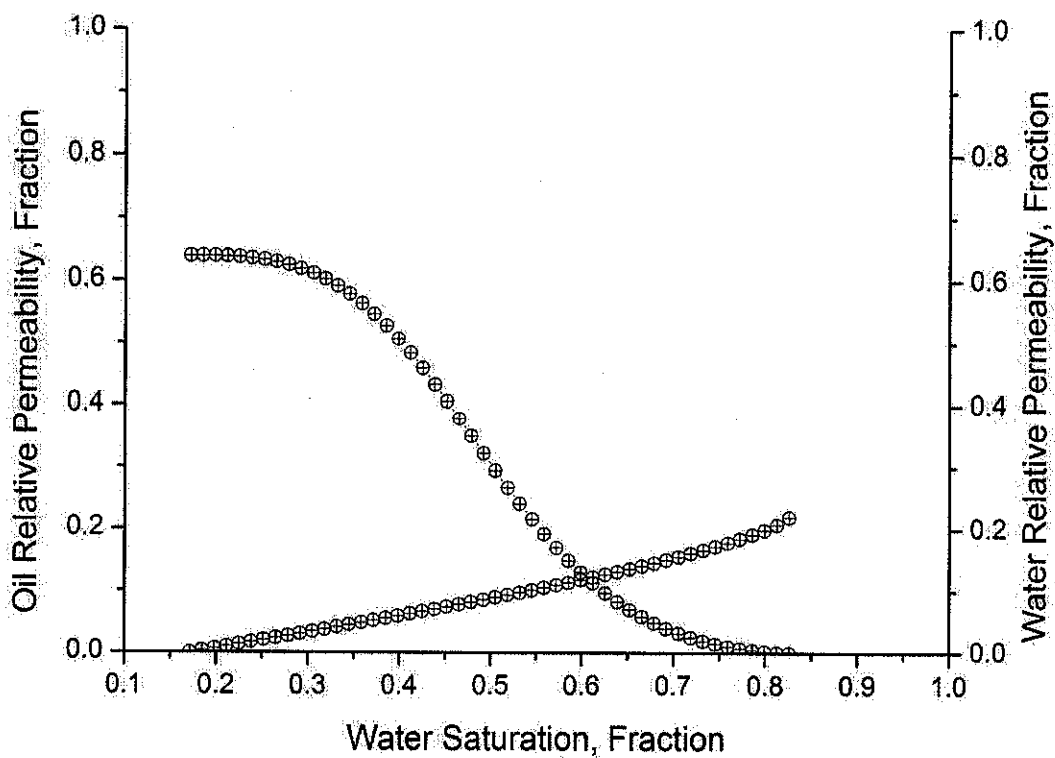


Figure A.43: Oil-water relative permeability for 50 % ratio of n-heptane–crude oil injection, (LET correlation, water-oil system)

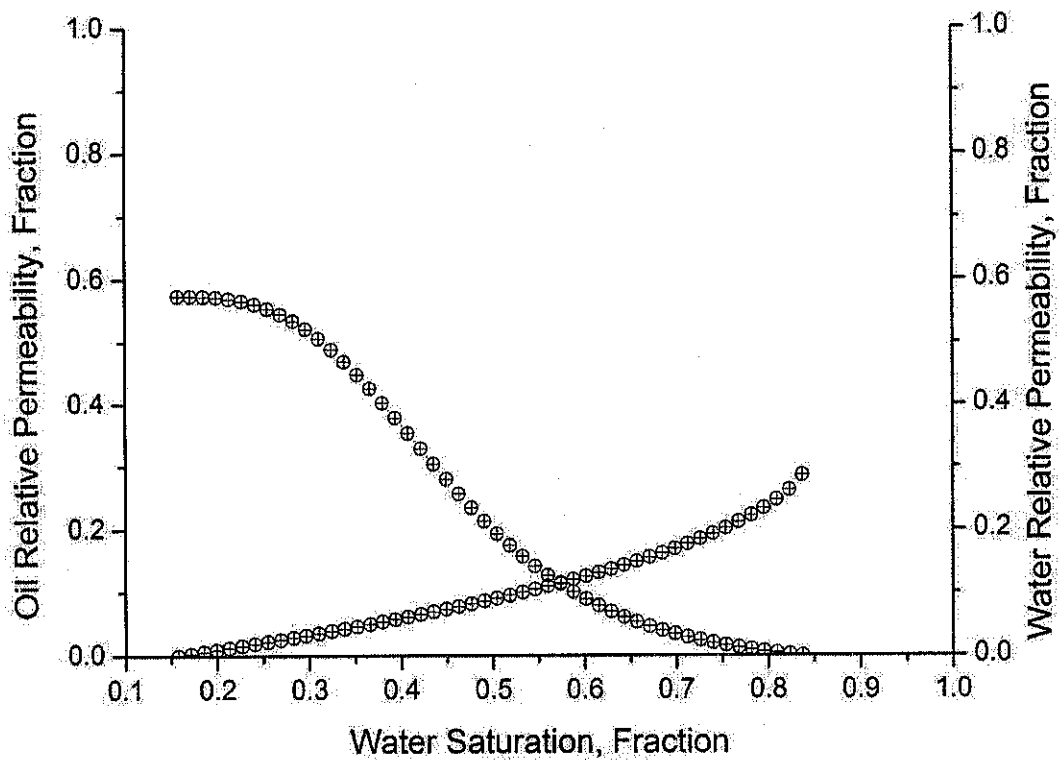


Figure A.44: Oil-water relative permeability for 80 % ratio of n-heptane–crude oil injection, (LET correlation, water-oil system)

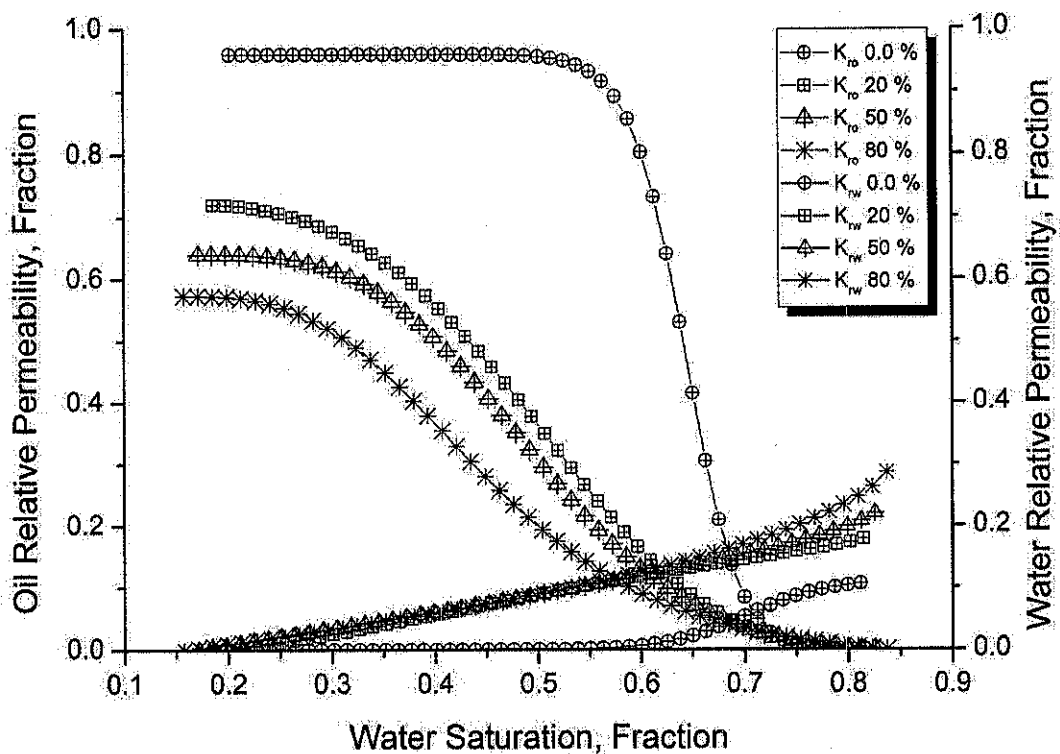


Figure A.45: Effect of asphaltene on relative permeability at various n-heptane–crude oil ratios injections, (LET correlation, water-oil system)

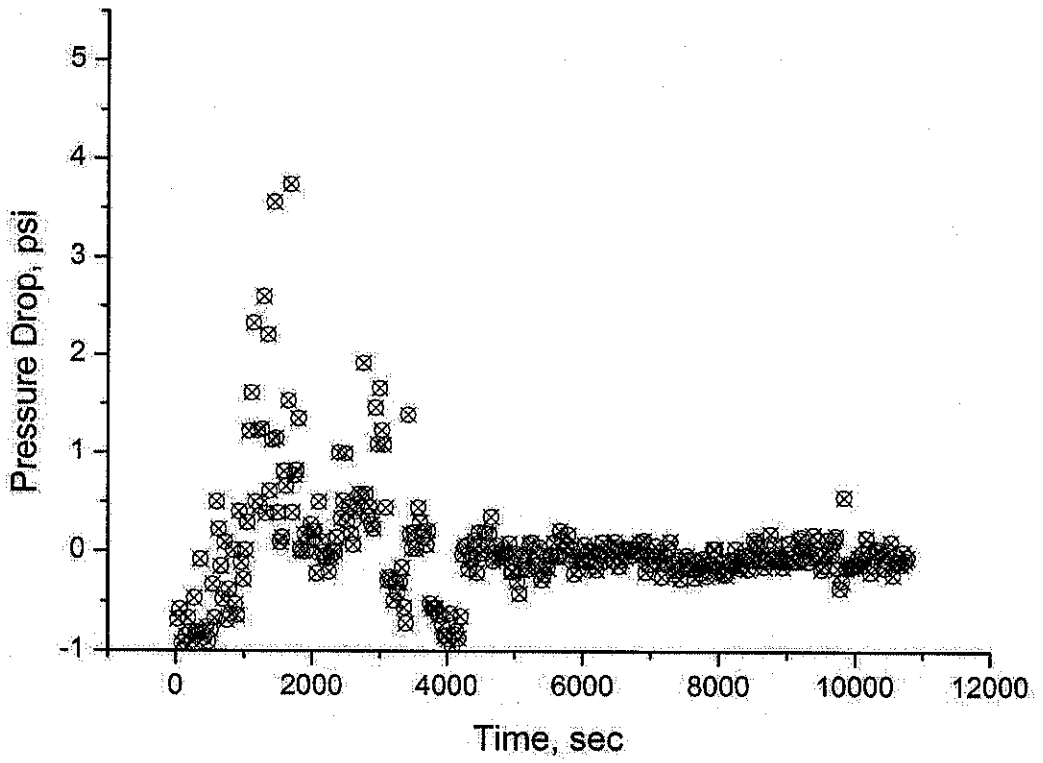


Figure A.46: Pressure drop across core sample during gas injection (zero % ratio of n-heptane–crude oil injection, gas-oil system)

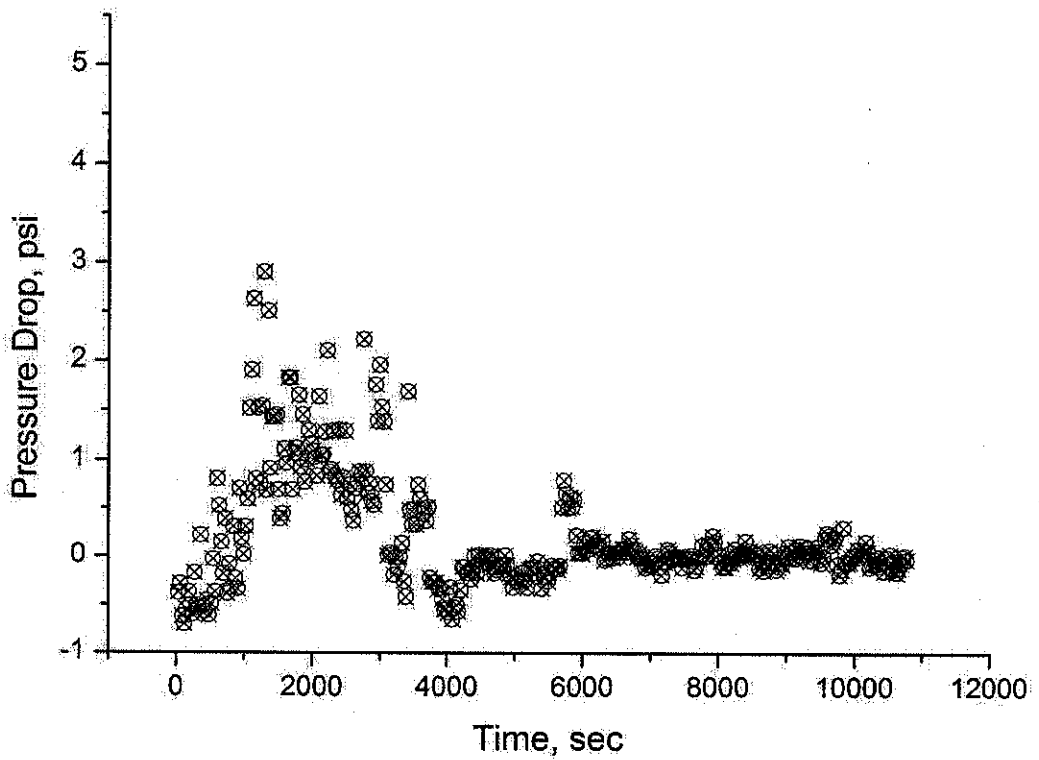


Figure A.47: Pressure drop across core sample during water injection (20 % ratio of n-heptane–crude oil injection, gas-oil system)

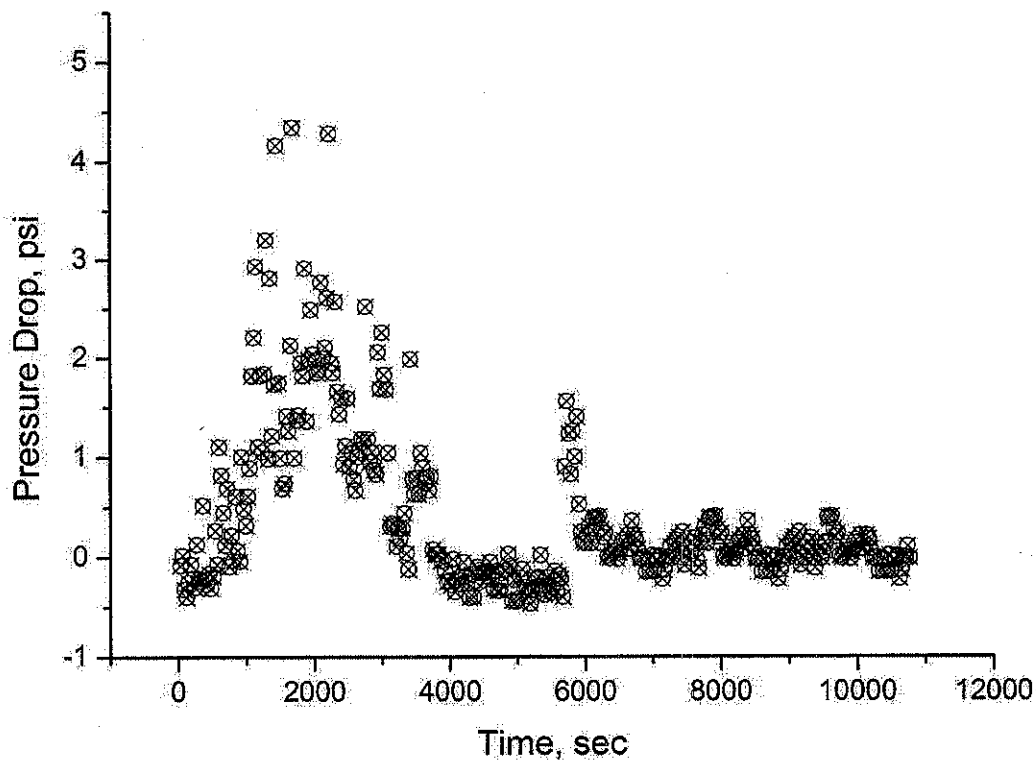


Figure A.48: Pressure drop across core sample during water injection (50 % ratio of n-heptane–crude oil injection, gas-oil system)

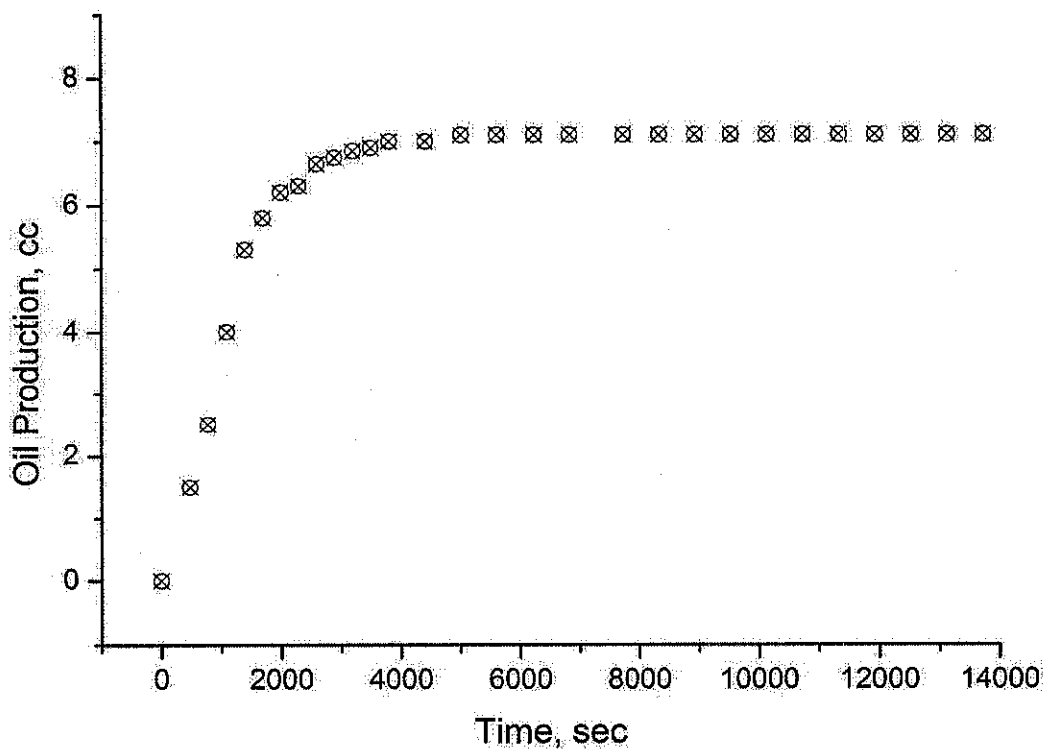


Figure A.49: Oil production from core sample during gas injection (zero % ratio of n-heptane–crude oil injection, gas-oil system)

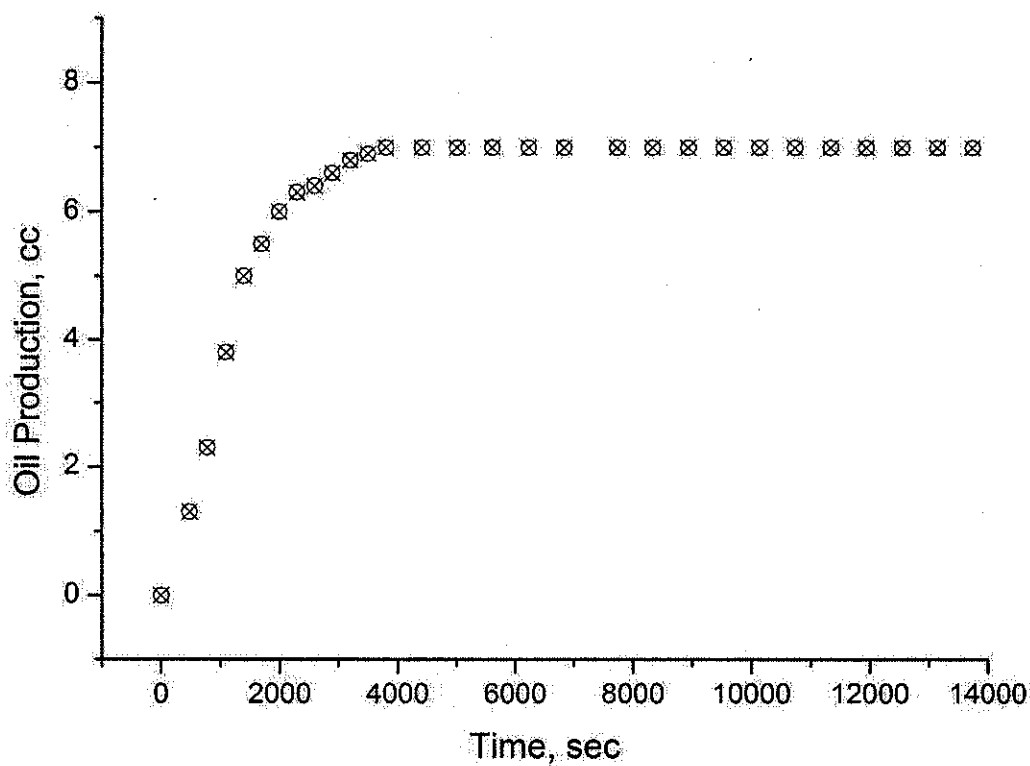


Figure A.50: Oil production from core sample during gas injection (20 % ratio of n-heptane-crude oil injection, gas-oil system)

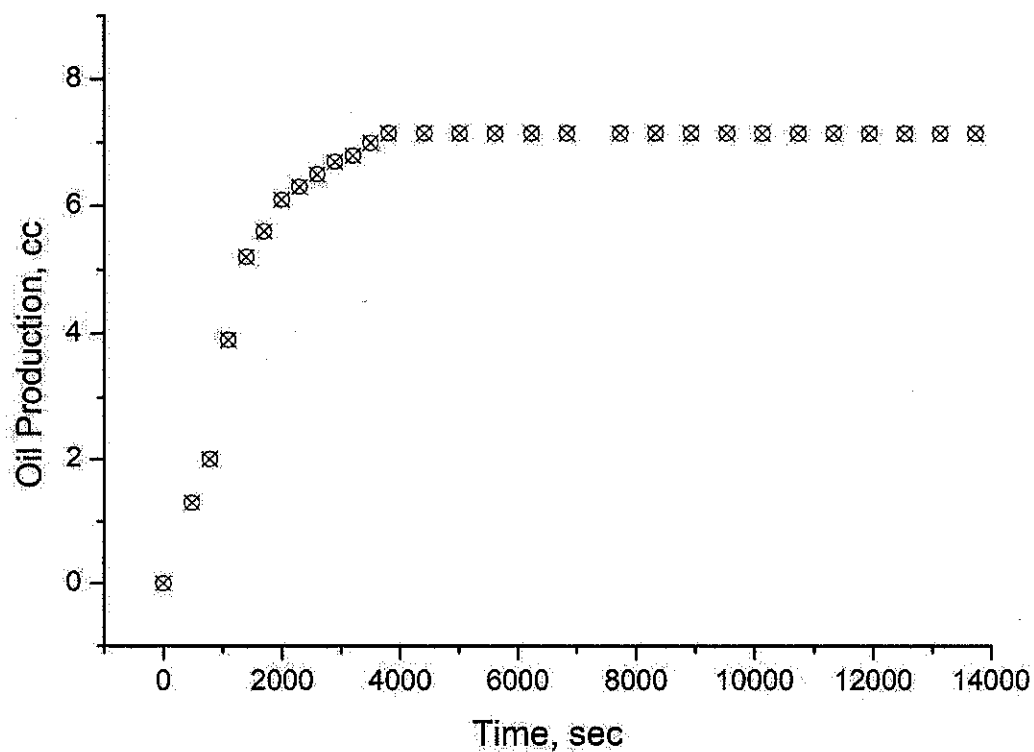


Figure A.51: Oil production from core sample during gas injection (50 % ratio of n-heptane-crude oil injection, gas-oil system)

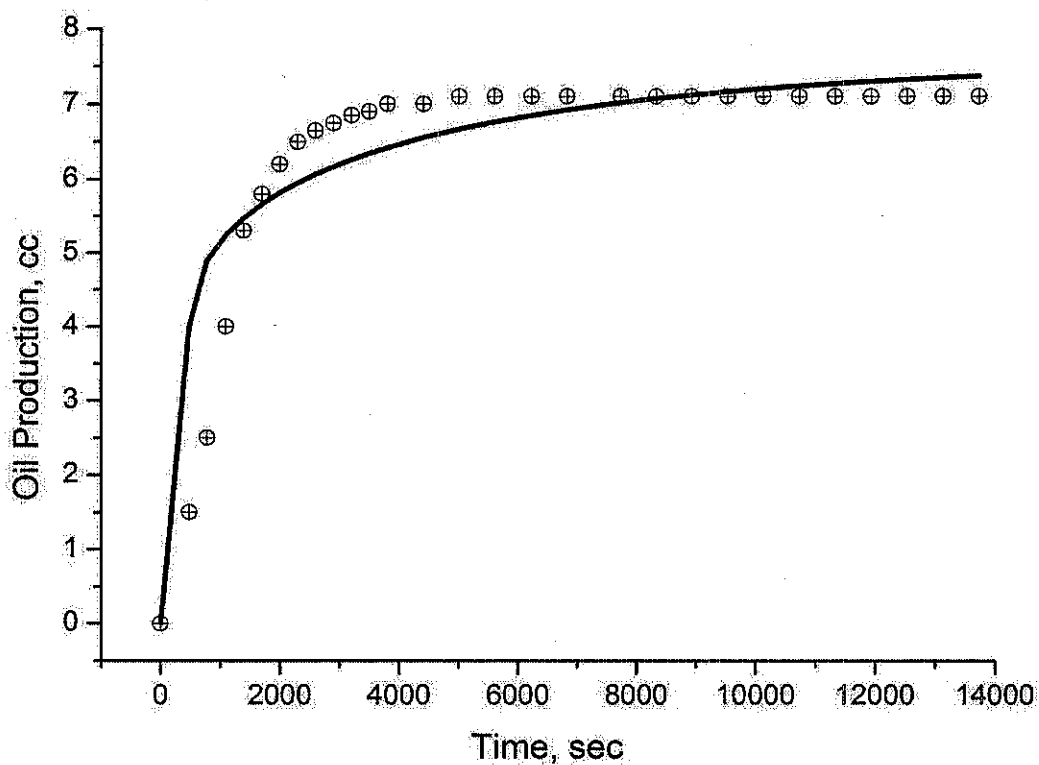


Figure A.52: Oil production history matching for zero % ratio of n-heptane–crude oil injection (Corey correlation, gas-oil system)

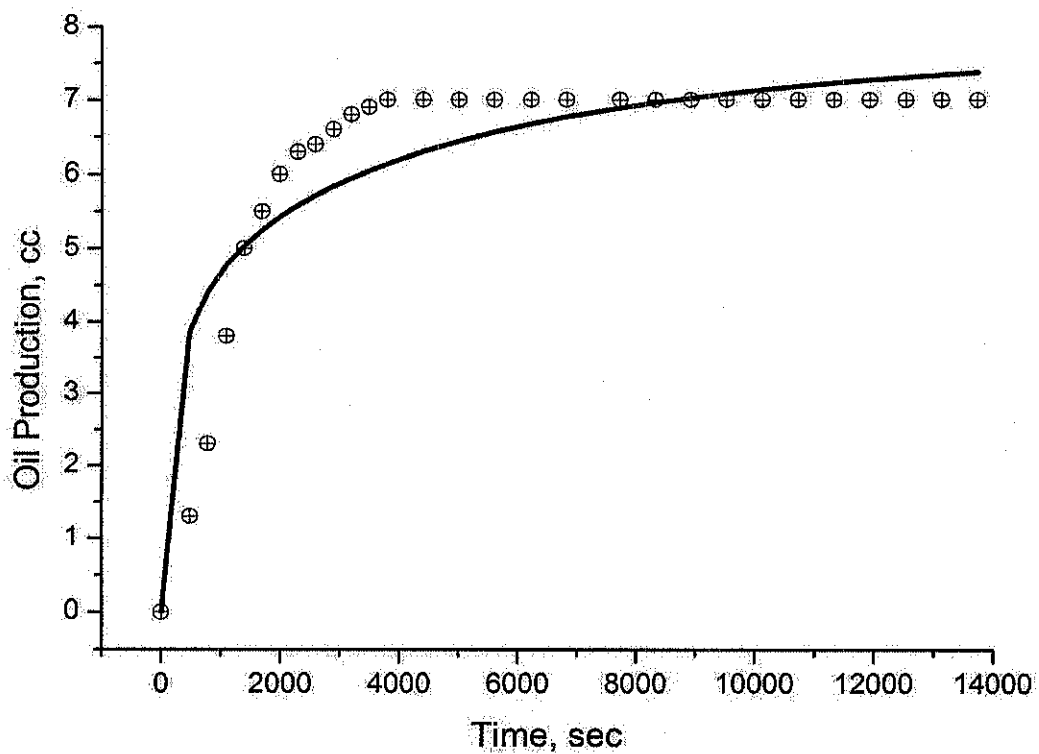


Figure A.53: Oil production history matching for 20 % ratio of n-heptane–crude oil injection (Corey correlation, gas-oil system)

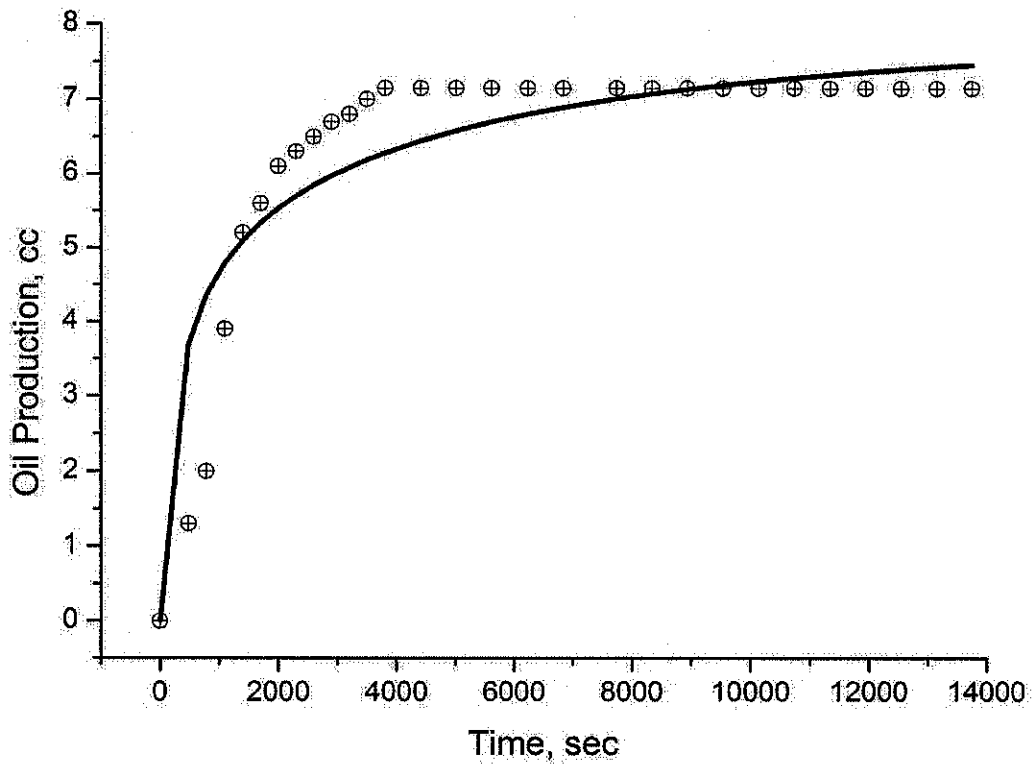


Figure A.54: Oil production history matching for 50 % ratio of n-heptane–crude oil injection (Corey correlation, gas-oil system)

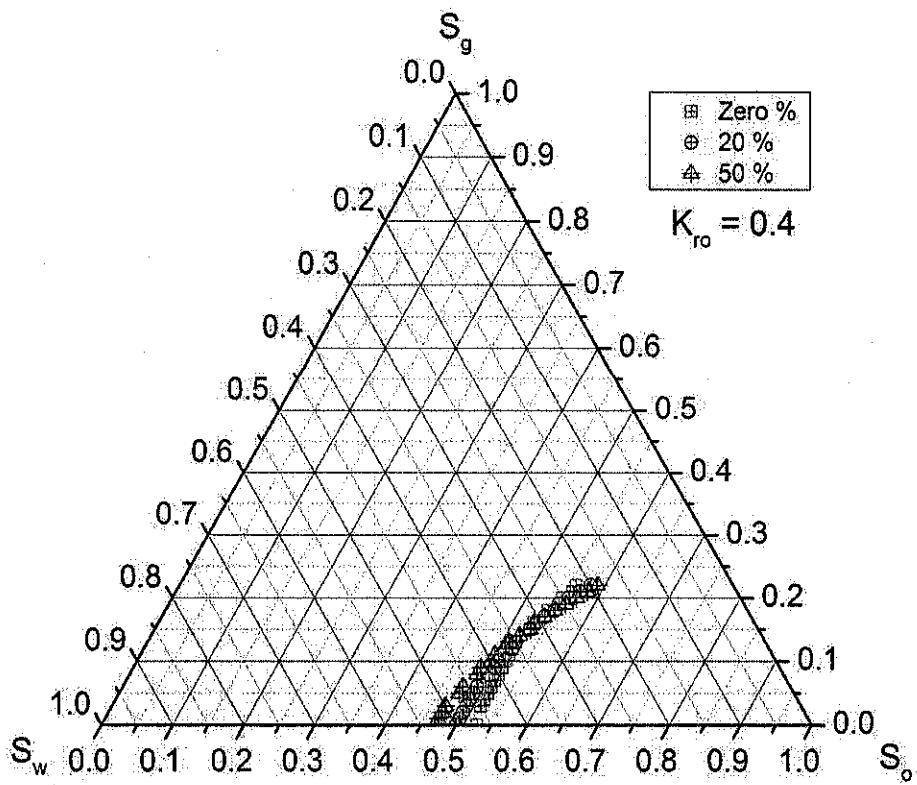


Figure A.55: Comparison of oil relative permeability equal to 0.4 for all cases

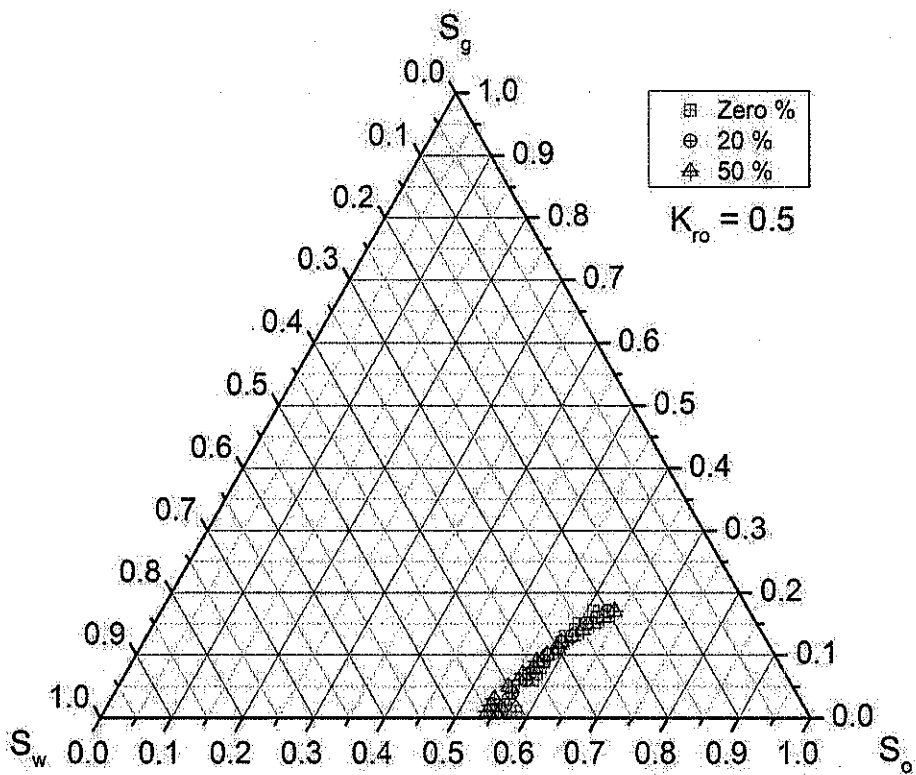


Figure A.56: Comparison of oil relative permeability equal to 0.5 for all cases

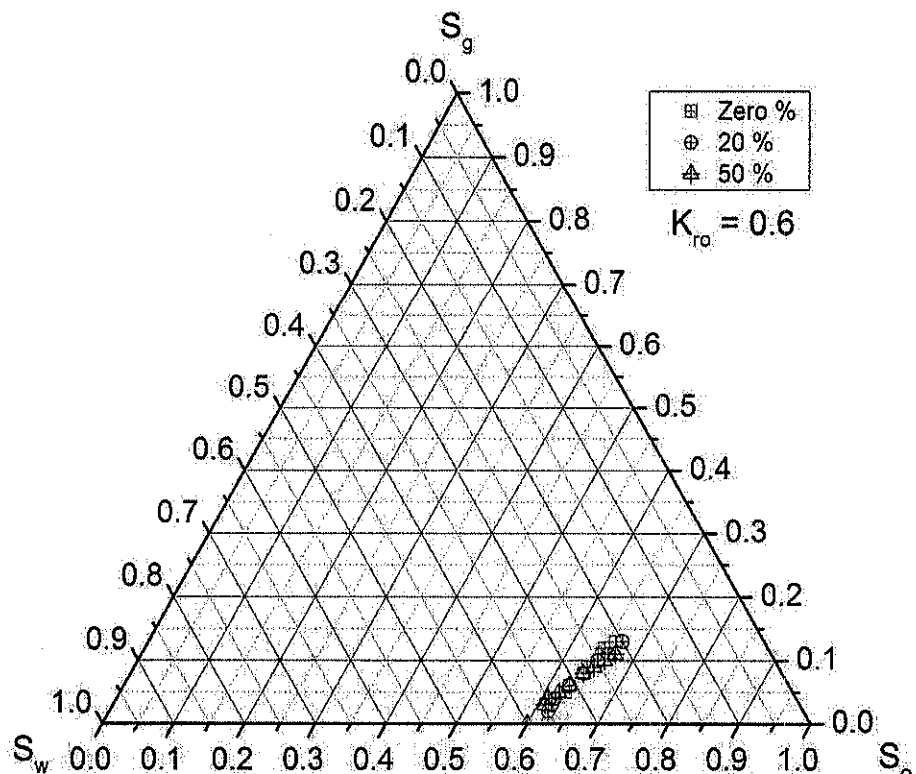


Figure A.57: Comparison of oil relative permeability equal to 0.6 for all cases

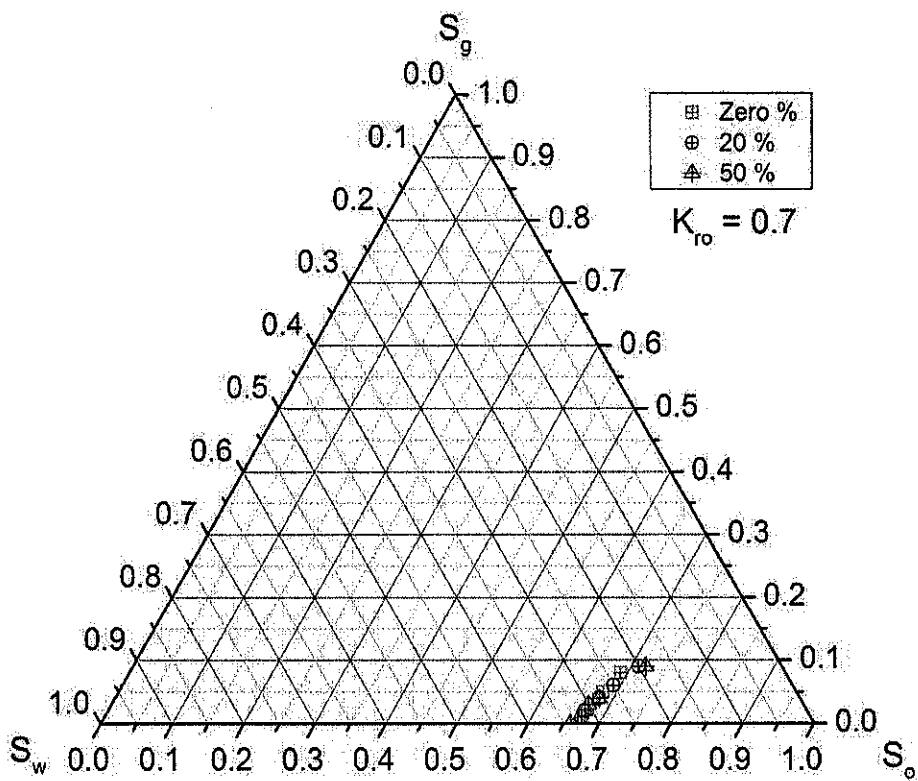


Figure A.58: Comparison of oil relative permeability equal to 0.7 for all cases

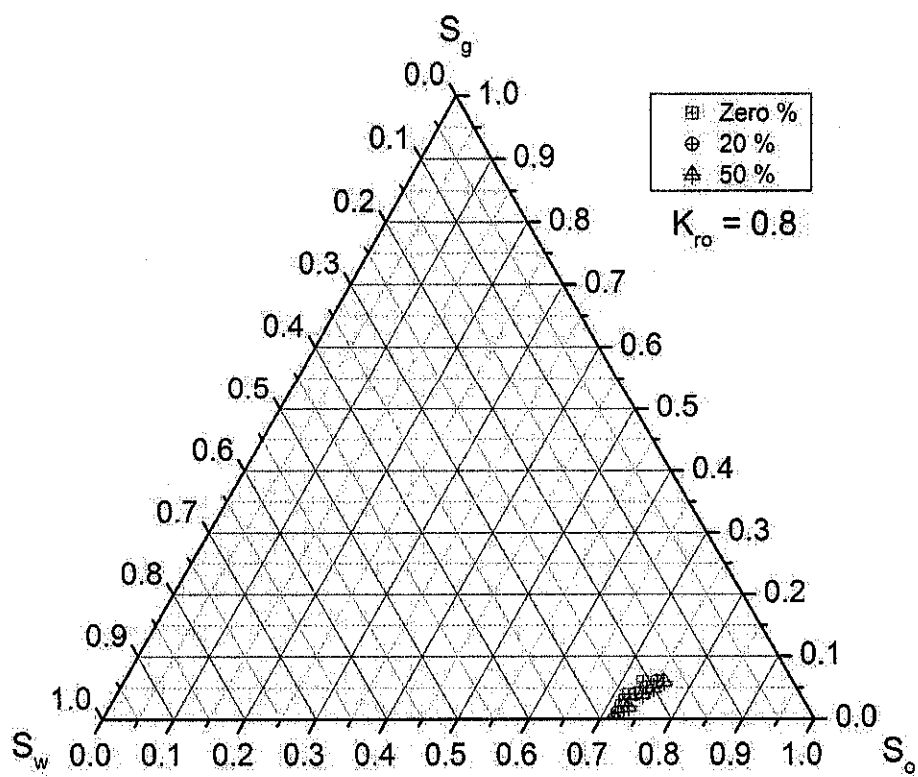


Figure A.59: Comparison of oil relative permeability equal to 0.8 for all cases

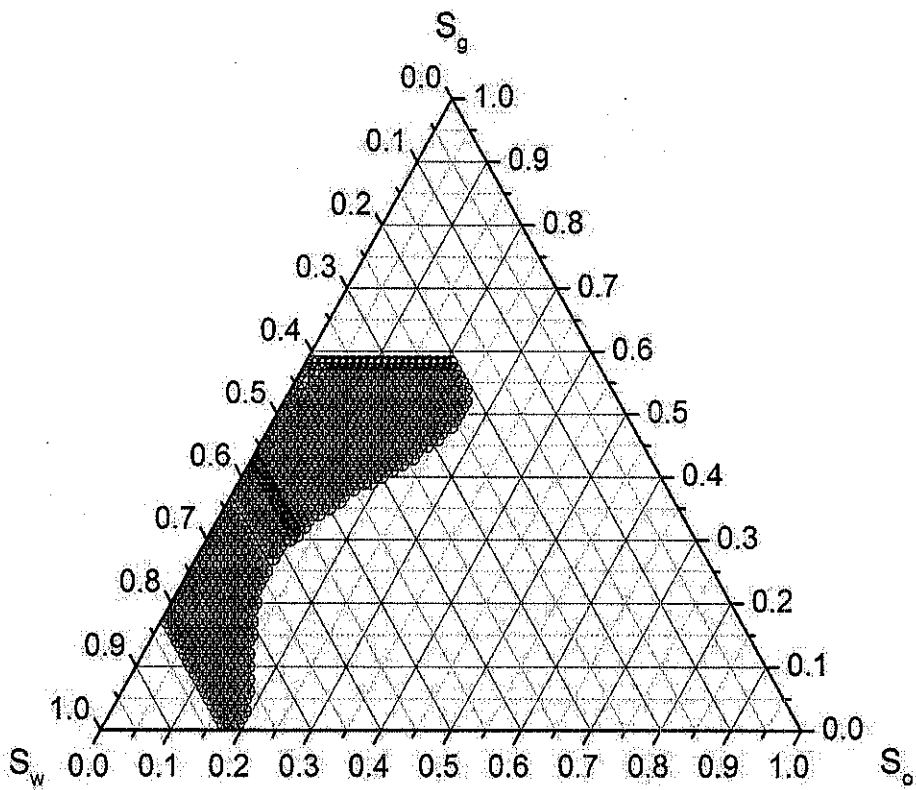


Figure A.60: Fluid saturation distribution for oil relative permeability for zero % ratio of n-heptane–crude oil injection

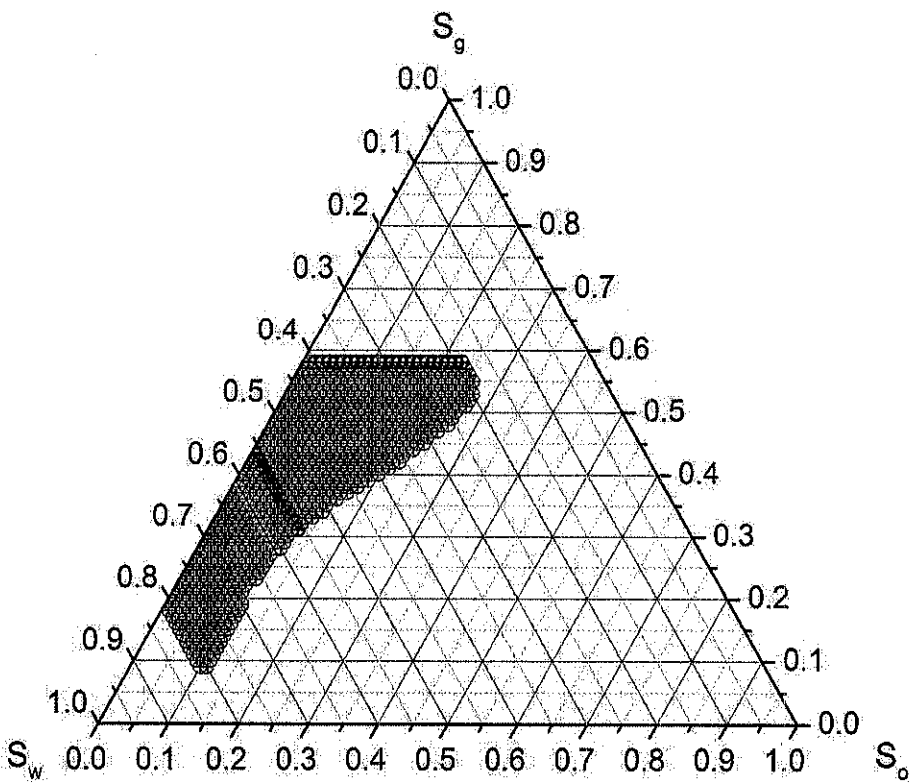


Figure A.61: Fluid saturation distribution for oil relative permeability for 20 % ratio of n-heptane–crude oil injection

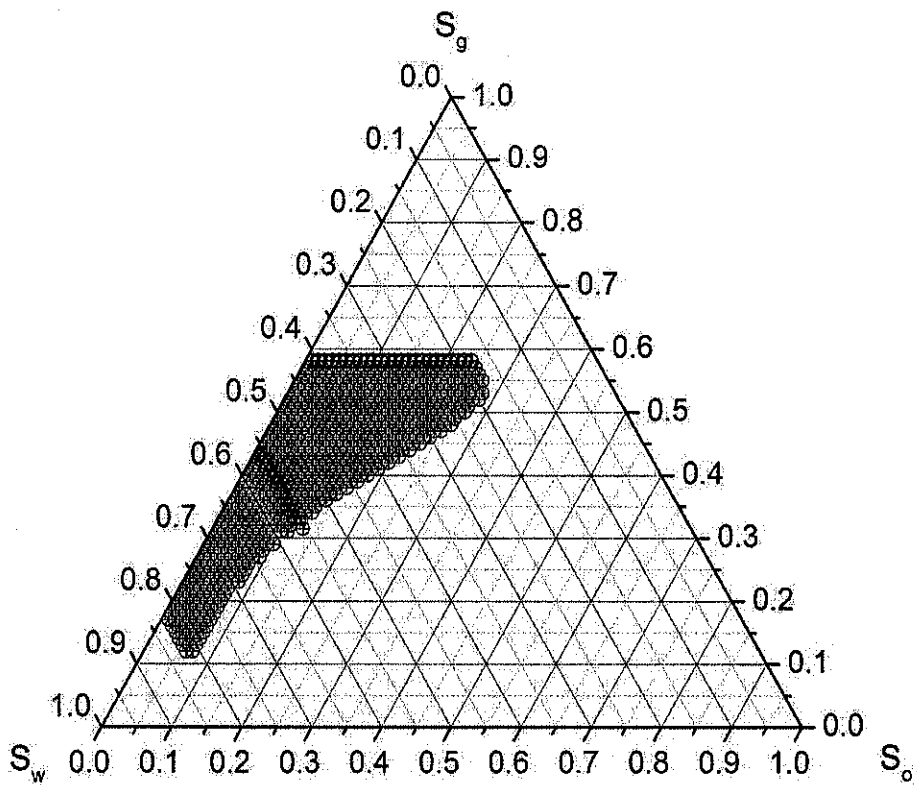


Figure A.62: Fluid saturation distribution for oil relative permeability for 50 % ratio of n-heptane–crude oil injection

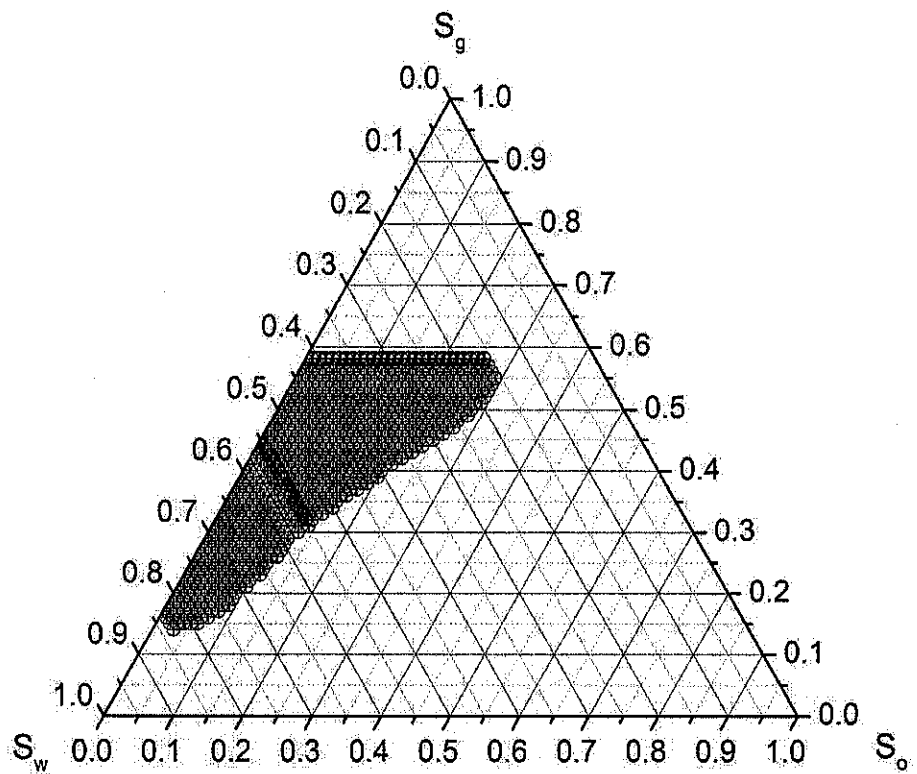


Figure A.63: Fluid saturation distribution for oil relative permeability for 80 % ratio of n-heptane–crude oil injection

APPENDIX B

PVT CELL SYSTEM AND ASPHALTNE MEASUREMENTS

B.1 Introduction

The mercury free fluid evaluation analyzer in its visual version is designed to study phase behavior of hydrocarbon fluids at reservoir conditions of pressure and temperature. Therefore, in order to conduct asphaltene precipitation and deposition experiments for live crude oil sample, PVT cell system which is equipped with some asphaltene supplements parts need to be used. The PVT cell system enables to identify solid particles and monitor change in size and morphology of wax crystals and asphaltenes solids as function of temperature, pressure, time and effect of various chemical treatments. This can be possible by equipping the PVT system with three different systems which are explained as following, Solid Detection System (SDS), High Pressure Microscope (HPM) and Solid Organic Filter (SOF) in one only.

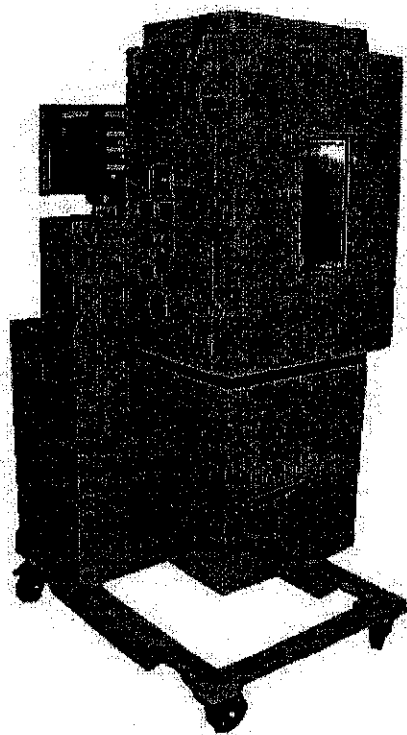


Figure B.1: Fluid evaluation system or PVT cell system

Figure B.1 shows a picture of PVT cell system which is used for asphaltene experiments of this study. The PVT cell system which is based on a window through cell offering full sample visibility through front and back windows is particularly interesting when visual observation of the fluid must be accomplished such as hydrates studies, swelling tests, volatile oil studies, gas condensates, etc. The general

features of this entire system are shown in Table B.1 and it can use for working pressure up to 15000 psi with pressure accuracy of 0.1 percent full scale, working temperature between -20°C to 175°C with temperature regulation of ± 0.5 °C, cell volume 500 cc with 100 cc visual and with volume accuracy of 0.01 ml, and with a magnetic drive stirring mechanism.

Table B.1: General description of PVT cell system

Item		Type / model / specification
Elements:		<input type="checkbox"/> 1 PVT cell of 500 cc <input type="checkbox"/> 2 accumulators of 200 cc <input type="checkbox"/> 1 injection pump
Operating pressure:		Up to 1,000 Bar – 15,000Psi
Operating Temperature:		<input type="checkbox"/> cooling system (down to – 20°C) <input type="checkbox"/> ambient to 175 °C
Chamber material:		Stainless steel
Connections:		1/8” LP Autoclave or Butech type (15000 Psi)
Stirring mechanism:		Magnetic drive
Solid Detection System:		<input type="checkbox"/> Dual wavelength (NIR) <input type="checkbox"/> Multiple wavelength (900 to 2500nm)
H P M	Microscope zoom:	Up to x 500
	Particles size Distribution:	Home-software
	Viewing area:	5mm diameter
Organic Solid Filter	Dead volume:	2 cc
	Filter size Range:	0.22 , 0.45, 1, 3 (pack of 50) um
Power requirement:		240 VAC 50/60Hz single phase plus ground power – 6 Kw
Dimensions: Weight:		LxWxH : 1890 mm x 1701 mm x 947 mm 820Kg

The well-known procedure and steps required for asphaltene experiments by using this PVT cell system which is equipped with SDS, HPM, and SOF are:

- a) Pre-measurement of relative heavy organic compounds by SARA test.
- b) Pre-requirements for asphaltene experiments, restoration, water content checking and asphaltene content measurement by ASTM method or IP143.

- c) Quality controls for asphaltene content before and after loading the sample into PVT cell.
- d) Constant mass expansion experiment (CME).
- e) Measurement the onset point of asphaltene precipitation by SDS system.
- f) Measurement the frequency of solid particles and monitor the change in size by HPM system.
- g) Measurement the amount of asphaltene precipitation in different temperatures, pressures or different CO₂ concentrations by SOF system.

Each system, HPM, SDS, and SOF can be operated together or isolated. The SDS and the HPM are automated process. The best is to combine all these techniques to improve the accuracy by data crosschecking. Every method complies with a specific function:

- a) Solid detection system (SDS) detects when the organic deposition takes place, in other words it measures the onset conditions of the live crude oil.
- b) High pressure microscope (HPM) identifies the solid particles and monitors the change in size and morphology of wax crystals and asphaltenes solids as function of temperature, pressure, time and effect of various chemical treatments.
- c) Organic solid filtration (SOF) enables to determine the amount of solids formed in the fluid sample when altering the pressure, temperature or composition of the fluid.

B.2 Sample Restoration

B.2.1 Restoration Methods

To conduct an asphaltene experiment preparation a good representative crude oil sample is very essential. Indeed, a sampling procedure is to obtain a representative sample of the original reservoir fluid under reservoir conditions for conducting the experiments. There are two main kinds of samples, bottom-hole sample and separator

sample. As can see in Figure B.2 the processes of sampling and restoration are very critical steps to prepare a good representative sample before starting asphaltene experiments and loading a sample inside the PVT cell system. Normally, after sampling, with loss of temperature and during shipment, phase behavior of sample can be altered (two phases). In order to have sample homogeneity inside the bottle, it needs to be restored properly. The restoration consists in mixing sample at reservoir pressure and reservoir temperature in a recombination cell. Figure B.3 shows the RCA 1000 instrument which is a recombination cell and it is used during this study.

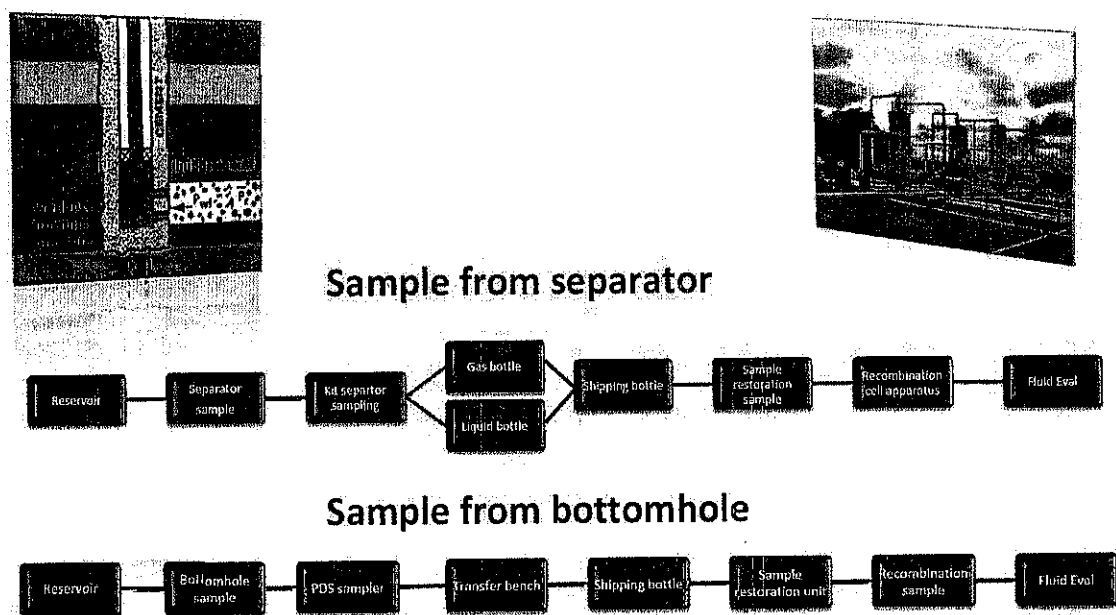


Figure B.2: Restoration processes of separator and bottom-hole samples

The RCA 1000 instrument is based on a high pressure, high temperature recombination cell in which oil and gas solutions are injected at pre-defined volume, stirred together, heated at a desired temperature and pressurized at pressure above the saturation pressure for few hours to give a homogeneous mixture of the reservoir fluid. The instrument comes with a recombination cell jacketed with a heating mantel for temperature control, a magnetic driven stirrer, a motorized rocking system used in conjunction with a mixing ring in the sample chamber of the cell for proper agitation of the heavy oil samples and a temperature and pressure display panel. The top of the cell is equipped with a bull's eye window to visualize the saturation pressure. The cell volume of this recombination cell is 2,000 cc with working pressure up to 15,000 psi and working temperature between ambient to 175°C. The pressure and temperature

accuracies are 0.1 percent full scale and $\pm 0.5\text{ }^{\circ}\text{C}$, respectively. The wetted material is stainless steel and viton.

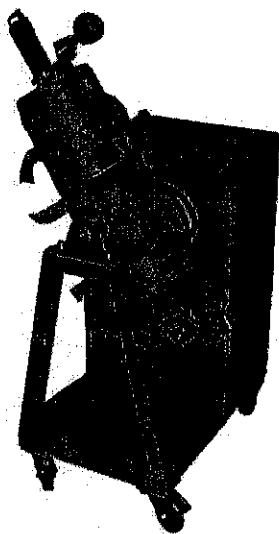


Figure B.3: RCA 1000 instrument, recombination cell

Typically, the re-pressurize process should be at 1000 psi above the expected bubble point pressure or static bottom-hole pressure (when bubble point pressure cannot be estimated). In case of heavy oil, waxy crudes, heat up $80\text{ }^{\circ}\text{C}$ at least is required. In case of gas condensate, the sampler chamber should be heated with a heating jacket to the reservoir temperature. Figure B.4 shows the schematic of three different of recombination instruments and position of recombination step which is important before loading the sample into PVT cell system.

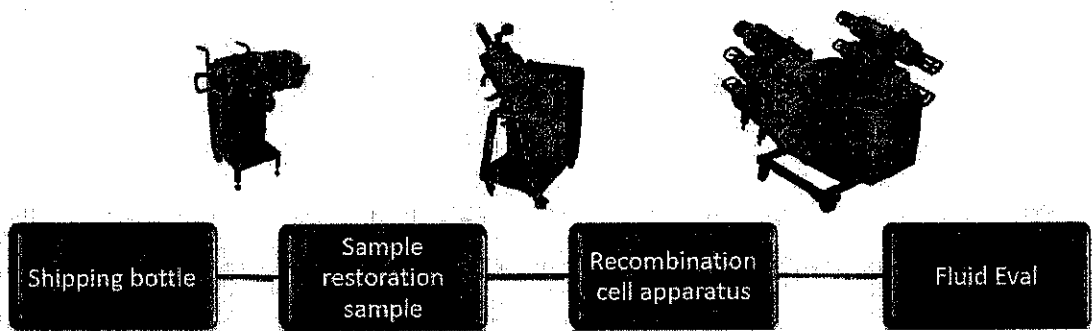


Figure B.4: Schematic of recombination instruments

For recombination the separator samples, gas and oil must be mixed into recombination cell according to production gas-oil ratio (GOR). The fluids can be

loaded by hydraulic pump from shipping bottles or accumulators. The gas sample needs to pressurize using a gas booster. The restoration of the sample inside the recombination cell at reservoir conditions or above usually takes time at least 5-7 days. As shown in Figure B.5, after the restoration process the sample can be transferred from recombination cell into PVT cell, whereas, as shown in Figure B.6 for bottom-hole samples; it can be loaded directly into the PVT cell system from the shipping bottles or accumulators using a hydraulic pump.

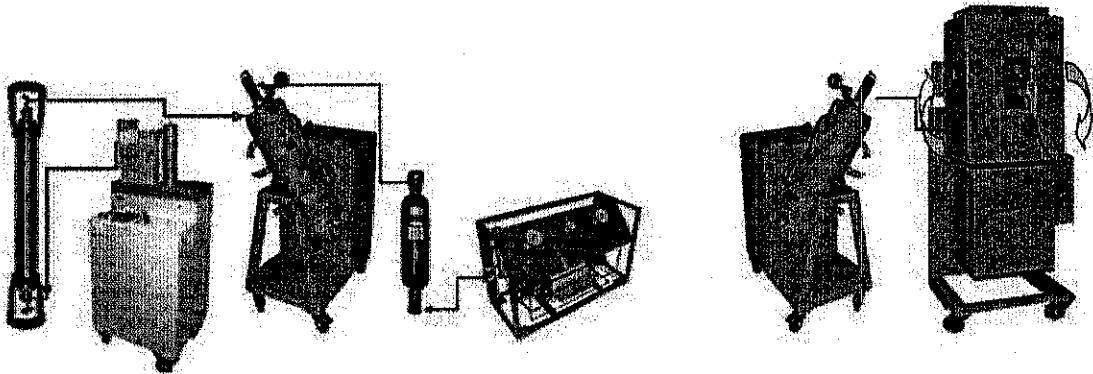


Figure B.5: Schematic of transferring separator samples into PVT cell

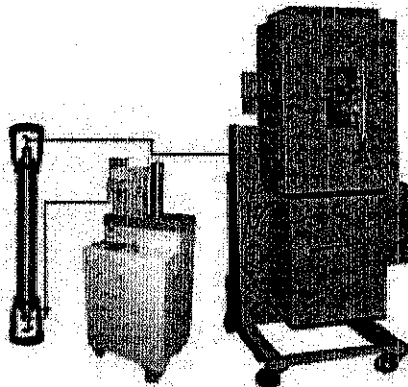


Figure B.6: Schematic of transferring bottom-hole samples into PVT cell

B.2.2 Recombination during This Study

In lack of the bottom-hole and separator samples, dead crude oil sample from Melaka Refinery in Malaysia is used to mix with available gases into recombination cell. The sixty percent CO_2 and forty percent methane are used during this recombination process to recombine with this dead crude oil. The gases and oil are recombined with nearby 500 gas-oil ratio (vol/vol) that almost close to the real reservoir conditions.

Furthermore, the recombination cell is heated up to 100 °C and re-pressurized to 6,000 psi. The magnetic stirrer and motorized rocking system are used in conjunction with a mixing ring in the sample chamber of the cell for proper agitation. The restoration period inside the recombination cell is taken more than twenty days. Moreover, the composition of recombined sample (live oil) is counted base on knowing the dead oil composition and computing the number of the moles of CO₂ and methane and using the material balance for components as shown in Table B.2.

Table B.2: Crude oil composition (dead and live oils)

Component	Dead crude oil		Live crude oil	
	Mole no.	Mole percent	Mole no.	Mole percent
CO ₂	0.000000	0.000000	1.023989	15.04741
C ₁	0.000000	0.000000	0.937300	13.77351
C ₅	0.000194	0.004005	0.000194	0.002846
C ₆	0.090288	1.863993	0.090288	1.326770
C ₇	0.373602	7.713000	0.373602	5.490038
C ₈	0.290482	5.996991	0.290482	4.268599
C ₉	0.178009	3.674989	0.178213	2.618821
C ₁₀	0.226641	4.678996	0.226641	3.330463
C ₁₁₊	3.684580	76.068026	3.684580	54.14447
Total	4.843796	100.000000	6.805289	100.000000

B.2.3 Basic Live Crude Oil Sample Measurements

The constant mass expansion (CME) experiment, differential vaporization (DV) experiment, viscosity and density measurements on some portion of live oil sample

are conducted. For this purpose 50 cc of live oil sample is transferred from the recombination cell into PVT cell. It is kept for 24 hours to reach again the equilibrium conditions which are 100 °C and 6,000 psi. The procedure of conducting the CME is certainly isothermal decreasing pressure process which is a non-destructive experiment. The pressure in the PVT cell is decreased continuously from 6,000 psi step by step and the total volume of the PVT cell in each step is recorded. The main window for the CME test can be shown in Figure B.7.

CME OIL FIELD

Stability criteria					Temp. Setpoint (deg C)	Pressure Setpoint (psig)	Temperature (deg C)	Pressure (psig)	Total Cell Volume Corr (cc)	Isotherm Compressibility Coefficient C (1/psi)x10 ⁶	Relative Volume (-)	Density (g/cc)
Stirring Duration (mn)	Pressure (psig)	Temp. (deg C)	Total Volume (cc)	Duration (mn)								
5	175	10.5	0.10	5	100.0	6000	100.1	5999.7	49.946			1.0000
						5000	100.1	4999.8	50.348			
						4000	100.0	3999.8	50.785			
						3000	100.0	2999.8	51.299			
						2500	100.0	2500.3	51.600			
						2300	100.1	2299.7	51.748			
						2250	100.0	2248.7	51.789			
						2200	99.9	2200.3	51.825			
						2150	100.0	2149.8	51.879			
						2100	100.0	2100.1	51.918			
						2050	100.0	2049.6	51.979			
						2045	100.0	2045	51.995			
						2040	100.0	2039.6	51.997			
						2035	99.9	2035	51.997			
						2030	100.1	2029.6	52.003			
						2000	100.0	2000	52.028			
						1900	100.0	1900.4	52.227			
						1800	99.9	1799.3	53.162			
						1500	99.9	1500.3	59.353			
						1400	100.0	1400	62.197			
						1300	100.0	1299.7	65.473			
						0						

Density at 1st step (g/cc)

1.000

Saturation Pressure (psig)

Saturation Volume (cc)

Units

Pressure

☒ Psig

☐ Psia

☐ Barg

☐ Bara

Temperature

☒ Deg C

☐ Deg F

Fill by operator

Measurement

Excel Calculation

Use "CME OIL.MA" Macro

Figure B.7: Main window during CME experiment in PVT system

Commonly, the bubble point pressure can be elicited from the sharp changing in total cell volume data versus pressure which is shown in Figure B.8. In addition, captured images of the camera from top of the PVT cell can be a visualize indication of bubble point pressure as well. According to these two indications the bubble point pressure of this live crude oil sample is estimated around 1720 psi at 100 °C. After this experiment the sample is recombined again at a pressure slightly higher than the estimated bubble point pressure. After reaching again the required equilibrium, in order to measure the oil viscosity at this pressure and 100 °C, some portion of sample

around 10 cc is transferred from the PVT cell into electromagnetic viscometer at fix conditions. In the same procedure the densitometer apparatus is used to measure the oil density at these conditions by transferring some other crude oil portion. The live crude oil viscosity and density which are obtained during these measurements are 0.772 cp and 0.774 g/cc respectively.

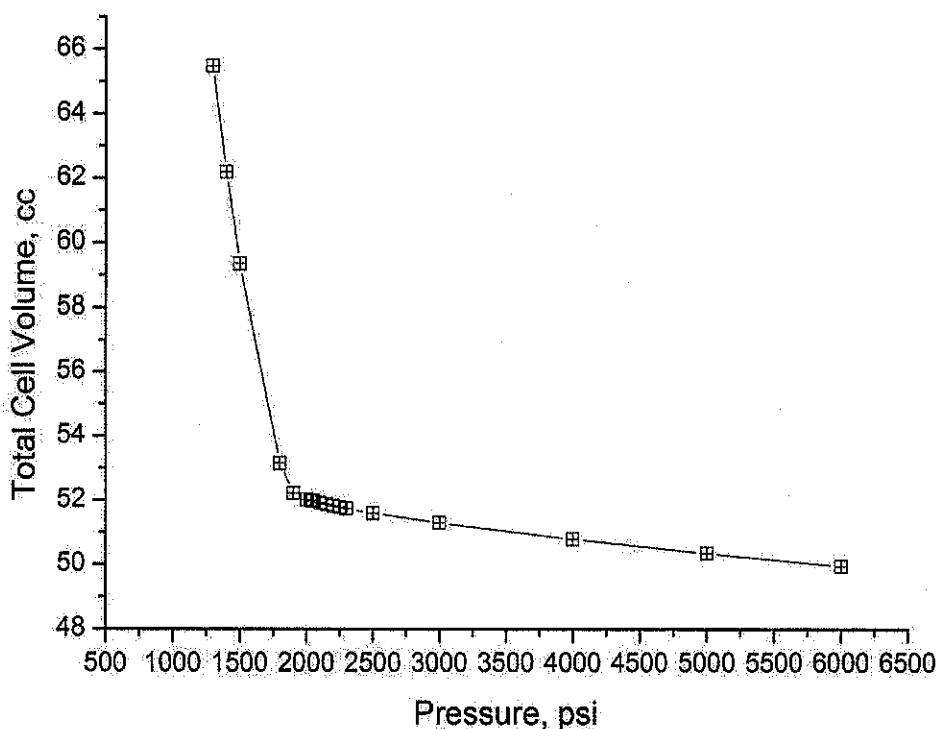


Figure B.8: Total PVT Cell volume versus pressure

B.3 Quality Control

Quality controls for asphaltene content before and after loading the sample into PVT cell and pre-filtration of crude oil sample before loading into PVT cell are compulsory. Typically, the quality controls should be done in two steps before and after loading a sample into PVT cell. The flow diagrams of these two steps are shown in Figure B.9 and Figure B.10. As clearly shown during these steps the content of asphaltene into crude oil sample is examined in order to get the homogenous samples. In addition, the pre-filtration for removing the non-organic particles such as sand, dust, and scale is necessary.

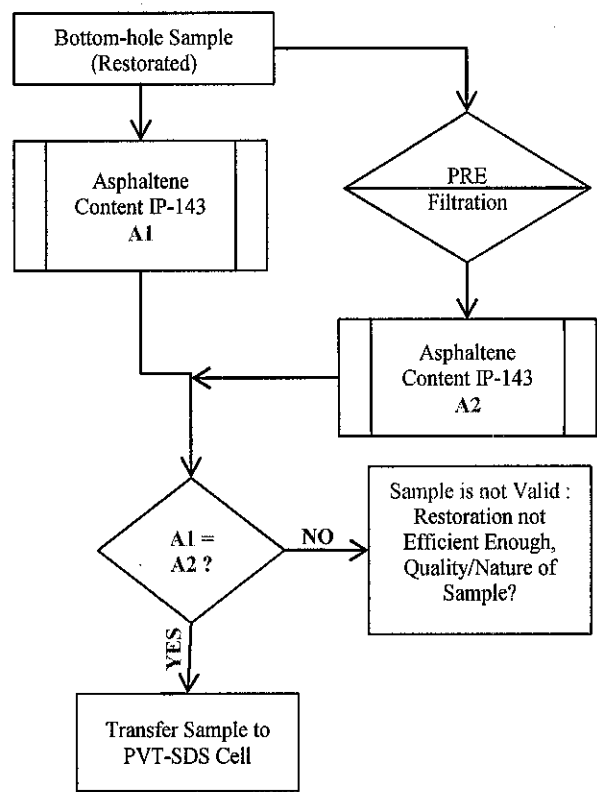


Figure B.9: Pre-filtration flow diagram before loading

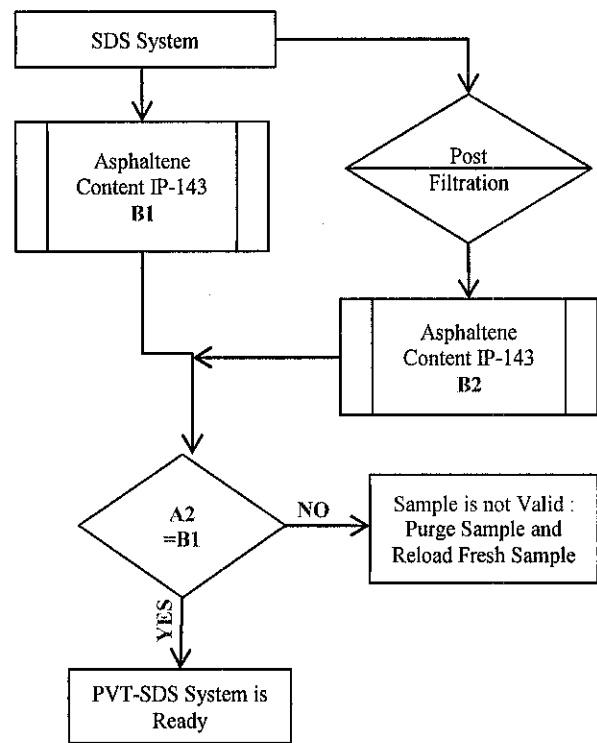


Figure B.10: Pre-filtration flow diagram after loading

Usually, the pre-filtration is done by passing the crude oil sample from 0.2 micro meter filter. If a sample is properly restored, the pre-filtration can remove only the non-organic particles, which could interfere with the experiment.

B.4 SDS System

B.4.1 How SDS System Work

The onset point of asphaltene precipitation can be detected and measured by using solid detection system (SDS) which schematically is shown in Figure B.11.

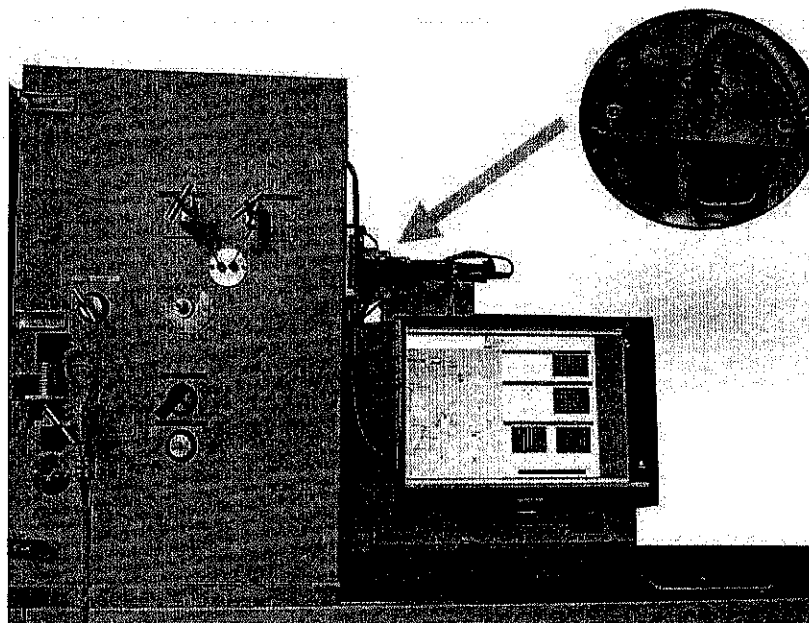


Figure B.11: Solid detection system (SDS)

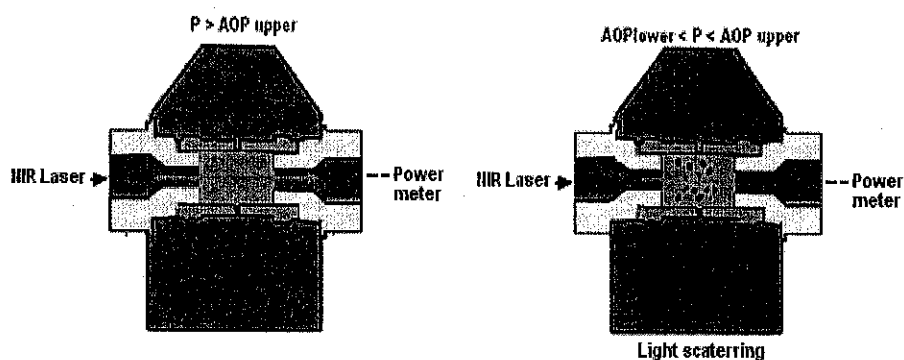


Figure B.12: Principle of light scattering technique

The solids detection system is based on the principle of light scattering technique that is illustrated in Figure B.12. The detection measures with accuracy the upper asphaltene precipitation (onset point) and with this information elaborates a corresponding saturation curve with plotting the power of transmitted light versus cell pressure. It is based on near-infrared study and it is an efficient way in detecting both bubble points and asphaltene aggregation onset pressures in high-pressure systems. The detection of solids is based on the level of transmitted light and it is directly related to the optical properties of the asphaltene in the near infrared range (ray light diffusion relation between asphaltene size and NIR wavelength range). The asphaltene aggregation contributes to the attenuation of the transmitted light by diffusion; at that time this point is easily identifiable in curves.

In a homogeneous fluid with no suspended asphaltene at a pressure above the asphaltene onset pressure (AOP) a light beam travels through the fluid with minimum scattering. While, at pressure below the AOP, asphaltene particles appear and cause partial light scattering. According to the amount and size of particles, a gradual reduction in light transmittance or transmitted light is observed until the bubble at which total scattering takes place. Approaching the lower AOP, the light transmittance starts increasing again. This can cause because the dissolution back of dispersed asphaltene particles into crude oil sample.

As remind of optical properties involved, the light transmittance depends on two main parameters, the fluid density and the quantity of solids particle presents in the fluid. Figure B.13 shows the relation between the light transmittance, density, and pressure for crude oil without having asphaltene. Moreover, Figure B.14 shows the same relationship but for crude oil with asphaltene potential. As can be seen, the light transmittance is inversely proportional to the density of oil sample. If the oil density decreases the light transmittance increases. As it is known for a live oil above the bubble point (single phase liquid), the density is proportional to the pressure. Hence, if the pressure decreases, the light transmittance increases proportionally. The light transmittance is inversely proportional to the size of the solid particle hence, if the solid size increases then the light transmittance decreases. The light transmittance is inversely proportional to the nucleation density of solids (appearance factor of solid

particle), hence, if it increases then the light transmittance decreases. The SDS optical setup is designed for precision measurements on petroleum fluids. The optimization of the optical loop and the amplification of the signal induce a better response of the system and consequently a better identification when asphaltenes precipitation or onset point pressure takes place.

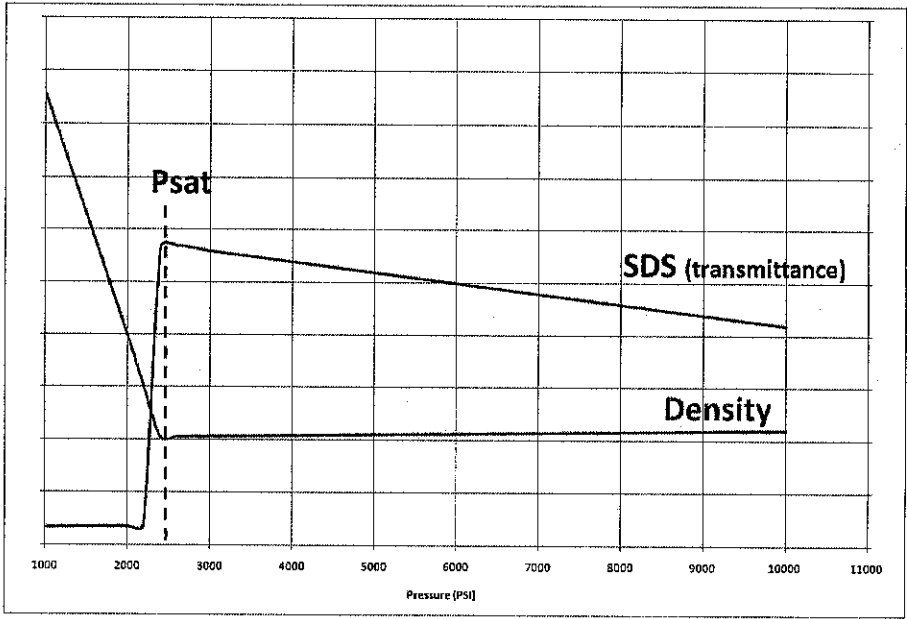


Figure B.13: Density and light transmittance versus pressure without asphaltene

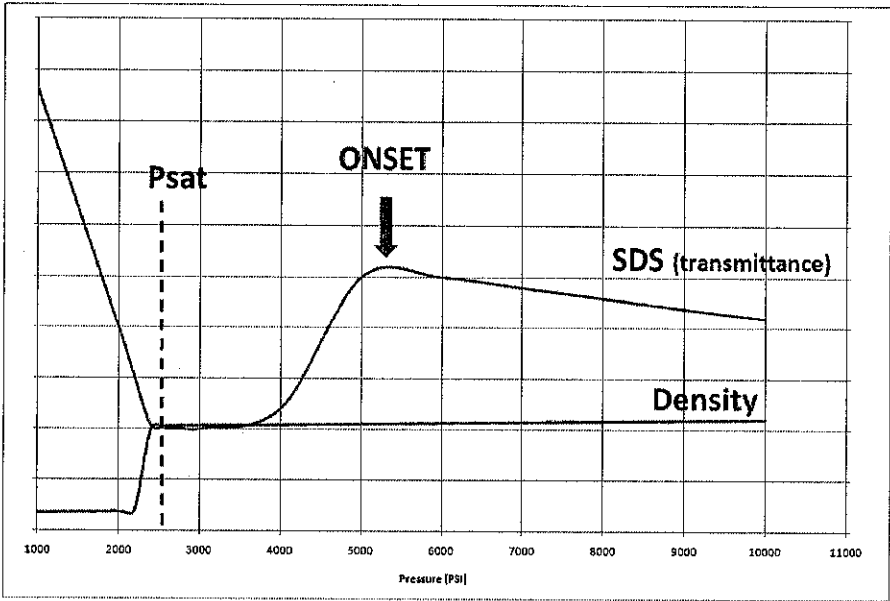


Figure B.14: Density and light transmittance versus pressure with asphaltene

B.4.2 SDS Procedure during This Study

The PVT cell which is equipped with SDS system is used to measure the onset of asphaltene precipitation. In this system, the fibre-optic light-transmittance probes are mounted across the windows of the visual cell. A computerized pump is controlled to maintain the system conditions during isothermal depressurization and/or isobaric injections of precipitating solvents for asphaltene precipitation studies. The process variables (temperature, pressure, time, and transmitted light power level) are recorded and displayed from the detector.

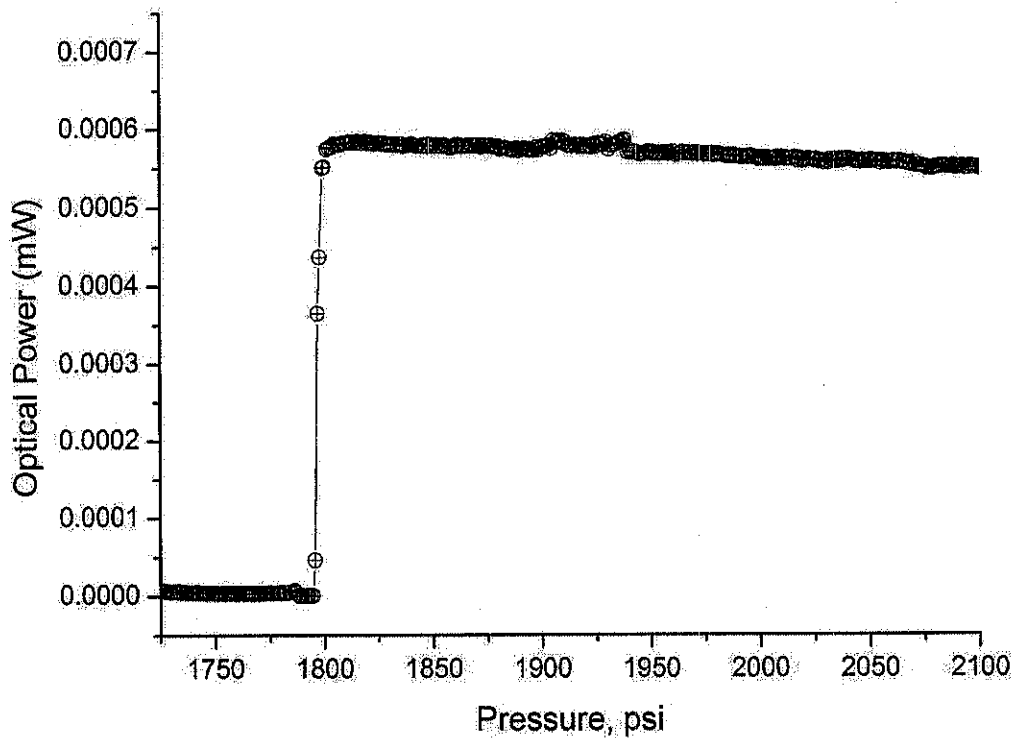


Figure B.15: Transmitted power as function of pressure

A typical experimental run involves charging a known volume of the recombined crude oil sample at or above the reservoir (or specified) temperature and pressure conditions. The total initial volume charge is around 50 ml. The cell content is homogenized at a maximum mixer speed of 1,400 rpm for about 30 min. Subsequently, the light-transmittance scan is conducted to establish the reference baseline. The depressurization experiment is started with simultaneous measurement of light transmittance power. The maximum depressurization rate used in this system is in the order of 40 psi/min. The average transmitted light power and the corresponding pressure are recorded every minute. Below the bubble point pressure,

the experiment is continued in discrete steps. At each pressure step, the cell content is allowed to stabilize, the generated gas is bled out, and the NIR response is monitored. Experiments are continued until an experimental abandonment pressure of 500 Pisa is attained.

Figure B.15 shows the transmitted power as function of cell pressure during the SDS process for this sample. As can be seen from these data the onset point of asphaltene cannot be obtained that it may because the recombined sample is not properly chosen for this kind of asphaltene experiment. The bubble point pressure 1790 psi can be estimated from this data. This value is slightly higher than previous CME data that is acceptable.

Table B.3: Description of HPM system

Description	Item	Type / model / specification
	Pressure range :	Ambient to 15000Psi
	Temperature range :	Ambient to 200°C (option -20°C)
	Detection based on:	Microscopic observation
	Viewing area :	5mm diameter
	Wetted material :	Stainless steel, sapphire, with custom-made coating for microscope analysis
	Microscope zoom :	up to x 500
	Results provided:	Particles size distribution from 1um
	CCD sensor:	Color 2.0MPixels GIGABIT Ethernet 15f/s 1600x1200

B.5 HPM System

The high pressure microscope (HPM) is specially designed to visualize accurately the wax and asphaltenes precipitation at onset point condition up to 15000 psi and 200 °C. The HPM is very easy to use and very simple to install. The schematic of this

system is shown in Figure B.16 and specification is given in Table B.3. The HPM enables to identify the solid particles and monitor the change in size and morphology of wax crystals and asphaltene solids as function of temperature, pressure, time and effect of various chemical treatments. The fluid under consideration is homogenized at the desired conditions in PVT cell and transferred from the PVT cell through the HPM cell by a re-circulator pump embedded which work under controlled pressure and flow rate. The PVT cell, HPM and pump are all inside the same air bath thus enabling correct thermal equilibrium. Subsequently, the fluid is depressurized at known pressure decrements, and transferred into the HPM cell. Any change in the observed reservoir fluid are recorded with the HPM video camera and then analyzed. The provided software measures the particle size distribution. The appearance of wax can create major problems by plugging flow lines and process equipment. It is primarily a surface problem rather than a reservoir problem when there are lowest temperatures. That is why the HPM is also compatible with negative temperature (-20°C) for detection of wax appearance temperature.

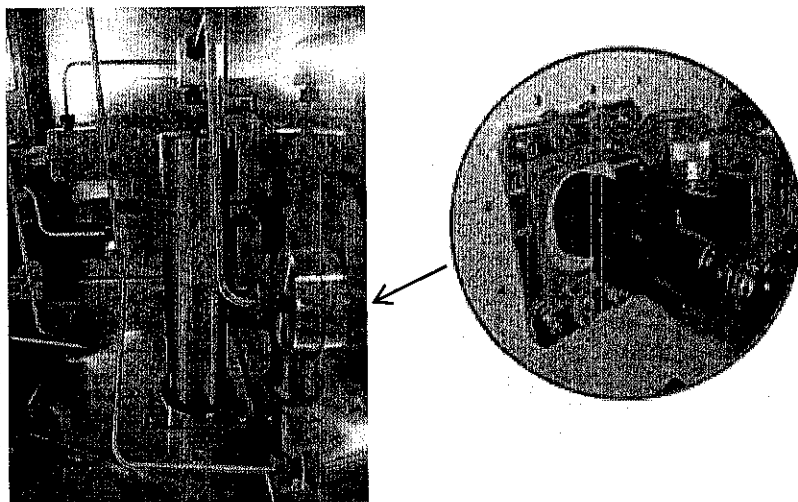


Figure B.16: Schematic of the HPM system

At high pressures in the reservoir, the asphaltenes are dissolved in the monophasic crude oil. When the pressure is reduced the molar volume and the solubility parameter difference between asphaltenes and the crude oil increases towards a maximum at the bubble point of the crude oil. As a result of the reduced solvating power, the asphaltenes may start to precipitate at some onset pressure higher than the bubble point. Prior to the precipitation a stepwise association of the asphaltene molecules will

take place. The final precipitation is due to a strong attraction between the colloidal particles and the formation of agglomerates. Once gas evolves, the light alkane fraction of the liquid phase is reduced, and thereby the solvating power for asphaltene molecules increases. Wax crystals can be visible in a crude oil below its wax appearance temperature.

The optical loops which include image processing, microscope, cell and backlight have been optimized for the study of petroleum fluid. The backlight is based on the modern technology of Xenon to provide high level of illumination for very opaque fluid ($\text{API} > 15^\circ$). The cell and the microscope have been designed to be compatible with industrial environment and to require little maintenance. The microscope is protected from any vibration and the macro and micro tuning of the focus is done with one accurate motion table. During the experiment, in case of asphaltene plugging inside the HPM cell, the cell can be isolated from the PVT cell and cleaned directly without losing the sample.

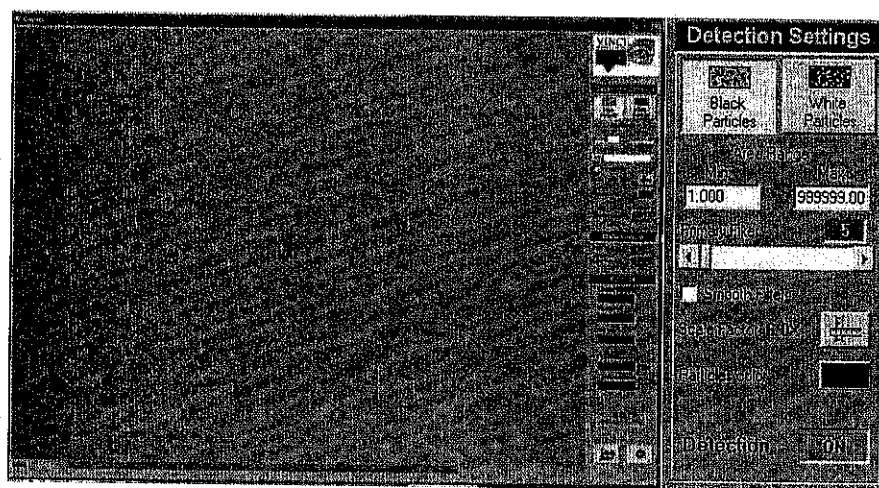


Figure B.17: Main window of the particle size analysis

The particle size analysis (PSA) is capable to detect particles from $1\ \mu\text{m}$, measures particle count, particle size and to give size distributions. The main window of this software is shown in Figure B.17. The data is recorded automatically and periodically. The file format of the results is compatible with excel. The software is quite easy to use, only few parameters (size range of detection, filter and scale factor) are required to launch auto detection. The particle detection is based on evolved algorithm which takes into account the nature of the solids observed (asphaltene or

wax). Indeed, the optical properties of the asphaltene induce important light scattering, it means than particles can appear with different size than the reality. Therefore, data processing on image with this kind of particle requires adequate treatment to provide reliable results.

During experiment and pressure decreasing process this software can import automatically the results from HPM system and plots some useful graphs. The main graphs are the particle size distribution of asphaltene particle (particle mean size of asphaltene) versus cell pressure. These graphs are very important for study the effect of kinetic on asphaltene precipitation and deposition. In addition the flocculation process which is a step between the precipitation and deposition steps can be clearly defined by using this data. Also it can be recommend that the onset point of deposition (OAD) which is condition that asphaltene start to deposit and different than OAP can be measured and defined. The examples of these graphs are shown in Figure B.18.

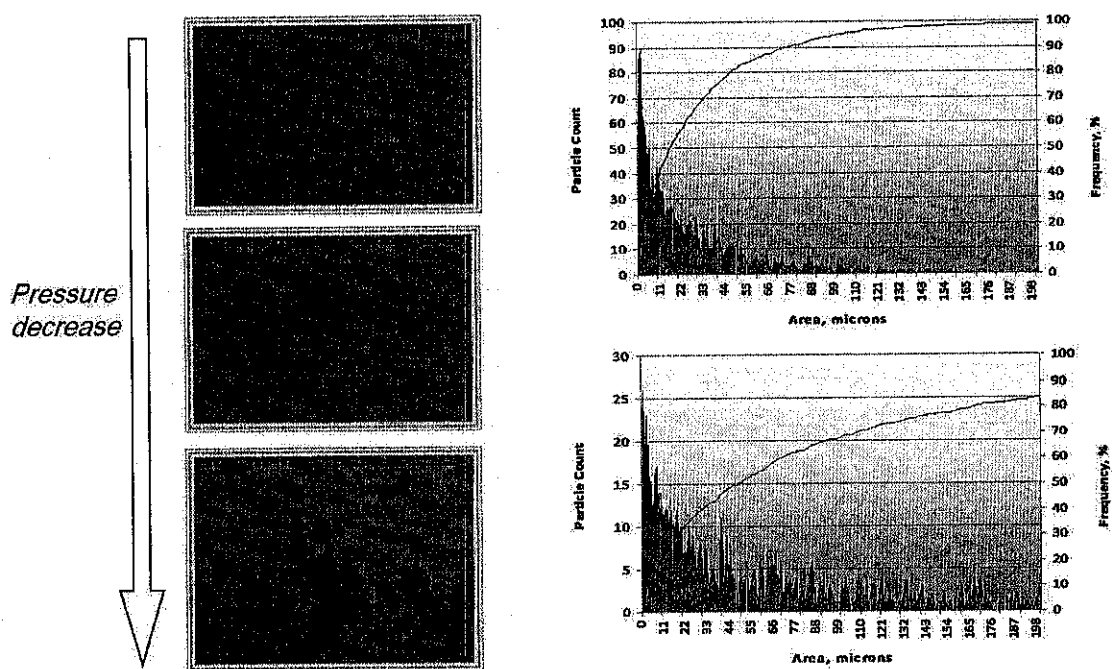


Figure B.18: Example of main output graphs from HPM system

Advanced studies can be performed to analysis the kinetic of the Asphaltene. For example, the particle size analysis from the HPM enables to follow the growth rate of the particles according to the nature of any inhibitor or additive used. Very good

studies can be done to study the effect of different inhibitors on asphaltene precipitation under reservoir condition by using this method. Figure B.19 shows such potential to study the effect of inhibitor on asphaltene precipitation.

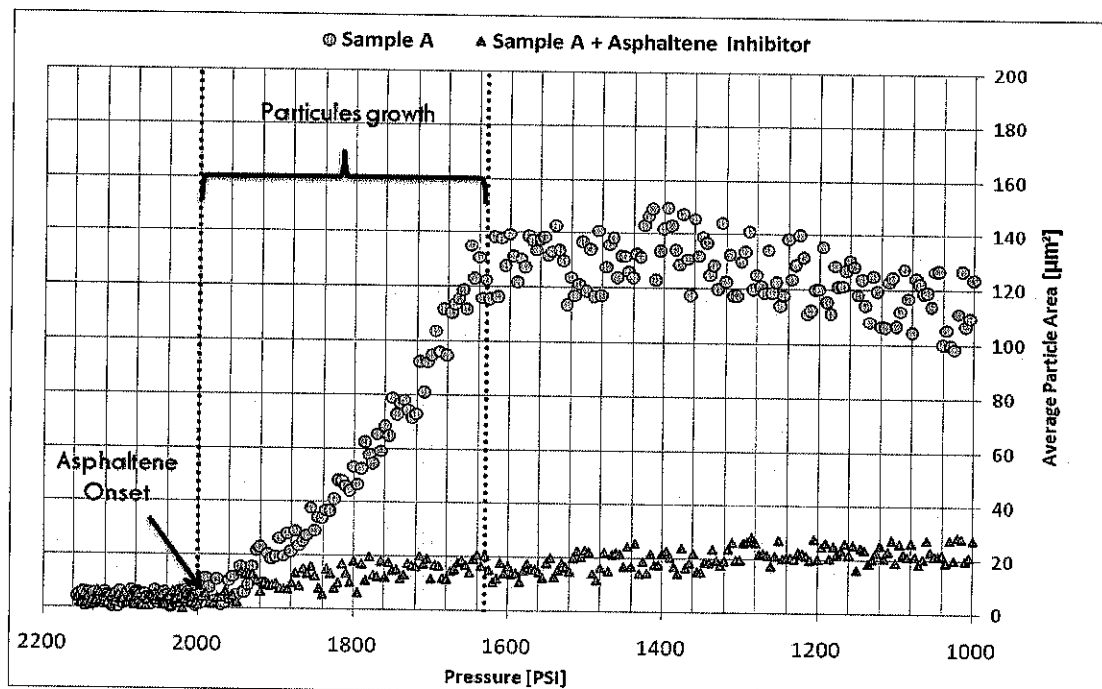


Figure B.19: Effect of inhibitor on asphaltene precipitation

B.6 SOF System

The high pressure high temperature organic solid filtration (SOF) is used to determine the amount of solids formed in the fluid sample when altering the pressure, temperature or composition of the fluid after a precipitation process. It is used in connection with PVT cell system to filter precise volumes of oil and solvent at reservoir conditions. The device is composed of a high pressure, high temperature stainless steel filter holder using filter disc to retain the solid particles. The fluid sample is transferred from the PVT cell to the floating piston accumulator through the filter at controlled pressure and flow rate. Different ranges of filter size are given along with this filter in Table B.4.

Amount of total asphaltene precipitation will be measured by filter unit in reservoir temperature and different reservoir pressures. It should note that filter unit in

this system is putted in air bath and its temperature is same the temperature of the fluid inside the cell. After fixing temperature and desired pressure inside the cell, some asphaltic oil passed through the filter unit at constant temperature and pressure and then filtered oil in the separator is separated from the gas. Then, the asphaltene content will be measured at fixed temperature and desired pressure by using IP-143 standard.

After washing and cleaning filter unit, by depressurization process the pressure inside the PVT cell will be decreased and the asphaltene content in new condition will be measured. At each pressure step, the cell content is allowed to stabilize. Experiments are continued until an experimental abandonment pressure of 3.45 MPa (500 psi) is attained. The schematic for high pressure and high temperature filter unit inside the PVT cell system is shown in Figure B.20.

Table B.1: Description of SOF system

Description	Item	Type / model / specification
	Minimum volume:	2cc
	Connections:	Autoclave 1/8"
	Maximum Pressure Working:	1000Bar (15000Psi)
	Maximum Temperature Working:	200°C
	Material:	Stainless Steel
	Wetted parts:	Stainless Steel, Hastelloy, Polypropylene Membrane, Viton
	Filter size range (µm):	0.22 , 0.45, 1, 3

From the results of the SDS and HPM which are recorded periodically, the upper and lower asphaltene onset condition can be determined and it is possible to delimit the stability zones for asphaltenes in solution. The example of asphaltene envelope can be plotted as shown in Figure B.21. The green area represents the condition where asphaltene flocculation has been observed or detected. As can see during the first CME at 130°C, the upper onset is about 10,000 psi, the saturation point is 3220 psi and the lower onset is 2460 psi. As pressure continues to decrease closer to the saturation pressure, more asphaltenes is precipitated, until the saturation pressure is reached, and gas is released from solution. With further pressure decrease, enough gas

has been removed from the system, and the asphaltene may begin to dissolve back into crude oil as shown in asphaltene lower locus.

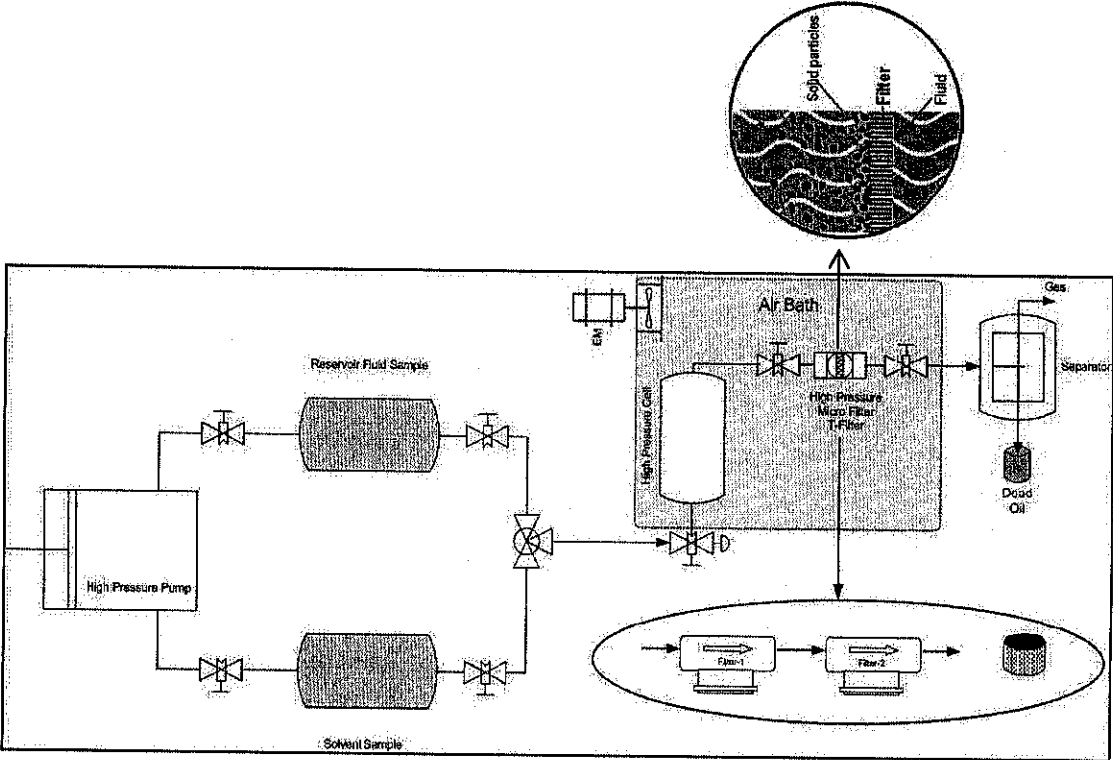


Figure B.20: Schematic of SOF system inside the PVT cell system

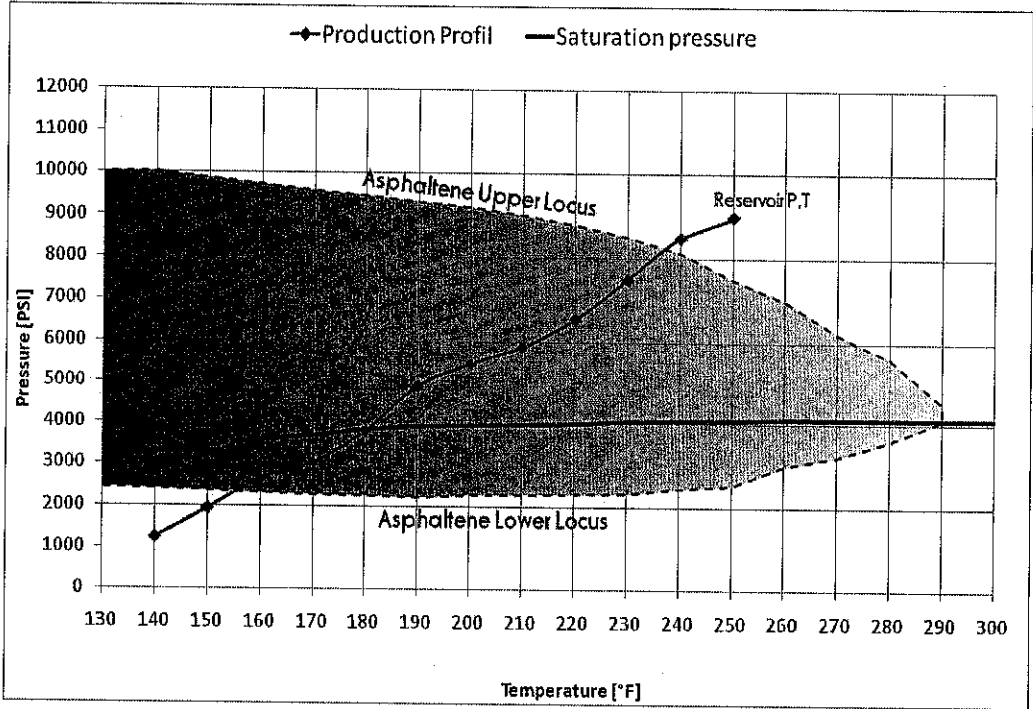


Figure B.21: Asphaltene phase behavior envelope

APPENDIX C

ASPHALTENE SIMULATION INPUT FILE DATA FOR ECLIPSE 300

RUNSPEC

TITLE

Asphaltene PRECIPITATION

START

1 JAN 2000 /

FIELD

GAS

OIL

WATER

DIMENS

100 1 1 /

COMPS

12 /

EQLDIMS

1 200 /

TABDIMS

1 1 2* 2 /

--AIM

FULLIMP

--NOSIM

UNIFIN

UNIFOUT

NOECHO

-- Switch on Asphaltene deposition model

ASPHALTE

WEIGHT PORO TAB /

GRID

--Basic grid block sizes

EQUALS

DX 80/
DY 80 /
DZ 20 /
PORO 0.224 /
PERMX 260 /
PERMY 260 /
PERMZ 80 /
TOPS 7500 4* 1 1 /
/
INIT
--Properties section-----
PROPS
--Water saturation functions
Pedersen
STONE2
--Gas saturation functions
SGFN
0.000000 0.000000 0.000000
0.050000 0.006005 0.010000
0.100000 0.031314 0.030000
0.150000 0.072661 0.100000
0.200000 0.123152 0.300000
0.250000 0.189110 0.600000
0.300000 0.266970 1.000000
0.350000 0.356149 1.500000
0.400000 0.456332 2.100000
0.450000 0.567132 2.800000
0.500000 0.694937 3.600000
0.550000 0.846386 4.500000
0.581700 1.000000 5.500000
/

--Oil saturation functions

SOF3

0.188100	0.000000	0.000000
0.200000	0.001923	0.001000
0.250000	0.025617	0.007270
0.300000	0.065423	0.033382
0.350000	0.117448	0.075186
0.400000	0.179906	0.126450
0.450000	0.251644	0.193003
0.500000	0.331889	0.271429
0.550000	0.420049	0.361158
0.600000	0.515624	0.461872
0.650000	0.618238	0.573522
0.700000	0.727555	0.702509
0.750000	0.843320	0.854067
0.780000	0.915764	0.946235
0.797500	1.000000	1.000000

/

--Water saturation functions

SWFN

0.202500	0.000000	20.000000
0.220000	0.000007	9.000000
0.250000	0.000087	5.000000
0.300000	0.000639	4.100000
0.350000	0.002027	3.300000
0.400000	0.004568	2.600000
0.450000	0.008564	2.000000
0.500000	0.014312	1.500000
0.550000	0.022074	1.100000
0.600000	0.032125	0.800000
0.650000	0.044720	0.600000
0.700000	0.060100	0.300000

0.750000	0.078514	0.100000
0.800000	0.100207	0.000000
0.811900	0.105870	0.000000

/

RPTPROPS

SOF3=5 SWFN=5 SGFN=5 /

--Rock properties

ROCK

-- pres cw

14.7 5.0E-6 /

-- Water properties

PVTW

-- pres bw cw vw

14.7 1.0 3.3E-6 0.7 /

-- Standard conditions

STCOND

--Temp Pressure

60 14.7 /

-- Reservoir temperature (deg F)

RTEMP

160 /

-- Equation of State

EOS

PR /

-- Component names

CNAMES

N2 CO2 C1 C2 C3

HC1 HC2 HC3 HC4

HC5 C36+ Asph

/

-- Reservoir EoS properties

-- Molecular weights

MW

28.013 44.01 16.043 30.07
44.097 64.1 96.52 134.556
245.556 433.542 649.644 649.644 /

-- Critical temperatures (R)

TCRIT

227.16 547.56 343.08 549.72
665.64 796.8618 970.9884 1116.891
1382.634 1646.541 1846.0458 1846.0458

/

-- Critical pressures (psi)

PCRIT

492.314325 1069.86516 667.19613 708.34479
615.760305 513.0650064 424.8011307 343.7382705
209.2115442 133.2922665 105.1348263 105.1348263

/

ZCRIT

0.290 0.277 0.264 0.257
0.245 0.235 0.235 0.236
0.290 0.277 0.264 0.257 /

-- Acentric factors

ACF

0.04 0.225 0.008 0.098
0.152 0.23027 0.30269 0.40879
0.72237 1.12962 1.34026 1.34026 /

-- Binary interaction coefficients

BIC

0.0

-0.02 0.0

0.031 0.103 0.0

0.042 0.13 0.0027 0.0

```

0.091 0.135 0.0085 0.0017 0.0
0.095 0.13 0.018 0.0069 0.0018 0.0
0.12 0.15 0.0319 0.0164 0.0077 0.0021 0.0
0.12 0.15 0.0471 0.028 0.0163 0.0073 0.0016 0.0
0.12 0.15 0.0833 0.058 0.041 0.0261 0.0137 0.006 0.0
0.12 0.15 0.1166 0.0874 0.0668 0.0479 0.0307 0.0186 0.0036 0.0
0.12 0.15 0.1329 0.1022 0.0802 0.0596 0.0404 0.0264 0.0075 0.0007 0.0 /
-- Specify initial liquid composition
ZMFVD
1000.0 0.0016 0.020002 0.333633 0.077107 0.073907 0.118313 0.112112 0.083608
0.138178 0.021569 0.019654968 0.000316
7500.0 0.0016 0.020002 0.333633 0.077107 0.073907 0.118313 0.112112 0.083608
0.138178 0.021569 0.019654968 0.000316
/
-- Asphaltene parameters
ASPFLOC
-- first last floc
11 11 12 /
--ASPP1P
--'P' /
-- asphaltene weight percentage
ASPREWG
-- pres %_wt
1000.0 10.0
2209.0 20.0
3000.0 20.0
10000.0 100.0 /
-- ... asphaltene floc rates
-- (set here to cause faster floc degradation than formation)
ASPFLRT
-- CMP6
0.1500

```

```

0.001 /
-- ... asphaltene deposition
ASPDEPO
-- adsorp plug entrain Vcr
0.10 0.10 0.0 2500 /
-- ... asphaltene damage ratio
ASPKDAM
-- exponent
3 /
-- ... asphaltene viscosity change
ASPVISO
-- vfrac mult
0.0 1.0
0.01 1.2
0.12 1.7
1.0 10.0 /
ASPKROW
-- SW KRW KRO
0.157600 0.000000 0.573100
0.200000 0.003594 0.515811
0.250000 0.012281 0.451320
0.300000 0.024272 0.390207
0.350000 0.039003 0.332602
0.400000 0.056172 0.278654
0.450000 0.075494 0.228459
0.500000 0.096869 0.182263
0.550000 0.120121 0.140208
0.600000 0.145135 0.102557
0.650000 0.171871 0.069686
0.700000 0.200206 0.041934
0.750000 0.230112 0.020035
0.800000 0.261505 0.005055

```

0.837300 0.285860 0.000000 /

ASPWETF

-- DEPOSIT F FACTOR

0.0 0.0

0.00804 0.5323

0.01171 0.70496

0.01884 1.0 /

SOLUTION

EQUIL

-- zdat pdat owc pcow goc pcog dummy dummy Ninit

7500 5500 10000 0 4000 0 1 1 1* /

RPTRST

PRESSURE SOIL SGAS SWAT XMF YMF RPORV ASPADS ASPDOT ASPEN

ASPFL ASPKDM ASPLU ASPREW ASPVOM ASPLIM ASPFRD /

SUMMARY

FGOR

FWCT

FOPR

FGPR

FWPR

FOPT

FGPT

FWPT

FPR

FOSAT

FGSAT

FLPR

FLPT

FOE
 FOEW
 TCPU
 ELAPSED
 NEWTON
 WBHP
 /
 WOPR
 /
 WWPR
 /
 WGPR
 /
 WWCT
 /
 WGOR
 /
 -- Asphaltene grid block parameters
 BPR
 1 1 1 /
 50 1 1 /
 100 1 1 /
 /
 BOKR
 1 1 1 /
 50 1 1 /
 100 1 1 /
 /
 BWKR
 1 1 1 /
 50 1 1 /
 100 1 1 /

/

BGKR

1 1 1/

50 1 1/

100 1 1/

/

BRPV

1 1 1/

50 1 1/

100 1 1/

/

BASPDOT

1 1 1/

10 1 1/

20 1 1/

30 1 1/

40 1 1/

50 1 1/

60 1 1/

70 1 1/

80 1 1/

90 1 1/

100 1 1/

/

BASPREW

1 1 1/

50 1 1/

100 1 1/

/

BASPKDM

1 1 1/

10 1 1/

20 1 1 /
30 1 1 /
40 1 1 /
50 1 1 /
60 1 1 /
70 1 1 /
80 1 1 /
90 1 1 /
100 1 1 /

/

BASPVOM

1 1 1 /
50 1 1 /
100 1 1 /

/

BDENO

1 1 1 /
50 1 1 /
100 1 1 /

/

BRPV

1 1 1 /
50 1 1 /
100 1 1 /

/

BOVIS

1 1 1 /
50 1 1 /
100 1 1 /

/

EXCEL

-- Asphaltene grid block parameters

RUNSUM

SCHEDULE

--Define injection and production wells

WELSPECS

-- Well Group I0 J0 depth phase

WATINJ FIELD 1 1 7500 WAT /

PROD FIELD 100 1 7500 OIL/

GASINJ FIELD 1 1 7500 GAS /

/

COMPDAT

-- Well I J K1 K2 Status

WATINJ 1 1 1 1 /

PROD 100 1 1 1 /

GASINJ 1 1 1 1 /

/

-- Composition of injected fluid (native oil)

WELLSTRE

-- name N2 CO2 C1 C2 C3 HC1 HC2 HC3 HC4 HC5 C36+ Asph

COMPINJ 0.0 1.0 0.0 0.0 0.0 0.0 0.0 0.0 0.0 0.0 0.0 0.0 /

/

WCONPROD

-- Well Status Mode Orat Wrat Grat Lrat Resv BHP

PROD OPEN BHP 1* 1* 1* 1* 1* 500 /

/

WINJGAS

GASINJ STREAM COMPINJ /

/

WCONINJE

-- Well Type Status Mode Surf Resv BHP

WATINJ WAT SHUT RATE 100 1* 5500/

```

GASINJ GAS SHUT RATE 500 1* 5500/
/
TSTEP
50*10/
--RPTPRINT
--1 1 0 0 0 1
TSTEP
0.01 /
-- Switch off producer and start injecting to re-pressurise
WELOPEN
-- Well Status
GASINJ SHUT /
WATINJ OPEN/
PROD OPEN/
/
TSTEP
50*10/
TSTEP
0.01 /
WELOPEN
-- Well Status
GASINJ OPEN /
WATINJ SHUT /
PROD OPEN/
/
TSTEP
50*10/

--RPTPRINT
--1 1 0 0 0 1
TSTEP
0.01 /

```

```
WELOPEN
-- Well Status
GASINJ SHUT /
WATINJ OPEN/
PROD OPEN/
/
TSTEP
50*10/
TSTEP
0.01 /
WELOPEN
-- Well Status
GASINJ OPEN /
WATINJ SHUT /
PROD OPEN/
/
TSTEP
50*10/
--RPTPRINT
--1 1 0 0 0 1
TSTEP
0.01 /
WELOPEN
-- Well Status
GASINJ SHUT /
WATINJ OPEN/
PROD OPEN/
/
TSTEP
50*10/
END
```

APPENDIX D

PAPER PUBLICATION

"Study of Asphaltene Precipitation and Deposition Phenomenon during WAG Application", SPE-143488, Ahmad Khanifar, Birol Demiral, Universiti Teknologi PETRONAS, Nasir Darman, PETRONAS, 2011 SPE Enhanced Oil Recovery Conference, 19-21 July 2011, Kuala Lumpur, Malaysia.

"The Effects of Asphaltene Precipitation and Deposition Control Parameters on Reservoir Performance: A Numerical Approach", SPE-146188, Ahmad Khanifar, Birol Demiral, Universiti Teknologi PETRONAS, Nasir Darman, PETRONAS, the 2011 SPE Reservoir Characterization and Simulation Conference and Exhibition (RCSC), 09-11 October 2011 in Abu Dhabi, UAE.

"Modeling of Asphaltene Precipitation and Deposition during WAG Application", IPTC-14147, Ahmad Khanifar, Birol Demiral, Universiti Teknologi PETRONAS, Nasir Darman, PETRONAS, International Petroleum Technology Conference (IPTC), 15-17 November 2011, in Bangkok, Thailand.

"A Simulation Study of Chemically Enhanced Water Alternating Gas (CWAG) Injection", SPE 154152, S. Majidaie, A. Khanifar, M. Onur, and Isa Tan, Universiti Teknologi PETRONAS, SPE EOR Conference at Oil and Gas West Asia, Muscat, Oman, 16-18 April 2012.

"Prediction of the Oil Properties Fluid Characterization after Gas Injection and Swelling Phenomena", Ahmad Khanifar, International Conference on Integrated Petroleum Engineering and Geosciences (ICIPEG 2010) Kuala Lumpur, Malaysia, 2010.

"Numerical Study of Asphaltene Control Parameters' Effects on Reservoir Performance", Ahmad Khanifar, Birol Demiral, Universiti Teknologi PETRONAS, Nasir Darman, PETRONAS, the Second International Conference on Integrated Petroleum Engineering and Geosciences 2012 (ICIPEG 2012), 12-14 June, Kuala Lumpur, Malaysia.

"The Potential of Immiscible Carbon Dioxide Flooding on Malaysian Light Oil Reservoir", S. Majidaie, A. Khanifar, Isa M. Tan, M. Onur, EOR Center, Universiti Teknologi PETRONAS, the Second International Conference on Integrated Petroleum

Engineering and Geosciences 2012 (ICIPEG 2012), 12-14 June, Kuala Lumpur, Malaysia.

"Investigation the Effects of Asphaltene Presence on Reservoir Performance", Ahmad Khanifar, Birol Demiral, Universiti Teknologi PETRONAS, National Postgraduate Conference (NPC) 2011, 19-20 Sept 2011, Malaysia.

"Study of Asphaltene Precipitation and Deposition Phenomenon", Ahmad Khanifar, Birol Demiral, Universiti Teknologi PETRONAS, Nasir Darman, PETRONAS, National Postgraduate Conference (NPC) 2011, 19-20 Sept 2011, Malaysia.

"Investigation the Effects of Asphaltene Presence on Relative Permeability Characteristics during WAG Process", Ahmad Khanifar, Birol Demiral, Universiti Teknologi PETRONAS, Nasir Darman, PETRONAS, The First Iranian Students Scientific Conference, 9-10 April 2011, Kuala Lumpur, Malaysia.

"Investigation of Water-Oil Relative Permeability Alteration due to Asphaltene Deposition under Reservoir Conditions", Ahmad Khanifar, Mustafa Onur, Universiti Teknologi PETRONAS, Birol Demiral, Schlumberger, Nasir Darman, PETRONAS, submitted to the Journal of Petroleum Science and Engineering, for possible publication July 2012.

"New Experimental Correlations to Predict Water-Oil Relative Permeability Curves Affected from Asphaltene Deposition", Ahmad Khanifar, Mustafa Onur, Universiti Teknologi PETRONAS, Birol Demiral, Schlumberger, Nasir Darman, PETRONAS, submitted to the 2013 Enhanced Oil Recovery Conference, 2-4 July 2013, Kuala Lumpur, Malaysia, for possible oral presentation and publication.

"Three-Phase Relative Permeability Alteration due to Asphaltene Deposition under WAG Process", Ahmad Khanifar, Mustafa Onur, Universiti Teknologi PETRONAS, Birol Demiral, Schlumberger, Nasir Darman, PETRONAS, submitted to the 2013 Enhanced Oil Recovery Conference, 2-4 July 2013, Kuala Lumpur, Malaysia, for possible oral presentation and publication.

